APPLICATIONS OF THE RHENIUM-OSMIUM ISOTOPIC SYSTEM, AND PLATINUM AND IRIDIUM ABUNDANCES IN ORGANIC-RICH MUD ROCKS: A GEOCHRONOLOGY, GEOCHEMISTRY, AND REDOX STUDY

A Dissertation Presented to

the Faculty of the Department of Earth and Atmospheric Sciences

University of Houston

In Partial Fulfillment

of the Requirements for the Degree

Doctor of Philosophy

By

Shawn Curtis Wright

August 2015

APPLICATIONS OF THE RHENIUM-OSMIUM ISOTOPIC SYSTEM, AND PLATINUM AND IRIDIUM ABUNDANCES IN ORGANIC-RICH MUD ROCKS: A GEOCHRONOLOGY, GEOCHEMISTRY, AND REDOX STUDY

_____

Shawn Curtis Wright

APPROVED:

_____

Dr. Alan Brandon, Chairman

_____

Dr. Henry Chafetz

_____

Dr. William Dupré

_____

Dr. Amy Kelly

_____

Dr. Eugene Domack

_____

Dean, College of Natural Sciences and Mathematics

“Every major achievement is almost always preceded by years of toil, hard work, failure, stress, tests of character, determination, and sleepless nights... All of which help form the network of roots that can then support real accomplishments.”

- Prakash Iyer

APPLICATIONS OF THE RHENIUM-OSMIUM ISOTOPIC SYSTEM, AND PLATINUM AND IRIDIUM ABUNDANCES IN ORGANIC-RICH MUD ROCKS: A GEOCHRONOLOGY, GEOCHEMISTRY, AND REDOX STUDY

An Abstract of a Dissertation

Presented to

the Faculty of the Department of Earth and Atmospheric Sciences

University of Houston

In Partial Fulfillment

of the Requirements for the Degree

Doctor of Philosophy

By

Shawn Curtis Wright

August 2015

ABSTRACT

This study demonstrates the utility of the Re-Os isotopic system by providing two precise, absolute ages for Permian sedimentary strata and by performing high-resolution chemostratigraphy across the globally-correlated oceanic anoxic event 2 (OAE2). In addition, the majority of Re-Os studies published to date are based on the organophilic behavior of Re and Os, however, there is not presently a thorough understanding of where in the organic matter Re and Os are complexed. In order to begin to provide an understanding of the location of these elements, measurement of Re and Os isotopes in organic (bitumen, kerogen, and oil) and inorganic (pyrite) phases from the Eagle Ford Shale was performed.

Absolute ages and calculated initial $^{187}Os/^{188}Os$ ratios of 264.3 ± 7.5 Ma ($^{187}Os/^{188}Os_i$ = 0.46 ± 0.09) for the Permian Brushy Canyon Fm. from the Delaware Basin, west Texas, and 298.0 ± 2.3 Ma ($^{187}Os/^{188}Os_i$ = 0.56 ± 0.02) for the Permian Tasmanite Shale provide some insight into the Os isotopic composition of their respective basins at the time of sediment deposition ($^{187}Os/^{188}Os_i$). These data coupled with a previously published compilation of $(^{187}Os/^{188}Os)_i$ values provide a first order examination of the Paleozoic seawater $^{187}Os/^{188}Os$ record.

High-resolution chemostratigraphy across OAE2 in the Eagle Ford Shale demonstrates an abrupt negative excursion in $(^{187}Os/^{188}Os)_i$ values ~340 kyr prior to OAE2. This represents a drastic shift in the $^{187}Os/^{188}Os$ of seawater during this anoxic period, likely due to the eruption of basaltic magma during the formation of a large igneous province.

This negative excursion, followed ~340 kyr later by a marked enrichment in Pt and Ir within highly oxic bottom-waters demonstrate the variable behavior of these elements in the water column. The variable enrichment of Os and Pt-Ir before and during OAE2 was ultimately caused by changes in insolation controlled by Milankovitch cycles.

Re and Os abundances in the various organic and inorganic fractions demonstrate that these elements predominantly reside in the kerogen, with only minor amounts in the bitumen and pyrite. However, these elements could be sequestered into micro-inorganic phases that are tightly held within the kerogen and not thoroughly removed during kerogen isolation.

TABLE OF CONTENTS

CHAPTER 2:

RHENIUM-OSMIUM GEOCHRONOLOGY AND GEOCHEMISTRY OF THE TASMANITE OIL SHALE, TASMANIA: PERMIAN TIME-SCALE CALIBRATION AND THE CONSTRUCTION OF THE PALEOZOIC SEAWATER $^{187}Os/^{188}Os$ CURVE.

CHAPTER 3:

RHENIUM-OSMIUM ISOTOPES AND PLATINUM AND IRIDIUM ABUNDANCES ACROSS THE OCEANIC ANOXIC EVENT 2: SOURCE AND ENRICHMENT MECHANISMS

CHAPTER 4:

RHENIUM AND OSMIUM ISOTOPES IN ORGANIC CONSTITUENTS, PYRITE, AND BULK-ROCKS FROM THE EAGLE FORD SHALE: CONSTRUCTING AN INTERNAL ISOCHRON

DISSERTATION INTRODUCTION

The discovery of the long-lived nature of ^{187}Re by Naldrett and Libby (1948) and the subsequent development of the Re-Os geochronometer provided an important tool for the geosciences, particularly in geochronology and isotopic studies. Following a period of hampered application due to analytical difficulties and the precise determination of the ^{187}Re decay constant (Herr et al., 1954; Hirt et al., 1963; Luck and Allegre, 1983, Lindner et al., 1989; Smoliar et al., 1996), the ^{187}Re-^{187}Os isotopic system is now routinely used for determining the crystallization ages of early solar system materials (Luck et al., 1980; Luck and Allegre, 1983; Horan et al., 1992; Morgan et al., 1992; Brandon et al., 1999), in understanding sulfide ore genesis (Hirt et al., 1963; Luck and Allegre, 1982; Foster et al., 1996; Markey et al,. 1996; Selby et al,. 2002) and mantle evolution and crustal growth (Morgan, 1986; Herzberg, 1993; Walker et al. 1994; Pearson et al., 1995; Pearson et al., 1998) among other applications.

Rhenium and Os are highly siderophile and chalcophile elements (Hart and Ravizza, 1996; Burton et al., 1999; Pearson et al., 2004; Fonseca et al., 2007), meaning that they are preferentially partitioned into metallic and sulphide phases in solid-melt systems. The mechanism that makes the Re-Os system useful for geochemistry is the difference in compatibility of Re and Os. During mantle melting, Re and Os behave incompatible, and moderately compatible, respectively (Walker et al., 1989). Therefore, during mantle melting, the bulk of mantle Re is partitioned into the melt and is subsequently enriched in the Earth's crust. Osmium, however, remains in mantle phases (most commonly in sulfides) and is depleted in the Earth's crust with respect to Re. This results in upper-

mantle sources having low Re/Os ratios, while crustal sources have an average Re/Os that is much higher than mantle sources. Because of a crustal enrichment in Re, the isotopic decay of ^{187}Re to ^{187}Os produces an increasing crustal enrichment in ^{187}Os with an increase in the age of crustal sources. Therefore, older crustal rocks have ^{187}Os/^{188}Os ratios that are much higher than the ^{187}Os/^{188}Os of younger rocks, and much, much higher than that of the mantle (^{187}Os/^{188}Os = 0.127).

It was recently discovered that during anoxic, reducing conditions, Re and Os are both organophilic, and thus have an affinity for organic complexes (Crusius et al., 1996). This becomes useful, as it is suggested that in sedimentary systems, more specifically, marine and lacustrine basins, these elements become sequestered by pelagic organisms within the water column. It is not presently known whether this is an adsorption process, or if these elements are complexed within the organic molecules that make up the organic matter (Miller, 2004). However, after deposition on the basin floor, the organic matter preserves the Re and Os isotopic signatures of seawater. This results in a relatively high abundance of both elements in organic-rich mud rocks (ORM) (hundreds of ppt to hundreds of ppb). Over time, the basin floor preserves a vertical sequence of changing seawater chemistry. This in turn provides constraints on the seawater chemistry at the time of deposition, and is controlled by processes such as climate, weathering rates, and tectonics (Esser and Turekian, 1988; Pegram et al., 1992; Peucker-Ehrenbrink et al., 1995; Oxburgh, 1998; Burton et al., 2010).

The utility of the Re-Os isotopic system has increased substantially in the past twenty years, mostly due to the development and implementation of higher-precision analytical

techniques and instrumentation and the associated ability to analyze very small quantities of sample (< 1 ppb Re; < 50ppt Os) with precision (Shirey and Walker, 1995; Volkening et al., 1991). From its initial use in the geosciences in the sub-disciplines of cosmochemistry and other high-temperature geochemistry, the Re-Os system has now evolved as a useful tool in ocean sciences and low temperature geochemistry. It has become particularly useful in sedimentary geochemistry and geochronology of ORM (Ravizza and Turekian, 1989; Selby and Creaser, 2003; Cohen et al., 2004; Hannah et al., 2004; Kendall et al., 2004; Kendall et al., 2009; Finlay et al., 2010; Rooney et al., 2012; Cumming et al., 2012).

Organic-rich mud rocks contain Re and Os abundances of parts-per-billion (ppb) and parts-per-trillion (ppt) quantities, respectively, and are enriched in these elements by orders of magnitude when compared to other crustal rocks (Horan et al., 1994). ^{187}Re decays to ^{187}Os with a half-life of 41.6 billion years, and provided that (1) sufficient fractionation between Re and Os occurs to produce a wide range in the measured $^{187}Re/^{188}Os$ and $^{187}Os/^{188}Os$ ratios, and (2) there is no post-depositional mobilization of Re or Os, then it is possible to use this system to determine an age for the deposition of ORM.

The Re-Os system was first applied to ORM by Ravizza and Turekian (1989) on the Mississippian/Devonian Bakken Shale in northern USA using a now-outdated, nickel-sulfide fire-assay procedure. This study achieved a source rock age of 354 ± 49 Ma (± 13.8%, 2σ) which is in agreement with the accepted age of the Bakken (~360Ma) (LeFever et al., 1991). Following this work, Cohen et al. (1999) implemented the use of

high-temperature Carius-tube digestion (Shirey and Walker, 1995) using inverse *aqua-regia* (1:3 HCl and HNO_3) for ORM dissolution. The use of Carius tubes and this highly reactive reagent provides a means for more-efficient sample dissolution and more-complete sample/spike equilibration (Shirey and Walker, 1995). Cohen et al. (1999) reported ages on Hettangian, Toarcian, and Kimmeridgian units in England of 207 ± 12Ma, 181 ± 13 Ma, and 155 ± 4.3 Ma (2σ), respectively, which are all indistinguishable from their accepted ages. The uncertainties in the isochrons in this study (average ± 5.2%, 2σ) provided a much-more-precise age determination than previous methods.

The past decade has seen key advances in sample selection and chemical extraction techniques which have subsequently led to a reduction in the uncertainties in shale Re-Os isochrons. Perhaps the largest step forward in these studies is the implementation of Jones Reagent ($Cr^{VI}O_3$ in H_2SO_4) as the digestion reagent (Selby and Creaser, 2003). It has been shown that dissolving ORM samples using inverse *aqua regia* accesses both the hydrogenous (derived from sea-water), and the non-hydrogenous (detrital material) component of whole-rock ORM (Selby and Creaser, 2003). However, Re-Os studies in ORM are only concerned with the hydrogenous component (Re-Os complexed with sulphides and organic carbon), any non-hydrogenous Re and Os that are dissolved during digestion result in isochrons with higher uncertainties. This is because non-hydrogenous, or detrital, Re and Os has no age correlation with hydrogenous Re and Os, as this material is likely of different and varying ages, and have different $^{187}Os/^{188}Os$ compositions at the time of deposition. Selby and Creaser (2003) pioneered the application of the Jones Reagent dissolution, and reported an age of 363.4 ± 5.6 Ma

(±1.5%, 2σ) for a black shale unit of the Exshaw Formation, Canada. This same unit, digested with inverse *aqua regia* resulted in a less precise age of 358 ± 10 Ma (±2.8%, 2σ). Selby and Creaser (2003) concluded that Jones Reagent, an organic oxidizer, only accesses the hydrogenous Re and Os of ORM, and in this study, produced an uncertainty which is significantly better than any previous used method. Currently, with careful sample selection, sample preparation, and digestion using Jones Reagent, uncertainties of ~1% (2σ) are achievable for ORM.

Temporal changes in local and global seawater geochemistry have been preserved in the rock record and recovered using predominantly O, C, and Sr isotopes. More recently, Os has also become a useful isotopic tracer that has begun to be applied to understanding the evolution of seawater during different time intervals. The Os isotopic composition of ORM reflects the $^{187}Os/^{188}Os$ composition of seawater at the time their respective sediments were deposited [$(^{187}Os/^{188}Os)_i$]. Rhenium and Os are redox-sensitive and organophilic in nature, and are suggested to be sequestered by organisms at, or below the sediment-water interface in both marine and lacustrine basins under suboxic, anoxic or euxinic conditions and are thus hydrogenous in nature (Koide, 1991; Colodner et al., 1993; Crusius et al., 1996; Morford et al., 2009; Cumming et al., 2012). Studies of seawater evolution using $^{87}Sr/^{86}Sr$ isotopes are hindered by the long residence time of Sr in seawater (1 – 4 Myr) resulting in smaller variation in the isotopic range compared to Os. Because of this, small temporal variations in seawater average out, or are muted and potentially miss influences on seawater chemistry on shorter timescales. The residence time of Os in seawater is ~10 – 50 kyr. (Peucker-Ehrenbrink and Ravizza, 2000).

Because of this, high-frequency isotopic changes, on the order of tens to hundreds of thousands of years, in seawater chemistry (such as orbitally forced, glacial-interglacial cycles) are potentially resolvable with Os isotopes. Rhenium and Os in ORM are being used more frequently in geochronology for providing depositional ages and for understanding potentially small chemical changes in the temporal evolution of seawater on shorter timescales which aren't captured by Sr isotopes (Ravizza and Turekian, 1989; Oxburgh, 1998; Cohen et al., 1999; Peucker-Ehrenbrink and Ravizza, 2000; Creaser et al., 2002; Selby and Creaser, 2003; Hannah et al., 2004; Kendall et al., 2004; Finlay et al., 2010; Rooney et al., 2010). The $^{187}Os/^{188}Os$ of seawater is derived from a balance of two primary inputs: (1) Radiogenic Os from river water during weathering and subsequent continental runoff of upper continental crust (Esser and Turekian, 1993; Peucker-Ehrenbrink and Jahn, 2001), and (2) non-radiogenic Os from the mantle via seafloor spreading and production of mid-ocean ridge basalts, flood basalt events, hydrothermal alteration of oceanic crust and from meteorite influx (Peucker-Ehrenbrink and Ravizza, 2000; Schmitz et al., 2004). The relative contributions of these sources have varied significantly throughout geologic history leading to significant variations in the $^{187}Os/^{188}Os$ of seawater. The evolution of the $^{187}Os/^{188}Os$ of seawater over the Earth's history can be reconstructed by measuring the $^{187}Os/^{188}Os$ of ORM throughout the geologic past. From the $^{187}Os/^{188}Os$ of ORM at any given time of formation, a mass-balance calculation can be used to determine the relative contribution of radiogenic and non-radiogenic Os to seawater. Inferences can then be made about leverate to the Os seawater budget from the degree of continental weathering (Ravizza et al., 2001; Schmitz et al., 2004), seafloor spreading rates, the eruption of flood basalts (Ravizza and Peucker-

Ehrenbrink, 2003; Turgeon and Creaser, 2008) as well as the timing and influx of meteorite impacts (Paquay et al., 2008).

The use of the Re-Os isotopic system has even-more recently been expanded to other portions of the petroleum system including the timing of petroleum generation. These studies obtained Re-Os ages for crude oil that agree with their modeled generation age (Selby et al., 2005; Selby and Creaser, 2005; Finlay et al., 2011). Traditionally, the timing of hydrocarbon generation involves the construction of basin models using parameters that are often grossly estimated (Ruble et al., 2001). Therefore, determining the absolute age of petroleum generation provides vital information in understanding the petroleum system, including source-rock maturation and hydrocarbon generation. Furthermore, Os isotopes have been successfully used in the fingerprinting of oils for source rock identification (Finlay et al., 2012). Oil-to-source correlations are commonly performed using carbon isotopes or biomarkers, however, these methods are hindered by biodegradation, as they rely heavily on the light fractions of oil (Peters et al., 1999; Peters et al., 2005). Rhenium and Os are located almost exclusively in the heavy, asphaltene fraction of oil and therefore isn't limited by biodegradation (Selby et al., 2007). These preliminary studies provide a strong case that the Re-Os isotopic system, when applied to the petroleum system, could be a valuable tool in petroleum exploration.

The aim of the work presented here is to demonstrate and expand the utility of the Re-Os isotopic system in ORM. In addition, the coupled use of Re-Os and Pt-Ir is introduced as a powerful tool in redox studies. This dissertation is presented in the format of scientific papers with four main research chapters written as distinct papers. Due to selecting this

style for the dissertation, some repetition exists, particularly in the introduction and methodology sections of each paper.

REFERENCES

Brandon A.D., Norman M.D., Walker R.J. and Morgan J.W. (1999) ^{186}Os-^{187}Os systematics of Hawaiian picrites. *Earth and Planetary Science Letters* **174**, 25-42.

Burton K.W., Bourdon B., Birck J.-L., Allegre C.J. and Hein J.R. (1999) Osmium isotope variations in the oceans recorded by Fe-Mn crusts. *Earth and Planetary Science Letters* **171**, 185-197.

Burton K.W., Gannoun A. and Parkinson I.J. (2010) Climate driven glacial-interglacial variations in the osmium isotope composition of seawater recorded by planktic foraminifera. *Earth and Planetary Science Letters* **295**, 58-68.

Cohen A.S., Coe A.L. Bartlett J.M. and Hawksworth C.J. (1999) Precise Re-Os ages of organic-rich mudrocks and the Os isotope composition of Jurassic seawater. *Earth and Planetary Science Letters* **167**, 159-173.

Cohen A.S. (2004) The rhenium-osmium isotope system: applications to geochronological and palaeoenvironmental problems. *Journal of the Geological Society of London* **161**, 729-734.

Colodner D., Sachs J., Ravizza G., Turekian K.K., Edmond J. and Boyle E. (1993) The geochemical cycles of rhenium: A reconnaissance. *Earth and Planetary Science Letters* **117**, 205-221.

Creaser R.A., Sannigrahi P., Chacko T. and Selby D. (2002) Further evaluation of the Re-Os geochronometer in organic-rich sedimentary rocks: A test of hydrocarbon maturation effects in the Exshaw Formation, Western Canada Sedimentary Basin. *Geochimica et Cosmochimica Acta* **66**, 3441-3452.

Crusius J., Calvert S., Pedersen T. and Sage D. (1996) Rhenium and molybdenum enrichments in sediments as indicator of oxic, suboxic and sulfidic conditions of deposition. *Earth and Planetary Science Letters* **145**, 65-78.

Cumming V.M., Selby D. and Lillis P.G. (2012) Re-Os geochronology of the lacustrine Green River Formation: Insights into direct depositional dating of lacustrine successions, Re-Os systematics and paleocontinental weathering. *Earth and Planetary Science Letters* **359-360**, 194-205.

Esser B.K. & Turekian K.K. (1988) Accretion rate of extraterrestrial particles determined from osmium isotope systematics of Pacific pelagic clay and manganese nodules. *Geochimica et Cosmochimica Acta* **52**, 1383-1388.

Esser B.K. and Turekian K.K. (1993) The osmium isotopic compositions of the continental crust. *Geochimica et Cosmochimica Acta* **57**, 3093-3104.

Finlay A.J., Selby D. and Grocke D.R. (2010) Tracking the Hirnantian glaciations using Os isotopes. *Earth and Planetary Science Letters* **293**, 339-348.

Finlay A.J., Selby D. and Osborne M.J. (2011) Re-Os geochronology and fingerprinting of United Kingdom Atlantic margin oil: Temporal implications for regional petroleum systems. *Geology* **39**, 475-478.

Finlay A.J., Selby D. and Osborne M.J. (2012) Petroleum source rock identification of United Kingdom Atlantic Margin oil fields and the Western Canadian Oil Sands using platinum, palladium, osmium and rhenium: Implications for global petroleum systems. *Earth and Planetary Science Letters* **313-314**, 95-104.

Fonseca R.O.C., Mallmann G., St.C.O'Neill H. and Campbell I.H. (2007) How chalcophile is rhenium? An experimental study of the solubility of Re in sulphide mattes. *Earth and Planetary Science Letters* **260**, 537-548.

Foster J.G., Lambert D.D., Frick L.R. and Maas R. (1996) Re-Os isotope evidence for genesis of archaean nickel ores from uncontaminated komatiites. *Nature* **382**, 703-706.

Hannah J.L., Bekker A., Stein H.J., Markey R.J. and Holland H.D. (2004) Primitive Os and 2316 Ma age for marine shale: Implications for Paleoproterozoic glacial events and the rise of atmospheric oxygen. *Earth and Planetary Science Letters* **225**, 43-52.

Hart S.R. & Ravizza G. (1996) Os partitioning between phases in lherzolite and basalt in earth processes: reading the isotopic code. *AGU Geophysical Monograph.*

Herr W., Hintenberger H. and Voshage H. (1954) Half-life of rhenium. *Physics Review* **95**, 1691.

Herzberg C.T. (1993) Lithosphere peridotites of the Kaapvaal Craton. *Earth and Planetary Science Letters* **120**, 13-29.

Hirt B., Tilton G.R., Herr W. and Hoffmeister W. (1963) The half-life of ^{187}Re. In: Geiss J. and Goldberg E. (Eds.), *Earth Science and Meteroritics,* North Holland, Amsterdam.

Horan M.F., Morgan J.W., Walker R.J. and Grossman J.N. (1992) Rhenium-osmium isotope constraints on the age of iron-meteorites. *Science* **255**, 1118-1121.

Horan M.F., Morgan J.W., Grauch R.I., Coveney Jr. R.M., Murowchick J.B. and Hulbert L.J. (1994) Rhenium and osmium isotopes in black shales and Ni-Mo-PGE-rich sulfide layers, Yukon Territory, Canada, and Hunan and Guizhou provinces, China. *Geochimica et Cosmochimica Acta* **58**, 257-265.

Kendall B.S., Creaser R.A., Ross G.M. and Selby D. (2004) Constraints on the timing of Marinoan 'Snowball Earth' glaciations by ^{187}Re-^{187}Os dating of a Neoproterozoic post-glacial black shale in Western Canada. *Earth and Planetary Science Letters* **222,** 729-470.

Kendall B.S., Creaser R.A. and Selby D. (2009) ^{187}Re-^{187}Os geochronology of Precambrian organic-rich sedimentary rocks. *Geological Society of London Special Publications* **326**, 85-107.

Koide M., Goldberg E.D., Niemeyer S., Gerlach D., Hodge V., Bertine K.K. and Padova A. (1991) Osmium in marine sediments. *Geochimica et Cosmochimica Acta* **55**, 1641-1648.

LeFever J.A., Martiniuk C.D., Dancsok E.F.R. and Mahnic P.A. (1991) Petroleum potential of the middle member of the Bakken Formation, Williston Basin. In: Christopher J.E. and Haidl F.M. (Eds.), *6th International Williston Basin symposium*. Saskatchewan Geological Society Special Publication **11**, 74-94.

Lindner M., Leich D.A., Russ G.P., Bazan J.M. and Borg R.J. (1989) Direct determination of the half-life of ^{187}Re. *Geochimica et Cosmochimica Acta* **53**, 1597-1606.

Luck J.M. and Allegre C.J. (1982) The study of molybdenites through the ^{187}Re-^{187}Os chronometer. *Earth and Planetary Science Letters* **61**, 291-296.

Luck J.M. and Allegre C.J. (1983) ^{187}Re-^{187}Os systematics in meteorites and cosmochemical consequences. *Nature* **302**, 130-132.

Luck J.M., Birck J.L. and Allegre C.J. (1980) ^{187}Re-^{187}Os systematics in meteorites: early chronology of the solar system and age of the galaxy. *Nature* **283**, 256-259.

Markey R., Stein H. and Morgan J. (1996) Highly precise Re-Os dating for molybdenite using

Miller C.A. (2004) Re-Os dating of algal laminites: reduction-enrichment of metals in the sedimentary environment and evidence for new geoporphyrins. MSc Thesis, University of Saskatchewan, Saskatoon, Canada.

Morford J.L., Martin W.R., Francois R. and Carney C.M. (2009) A model for uranium, rhenium, and molybdenum diagenesis in marine sediments based on results from coastal locations. *Geochimica et Cosmochimica Acta* **73**, 2938-2960.

Morgan J.W., Walker R.J. and Grossman J.N. (1992) Rhenium-osmium isotope systematics in meteorites 1. Magmatic iron meteorite group-IIab and group-IIIab. *Earth and Planetary Science Letters* **108**, 191-202.

Morgan J.W. (1986) Ultramafic xenoliths – clues to Earths le accretionary history. *Journal of Geophysical Research – Solid Earth and Planets* **91**, 2375-2384.

Naldrett S.N. and Libby W.F. (1948) Natural radioactivity of rhenium. *Physics Review* **73**, 487-493.

Oxburgh R. (1998) Variations in the osmium isotope composition of sea water over the past 200,000 years. *Earth and Planetary Science Letters* **159**, 183-191.

Pearson D.G., Carlson R.W., Shirey S.B., Boyd F.R. and Nixon P.H. (1995) Stabilization of archean lithospheric mantle – a Re-Os isotope study of peridotite xenoliths from the Kaapvaal Craton. *Earth and Planetary Science Letters* **134**, 341-357.

Pearson D.G., Shirey S.B., Harris J.W. and Carlson R.W. (1998) Sulphide inclusions in diamonds from the Koffiefontein kimberlite, S. Africa: constraints on diamond ages and mantle Re-Os systematics. *Earth and Planetary Science Letters* **160**, 311-326.

Pearson D.G., Irvine G.J., Ionov D.A., Boyd F.R. and Dreibus G.E. (2004) Re-Os isotope systematics and platinum group element fractionation during mantle melt extraction: a study of massif and xenoliths peridotite suites. *Chemical Geology* **208**, 29-59.

Pegram W.J., Krishnaswami S., Ravizza G.E. and Turekian K.K. (1992) The record of sea water $^{187}Os/^{186}Os$ variation through the Cenozoic. *Earth and Planetary Science Letters* **113**, 569-576.

Peters K.E, Fraser T.H., Amris W., Rustanto B. and Hermanto E. (1999) Geochemistry of crude oils from eastern Indonesia. *AAPG Bulletin* **83**, 1924-1927.

Peters K.E., Walters C.C. and Moldowan J.M. (2005) The Biomarker Guide Volume 1: Biomarkers and Isotopes in the Environment and Human History, Cambridge University Press.

Peucker-Ehrenbrink B. and Jahn B.-M. (2001) Rhenium-osmium isotope systematics and platinum group element concentrations: Loess and the upper continental crust. *Geochemistry Geophysics Geosystems* **2**, 1-22.

Peucker-Ehrenbrink B. and Ravizza G. (2000) The marine osmium isotope record. *Terra Nova* **12**, 205-219.

Peucker-Ehrinbrink B., Ravizza G. and Hoffmann A.W. (1995) The marine $^{187}Os/^{188}Os$ record of the past 80 million years. *Earth and Planetary Science Letters* **130**, 155-176.

Ravizza G. and Turekian K.K. (1989) Applications of the ^{187}Re-^{187}Os system to black shale geochronometry. *Geochimica et Cosmochimica Acta* **53**, 3257-3262.

Ravizza G., Turekian K.K. and Hay B.J. (2001) The geochemistry of rhenium and osmium in recent sediments from the Black Sea. *Geochimica et Cosmochimica Acta* **55**, 3741-3752.

Rooney A.D., Selby D., Houzay J.-P. and Renne P.R. (2010) Re-Os geochronology of a Mesoproterozoic sedimentary succession, Taoudeni Basin, Mauritania: Implications for basin-wide correlations and Re-Os organic-rich sediments systematics. *Earth and Planetary Science Letters* **289**, 486-496.

Rooney A.D., Chew D.M. & Selby D. (2011) Re-Os geochronology of the Neoproterozoic-Cambrian Dalradian Supergroup of Scotland and Ireland: Implications for Neoproterozoic stratigraphy, glaciations and Re-Os systematics. *Precambrian Research* **185**, 202-214.

Rooney A.D., Selby D., Lewan M.D., Lillis P.G. and Houzay J.-P. (2012) Evaluating Re-Os systematics in organic-rich sedimentary rocks in response to petroleum generation using hydrous pyrolysis experiments. *Geochimica et Cosmochimica Acta* **77**, 275-291.

Ruble T.E., Lewan M.D. and Philp R.P. (2001) New insights on the Green River petroleum system in the Uinta basin from hydrous-pyrolysis experiments. *AAPG Bulletin* **85**, 1333-1371.

Schmitz B., Peucker-Ehrenbrink B., Heilmann-Clausen C., Aberg G., Asaro F. and Lee C.A. (2004) Basaltic explosive volcanism, but no comet impact, at the Paleocene-Eocene boundary: High-resolution chemical and isotopic records from Egypt, Spain and Denmark. *Earth and Planetary Science Letters* **225**, 1-17.

Selby D. and Creaser R.A. (2003) Re-Os geochronology of organic rich sediments: An evaluation of organic matter analysis methods. *Chemical Geology* **200**, 225-240.

Selby D. and Creaser R.A. (2005) Direct radiometric dating of hydrocarbon deposits using rhenium-osmium isotopes. *Science* **308**, 1293-1295.

Selby D., Creaser R.A., Hart C.J.R., Rombach C.S., Thompson J.F.H. Smith M.T., Bakke A.A. and Goldfarb R.J. (2002) Absolute timing of sulfide and gold mineralization: a comparison of Re-Os molybdenite and Ar-Ar mica methods from the Tintina Gold Belt, Alaska. *Geology* **30**, 791-794.

Selby D., Creaser R.A., Dewing K. and Fowler M. (2005) Evaluation of bitumen as a ^{187}Re-^{187}Os geochronometer for hydrocarbon maturation and migration: A test case from the Polaris MVT deposits, Canada. *Earth and Planetary Science Letters* **235**, 1-15.

Selby D., Creaser R.A. and Fowler M.G. (2007) Re-Os elemental and isotope systematics in crude oils. *Geochimica et Cosmochimica Acta* **71**, 378-386.

Shirey S.B. & Walker R.J. (1995) Carius Tube Digestion for Low-Blank Rhenium-Osmium Analysis. *Analytical Chemistry* **67**, 2136-2141.

Smoliar M.I., Walker R.J. and Morgan J.W. (1996) Re-Os isotope constraints on the age of Group IIA, IIIA, IVA, and IVB iron meteorites. *Science* **271**, 1099-1102.

Turgeon S.C. and Creaser R.A. (2008) Cretaceous oceanic anoxic event 2 triggered by a massive magmatic episode. *Nature Letters* **454**, 323-326.

Volkening J., Walczyk T. and Heumann K.G. (1991) Osmium isotope ratio determinations by negative thermal ionization mass spectrometry. *International Journal of Mass Spectrometry and Ion Processes* **105**, 147-159.

Walker R.J., Morgan J.W., Horan M.F., Czamanske G.K., Krogstad E.J., Fedorenko V.A. and Kunilov V.W. (1994) Re-Os isotope evidence for an enriched-mantle source for the Norilsk-type ore-bearing intrusions, Siberia. *Geochimica et Cosmochimica Acta* **58**, 4179-4197.

Walker R.J., Carlson R.W., Shirey S.B. and Boyd F.R. (1989) Os, Sr, Nd, and Pb isotope systematics of southern Africa peridotite xenoliths: Implications for the chemical evolution of subcontinental mantle. *Geochimica et Cosmochimica Acta* **53**, 1583-1595.

CHAPTER 1:

RHENIUM-OSMIUM GEOCHRONOLOGY AND GEOCHEMISTRY OF THE PERMIAN BRUSHY CANYON FORMATION: INSIGHT INTO THE EVOLUTION OF PERMIAN SEAWATER.

1.1. INTRODUCTION

The Permian strata of the Delaware Basin of West Texas potentially record geochemical evidence of significant geologic and paleo-climatic changes that occurred during the Permian Period (Figure 1.1). The Early Permian (Sakmarian; 295.0 – 290.1 Ma) was marked by significant reduction in the glaciers covering large parts of Gondwana during the Permo-Carboniferous glaciation (Schwarzbach, 1974; Frakes et al., 1992). Simultaneously, a drastic change in global climate from predominantly humid conditions during the Asselian (298.9 – 295.0 Ma) and Early Sakmarian to a dominantly dry climate during the Artinskian (290.1 – 283.5 Ma) and Kungurian (283.5 – 272.3 Ma) occurred, which persisted throughout much of the Late Permian (Kozur, 1984) with more humid conditions returning by only the latest Permian (Korte et al., 2006). In addition, opening of the Neotethys occurred during the Sakmarian and continued into the Middle Permian with a markedly increased spreading rate during the Guadalupian (Stampfli, 2000; Stampfli et al., 2001). Evidence for this is preserved by widespread Guadalupian Neotethyan pillow basalts overlain by Wordian-Capitanian radiolarites and pelagic limestones in Oman (Bechennec, 1988; Blendinger, 1988; Pillevuit et al., 1997). Coincident with cessation of Neotethys spreading during the Guadalupian was the diminishing of spreading in the Paleo-tethys, with spreading having stopped altogether by the Lopingian (260 – 251 Ma) (Bagheri et al., 2003).

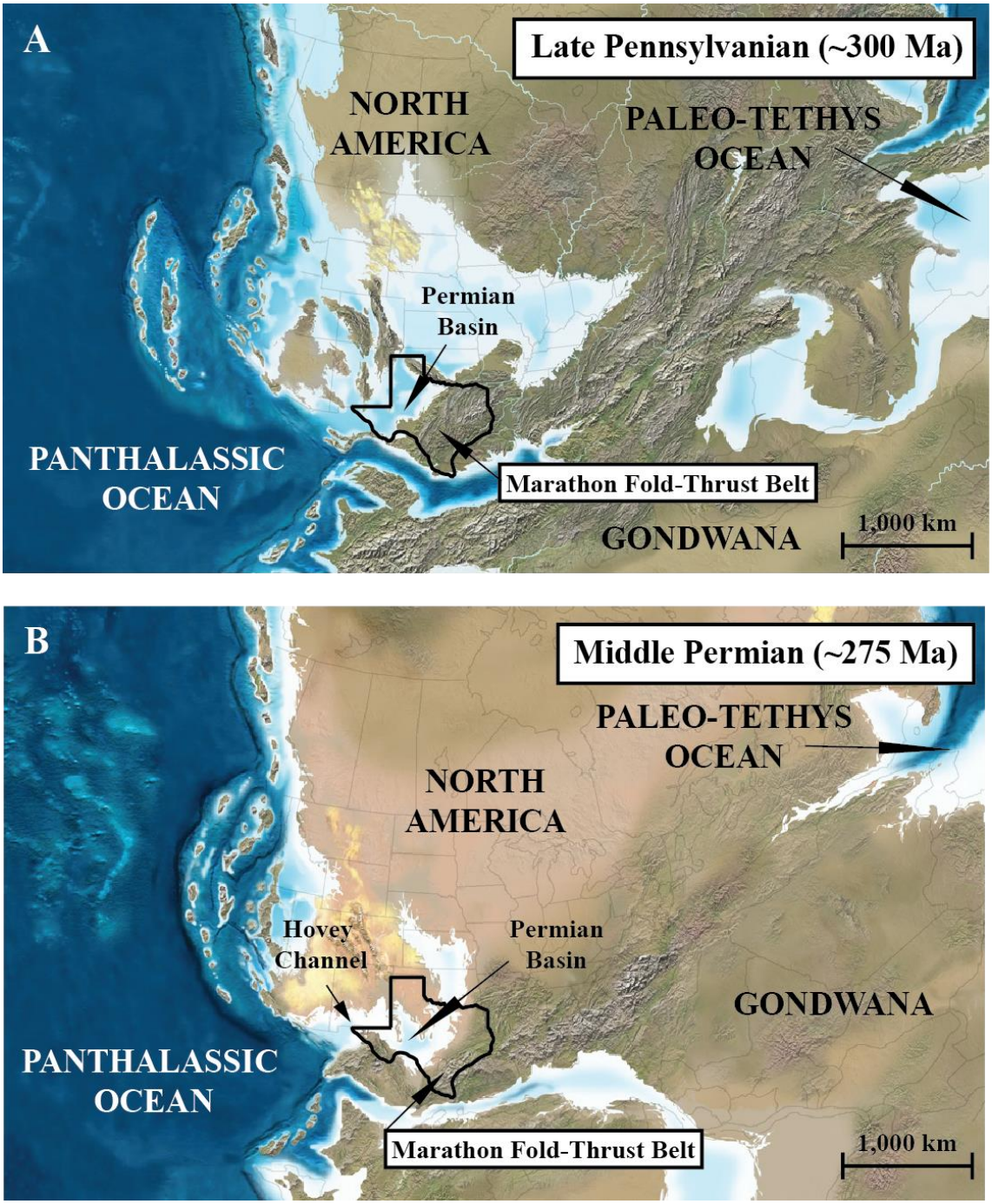

Figure 1.1. Paleoreconstruction of the southern Laurentian margin during the (A) Late Pennsylvanian, and (B) Middle Permian. Texas is outlined in black, with the location of the Permian Basin highlighted in each. Modified from Ron Blakey and Colorado Plateau Geosystems, Inc.

Locally, rapid sedimentation during the Early Permian caused rapid basin subsidence, which in turn caused enormous compressional stresses in the underlying crustal rocks resulting in uplift of the fault-block separating the Delaware Basin from the Midland Basin to the east. In addition, the Diablo Arch to the west was also significantly uplifted (Adams, 1965). During the Permian, the Delaware Basin was just north of the equator (Ziegler et al., 1997), within an arid climate zone, inferred from the presence of aeolian siliciclastics preserved throughout the region (King, 1948; Oriel et al., 1967; Fischer and Sarnthein, 1988; Soreghan and Soreghan, 2013).

Temporal changes in local and global seawater geochemistry have been preserved in the rock record and recovered using predominantly O, C, and Sr isotopes. Because of recent advances in analytical geochemistry, the ^{187}Re-^{187}Os isotopic system ($t_{1/2}$ = 41.6 by; Smoliar et al., 1996) has also become a useful geochronometer and isotopic tracer that has begun to be applied to understanding the evolution of seawater during different time intervals. The Os isotopic composition of organic-rich mud rocks (ORM) reflects the $^{187}Os/^{188}Os$ composition of seawater at the time their respective sediments were deposited. Rhenium and Os are redox-sensitive and organophilic in nature, and are suggested to be sequestered by organisms at, or below the sediment-water interface in both marine and lacustrine basins under suboxic, anoxic, or euxinic conditions and are thus hydrogenous in nature (Koide, 1991; Colodner et al., 1993; Crusius et al., 1996; Morford et al., 2009; Cumming et al., 2012). Studies of seawater evolution using $^{87}Sr/^{86}Sr$ isotopes are hindered by the long residence time of Sr in seawater (1 – 4 Myr) resulting in smaller variation in the isotopic range compared to Os. Because of this, small temporal

variations in seawater are averaged out, or are muted, and potentially miss influences on seawater chemistry on shorter timescales. The residence time of Os in seawater is ~10 – 50 kyr (Peucker-Ehrenbrink and Ravizza, 2000). Because of this, high-frequency isotopic changes, on the order of tens to hundreds of thousands of years, in seawater chemistry (such as orbitally forced, glacial-interglacial cycles) are potentially resolvable with Os isotopes. Rhenium and Os in ORM are being used more frequently in geochronology for providing depositional ages and for understanding potentially small chemical changes in the temporal evolution of seawater on shorter timescales which aren't captured by Sr isotopes (Ravizza and Turekian, 1989; Oxburgh, 1998; Cohen et al., 1999; Peucker-Ehrenbrink and Ravizza, 2000; Creaser et al., 2002; Selby and Creaser, 2003; Hannah et al., 2004; Kendall et al., 2004; Finlay et al., 2010; Rooney et al., 2010). The $^{187}Os/^{188}Os$ of seawater is derived from a balance of two primary inputs: (1) Radiogenic Os from river water during weathering and subsequent continental runoff of upper continental crust (Esser and Turekian, 1993; Peucker-Ehrenbrink and Jahn, 2001), and (2) non-radiogenic Os from the mantle via seafloor spreading and production of mid-ocean ridge basalts, flood basalt events, or hydrothermal alteration of oceanic crust or from meteorite influx (Peucker-Ehrenbrink and Ravizza, 2000; Schmitz et al., 2004). The relative contributions of these sources have varied significantly throughout geologic history leading to significant variations in the $^{187}Os/^{188}Os$ of coeval seawater. The evolution of the $^{187}Os/^{188}Os$ of seawater over the Earth's history can be reconstructed by measuring the $^{187}Os/^{188}Os$ of ORM throughout the geologic past. From the $^{187}Os/^{188}Os$ of ORM at any given time of formation, a mass-balance calculation can be used to determine the relative contribution of radiogenic and non-radiogenic Os to seawater. Inferences can

then be made about leverate to the Os seawater budget from the degree of continental weathering (Ravizza et al., 2001; Schmitz et al., 2004), seafloor spreading rates, the eruption of flood basalts (Ravizza and Peucker-Ehrenbrink, 2003; Turgeon and Creaser, 2008) as well as the timing and flux of meteorite impacts (Paquay et al., 2008).

Within this context, this study presents Re-Os geochronology and geochemical data for the Guadalupian Brushy Canyon Formation in order to provide its precise and accurate absolute age as well as understand the Os isotopic chemistry of seawater in the Delaware Basin during the Guadalupian. These data will help in understanding global ocean geochemistry during the Permian which can further lead to a better understanding of the global geologic processes that were occurring at that time.

1.2. GEOLOGIC SETTING

The Permian Basin of West Texas and southern New Mexico developed during the Early Pennsylvanian on the southern edge of Laurentia as a foreland basin as a result of cratonic depression associated with uplift of the Marathon Fold Belt during the assembly of Pangea (Hills, 1984; Beaubouef et al., 1999) (Figure 1.1). The greater Permian Basin is made up of several small sub-basins: the Midland Basin, the Marfa Basin, and the Delaware Basin. The western-most Delaware Basin formed during the Early Permian (Wolfcampian Epoch) and was the second-largest of the sub-basins, covering an area of over 26,000 km^2 of Laurentia, in what is now west Texas (King, 1948) (Figure 1.2). During the Middle Permian, the Delaware Basin was approximately 160 km in diameter and is estimated to have been 300 – 600 m deep and accommodated approximately 1,000 – 1,600 m of terrigenous silt, sand and mud of the Guadalupian Delaware Mountain

Group (King, 1948; Newell et al., 1953; Meissner, 1972; Harms, 1974; Harms and Williamson, 1988; Kerans et al., 1992) (Figure 1.2). Strata of the Delaware Mountain Group preserve a succession of slope and basin deposits in the Delaware Basin (Gardner, 1977) and are divided into the Brushy Canyon, Cherry Canyon, and Bell Canyon Formations, from oldest to youngest (Kerans et al., 1992) (Figure 1.3).

During the Guadalupian and throughout the majority of the Permian, the Delaware Basin was connected to the Panthalassa Ocean to the west by the Hovey Channel, a narrow inlet that supplied new seawater to the basin (King, 1948) (Figures 1.1 and 1.2). During eustatic sea level changes and subsidence rate fluctuations in the basin, the influx of seawater was sporadic throughout the final filling stages of the Delaware Basin during the Late Permian. Intermittent marine conditions existed in the Delaware Basin into the Ochoan until evaporate accumulation prompted progressive restriction from marine influence (King, 1948).

Variations in relative sea level within the Permian Basin during the Guadalupian are preserved in the Delaware Mountain Group by cyclic interbedded sandstone and organic-rich siltstone (Meissner, 1972; Fischer and Sarnthein, 1988; Gardner, 1992; Gardner, 1997a, b).

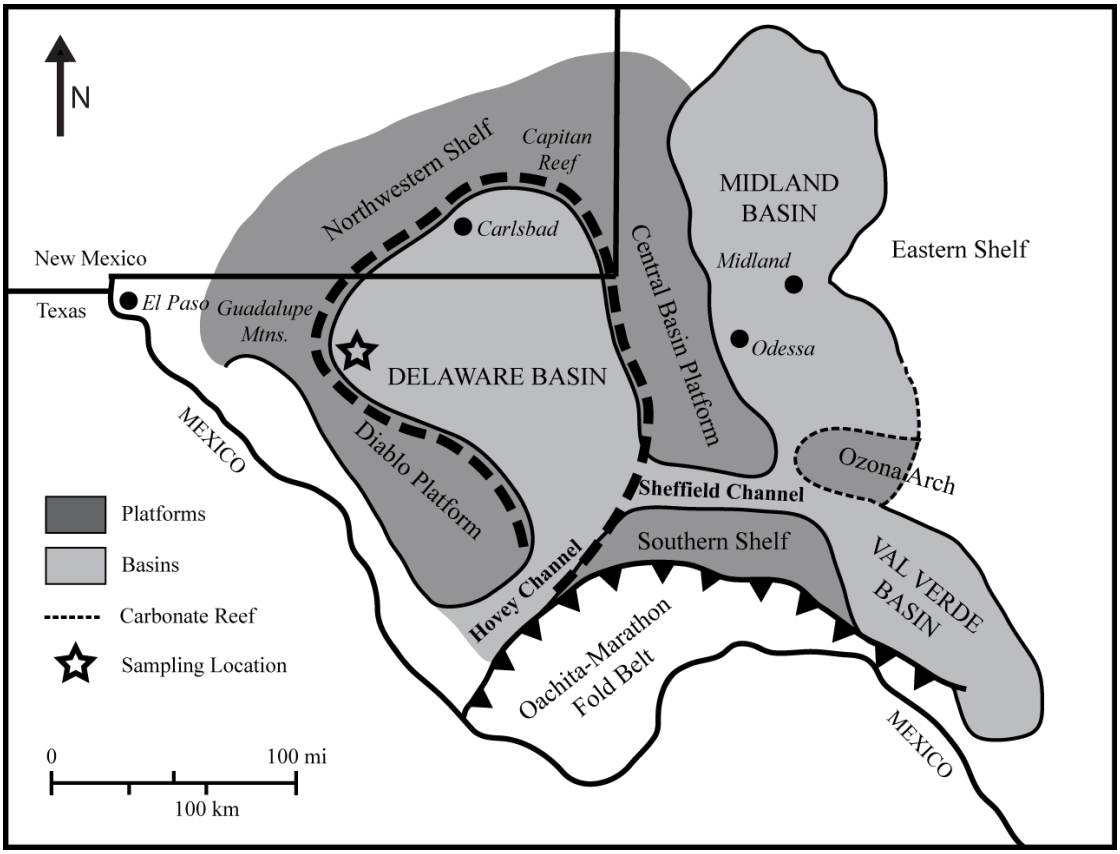

Figure 1.2. Present-day map of the Permian Basin, west Texas showing the locations of the three sub-basins that comprise the greater Permian Basin. The black star represents the location of both cores used in this study (DB-01 and DB-02). Modified after Comer (1991) and Harris et al. (2013).

During relative sea-level high-stands, widespread, organic-rich siltstones of varying thickness accumulated on the basin floor by the hemi-pelagic settling of marine algal material and detrital silt and mud through both aeolian and marine processes. Sands were restricted from entering the basin due to their entrapment behind a broad, flooded shelf and carbonate platform (Meissner, 1972; Dutton et al., 2003). During exposure of the carbonate shelf during subsequent sea-level low-stands, sands were transported to the shelf margin via aeolian dune progradation and fluvial processes (Fischer and Sarnthein, 1988) and were carried to the basin floor predominantly by turbidity currents and deposited as major submarine fan complexes (Newell et al., 1953; Payne, 1976; Berg, 1979; Gardner, 1992; Zelt and Rossen, 1995; Bouma, 1996; Beaubouef et al., 1999; Gardner and Borer, 2000; Dutton et al., 2003).

The Brushy Canyon Formation represents a major third-order low-stand wedge deposited in slope to basin environments over a 2 – 4 Myr duration during the Guadalupian (Kerans et al., 1993; Gardner and Sonnenfeld, 1996; Sageman et al., 1998; Gardner et al., 2003). It consists primarily of low-stand turbidite deposits with ubiquitous, widely traceable, <0.1 to >2 m thick, organic-rich siltstone marker beds (Gardner, 1992; Sageman et al., 1998). These beds are interpreted as high-stand, sediment-starved suspension deposits marking the basinward equivalent of marine flooding surfaces (Gardner and Sonnenfeld, 1996) and are proven source rocks for oil found in sandstone reservoirs within the Brushy Canyon Formation (Hays and Tieh, 1992).

The interbedded, organic-rich siltstones contain ~0.5% to ~3% total organic carbon (TOC) and a mixture of oxygen-rich Type II and Type III kerogen consistent with marine

algal input and downslope transport of terrestrial organic matter (Hays and Tieh, 1992; Sageman et al., 1998). The TOC increases during retrogradation, or depositional system back-stepping during sea-level transgressions and high-stands, and is negatively correlated with both grain size and abundance of Type III kerogen, indicated by higher hydrogen index (HI) associated with zones of higher TOC (Hays and Tieh, 1992). Conversely, HIs are lowest in organic carbon-poor regions of maximum low-stand, reflecting higher input of terrigenous organic matter, or oxidation of marine organic matter (Pratt, 1984). The frequency of organic-rich siltstones is also higher during relative high-stands of sea-level (Sageman et al., 1998). Biomarker evidence indicates that petroleum reservoirs within the Brushy Canyon Formation are sourced primarily by the Type II marine kerogen, with only traces of compounds specific to Type III kerogen (Hays and Tieh, 1992). The temperature of maximum hydrocarbon formation (T_{max}) was measured at 439 to 448°C during Rock-Eval pyrolysis, and thermal alteration index (TAI) values between 2.4 and 2.8 indicates the Brushy Canyon Formation has been thermally matured to depths associated with the oil generation window (Justman, 2001).

The formations of the Delaware Mountain Group in the Guadalupe Mountains are the Global Boundary Stratotype Section and Point (GSSP) for Guadalupian strata (Figure 1.3). The GSSP are based on the evolution of a single conodont genus, *Jinogondolella* first recognized by Girty (1908) in the Guadalupe Mountains, Texas. The GSSP for the Roadian, the basal stage of the Guadalupian, is marked by the first appearance of *Jinogondolella nankingensis* in a black, thin-bedded limestone in the

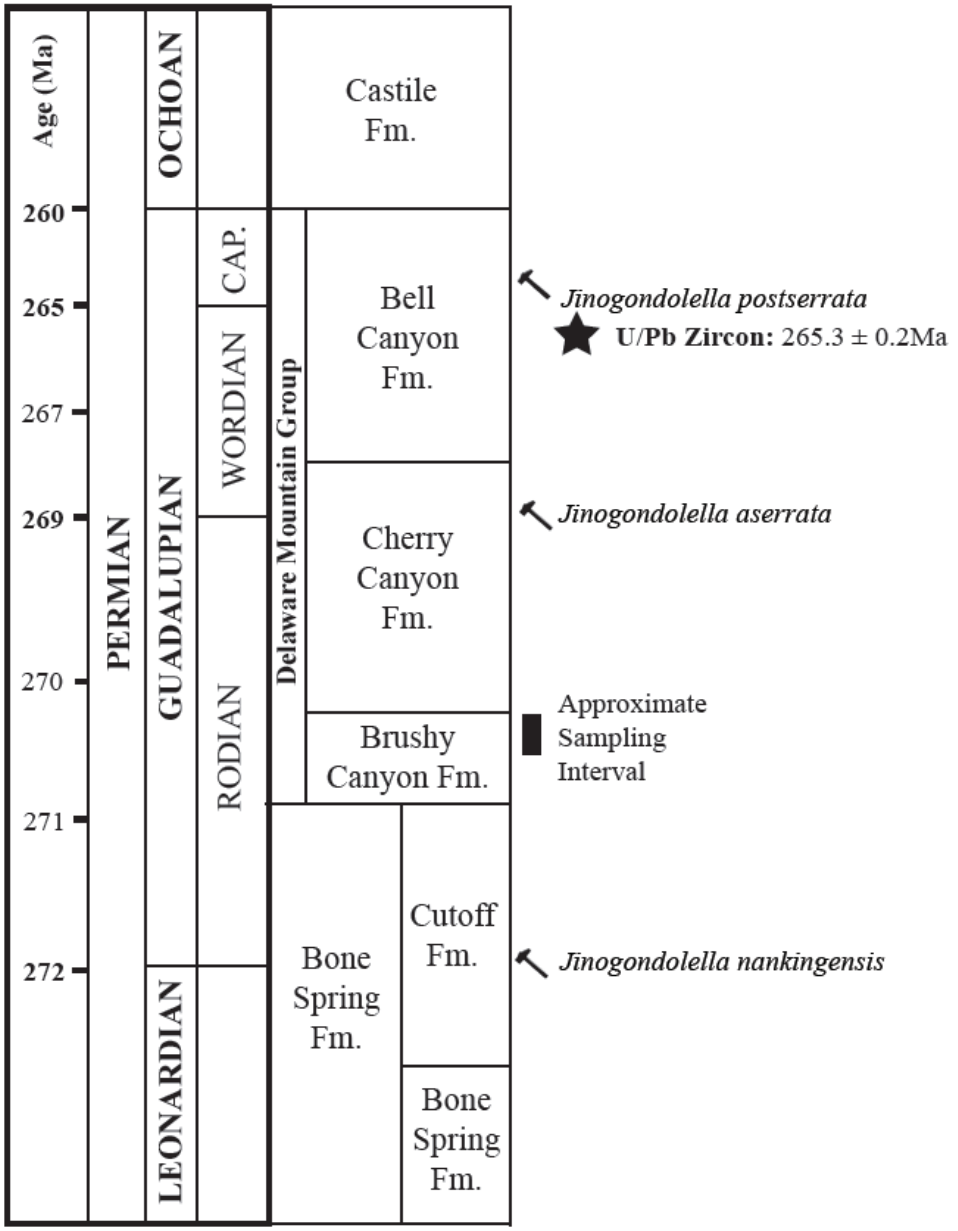

Figure 1.3: Generalized stratigraphic column of the Permian strata of the Delaware Basin after Dutton et al. (2003). Small black hammers represent GSSP described by Glenister et al. (1999) and further discussed in this paper. The U/Pb age (black star) is a zircon age from an interbedded tuff unit from Bowring et al. (1998). Ages on the left hand side are statistically calculated by Agterberg et al. (2012) based on the U/Pb age of Bowring et al. (1998). All samples used in this study were taken from a two foot, time-correlative interval, across the two cores, shown by the black rectangle.

Cutoff Formation, which lies just below the Delaware Mountain Group (Glenister et al., 1999; Mei and Henderson, 2002). The GSSP for the beginning of the Wordian is marked by the first appearance of *Jinogondolella aserrata* in a skeletal carbonate mudstone just below the top of the Cherry Canyon Formation (Glenister et al., 1999). The marker horizon for the Capitanian Stage is the first evolutionary appearance of the *Jinogondolella postserrata* within the upper Piney Limestone member of the Bell Canyon Formation (Glenister et al., 1999). The top of the Permian is marked by a global regression of sea level with very few complete, continuous sections being preserved that span the Guadalupian/Lopingian boundary. The Laibin syncline in the Guangxi Province, China, is the only section that contains a complete, regionally correlatable succession of marine conodonts and is the GSSP for the end of the Guadalupian (Henderson et al., 2002).

The only absolute age constraint available for the Delaware Mountain Group, or any other Guadalupian strata are from $^{206}Pb/^{238}U$, $^{207}Pb/^{235}U$ and $^{207}Pb/^{206}Pb$ ages of zircons from an ash bed 37m below the base Capitanian GSSP yielding ages of 265.3 ± 0.2 Ma, 265.4 ± 0.3 Ma and 266.5 ± 1.8 Ma, respectively (Bowring et al., 1998). The best estimate of 265.3 ± 0.2 Ma for this ash bed provides a maximum estimate for the age of the base of the Capitanian (Bowring et al., 1998) (Figure 1.3).

All other ages for Guadalupian stage boundaries are estimated using a cubic spline fit. Cubic spline fitting is a graphical, curve-fitting statistical method that relates measured radiometric ages to stage boundaries without absolute ages based on their stratigraphic position and thickness. A full discussion of the method can be found in Agterberg et al.

(2012). The section in Figure 3 is calibrated to absolute time using this method tied to the U-Pb age of Bowring et al. (1998).

1.3. SAMPLING AND ANALYTICAL PROCEDURES

1.3.1. Sampling

Samples used in this study were taken from a two research cores that were drilled in the Delaware Basin by Gulf Oil in 1980's (Figure 1.2). The research cores penetrate portions of the Guadalupian Cherry Canyon and Brushy Canyon Formations and therefore contain the formation contact. Eight 1-inch core plugs were taken from an organic-rich interval of the Brushy Canyon Formation that was proximal to the Cherry Canyon-Brushy Canyon Formation contact based on lithologic interpretations and geochemical correlations by Milliken (1994). Sampling close to a previously correlated marker horizon limits the age variance between samples taken from multiple cores that are intended to be the same age. This marker horizon was correlated between the two cores based on available gamma well log data. Six core plugs were taken from the more proximal DB-01 core, and two plugs from the more distal DB-02 core. The entire outer surface of the core plugs were sanded with silicon carbide to remove any drill markings and possible metal contamination that could have been obtained during coring, cleaned with ethanol, and left to air dry. A 20-g aliquot of each plug, representing a stratigraphic interval of ~2cm, was then broken into chips and powdered using a mortar and pestle. While the actual amount of powder used for each Re-Os analysis is much less, larger aliquots of powdered sample negate the effects of Re and Os heterogeneity within a sample (Kendall et al., 2009).

1.3.2. Organic Characterization (TOC and Pyrolysis)

Total organic carbon (TOC) content was determined by the dry combustion of an aliquot of the powdered sample using a Leco CS244 carbon analyzer at Weatherford Laboratories in Houston, Texas. First, samples were pretreated with 2% HCl acid in order to remove any carbonate-associated carbon, and then dried. The demineralized sample was then placed in a crucible and heated to 1,350°C in an oxygen atmosphere. Carbon is oxidized to form CO_2 which is carried by the gaseous oxygen flow through scrubbers in order to remove chlorine gas and any residual moisture. The CO_2 is then measured by an infrared detector and corrected to weight percent carbon (TOC %).

Organic matter type and maturity were determined via Rock-Eval pyrolysis at Weatherford Laboratories in Houston, Texas. The Rock-Eval pyrolysis method involves step-heating of a sample in an inert atmosphere. In brief, samples are heated to 300°C for 3 minutes in order to volatilize free hydrocarbons (bitumen) within the sample. Free hydrocarbons are hydrocarbons that have already, naturally, been generated in the sample and are reported in mg of hydrocarbons per gram of TOC (mgHC/gTOC) and are termed S_1. The temperature then increases slowly from 300°C to 550°C in order to artificially thermally crack and volatilize the heavy carbon compounds (kerogen), are reported in mgHC/gTOC and are termed S_2. The temperature of maximum hydrocarbon formation after free hydrocarbons are removed is termed T_{max} and is dependent upon the thermal maturity and organic matter type present in the sample. CO_2 that is created during the thermal cracking of the heavy-carbon compounds is measured and reported as

$mgCO_2/gTOC$, is termed S_3 and is an indication of the amount of oxygen in the kerogen which is also dependent upon organic matter type.

1.3.3. Re-Os Geochemistry

Approximately 0.3 g of powdered sample was weighed and transferred to a thick-walled, internally cleaned, borosilicate glass Carius tube along with a known amount of a mixed ^{185}Re + ^{190}Os spike and 8 mL of a chromic-acid solution created by dissolving $Cr^{VI}O_3$ powder into 4N H_2SO_4 (0.25 g/mL). The CrO_3-H_2SO_4 method was used to preferentially dissolve and oxidize hydrogenous Re and Os which yields more accurate and precise ages (Selby and Creaser, 2003). The Carius tubes were sealed, and sample and spike were digested and equilibrated at 240°C for 48 hours. Digestion dissolves sample powders and oxidizes sample Re and Os to ReO_3^- and OsO_4^- species, respectively. Following digestion the Carius tubes were frozen in a dry ice – ethanol slurry, opened, then thawed, and Os was isolated from the CrO_3-H_2SO_4 solution using $CHCl_3$ solvent extraction at room temperature (Cohen and Waters, 1996), back extracted into 9N HBr and further purified via micro-distillation (Birck et al., 1997). Rhenium was removed from the CrO_3-H_2SO_4 solution by anion column chromatography following reduction of the Cr^{VI} to Cr^{III} using Milli-Q and bubbling with SO_2 gas. Rhenium was further purified by passing the output of the first column through a second anion column. The isolated Re and Os were then loaded onto ultra-pure (>99.99%) Ni and Pt filaments, respectively, and coated with activator solutions of $Ba(NO_3)_2$ and $Ba(OH)_2$, respectively.

The Re and Os isotopic compositions were determined by isotope-dilution-negative-thermal-ionization mass spectrometry (ID-NTIMS) on a ThermoElectron TRITON Plus

TIMS at the University of Houston (Creaser et al., 1991; Volkening et al., 1991). Rhenium was measured as ReO_4^- via static Faraday collection and Os as OsO_3^- via ion-counting using a secondary electron multiplier in peak-hopping mode.

Measured isotopic ratios were spike stripped, corrected for isobaric oxygen interference, instrumental mass fractionation (using $^{185}Re/^{187}Re=0.59738$ and $^{192}Os/^{188}Os=3.08761$), and procedural blank contributions. Uncertainties were obtained through the error propagation of uncertainties in blank abundance and isotopic composition, spike abundance values, mass spectrometry measurements of Re and Os, and the reproducibility of the Re and Os isotopic values of the standard. Average procedural blanks were 19 ± 10 (2σ, n=16) pg for Re and 0.60 ± 1.1 (2σ, n=18) pg for Os with a $^{187}Os/^{188}Os = 0.16 \pm 0.02$ (2σ, n=18).

Repeat measurements of Re and Os standards were performed throughout the analytical campaign. The Re standard, made form zone-refined Re ribbon, yields an average $^{185}Re/^{187}Re$ ratio of 0.59783 ± 0.00022 (2σ, n=16) for 1.5 ng loads using static Faraday collection. The difference between the measured Re standard value and the established standard value of 0.59738 ± 0.0039 (Gramlich et al., 1973) was used to correct the measured $^{185}Re/^{187}Re$ ratios of samples used in this study. The University of Maryland Os standard (Brandon et al., 1999), yielded a $^{187}Os/^{188}Os$ ratio of 0.11385 ± 0.00026 (2σ, n=18) for 500pg loads using a secondary electron multiplier and is, within uncertainty, identical to that reported by Brandon et al. (1999).

The Re-Os ages and $(^{187}Os/^{188}Os)_i$ are obtained via modified York regression (York, 1969) of the reduced isotopic data and propagated 2σ uncertainties using *Isoplot v. 4.15*

(Ludwig, 2008). Errors are calculated using the maximum-likelihood estimation algorithm and are reported as 2σ.

1.4. RESULTS

1.4.1. Organic Characterization (TOC and Pyrolysis)

The TOC values for Brushy Canyon samples range from 0.97 to 4.04% with an average of 2.89% and no observed trend with depth (Table 1.1). All but one sample have TOC values > 1% making them fair – good source rocks.

Rock-Eval pyrolysis yielded T_{max} (a measure of thermal maturity using the temperature of maximum generation of hydrocarbons during pyrolysis) values of 437 – 443°C indicating slight to moderate thermal maturity, bordering the onset of oil generation for Type II marine kerogen. The type of organic matter that make up the samples is determined through the co-variance of ratios (hydrogen index and oxygen index) that are proxies for the amount of H, C, and O in the kerogen, traditionally represented on the classic van Krevelen atomic H/C versus O/C diagram (Espitalie et al., 1977; Peters, 1986) (Figure 1.4). Hydrogen Index (HI) ([100*S_2]/TOC), a proxy for atomic H/C, is a measure of the amount of hydrogen in the kerogen. Marine organisms and algae are generally composed of lipid- and protein-rich organic matter, which has a higher proportion of hydrogen than the carbohydrate-rich land plant constituents. Oxygen Index (OI) ([100*S_3]/TOC), a proxy for atomic O/C, is a measure of the amount of oxygen in the kerogen. Polysaccharide-rich remains of land plants and inert organic matter are

Sample	TOC (%)	S1	S2	S3	T_{max}	OI	HI
Core: DB-01							
BC1-1	0.97	0.47	2.22	0.50	442	51	228
BC1-1.5	2.65	1.39	8.10	0.74	441	34	328
BC1-2	1.91	0.94	6.28	0.65	438	21	393
BC1-2.5	3.19	1.76	11.78	0.70	437	19	382
BC1-3	3.46	1.58	13.58	0.73	441	16	377
BC1-3.5	4.04	2.09	15.55	0.78	438	23	311
BC1-4	3.88	2.30	14.81	0.74	443	28	306
BC1-4.5	2.71	1.19	9.02	0.63	441	22	370
BC1-5	3.38	1.68	12.73	0.54	442	19	385
BC1-6	2.75	1.23	8.54	0.64	439	23	333

Table 1.1. TOC and Rock-Eval data for Brushy Canyon organic-rich mud rocks. TOC = Total organic carbon and is given in weight percent. S1, S2 are in mg of hydrocarbons per gram of TOC (mgHC/gTOC), S3 is in mg CO_2 per gram of TOC (mgCO_2/gTOC), T_{max} is in °C, Oxygen Index (OI) = S3/TOC, Hydrogen Index (HI) = S2/TOC.

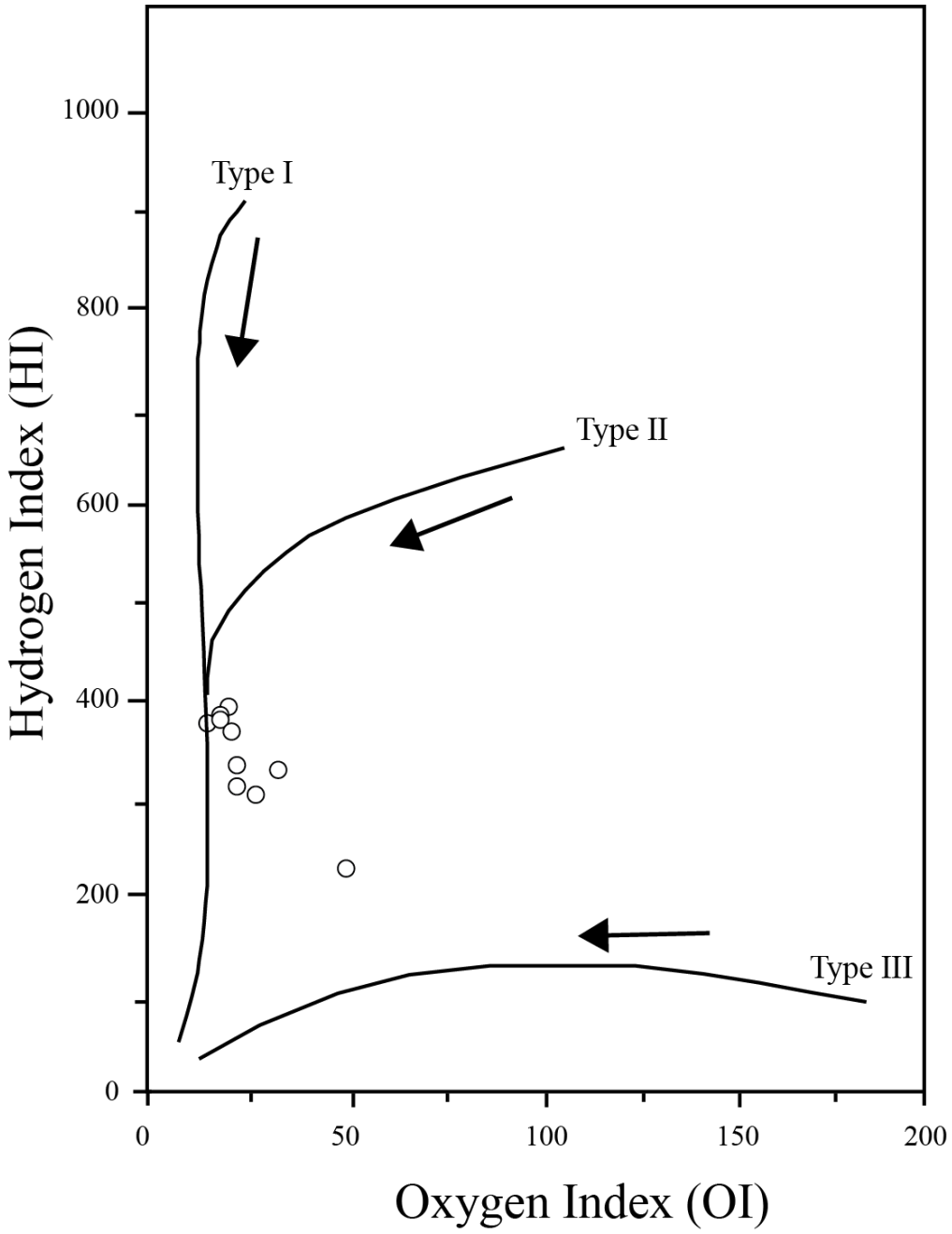

Figure 1.4. Modified Van Krevelen diagram showing the co-variation of Hydrogen Index (S2/TOC) and Oxygen Index (S3/TOC), both indicators of organic matter type. Black arrow indicates increasing thermal maturity for each organic matter type.

generally much higher in OI than in marine sediments. Therefore, a thermally immature kerogen created from the remains of terrestrial organic matter (Type III). The co-variation of HI and OI is also useful in the estimation of thermal maturity, as samples follow paths on a modified van Krevelen diagram during burial and thermal maturity due to a loss of H and O relative to C during hydrocarbon generation (Figure 1.4). The HI (228-393 mgHC/gTOC) and OI (16-51 $mgCO_2$/gTOC) data for Brushy Canyon samples illustrate that they are comprised of slightly to moderately mature Type II kerogen, consistent with a marine kerogen and previous studies of the Brushy Canyon Formation (Hays and Tieh, 1992; Sageman et al., 1998) (Table 1.1, Figure 1.4).

1.4.2. Re-Os Geochemistry

The Re-Os abundances and isotopic compositions for Brushy Canyon samples are presented in Table 1.2. All samples are enriched in Re (17-92 ppb) and Os (149-887 ppt) compared to modern-day average continental crust (~1 ppb Re and 30-50 ppt Os; Esser and Turekian, 1993) and have typical abundances for ORM (Ravizza and Turekian, 1989; Cohen et al., 1999; Creaser et al., 2002; Selby and Creaser, 2003; Hannah et al., 2004; Kendall et al., 2004; Finlay et al., 2010; Rooney et al., 2010). The $^{187}Re/^{188}Os$ ratios range from 436 to 967 and are positively correlated with $^{187}Os/^{188}Os$ ratios of 2.42 to 4.79.

Sample	$\frac{^{187}Re}{^{188}Os}$	±	$\frac{^{187}Os}{^{188}Os}$	±	Re (ppb)	±	Os (ppt)	±
Core: DB-01								
BC1-1	864.24	8.64	4.34	0.04	17.31	0.07	149.57	2.67
BC1-1.5	910.29	9.10	4.46	0.05	57.93	0.21	480.00	4.35
BC1-2	700.93	7.01	3.57	0.05	32.89	0.12	327.70	3.35
BC1-2.5	861.21	6.91	4.28	0.03	82.12	0.29	708.27	5.21
BC1-3	747.19	6.09	3.77	0.03	69.34	0.24	659.69	4.76
BC1-3.5	436.46	4.20	2.42	0.02	49.63	0.18	711.61	5.11
BC1-4	809.95	5.53	4.02	0.03	91.76	0.32	823.06	5.40
BC1-4.5	967.78	9.68	4.79	0.07	69.68	0.25	558.12	5.87
BC1-5	728.40	5.28	3.65	0.02	78.26	0.27	755.93	5.03
BC1-6	579.96	5.90	3.02	0.03	41.54	0.15	475.50	3.75
Core: DB-02								
BC2-1	721.74	2.83	3.62	0.01	91.33	0.32	887.71	3.74
BC2-2	572.06	2.51	2.98	0.01	49.16	0.17	568.36	2.58

Table 1.2. Re-Os isotopic data for Brushy Canyon organic-rich mud rocks. Uncertainties for Re-Os isotopic data are 2σ.

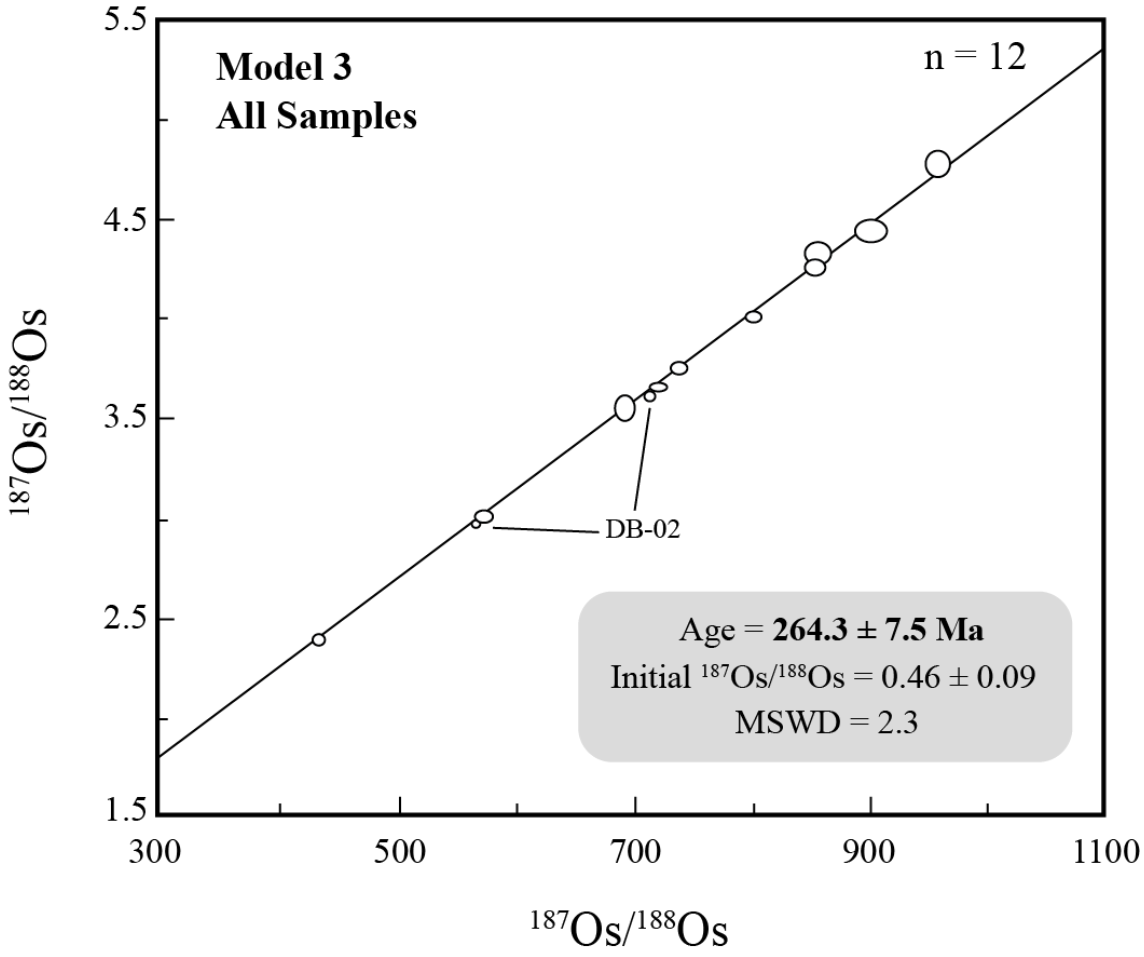

Figure 1.5. Re-Os isochron for the Brushy Canyon Formation. Samples from core DB-02 are labeled as such. All other samples are from core DB-01. Uncertainty is reported as 2σ.

1.5. DISCUSSION

1.5.1. Re-Os Geochronology

Regression of all data points from the Brushy Canyon Formation yields a Model 3 age of 264.3 ± 7.5 Ma (2.8% age uncertainty, 2σ, n=12, mean square of weighted deviates [MSWD] = 2.3). Within uncertainty, this agrees with the expected age for this formation (see *Geologic Setting*) (Figure 1.5). The calculated $(^{187}Os/^{188}Os)_i$ at 264 Ma for all samples range from 0.43 to 0.51 with no clear correlation with stratigraphic level (using $\lambda=1.666 \times 10^{-11}a^{-1}$; Smoliar et al., 1996). This, and the MSWD of 2.3, indicates that Os input into the basin had some small variations over the length of the sampled section (~1 m) and was non-systematic or there has been some degree of post-depositional mobility of Os on the scale of the 20 g sample size. Model 3 ages assume that the scatter about the isochron is not due a result of analytical uncertainty and includes geologic factors (e.g., a change in $(^{187}Os/^{188}Os)_i$, or post-depositional mobility of Os) (Ludwig, 2008).

1.5.2. Comparison to Established Age

Whereas there are no previously reported absolute ages for the Guadalupian, Agterberg et al. (2012) estimated the age for the upper and lower Guadalupian boundaries using a cubic spline fit based on a radiometric age obtained for the base of the Capitanian at 265.3 ± 0.2 Ma (Bowring et al. 1998). Based on this cubic spline fit, the Guadalupian Epoch spanned from 272 Ma to 260 Ma (Figure 1.3). Based on the stratigraphic position of the Brushy Canyon (between the Cherry Canyon and Bone Springs Formation) and the locations of the Wordian and Roadian GSSP's (see section), the Brushy Canyon

Formation is Roadian in age and therefore has an age of 272 – 269 Ma (Figure 1.3). The calculated Model 3 age of 264.3 ± 7.5 Ma from this study agree with the expected age based on calculations from Agterberg et al. (2012), however, with large uncertainty.

In order to obtain precise isochron ages, three conditions must be met: (1) There must be a significant spread in measured $^{187}Re/^{187}Os$, which leads to a significant spread in measured $^{187}Os/^{188}Os$ after significant time, (2) The $(^{187}Os/^{188}Os)_i$ for all samples must have been the same, and (3) There must be no post-depositional mobilization of Re or Os. With ranges in $^{187}Re/^{188}Os$ of 431- 896 and $^{187}Os/^{188}Os$ of 2.39 – 4.15 for the isochron presented here, there is adequate spread in both ratios for a precise age. Calculated $(^{187}Os/^{188}Os)_i$ at 264 Ma range from 0.43 – 0.51, and as previously discussed, have no clear correlation with stratigraphic level, indicating that the variation in calculated initials have resulted from post-depositional mobility of Os rather than a systematic change in seawater $^{187}Os/^{188}Os$ compositions.

1.5.3. Relationship between Re and Os Abundances and TOC

The uptake of Re and Os in the water column occurs under suboxic to anoxic conditions with complexation likely occurring through a combination of reductive capture (Colodner et al., 1993; Yamashita et al., 2007) and adsorption onto organic complexes (Koide, 1991; Crusius et al., 1996; Levasseur et al., 1998; Oxburgh, 1998; Cohen et al., 1999; Morford and Emerson, 1999). Several experimental studies have demonstrated that the uptake mechanism varies for each element with soluble Re ($Re^{VII}O_4^-$) being removed from seawater by reductive capture during diffusion into anoxic pore waters and converted to the insoluble Re^{IV} form under low-oxidation-potential (Eh) conditions

(Colodner et al., 1993). Removal of Os from seawater (as soluble Os^{IV}) is suggested to be directly associated with the presence of organic matter (Yamashita et al., 2007). Over a wide range of Eh and pH conditions, Os enters oxic sediment, first as Os^{IV}, and is then converted to Os^{III} after further reduction during organic complexation (Yamashita et al., 2007). Osmium removal from seawater is fast compared to Re removal (hours vs. weeks) and is complexed into ferromanganese oxides as well as organic-rich sediments, whereas Re is only removed to sediment under highly reducing conditions leading to high $^{187}Re/^{188}Os$ ratios in organic-rich sediments (Yamashita et al., 2007; Poirier et al., 2011).

Whereas the removal of Os from seawater has been directly linked to organic matter, the rate of removal is controlled not only by the type and abundance of organic matter, but also the redox conditions and sediment accumulation rates. The rate of removal of Re from seawater, however, is controlled by precipitation kinetics and has been demonstrated to be unaffected by changes in sediment accumulation rate and sulfide abundance (Crusius and Thompson, 2000; Sundby et al., 2004). However, Rooney et al. (2010) suggests that the enrichment of Re and Os in ORM may be related to local factors such as the duration that the pore-water sediment interface is open, and changes in the oxic-anoxic boundary of the water column, both of which can be related to sediment accumulation rate. Further, the behavior of other redox-sensitive elements such as Ni and Mo who's dominant enrichment factor is sediment accumulation rate, are very similar to that of Re and Os, indicates a common dominant enrichment factor (Lewan and Maynard, 1982; Kendall et al., 2009; Rooney et al., 2010).

Some recent studies have shown that Re and Os abundances do not always correlate with TOC values. However, these studies either used inverse *aqua-regia* instead of CrO_3-H_2SO_4 for sample digestion (Cohen et al., 1999), or were performed on organic-rock mudrocks from restricted basins (McArthur et al., 2008; Baioumy et al., 2011; Cumming et al., 2012). Sample digestion using inverse *aqua-regia* alleviates and oxidizes Re and Os from both hydrogenous and non-hydrogenous, detrital sources. Since non-hydrogenous sources aren't related to seawater and unrelated to organic matter, a strong correlation between Re and Os abundances and TOC isn't expected. In fact, there is a weak correlation between Re and Os abundance and TOC for the Jurassic ORM reported by Cohen et al. (1999) and perhaps a stronger correlation would result from analysis using the CrO_3-H_2SO_4 method.

Baioumy et al. (2011) reported Re-Os data for laterally correlated marine and non-marine shales and coals from Egypt. The marine shales showed a strong positive correlation between TOC and both Re and Os abundances (R^2=0.87 and 0.89, respectively), and a lack of correlation in the laterally correlated non-marine gray shales and coals (R^2=0.19 and 0.37, respectively). Cumming et al. (2012) also reported a lack of correlation between TOC and Os in both distal and proximal (R^2= 0.56 and 0.41, respectively) lacustrine deposits from the Green River Basin. A lack of correlation is also observed between TOC and Re in the proximal, lake margin Douglas Creek Member (R^2=0.17). However, the Mahogany Zone which represents distal lake center deposits showed a moderate positive correlation between TOC and Re (R^2 = 0.73) (Cumming et al., 2012). The Mahogany Zone was deposited in the lake center when lake levels were at their

maximum and sedimentation rates were slow and steady under a stratified water column (Bradley, 1931; Boyer, 1982; Tuttle and Goldhaber, 1993; Cumming et al., 2012). In contrast, the Douglas Creek Member was deposited on the lake margin during fluctuating lake-levels and a variation in sedimentation rate, possibly allowing much higher variation in the Re-Os uptake and fractionation compared to the more stable lake center where association of Re and Os with organic matter would have been greater (Cumming et al., 2012). It has been suggested that in restricted basins, organic matter sedimentation draws down dissolved Re and Os from the water column resulting in a shortening of the residence time subsequently causing rapid variations in the availability of those elements in the water column (McArthur et al., 2008). This results in rapid variations in the $(^{187}Os/^{188}Os)_i$ of the sediments. However, the proximal lacustrine zones discussed in Cumming et al. (2012) that had the weakest correlation between TOC and both Re and Os, provided a more precise isochron than the distal shales from the lake center.

If there is a relationship between TOC, sedimentation rate, and the abundances of Re and Os, it can be expected that the slope of a line correlating points from various ORM on a TOC vs. Re (or Os) plot would be related to the sediment accumulation rate (Figure 1.6). Because TOC decreases during decreased sedimentation rates due to scavenging of organic matter by benthic organisms, while Os (or Re) abundances would increase due to a longer duration of interaction between pore-waters and the sediment interface, this correlation would be negative, with larger slopes (higher Re/TOC or Os/TOC) representing slower accumulation rates. In fact, there is a rough correlation between the slope of the correlation line and the R^2 value for most marine and non-marine shales, with

slopes of Re/TOC and Os/TOC of up to 18.7 and 350.7, respectively, and R^2 values of 0.97 for both (Figure 1.6). This indicates that the slower sedimentation rates in less-restricted, marine conditions, provides adequate time for the complexing of Re and Os with organic matter. However, the implication of this correlation may not be straight-forward. In addition to sedimentation rate, the amount of preserved organic matter in sediment can be related to water depth, redox conditions, diagenetic processes following deposition and burial, as well as degree of restriction of the basin. Molybdenum concentration in organic-rich mud rocks is a particularly useful indicator of paleoredox state as the uptake of Mo from seawater requires low O_2 to anoxic waters with H_2S present in the sediment pore fluid (Zheng et al., 2000). Georgiev et al. (2011) reported a positive relationship between TOC and molybdenum abundance for Upper Permian shales from Greenland and the mid-Norwegian shelf and also attributed the correlation to the degree of basin restriction. In stagnant, restricted basins with limited deep water renewal, Mo drawdown into basin floor sediments progressively depletes the dissolved Mo of seawater, resulting in shales that are deposited in this setting to have lower Mo/TOC than shales deposited in less restricted basins with continued Mo renewal (Georgiev et al., 2011). Therefore, ORM with low Mo/TOC are suggested to be deposited in a more restricted basin setting than those with high Mo/TOC (Tribovillard et al., 2006). Non-marine shales discussed here all plot with low Re/TOC and Os/TOC, in a distinct field, separate from the marine shales with high Re/TOC and Os/TOC (Figure 1.6). If the only factor controlling the slopes of the correlation lines on this diagram was sediment accumulation rates, this divergence of marine and lacustrine shales wouldn't occur, as sediment accumulation rates are similar for some lacustrine and marine settings.

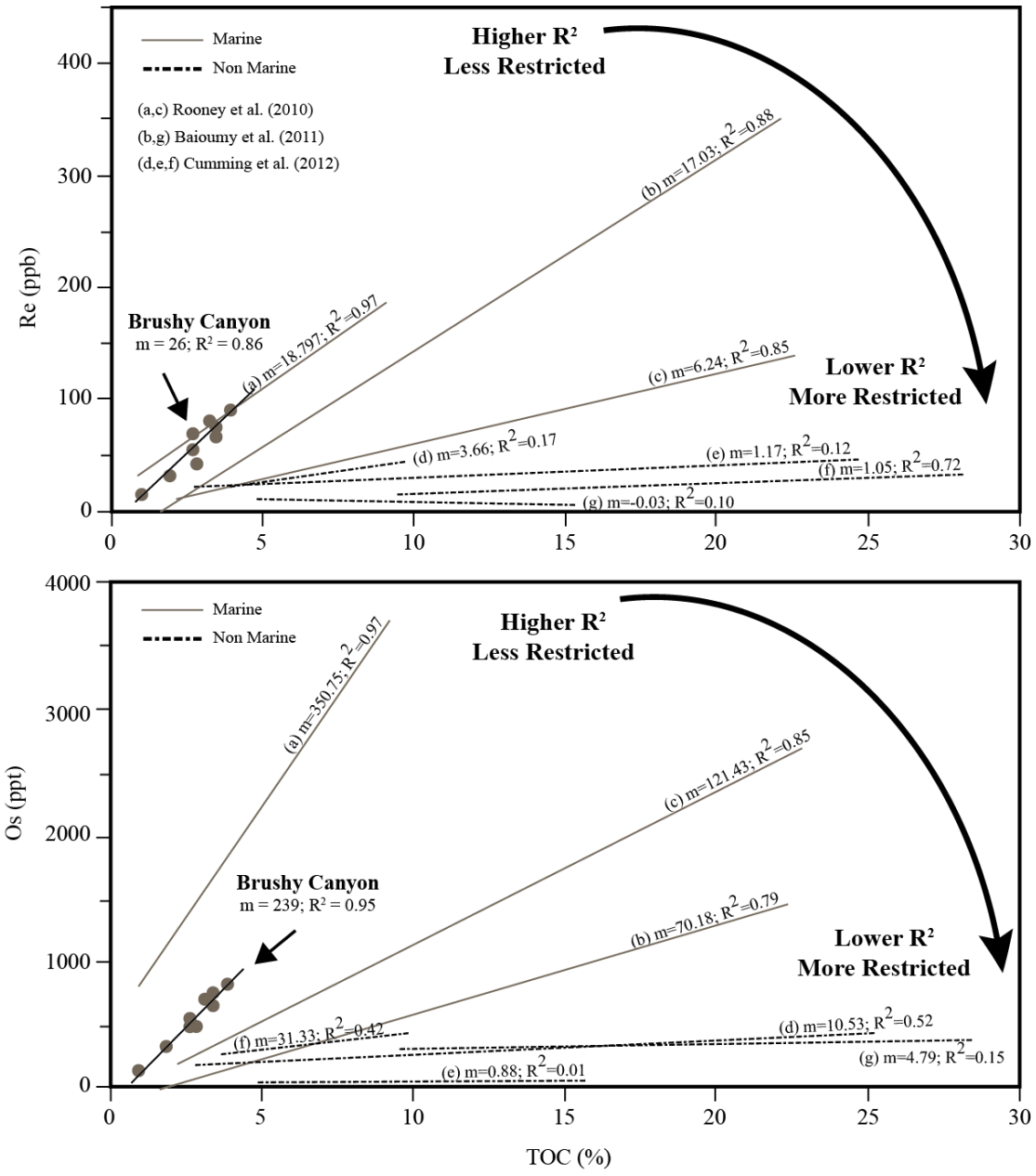

Figure 1.6. (A) Re abundance (in ppb) vs. Total organic carbon (in weight percent), (B) Os abundance (in ppt) vs. Total organic carbon (in weight percent). Solid gray lines represent marine shales from: (a, c) Rooney et al. (2010) and (b) Baioumy et al. (2011). Dashed black lines represent non-marine shales from: (g) Baioumy et al. (2011), (d, e) proximal lacustrine shale from Cumming et al. (2012) and (f) distal lacustrine shales from Cumming et al. (2012).

The covariation of Re and Os with TOC therefore has implications for Re and Os renewal which is controlled by the degree of basin restrictivity, similar to that of Mo. Also, the degree of basin restrictivity does have some control on the rate of sediment accumulation.

The TOC values for Brushy Canyon samples range from 0.97 to 4.04% and are positively correlated with both Re and Os abundances (Figure 1.6). The slope of Re/TOC and Os/TOC for Brushy Canyon samples is 26 and 239, respectively, with R^2 values of 0.86 and 0.95, respectively. These samples have the highest Re/TOC slope and second highest Os/TOC slope of all plotted samples. Based on the discussion above, Brushy Canyon samples were deposited in an open, unrestricted marine setting possibly under very slow sediment accumulation.

In summary, in the present understanding of the uptake and fractionation behavior of Re and Os in the water column is weak. It is however, likely an intricate balance of degree of anoxia, depositional rates, organic matter type, water depth, salinity, pH, and temperature that controls the kinetics of Re and Os removal from seawater. A better understanding of the types of organic molecules that are involved in Re and Os sequestration is clearly necessary to understand their behavior in the water column. In addition, future work is necessary to calibrate the Re/TOC and Os/TOC slopes to actual geologic controls such as redox conditions or sediment accumulation rate.

1.5.4. Dependence of Re and Os Abundance on Organic Matter Type

The trend in HI vs. OI observed in Figure 1.4 cannot be explained by varying degrees of thermal maturation, as all of the samples have similar T_{max} values. The trend is oblique to the direction of thermal maturity, and trends toward Type III kerogen values indicate some contribution of Type III terrestrial kerogen to the organic matter in these samples. This is consistent with work by Hays and Tieh (1992) who suggested a mixture of oxygen-rich Type II and Type III kerogen indicating marine algal input and downslope transport of terrestrial organic matter.

It has been previously suggested that the abundance of Re and Os are heavily dependent upon the organic matter type that comprises the samples, caused by variation in the type of organic ligands that are present (Miller, 2004). As noted above, Hydrogen Index is a proxy of the hydrogen content in kerogen, which varies depending on the pre-cursor organic matter that makes up the kerogen. Marine organisms and lacustrine algae are generally composed of lipid- and protein-rich organic matter, which has a higher proportion of hydrogen, and thus a higher HI than the carbohydrate-rich land plant constituents. This results in Type I and II, algal kerogen having higher HI than Type III kerogen that is terrestrial in origin (Figure 1.4). There is a positive correlation between both Re and Os abundances and HI for the Brushy Canyon samples, with R^2 values of 0.59 and 0.83, respectively (Figure 1.7a). This indicates that the abundances of Re and Os are to some degree dependent on the amount of organically bound hydrogen in the kerogen, with more hydrogen rich kerogen containing a higher abundance of Re and Os. This dependence seems to be more prevalent in the Os abundances. The variable

dependence between Re and Os supports previous studies that show differences in the uptake mechanism between Re and Os, with the sequestration of Os being directly related to the presence of organic matter (Yamashita et al., 2007). Also noted above, Oxygen Index is a proxy for the oxygen content in kerogen, which also varies depending on the organic matter type or degree of oxidation of the organic matter (Peters, 1986). Polysaccharide-rich remains of land plants and inert organic matter generally have a much higher OI than marine and lacustrine sediments, resulting in Type I and II, algal kerogen having lower OI than Type III terrestrial kerogen (Figure 1.4). There is a correlation between both Re and Os abundances and OI for the Brushy Canyon samples, with R^2 values of 0.63 and 0.85, respectively, however, this correlation is negative (Figure 1.7b). This indicates that the abundances of Re and Os are also to some degree inversely dependent on the amount of oxygen in the kerogen, with more oxidized kerogen containing lower abundances of both Re and Os. Cumming (2013) reported a lack of correlation between Re and Os abundances and OI values of ~15 and suggested that Re and Os enrichment requires lower oxygen-bearing kerogen or lower oxygen conditions during organic matter deposition. In the Brushy Canyon samples, a correlation does exist above an OI of 15 so additional factors must be involved that are specific to each sample suite. Regardless, the amount of oxygen in kerogen has a significant effect on the abundance of Re and Os in kerogen, likely due to the difference in chelating site precursors that are available during deposition and early burial (Cumming, 2013). A similar relationship is seen in vanadium and nickel abundances in kerogen. Vanadium and nickel are organically bound in tetrapyrroles (Lewan and Maynard, 1982). Chlorophyll, which is converted to a tetrapyrrole during burial, is very sensitive to

oxygen as it expands its ring structure making it incapable of hosting metals (Lewan and Maynard, 1982). Therefore, sediments and organic matter settling in an oxygenated water column have less chance to bind V and Ni in these tetrapyrroles (Lewan and Maynard, 1982). The similarity of the behaviors of Re and Os to V and Ni indicates the possibility of these elements being held in similar chelating sites in similar organic complexes.

Both HI and OI are interdependent upon TOC, and since TOC has long been recognized to correlate with Re and Os abundance, it is possible that the correlation of HI and OI with Re and Os abundances in the Brushy Canyon samples is strongly dependent upon the underlying correlation with TOC. The ratio of S_2/S_3 represents the amount of hydrocarbons that can be generated from a source rock relative to the amount of organic CO_2 released during Rock-Eval pyrolysis. S_2/S_3 ratios are considerably higher for Type I and II kerogen than for Type III kerogen because terrestrial derived organic matter contains substantially more oxygen than marine or lacustrine algal organic matter. There is a moderate to strong correlation between the S_2/S_3 ratio and both Re and Os abundances for Brushy Canyon samples, with R^2 values of 0.62 and 0.91, respectively (Figure 1.7c). This correlation is a TOC independent linkage between the type of organic matter in the rock and Re and Os abundances and provides the most robust evidence to date for the dependence of organic matter type on the abundance of Re and Os, with hydrogen rich, oxygen poor algal kerogen possibly providing more available chelating site for these elements.

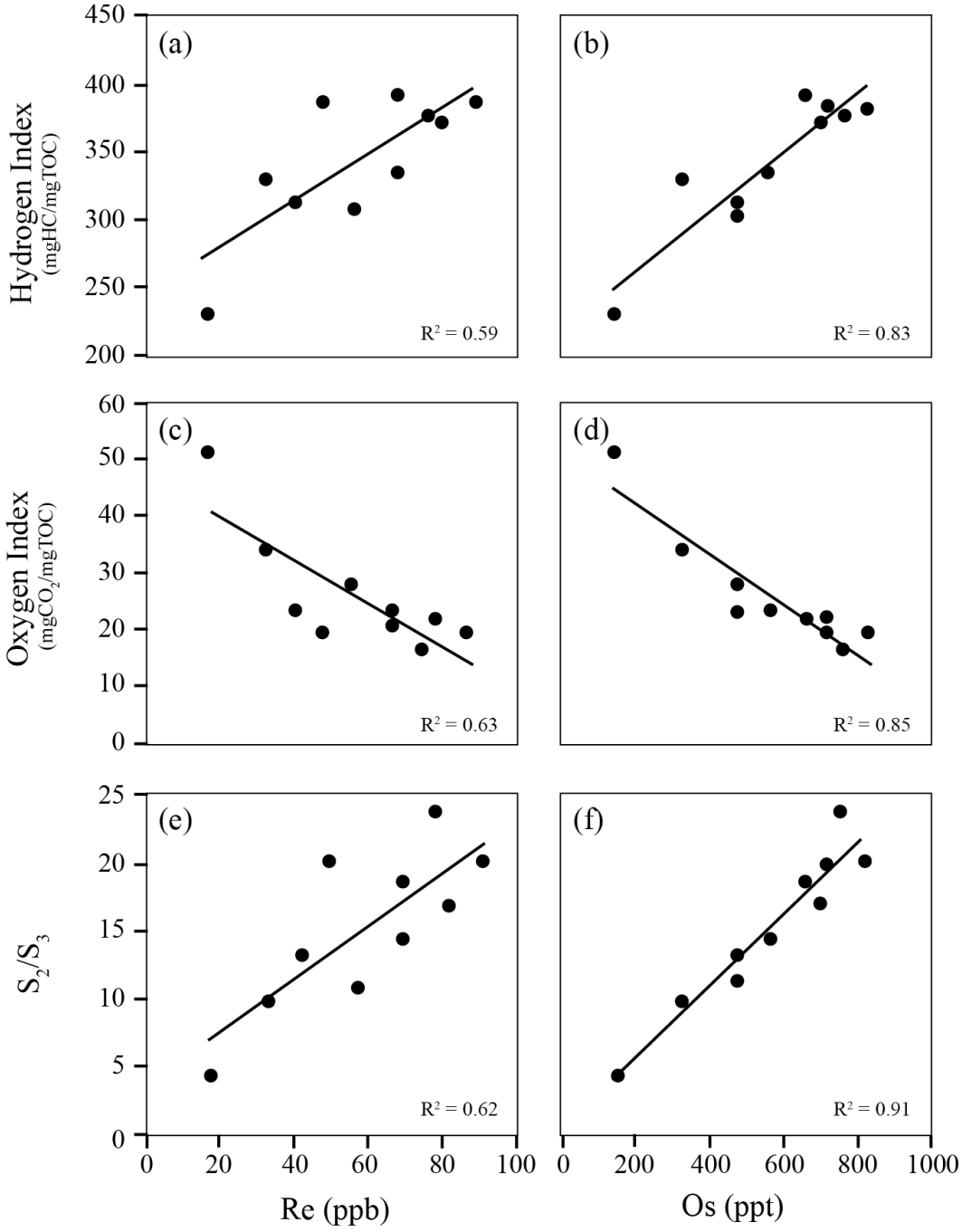

Figure 1.7. Crossplots of (a) Hydrogen Index (S2/TOC) and Re (ppb); (b) Hydrogen Index and Os (ppt); (c) Oxygen Index (S3/TOC) and Re (ppb); (d) Oxygen Index and Os (ppt); (e) S2/S3 (or HI/OI) and Re (ppb); (f) S2/S3 (or HI/OI) and Os (ppt) showing the correlation of Re and Os with proxies for organic matter type.

1.5.5. Implications of the $(^{187}Os/^{188}Os)_i$ at ~265 Ma

The $(^{187}Os/^{188}Os)_i$ obtained from the regression of 0.46 ± 0.09 is interpreted to represent the $^{187}Os/^{188}Os$ of seawater at the time of deposition (Ravizza and Turekian, 1989; Cohen et al., 1999). The $^{187}Os/^{188}Os$ ratio of seawater is derived from a balance of input from: (1) Radiogenic Os from river water during weathering and subsequent continental runoff of upper continental crust ($^{187}Os/^{188}Os$ = 1.4) (Esser and Turekian, 1993; Peucker-Ehrenbrink and Jahn, 2001), and (2) non-radiogenic Os from the mantle via seafloor spreading and production of mid-ocean ridge basalts, flood basalt events, or hydrothermal alteration of oceanic crust or from meteorite influx ($^{187}Os/^{188}Os$ = 0.13) (Peucker-Ehrenbrink and Ravizza, 2000; Walker et al., 2002; Schmitz et al., 2004).

Significant changes over time in the $^{187}Os/^{188}Os$ of seawater are observed in the rock record. These shifts can be caused by the relative change in the contribution of the various sources such as during periods of increased seafloor spreading, accelerated crustal weathering during deglaciation, or meteorite impacts. Changes on the order of orbitally forced, glacial-interglacial cycles can be resolved due to the short residence time of Os in the ocean (Oxburgh, 1998). The isotopic composition of present day seawater (~1.06; Peucker-Ehrenbrink and Ravizza, 2000) indicates a dominance of contribution from radiogenic crustal Os delivered to the oceans via rivers ($^{187}Os/^{188}Os$ = 1.54; Levasseur et al., 1999). The less-radiogenic $^{187}Os/^{188}Os$ for the Brushy Canyon Formation of 0.52 ± 0.11 indicates that the Delaware Basin received significantly lower relative contributions of crustal Os than did the present-day ocean. Similar conditions existed just prior to the Cretaceous-Paleocene boundary and throughout much of the Eocene leading

into the Eocene-Oligocene boundary (Burton et al., 1999; Pegram et al., 1992; Turgeon and Creaser, 2008).

Although seawater $^{187}Os/^{188}Os$ at any given time in Earth's history can be known by measuring Os isotopes in marine ORM, constraining the relative amount of contributions from the various sources is a challenge. This could be manifested in spatial and temporal variations in the $^{187}Os/^{188}Os$ of the eroding upper continental crust (e.g., weathering of ORM with $^{187}Os/^{188}Os \leq 13.6$; Peucker-Ehrenbrink and Blum, 1998). The unradiogenic component could be the product of a mixture of contributions from the various unradiogenic sources of Os.

The unradiogenic $(^{187}Os/^{188}Os)_i$ of the Brushy Canyon is, within uncertainty, identical to those for marine ORM from the mid-Norwegian shelf and Eastern Greenland at 252.1Ma (0.57 ± 0.04 and 0.62 ± 0.11, respectively), just prior to the end of the Permian (Georgiev et al. 2011) (Figure 1.8). This suggests that either: (1) There was no significant variation in the $(^{187}Os/^{188}Os)_i$ of global seawater across the ~13 Myr interval between the Guadalupian and the end of the Permian or (2) There was some degree of change in seawater conditions between these two times. However, due to small sample resolution, the $(^{187}Os/^{188}Os)_i$ is known for only these two distinct times. The data points discussed here are the only available $^{187}Os/^{188}Os$ data for Permian seawater. Therefore, any further $^{187}Os/^{188}Os$ trends in Permian seawater are unknown at this time.

Fluctuation in $^{87}Sr/^{86}Sr$ can also be used as a proxy for evaluating relative contributions of radiogenic and unradiogenic Sr to the oceans, however, with a much longer residence time (Cohen et al., 1999; Peucker-Ehrenbrink and Ravizza, 2000). This results in the

curve of $^{87}Sr/^{86}Sr$ being smoother than that for $^{187}Os/^{188}Os$ as a result of the temporal resolution of Sr being less than that of Os (~10 – 50 kyr; Peucker-Ehrenbrink and Ravizza, 2000). The Sr isotopic record of seawater records a general decrease in $^{87}Sr/^{86}Sr$ from a more radiogenic value of ~0.7080 to a less radiogenic value of 0.70685 from the start of the Permian into the Middle Guadalupian (~266Ma) followed by a slow increase, recovering to a $^{87}Sr/^{86}Sr$ value of 0.70715 by the end of the Permian (Korte et al., 2006) (Figure 1.8).

The trend toward unradiogenic Sr throughout the majority of the Permian represents one of the most rapid changes in the Sr isotopic record of the entire Phanerozoic and is explained by a coupling of (1) the waning of glacial ice retreat that covered large parts of the Late Paleozoic Southern Hemisphere continents, and (2) the opening of the Neotethys sea throughout the Cisuralian and into the Guadalupian (Korte et al., 2006). The Gondwanan Permo-Carboniferous glaciation culminated in the Asselian and Early

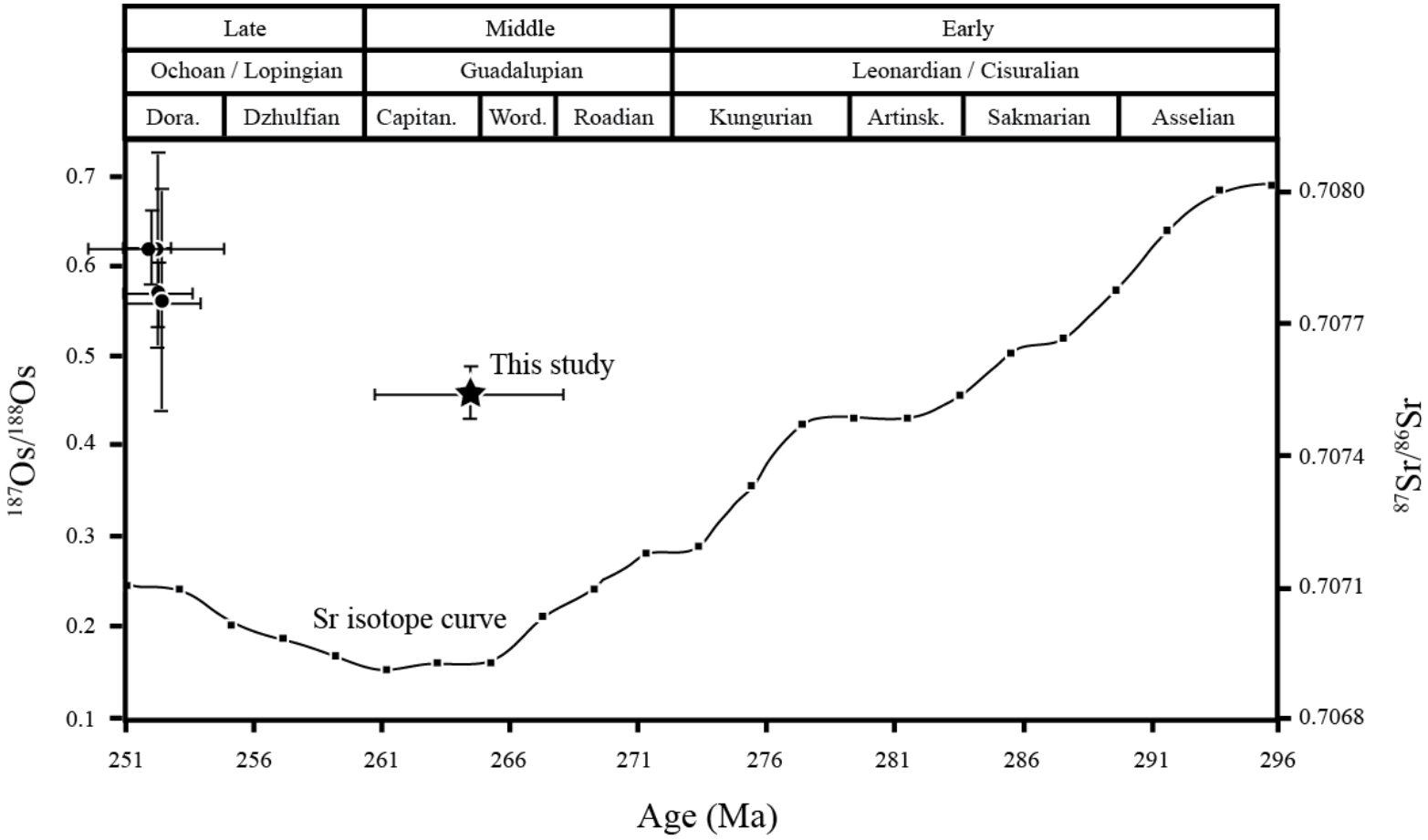

Figure 1.8. Strontium and osmium isotopic signature of seawater throughout the Permian. Solid black line represents the $^{87}Sr/^{86}Sr$ of seawater from Korte et al. (2006) as inferred from Sr isotopes of articulate brachiopod shells. Solid black circles represent $^{187}Os/^{188}Os$ data from Georgiev et al. (2011) from Permo-Triassic shales. Solid black star represents data from this study.

Sakmarian (Frakes et al., 1992) and glacial ice had waned and vanished by the Late Sakmarian (Banks and Clarke, 1987; Dickins and Shah, 1987). The beginning of the Permian is marked by radiogenic $^{87}Sr/^{86}Sr$ values, coinciding with a period of deglaciation in the Southern Hemisphere. Deglaciation accelerates continental erosion and thus provides an enhanced riverine flux of radiogenic Sr to the coeval oceans. During the waning stage of deglaciation during the Sakmarian, the rate of continental weathering decreased resulting in a decrease in the flux of radiogenic crustal material to the oceans. This coupled with the enhanced flux of unradiogenic strontium from hydrothermal circulation within the young oceanic crust created during the widespread volcanism associated with the opening of the Neotethys Ocean during the Cisuralian and into the Guadalupian resulted in the steep decrease in the $^{87}Sr/^{86}Sr$ during this time (Korte et al., 2006). Following the cessation of the opening of the Neotethys during the Wordian, coeval seawater $^{87}Sr/^{86}Sr$ began a slow trend toward more radiogenic values due to a larger contribution from radiogenic continental material via riverine flux (Korte et al., 2006).

In addition to these major geologic processes, secondary processes such as climate type (humid vs. arid) may have had an effect on the Sr isotopic record. The Asselian and Early Sakmarian was characterized by a comparatively higher worldwide humidity compared to a more arid climate in the Artinskian-Late Permian interval (Kozur, 1984; Korte et al., 2006). Humid climates are more conducive to chemical weathering of continental materials, and thus provide a larger flux of radiogenic Sr to the oceans compared to arid climate regimes. While the steep slope of the Sr isotopic curve throughout much of the

Permian is believed to be the result of decreased continental weathering due to waning of deglaciation, the curve could be affected by decreased weathering under an arid climate regime (Korte et al., 2006). In addition, the slower rate of increase in the $^{87}Sr/^{86}Sr$ following cessation of the opening of the Neotethys could be due to slower weathering rates under an arid climate regime (Korte et al., 2006).

Locally, high sedimentation rates during the Early Permian caused rapid basin subsidence which in turn caused enormous compressional stresses in the underlying crustal rocks resulting in uplift of the fault-block separating the Delaware Basin from the Midland Basin to the east. In addition, the Diablo Arch to the west was also significantly uplifted (Adams, 1965). During this time, massive sediment loads were being dumped into the Delaware Basin. Subsidence continued during the Leonardian although not as rapidly as during the Early Permian resulting in a slowed uplift of surrounding areas and an eventual leveling of the mountains to the west and northwest of the basin (Adams, 1965). Sedimentation continued into the Guadalupian and Ochoan, with Upper Permian strata reaching ~2,100 m thick. About one-third of the sediment thickness was attained by filling the depression inherited from the Early Permian, the rest was provided by regional downwarping and late rotational tilting (Adams, 1965). Around the margin of the Delaware Basin, marginal reefs rose ~450-600 m about the floor of the central Delaware Basin (Adams, 1965). During relative sea level high-stands, widespread, organic-rich siltstones of varying thickness accumulated on the basin floor by the hemi-pelagic settling of marine algal material and detrital silt and mud through both aeolian and marine processes while sands were restricted from entering the basin due to their entrapment

behind the broad, flooded shelf and carbonate platform (Meissner, 1972; Dutton et al., 2003). During exposure of the carbonate shelf during subsequent low-stands, sands were transported to the shelf margin via aeolian dune progradation and fluvial processes (Fischer and Sarnthein, 1988) and were carried to the basin floor predominantly by turbidity currents and deposited as major submarine fan complexes (Newell et al., 1953; Payne, 1976; Berg, 1979; Gardner, 1992; Zelt and Rossen, 1995; Bouma, 1996; Beaubouef et al., 1999; Gardner and Borer, 2000; Dutton et al., 2003). Basinal subsidence slowed during the Guadalupian, from 3.7cm/ky. in the Early Permian to 0.8cm/ky. in the Guadalupian as the area attained tectonic stability (Ye and Kerans, 1996). Intermittent marine conditions existed in the Delaware Basin into the Ochoan until evaporate accumulation prompted progressive restriction from marine influence (King, 1948) and an eventual filling of the basin by the end of the Permian.

During the Permian, the Delaware Basin was located just north of the equator (Ziegler et al., 1997), within an arid climate zone, inferred from the presence of aeolian siliciclastics and massive marine evaporate deposits of the Castile, Salado, and Rustler evaporates preserved throughout the region (King, 1948; Oriel et al., 1967; Magaritz et al., 1983; Fischer and Sarnthein, 1988; Soreghan and Soreghan, 2013).

Rapid sedimentation during the Early Permian would have provided an increase in radiogenic continental crustal material to the oceans, resulting in an increase in the $^{187}Os/^{188}Os$ of coeval seawater. To further enhance this radiogenic flux, the uplifting of the areas around the Delaware Basin would have exposed more continental material providing more radiogenic continental crust to weathering. There are no available

$^{187}Os/^{188}Os$ data for Early Permian seawater. However, during slowed sedimentation following the attainment of tectonic stability of the Delaware Basin during the Guadalupian, the flux of radiogenic material to the Delaware Basin, and thus to global seawater, would have been less. Coupled with the decreased chemical weathering under the arid climate regime that existed in the region during much of the Permian, the contribution of radiogenic Os to the oceans via riverine input from the continents was likely to be significantly less than during the Early Permian, resulting in a lower $^{187}Os/^{188}Os$ than Early Permian seawater.

Within uncertainty, the Os isotopic curve parallels the Sr isotopic curve for the Late Permian, within the limited data that is available (Figure 1.8). This indicates that there was a slight increase in the flux of radiogenic continental crustal material to the ocean over the 13 Myr interval between the Guadalupian and the end of the Permian. However, it could be argued that the overlap of the data points voids any conclusion about changes in seawater chemistry, as these data points could represent the same value, $^{187}Os/^{188}Os$ = ~0.55. Regardless, the $^{187}Os/^{188}Os$ of seawater at ~264 Ma is 0.46 ± 0.09 and is much less than that of present day seawater (~1.06; Peucker-Ehrenbrink and Ravizza, 2000) which indicates a significantly smaller relative contribution of radiogenic continental crustal material than the present day ocean is receiving, similar to times just prior to the Cretaceous-Paleocene boundary and throughout much of the Eocene leading into the Eocene-Oligocene boundary (Burton et al., 1999; Pegram et al., 1992; Turgeon and Creaser, 2008).

1.6. CONCLUSIONS

New Re-Os geochronology of the Brushy Canyon Formation from the Delaware Basin of west Texas yields a Model 3 age of 264.3 ± 7.5 Ma (2.8% age uncertainty, 2σ, n=12, mean square of weighted deviates [MSWD] = 2.3) and, within uncertainty, agrees with the expected estimate age of this formation. This data provides the first absolute age for Guadalupian strata. As there is no systematic trend seen in the calculated $(^{187}Os/^{188}Os)_i$ with depth, the large uncertainty in the age is most likely due to post-depositional mobility of Re and/or Os.

In addition, the $(^{187}Os/^{188}Os)_i$ obtained from the isochron regression provides the $^{187}Os/^{188}Os$ composition of seawater at the time that the Brushy Canyon Formation was deposited (~265Ma). The $(^{187}Os/^{188}Os)_i$ of 0.46 ± 0.09 is much less radiogenic than present-day seawater (~1.06; Peucker-Ehrenbrink and Ravizza, 2000), similar to conditions that existed just prior to the Cretaceous-Paleocene boundary and throughout much of the Eocene leading into the Eocene-Oligocene boundary. This indicates that vastly different conditions existed in the Guadalupian than today. Specifically, present day seawater is receiving a larger relative amount of radiogenic continental crustal material than Guadalupian seawater was receiving. This is likely largely due to decreased continental weathering following a period of deglaciation associated with the Permo-Carboniferous glaciation that culminated in the Asselian, with much of the glaciers having vanished by the Late Sakmarian (Banks and Clarke, 1987; Dickins and Shah, 1987). Within the Delaware Basin, denudation had slowed following tectonic stability during the Middle Permian. In addition, an arid climate regime slowed chemical

weathering of exposed continental crust, further restricting the flux of radiogenic continental crustal material to the Late Permian Ocean.

The lack of available Os isotopic data for Permian seawater inhibits any conclusions on trends in the $^{187}Os/^{188}Os$. However, given the few data available (n=2), the Os isotopic curve seems to parallel the Sr isotopic curve with both exhibiting an increase in contribution of radiogenic material over the 13 Myr interval bounded by the data points within the Late Permian.

Re and Os abundances correlate with HI, OI, and the ratio of S_2/S_3, all indicating a relationship between these elemental abundances and the type of organic matter that makes up the samples. This correlation is positive for HI and S_2/S_3, and negative for OI. The positive relationship between the abundances of Re and Os and both HI and S_2/S_3 indicate that the presence of hydrogen rich, oxygen poor organic matter, such as Type I and Type II algal kerogen, yield higher abundances of Re and Os in these samples. On the other hand, the negative correlation between the elemental abundances and OI means that the amount of oxygen in kerogen has a significant effect on the abundance of Re and Os in kerogen, likely due to the difference in chelating site precursors that are available during deposition and early burial, similar to the relationship seen with vanadium and nickel in organic matter. However, these correlations may be complicated by other controlling factors such as variability in redox conditions.

REFERENCES

Adams J.E. (1965) Stratigraphic-tectonic development of Delaware Basin. *AAPG Bulletin* **49**, 2140-2148.

Agterberg F.P., Hammer O. and Gradstein F.M. (2012) Statistical procedures, Chapter 14. In: Gradstein F.M., Ogg J.G., Schmitz M. and Ogg G. (Eds). *The Geological Time Scale 2012*, Elsevier, Amsterdam, 269-274.

Bagheri S., Kozur H.W. and Stampfli G. (2003) The Palaeotethyan suture in NE Iran and its displaced continuation in Central Iran (Anarak-Nakhlak area). *22nd IAS Meeting of Sedimentology Abstract Book* **9**.

Baioumy H.M., Eglinton L.B., and Peucker-Ehrenbrink B. (2011) Rhenium-osmium isotope and platinum group element systematics of marine vs. non-marine organic-rich sediments and coals from Egypt. *Chemical Geology* **285**, 70-81.

Banks M.R. and Clarke M.J. (1987) Changes in the geography of the Tasmania Basin in the Late Paleozoic. In: McKenzie G.D. (Ed.), Gondwana Six: Stratigraphy, Sedimentology and Paleontology. *Geophysical Monograms* **41**, 1-14.

Beaubouef R.T., Rossen C., Zelt F.B., Sullivan M.D., Mohrig D.C. and Jennette D.C. (1999) Deep-water Sandstones, Brushy Canyon Formation, West Texas, Field Guide for AAPG Hedberg Field Research Conference – April 15-20, 1999. *AAPG Continuing Education Course Note Series* **40**, 1-48.

Bechennec F. (1988) Geologie des nappes d'Hawasina dans les parties orientales et centrales des montagnes d'Oman. *Documents du B.R.G.M., Bureau de Recherches Geologiques et Minieres, Orleans* **127**, 1-474.

Berg R.R. (1979) Reservoir sandstones of the Delaware Mountain Group, southeast New Mexico. In: Sullivan N.M. (Ed.), Guadalupian Delaware Mountain Group of west Texas and southeast New Mexico, Symposium and Field Trip Conference Guidebook. *SEPM Publications, Permian Basin Section* **79-18**, 75-95.

Birck J.-L., RoyBarman M. and Capmas F. (1997) Re-Os measurements at the femtomole level in natural samples. *Geostandards Newsletter* **20**, 19-27.

Blendinger W. (1988) Permian to Jurassic deep water sediments of the Eastern Oman Mountains: Their significance for the evolution of the Arabia margin of South Tethys. *Facies* **19**, 1-32.

Bouma A.H. (1996) Initial comparison between fine- and coarse-grained submarine fans and the Brushy Canyon Formation sandstones. In: DeMis W.D. and Cole A.G. (Eds.), The Brushy Canyon play in outcrop and subsurface: Concepts and examples: Guidebook. *SEPM Publication, Permian Basin Section* **96-38**, 41-50.

Bowring S.A., Erwin D.H., Jin Y.G., Martin M.W., Davidek K., Wang W. (1998) U/Pb zircon geochronology and tempo of the end-Permian mass extinction. *Science* **280**, 1039-1045.

Boyer B.W. (1982) Green River laminites: Does the playa-lake model really invalidate the stratified-lake model? *Geology* **10**, 321-324.

Bradley W.H. (1931) Origin and microfossils of the oil shale of the Green River Formation of Colorado and Utah. *U.S. Geological Survey, Professional Paper* **168.**

Brandon A.D., Norman M.D., Walker R.J. and Morgan J.W. (1999) ^{186}Os-^{187}Os systematics of Hawaiian picrites. *Earth and Planetary Science Letters* **174**, 25-42.

Burton K.W., Bourdon B., Birck J.-L., Allegre C.J. and Hein J.R. (1999) Osmium isotope variations in the oceans recorded by Fe-Mn crusts. *Earth and Planetary Science Letters* **171**, 185-197.

Cohen A.S. and Waters F.G. (1996) Separation of osmium from geological materials by solvent extraction for analysis by TIMS. *Analytical Chimica Acta* **332**, 269-275.

Cohen A.S., Coe A.L. Bartlett J.M. and Hawksworth C.J. (1999) Precise Re-Os ages of organic-rich mudrocks and the Os isotope composition of Jurassic seawater. *Earth and Planetary Science Letters* **167**, 159-173.

Colodner D., Sachs J., Ravizza G., Turekian K.K., Edmond J. and Boyle E. (1993) The geochemical cycles of rhenium: A reconnaissance. *Earth and Planetary Science Letters* **117**, 205-221.

Creaser R.A., Papanastassiou D.A. and Wasserburg G.J. (1991) Negative thermal ion mass spectrometry of osmium, rhenium and iridium. *Geochimica et Cosmochimica Acta* **55**, 397-401.

Creaser R.A., Sannigrahi P., Chacko T. and Selby D. (2002) Further evaluation of the Re-Os geochronometer in organic-rich sedimentary rocks: A test of hydrocarbon maturation effects in the Exshaw Formation, Western Canada Sedimentary Basin. *Geochimica et Cosmochimica Acta* **66**, 3441-3452.

Crusius J. and Thompson J. (2000) Comparative behavior of authigenic Re, U, and Mo during reoxidation and subsequent long-term burial in marine sediments. *Geochimica et Cosmochimica Acta* **64**, 2233-2242.

Crusius J., Calvert S., Pedersen T. and Sage D. (1996) Rhenium and molybdenum enrichments in sediments as indicator of oxic, suboxic and sulfidic conditions of deposition. *Earth and Planetary Science Letters* **145**, 65-78.

Cumming V.M., Selby D. and Lillis P.G. (2012) Re-Os geochronology of the lacustrine Green River Formation: Insights into direct depositional dating of lacustrine successions, Re-Os systematics and paleocontinental weathering. *Earth and Planetary Science Letters* **359-360**, 194-205.

Cumming V.M. (2013) Rhenium-osmium geochronology and geochemistry of ancient lacustrine sedimentary and petroleum systems, Durham theses, Durham University. Available at Durham E-Thesis Oline: http://ethesis.dur.ac.uk/6945

Dickins J.M. and Shah S.C. (1987) The relationship of the Indian and western Australian Permian marine faunas. In: McKenzie G.D. (Ed.), Gondwana Six: Stratigraphy, Sedimentology and Paleontology. *Geophysical Monograms* **41**, 15-21.

Dutton S.P., Flanders W.A. and Barton M.D. (2003) Reservoir characterization of a Permian deep-water sandstone, East Ford field, Delware Basin, Texas. *AAPG Bulletin* **87**, 609-627.

Esser B.K. and Turekian K.K. (1993) The osmium isotopic compositions of the continental crust. *Geochimica et Cosmochimica Acta* **57**, 3093-3104.

Finlay A.J., Selby D. and Grocke D.R. (2010) Tracking the Hirnantian glaciations using Os isotopes. *Earth and Planetary Science Letters* **293**, 339-348.

Fischer A.G. and Sarnthein M. (1988) Airborne silts and dune-derived sands in the Permian of the Delaware Basin. *Journal of Sedimentary Petrology* **58**, 637-643.

Frakes L.A., Francis J.E., and Syktus J.I. (1992) Climate modes of the Phanerozoic: The history of Earth's climate over the past 600 million years. *Cambridge University Press,* Cambridge

Gardner M.H. and Borer J.M. (2000) Submarine channel architecture along a slope to basin profile, Brushy Canyon Formation, West Texas. In: Bouma A.H. and Stone C.G. (Eds.), Fine-grained turbidite systems. *AAPG Memoir* **72**, 195-215.

Gardner M.H. and Sonnenfeld M.D. (1996) Stratigraphic changes in facies architecture of the Permian Brushy Canyon Formation in Guadalupe Mountains National Park, West Texas. In: DeMis W.D. and Cole A.G. (Eds.), The Brushy Canyon play in outcrop and subsurface: Concepts and examples. *Permian Basin Section of the Society of Economic Paleontologists and Mineralogists Publication* **96-38**, 17-40.

Gardner M.H. (1992) Sequence stratigraphic and eolian-derived turbidites: Patterns of deep-water sedimentation along an arid carbonate platform, Permian (Guadalupian) Delaware Mountain Group, West Texas. In: Murk D.H. and Curran B.C. (Eds.), Permian Basin exploration and production strategies: Applications of sequence stratigraphic and reservoir characterization concepts. *West Texas Geological Society Publication* **92-91**, 7-12.

Gardner M.H. (1997a) Characterization of deep-water siliciclastic reservoirs in the upper Bell Canyon and Cherry Canyon Formations of the northern Delaware Basin, Culberson and Reeves Counties, Texas. In: Major R.P. (Ed.), Oil and gas on Texas state lands: An assessment of the resource and characterization of type reservoirs. *University of Texas, Bureau of Economic Geology Report of Investigations* **241**, 137-146.

Gardner M.H. (1997b) Sequence stratigraphy and hydrocarbon habitat of the Permian (Guadalupian) Delaware Mountain Group, Delaware Basin, west Texas. In: Major R.P. (Ed.), Oil and gas on Texas state lands: An assessment of the resource and characterization of type reservoirs. *University of Texas, Bureau of Economic Geology Report of Investigations* **241**, 147-157.

Gardner M.H., Borer J.M., Melick J.J., Mavilla N., Dechesne M. and Wagerle R.N. (2003) Stratigraphic process-response model for submarine channels and related features from studies of Permian Brushy Canyon outcrops, West Texas. *Marine and Petroleum Geology* **20**, 757-787.

Georgiev S., Stein H.J., Hannah J.L., Bingen B., Weiss H.M. and Piasecki S. (2011) Hot acidic Late Permian seas stifle life in record time. *Earth and Planetary Science Letters* **310**, 389-400.

Girty G.H. (1908) The Guadalupian Fauna. *United States Geological Survey Professional Paper* **58**, 1-683.

Glenister B.F., Wardlaw B.R., Lambert L.L., Spinosa C., Bowring S.A., Erwin D.H., Menning M. and Wilde G.L. (1999) Proposal of Guadalupian and component Roadian, Wordian and Capitanian Stages as International Standards for the Middle Permian Series. *Permophiles* **34**, 3-11.

Gramlich J.W., Murphy T.J., Garner E.L. and Shields W.R. (1973) Absolute isotopic abundance ratio and atomic weight of a reference sample of rhenium. *Journal of Research of the National Bureau of Standards* **77A**, 691-698.

Hannah J.L., Bekker A., Stein H.J., Markey R.J. and Holland H.D. (2004) Primitive Os and 2316 Ma age for marine shale: Implications for Paleoproterozoic glacial events and the rise of atmospheric oxygen. *Earth and Planetary Science Letters* **225**, 43-52.

Harms J.C. and Williamson C.R. (1988) Deep-water density current deposits of Delaware Mountain Group (Permian), Delaware Basin, Texas and New Mexico. *AAPG Bulletin* **72**, 299-317.

Harms J.C. (1974) Brushy Canyon Formation, Texas: A deep-water density current deposit. *GSA Bulletin* **85**, 1763-1784.

Harris N.B., Mnich C.A., Selby D. and Korn D. (2013) Minor and trace element and Re-Os chemistry of the Upper Devonian Woodford Shale, Permian Basin, west Texas: Insights into metal abundance and basin processes. *Chemical Geology* **356**, 76-93.

Hays P.D. and Tieh T.T. (1992) Organic geochemistry and diagenesis of the Delaware Mountain Group, West Texas and southeast New Mexico. *Transactions of American Association of Petroleum Geologists, Southwest Section* **92-90**, 155-175.

Henderson C.M., Mei S.L. and Wardlaw B.R. (2002) New conodont definition at the Guadalupian-Lopingian boundary. In: Hills L.V., Henderson C.M. and Bamber E.W. (Eds.), Carboniferous and Permian of the World. *Canadian Society of Petroleum Geologists Memoir* **19**, 725-735.

Hills J.M. (1984) Sedimentation, Tectonism, and Hydrocarbon Generation in Delaware Basin, West Texas and Southeastern New Mexico. *AAPG Bulletin* **68**, 250-267.

Justman H.A. (2001) Petroleum source rocks in the Brushy Canyon Formation (Permian), Delaware Basin, southestern New Mexico. M.S. Thesis, Earth and Environmental Sciences Department, New Mexico Institute of Mining and Technology, 106 pp.

Kendall B.S., Creaser R.A., Ross G.M. and Selby D. (2004) Constraints on the timing of Marinoan 'Snowball Earth' glaciations by ^{187}Re-^{187}Os dating of a Neoproterozoic post-glacial black shale in Western Canada. *Earth and Planetary Science Letters* **222,** 729-470.

Kendall B.S., Creaser R.A. and Selby D. (2009) ^{187}Re-^{187}Os geochronology of Precambrian organic-rich sedimentary rocks. *Geological Society of London Special Publications* **326**, 85-107.

Kerans C., Fitchen W.M., Gardner M.H., Sonnenfeld M.D., Tinker S.W., and Wardlaw B.R. (1992) Styles of sequence development within uppermost Leonardian through Guadalupian strata of the Guadalupe Mountains, Texas and New Mexico. In: Murk D.H. and Curran B.C. (Eds.), Permian Basin exploration and production strategies: Applications of sequence stratigraphic and reservoir characterization concepts. *West Texas Geological Society Publication* **92-91**, 1-7.

Kerans C., Fitchen W.M., Gardner M.H. and Wardlaw B.R. (1993) A contribution to the evolving stratigraphic framework of latest Leonardian-Guadalupian strata of the Delaware Basin. In: Adams J.W. and others (Eds.), Carlsbad Region, Permian Basin, new Mexico and Texas. *New Mexico Geological Society 44th Annual Field Conference Guidebook,* 175-184.

King P.B. (1948) Geology of the southern Guadalupe Mountains, Texas. *United States Geological Survey Professional Paper* **251**, 183.

Koide M., Goldberg E.D., Niemeyer S., Gerlach D., Hodge V., Bertine K.K. and Padova A. (1991) Osmium in marine sediments. *Geochimica et Cosmochimica Acta* **55**, 1641-1648.

Korte C., Jasper T., Kozur H.W. and Veizer J. (2006) $^{87}Sr/^{86}Sr$ record of Permian seawater. *Palaeo* **240**, 89-107.

Kozur H. (1984) Perm. In: Troger K.-A. (Ed.), Abriβ der Historischen Geologie. Akademie-Verlag, Berlin 270-307.

Levasseur S., Birck J. and Allegre C.J. (1998) Direct measurement of femtomoles of osmium and the $^{187}Os/^{186}Os$ ratio in seawater. *Science* **282**, 272-274.

Levasseur S., Birck J. and Allegre C.J. (1999) The osmium riverine flux and oceanic mass balance of osmium. *Earth and Planetary Science Letters* **174**, 7-23.

Lewan M.D. and Maynard J.B. (1982) Factors controlling enrichment of vanadium and nickel in the bitumen of organic sedimentary rocks. *Geochimica et Cosmochimica Acta* **46**, 2547-2560.

Ludwig K. (2008) Isoplot, version 4.0: A geochronological toolkit for Microsoft Excel. *Berkeley Geochronology Center Special Publication* **4,** 1-12.

Magaritz M., Anderson R.Y., Holser W.T., Saltzman E.S. and Garber J. (1983) Isotope shifts in the Late Permian of the Delaware Basin, Texas, precisely timed by varved sediments. *Earth and Planetary Science Letters* **66**, 111-124.

Markey R.J., Stein H.J., Hannah J.L., Zimmerman A., Selby D. and Creaser R.A. (2007) Standardizing Re-Os geochronology: A new molybdenite reference material (Henderson, USA) and the stoichiometry of Os salts. *Chemical Geology* **244**, 74-87.

McArthur J.M., Algeo T.J., van de Schootbrugge B., Li Q. and Howarth R.J. (2008) Basinal restriction, black shales, Re-Os dating, and the Early Toarcian (Jurassic) oceanic anoxic event. *Paleoceanography* **23**, PA4217.

Mei S.L. and Henderson C.M. (2002) Conodont definition of the Kungurian (Cisuralian) and Roadinian (Guadalupian) boundary. In: Hills L.V., Henderson C.M. and Bamber E.W. (Eds.), Carboniferous and Permian of the World. *Canadian Society of Petroleum Geologists Memoir* **19**, 529-551.

Meissner F.F. (1972) Cyclic sedimentation in Middle Permian strata of the Permian Basin, West Texas and New Mexico. In: Elam J.G. and Chuber S. (Eds.), Cyclic sedimentation in the Permian Basin (2nd edition), *West Texas Geological Society* **72-60,** 203-232.

Milliken M.S. (1994) Correlation and depositional environment using major elements and trace elements: Cores DB-01 and DB-02, northwest shelf of the Delaware Basin, Culberson County, Texas. Unpublished Thesis, *University of Houston, Houston, TX*.

Morford J.L. and Emerson S. (1999) The geochemistry of redox sensitive trace metals in sediments. *Geochimica et Cosmochimica Acta* **63**, 1735-1750.

Morford J.L., Martin W.R., Francois R. and Carney C.M. (2009) A model for uranium, rhenium, and molybdenum diagenesis in marine sediments based on results from coastal locations. *Geochimica et Cosmochimica Acta* **73**, 2938-2960.

Newell N.D., Rigby J.K., Fischer A.G., Whiteman A.J., Hickox J.E. and Bradley J.S. (1953) The Permian Reef Complex of the Guadalupe Mountains Region, Texas and New Mexico. *Publisher W.H. Freeman, San Francisco, CA.*

Oriel S.S., Myers D.A. and Crosby E.J. (1967) West Texas Permian Basin Region. In: McKee E.D., Oriel S.S. and others (Eds.), 1967 Paleotectonics investigations of the Permian system in the United States. *United States Geological Survey Professional Paper* **515**, 21-60.

Oxburgh R. (1998) Variations in the osmium isotope composition of sea water over the past 200,000 years. *Earth and Planetary Science Letters* **159**, 183-191.

Payne M.W. (1976) Basinal sandstone facies, Delaware Basin, West Texas and Southeast New Mexico. *AAPG Bulletin* **60**, 514-527.

Pegram W.J., Krishnaswami S., Ravizza G.E. and Turekian K.K. (1992) The record of sea water $^{187}Os/^{186}Os$ variation through the Cenozoic. *Earth and Planetary Science Letters* **113**, 569-576.

Peucker-Ehrenbrink B. and Blum J.D. (1998) Re-Os isotope systematics and weathering of Precambrian crustal rocks: Implications for the marine osmium isotope record. *Geochimica et Cosmochimica Acta* **62**, 3193-3203.

Peucker-Ehrenbrink B. and Jahn B.-M. (2001) Rhenium-osmium isotope systematics and platinum group element concentrations: Loess and the upper continental crust. *Geochemistry Geophysics Geosystems* **2**, 1-22.

Peucker-Ehrenbrink B. and Ravizza G. (2000) The marine osmium isotope record. *Terra Nova* **12**, 205-219.

Pillevuit A., Marcoux J., Stampfli G., Baud A. (1997) The Oman exotics: A key to the understanding of the Neotethyan geodynamic evolution. *Geodin. Acta* **10**, 209-238.

Poirier A., Hillaire-Marcel, C. (2011) Improved Os-isotopic stratigraphy of the Arctic Ocean. *Ocean. Geophys. Res. Lett.* **38**, L14607.

Pratt L.M. (1984) Influence of paleoenvironmental factors on the preservation of organic matter in Middle Cretaceous Greenhorn Formation near Pueblo, Colorado. *AAPG Bulletin* **68**, 1146-1159.

Ravizza G.E. and Peucker-Ehrenbrink B. (2003) The marine $^{187}Os/^{188}Os$ record of the Eocene-Oligocene transition: The interplay of weathering and glaciations. *Earth and Planetary Science Letters* **210**, 151-165.

Ravizza G. and Turekian K.K. (1989) Applications of the ^{187}Re-^{187}Os system to black shale geochronometry. *Geochimica et Cosmochimica Acta* **53**, 3257-3262.

Ravizza G., Turekian K.K. and Hay B.J. (2001) The geochemistry of rhenium and osmium in recent sediments from the Black Sea. *Geochimica et Cosmochimica Acta* **55**, 3741-3752.

Rooney A.D., Selby D., Houzay J.-P. and Renne P.R. (2010) Re-Os geochronology of a Mesoproterozoic sedimentary succession, Taoudeni Basin, Mauritania: Implications for basin-wide correlations and Re-Os organic-rich sediments systematics. *Earth and Planetary Science Letters* **289**, 486-496.

Sageman B.B., Gardner M.H., Armentrout J.M. and Murphy A.E. (1998) Stratigraphic hierarchy of organic carbon-rich siltstones in deep-water facies, Brushy Canyon Formation (Guadalupian), Delaware Basin, West Texas. *Geology* **26**, 451-454.

Schmitz B., Peucker-Ehrenbrink B., Heilmann-Clausen C., Aberg G., Asaro F. and Lee C.A. (2004) Basaltic explosive volcanism, but no comet impact, at the Paleocene-Eocene boundary: High-resolution chemical and isotopic records from Egypt, Spain and Denmark. *Earth and Planetary Science Letters* **225**, 1-17.

Schwarzbach M. (1974) Das Klima der Vorzeit. *Eine Einfuhrung in die Palaoklimatologie*. Enke, Stuttgart.

Selby D. and Creaser R.A. (2001) Re-Os geochronology and systematics in molybdenite from the Endako porphyry molybdenum deposit, British Columbia, Canada. *Economic Geology* **96**, 197-204.

Selby D. and Creaser R.A. (2003) Re-Os geochronology of organic rich sediments: An evaluation of organic matter analysis methods. *Chemical Geology* **200**, 225-240.

Smoliar M.I., Walker R.J. and Morgan J.W. (1996) Re-Os isotope constraints on the age of Group IIA, IIIA, IVA, and IVB iron meteorites. *Science* **271**, 1099-1102.

Soreghan G.S. and Soreghan M.J. (2013) Tracing clastic delivery to the Permian Delaware Basin, U.S.A.: Implications for paleogeography and circulation in westernmost equatorial Pangea. *Journal of Sedimentary Research* **83**, 786-802.

Stampfli G.M., Mosar J., Favre P., Pillevuit A., and Vannay J.-C. (2001) Permo-Mesozoic evolution of the western Tethyan realm: The Neotethys/East-Mediterranean connection. In: Zielger P.A., Cavazza W., Roberson A.H.F. and Crasquiin-Soleau S. (Eds.), PeriTethys Memoir 6: Peritethyan rift/Wrench basins and passive margins, IGCP 369. Mem Museum of Natural History **186**, 51-108.

Stampfli G.M. (2000) Tethyan oceans. In: Bozkurt E., Winchester J.A. and Piper J.D.A. (Eds.), Tectonics and Magmatism in Turkey and surrounding area. Geological Society of London, Special Publication **173**, 1-23.

Sundby B., Martinez P. and Gobeil C. (2004) Comparative geochemistry of cadmium, rhenium, uranium, and molybdenum in continental margin sediments. *Geochimica et Cosmochimica Acta* **68**, 2485-2493.

Tribovillard N., Algeo T., Lyons T.W. and Riboulleau A. (2006) Trace metals as paleoredox and paleoproductivity proxies: An update. *Chemical Geology* **232**, 12-32.

Turgeon S.C. and Creaser R.A. (2008) Cretaceous oceanic anoxic event 2 triggered by a massive magmatic episode. *Nature Letters* **454**, 323-326.

Tuttle M.L. and Goldhaber M.B. (1993) Sedimentary sulfur geochemistry of the Paleogene Green River Formation, western USA: Implications and geochemical approach, Devonian Appalachian Basin. *Paleogeography, Paleoclimatology, Paleoecology* **304**, 54-73.

Volkening J., Walczyk T. and Heumann K.G. (1991) Osmium isotope ratio determinations by negative thermal ionization mass spectrometry. *International Journal of Mass Spectrometry and Ion Processes* **105**, 147-159.

Walker R.J., Prichard H.M., Ishiwatari A., Pimentel M. (2002) The osmium isotopic composition of convecting upper mantle deduced from ophiolite chromites. *Geochimica et Cosmochimica Acta* **66**, 329-345.

Yamashita Y., Takahashi Y., Haba H., Enomoto S. and Shimizu H. (2007) Comparison of reductive accumulation of Re and Os in seawater-sediment systems. *Geochimica et Cosmochimica Acta* **71**, 3458-3475.

Ye Q. and Kerans C. (1996) Reconstructing Permian Eustasy from 2-D backstripping and its use in forward models; Lower and Middle Guadalupian facies, Stratigraphy, and reservoir geometries; San Andres/Grayburg Formations, Guadalupe Mountains, New Mexico and Texas. In: Moore G.E. and Wilde G.L. (Eds.), Symposium and Guidebook *SEPM, Permian Basin Section* **86-25; 69-74.**

York D. (1969) Least-squares fitting of a straight line with correlated errors. *Earth and Planetary Science Letters* **5**, 320-324.

Zelt F.B. and Rossen C. (1995) Geometry and continuity of deep-water sandstones and siltstones, Brushy Canyon Formation (Permian) Delaware Mountains, Texas. In: Pickering K.T., Hiscott R.N., Kenyon N.H., Ricci-Luchi F. and Smith R.D.A. (Eds.), Atlas of deep water environments, architectural style in turbidite Systems. *London: Chapman and Hill*, 167-183.

Ziegler A.M., Hulver M.L. and Rowley D.B. (1997) Permian world topography and climate. In: Martini I.P. (Ed.), Late glacial and postglacial environmental changes: Quaternary, Carboniferous-Permian, and Proterozoic. *Oxford, U.K. Oxford University Press*, 111-146.

CHAPTER 2:

RHENIUM-OSMIUM GEOCHRONOLOGY AND GEOCHEMISTRY OF THE TASMANITE OIL SHALE, TASMANIA: PERMIAN TIME-SCALE CALIBRATION AND THE CONSTRUCTION OF THE PALEOZOIC SEAWATER $^{187}Os/^{188}Os$ CURVE.

2.1. INTRODUCTION

Temporal changes in local and global seawater geochemistry have been preserved in the rock record and are traditionally recovered using predominantly O, C, and Sr isotopes. Because of recent advances in analytical geochemistry, the ^{187}Re-^{187}Os isotopic system ($t_{1/2}$ = 41.6 by; Smoliar et al., 1996) has also become a useful geochronometer and isotopic tracer that has begun to be applied to understanding the evolution of seawater during different time intervals. The Os isotopic composition of organic-rich mud rocks (ORM) reflects the $^{187}Os/^{188}Os$ composition of seawater at the time their respective sediments were deposited. Rhenium and Os are redox-sensitive and organophilic in nature, and are suggested to be sequestered by organisms at, or below the sediment-water interface in both marine and lacustrine basins under suboxic, anoxic, or euxinic conditions and are thus hydrogenous in nature (Koide, 1991; Colodner et al., 1993; Crusius et al., 1996; Morford et al., 2009; Cumming et al., 2012). Studies of seawater evolution using $^{87}Sr/^{86}Sr$ ratios have demonstrated Sr variation throughout the Phanerozoic (Veizer and Compston, 1974; Burke et al., 1982; Denison et al., 1994; Denison et al., 1997; Veizer et al., 1999; Ebneth et al., 2001). However, the long residence time of Sr of 1-4 Myr means that Sr isotopes are averaged out, or muted and potentially miss influences on seawater chemistry on shorter timescales. The residence time of Os in seawater is a ~10,000 – 50,000 yrs. (Peucker-Ehrenbrink and Ravizza, 2000). Because of this, high-frequency isotopic changes on the order of tens to hundreds of thousands of years in seawater chemistry (such as orbitally forced, glacial-interglacial cycles) are potentially resolvable with Os isotopes. Rhenium and Os in ORM are being

used more frequently in geochronology for providing depositional ages for these rocks (Ravizza and Turekian, 1989; Cohen et al., 1999; Creaser et al., 2002; Selby and Creaser, 2003; Hannah et al., 2004; Kendall et al., 2004; Finlay et al., 2010; Rooney et al., 2010). In addition, the $(^{187}Os/^{188}Os)_i$ (isotopic ratio at the time of rock formation) of ORM can be used to investigate potentially small chemical changes in the temporal evolution of seawater on shorter timescales which aren't captured by Sr isotopes (Oxburgh, 1998; Peucker-Ehrenbrink and Ravizza, 2000). The $^{187}Os/^{188}Os$ ratio of seawater is derived from a balance of two primary inputs: (1) Radiogenic Os from river water during weathering and subsequent continental runoff of upper continental crust (Esser and Turekian, 1993; Peucker-Ehrenbrink and Jahn, 2001), and (2) less-radiogenic Os from the mantle via seafloor spreading and production of mid-ocean ridge basalts, flood basalt events, hydrothermal alteration of oceanic crust, or from meteorite influx (Peucker-Ehrenbrink and Ravizza, 2000; Schmitz et al., 2004). The relative contributions of these sources have varied significantly throughout geologic history leading to significant variations in the $^{187}Os/^{188}Os$ of seawater. From the $(^{187}Os/^{188}Os)_i$ of ORM at any given time of formation, a mass balance calculation can be used to determine the relative contribution of radiogenic and non-radiogenic Os to seawater. Inferences can then be made about the degree of continental weathering (Ravizza et al., 2001; Schmitz et al., 2004), seafloor spreading rates, the eruption of flood basalts (Cohen et al., 1999; Ravizza and Peucker-Ehrenbrink, 2003; Turgeon and Creaser, 2008) as well as the timing and size of meteorite impacts (Paquay et al., 2008).

The majority of ORM studies have focused on $^{187}Os/^{188}Os$ ratio stratigraphy not only to construct the marine Os isotopic curve through time, but also to examine temporal perturbations in the record as they apply to changes in global ocean geochemistry caused by paleoclimate, tectonic, or extraterrestrial processes (Widom et al., 2004; Turgeon et al., 2007; Turgeon and Creaser, 2008; Du Vivier et al., 2014). The Cenozoic has received considerable attention. These studies have reported a steady increase in the $^{187}Os/^{188}Os$ ratio of seawater throughout the Cenozoic, increasing from a $^{187}Os/^{188}Os$ value of 0.20 at the K-T boundary to 1.06 at present day (Pegram et al., 1992; Ravizza, 1993; Peucker-Ehrenbrink et al., 1995; Turekian and Pegram, 1997; Pegram and Turekian, 1999; Peucker-Ehrenbrink and Ravizza, 2000). This $^{187}Os/^{188}Os$ trend is similar to the trend observed in increasing $^{87}Sr/^{86}Sr$ of this time interval. This progressive increase is interpreted to reflect an increase in continental weathering likely resulting from the uplift of the Himalayas (Raymo and Ruddiman, 1992; Richter et al., 1992). This tectonic forcing results in a consequent increase in the flux of crustal, radiogenic Os to the oceans. If Os-enriched rocks such as ORM and Precambrian crust ($^{187}Os/^{188}Os \leq 13.6$) are exposed to weathering, the resultant effect on the $^{187}Os/^{188}Os$ ratio of seawater is magnified (Peucker-Ehrinbrink and Blum, 1998).

Efforts to reconstruct the pre-Cenozoic record of seawater $^{187}Os/^{188}Os$ focus on specific geologic events such as pre-Cambrian glaciations (Kendall et al., 2004; Rooney et al., 2014), orogenic events (Rooney et al., 2010; Rooney et al., 2011), the onset of atmospheric oxygenation (Hannah et al., 2004) and important stratigraphic boundaries (Selby and Creaser, 2005; Turgeon et al., 2007; Selby et al., 2009; Du Vivier et al.,

2014). Few studies have focused on the Paleozoic. The few extant data suggest that Paleozoic seawater had radiogenic $^{187}Os/^{188}Os$ compositions, within the range of Cenozoic values (Peucker-Ehrenbrink and Ravizza, 2012). However, despite the 289 Myr span of the Paleozoic, most of the available $^{187}Os/^{188}Os$ data are grouped around the Devonian/Mississippian boundary, and many of these data have large uncertainty. The lack of data for the Paleozoic is present primarily due to the substantial analytical effort required to obtain accurate and precise $^{187}Os/^{188}Os$ values (Peucker-Ehrenbrink and Ravizza, 2012).

In order to begin to establish the Os-isotope evolution of seawater during the Paleozoic, this study reports new Re-Os geochronology for the Permian Tasmanite oil shale from Tasmania and provides a $^{187}Os/^{188}Os$ value for seawater in the earliest Permian. This is coupled with a compilation of previously published Re-Os isotope data, many of which have not been included in previous review papers, to present a first-order examination of the Paleozoic seawater $^{187}Os/^{188}Os$ record. The long-term goal of this work is to determine the processes that control the $^{187}Os/^{188}Os$ of seawater within the Paleozoic and to compare these constraints to what occurred during other times.

2.2. GEOLOGIC SETTING

During the Late Pennsylvanian and Early Permian, Tasmania was positioned within the southern polar circle, close to a polar latitude of ~80° (Li and Powel, 2001) as part of Gondwana (Figure 2.1). The onshore Tasmania Basin was glaciated during this time in the Late Paleozoic Ice Age (Veevers and Powell, 1987; Clarke and Forsyth, 1989; Dickins, 1996; Lopez-Gamundi, 1997; Isbell et al., 2003). This basin contains a

glaciomarine to terrestrial sequence of Late Carboniferous to Late Triassic age which unconformably overlies Precambrian and Paleozoic folded and metamorphosed sedimentary and igneous rocks (Reid and Burrett, 2004). This sequence, The Parmeener Supergroup was deposited in an intra-cratonic basin that was active during the Pennsylvanian to Late Triassic where sediment accumulated over a glacially-influenced, fragmented shelf with local topographic highs, in a fjord-like seaway (Clarke and Forsyth, 1989; Hand, 1993; Lopez-Gamundi, 2010). The Parmeener Supergroup is subdivided into the Lower Parmeener and Upper Parmeener Supergroups based on lithostratigraphic properties. This study will focus on the Lower Parmeener Supergroup (Figure 2.2).

The Late Pennsylvanian-Middle Permian Lower Parmeener Supergroup is predominantly glaciomarine. The confinement of glacigenic formations within this unit, deep structural depo-centers, abrupt lateral facies changes and pinching out of sedimentary units onto marginal structural highs, suggests that the majority of the lower Early Permian strata were deposited in a series of grabens or half-grabens separated by uplifted horsts during a period of extensional subsidence within the basin (Fielding et al., 2010) and throughout eastern Australia (Korsch et al., 2009). This wide-spread extension created a large number of discrete intra-cratonic basins, some of which later coalesced to form the larger Bowen-Gunnedah-Sydney Basin system (Clarke, 1989*)*. The base of the Lower Parmeener Supergroup is characterized by thick Late Pennsylvanian diamictites, glacial outwash conglomerates and sandstones, and local mudstones and rythmites of the

Wynyard Formation, also called the Truro or Stocker's Tillite (Clarke, 1989; Hand, 1993).

The Quamby mudstone represents a widespread marine transgression that covered most of Tasmania as glaciers retreated during the Asselian (Brakel and Totterdell, 1993; Hand, 1993; Lopez-Gamundi, 2010). The low terrigenous content and high concentration of pelagic organic carbon of the Tasmanite horizon, in addition to the overall facies succession of the Quamby Mudstone have been interpreted to indicate that the Tasmanite horizon represents the maximum flooding surface of the post-glacial marine transgression, and thus is a global, time-synchronous horizon in the succession of post-glacial events in the Early Permian (Lopez-Gamundi, 2010).

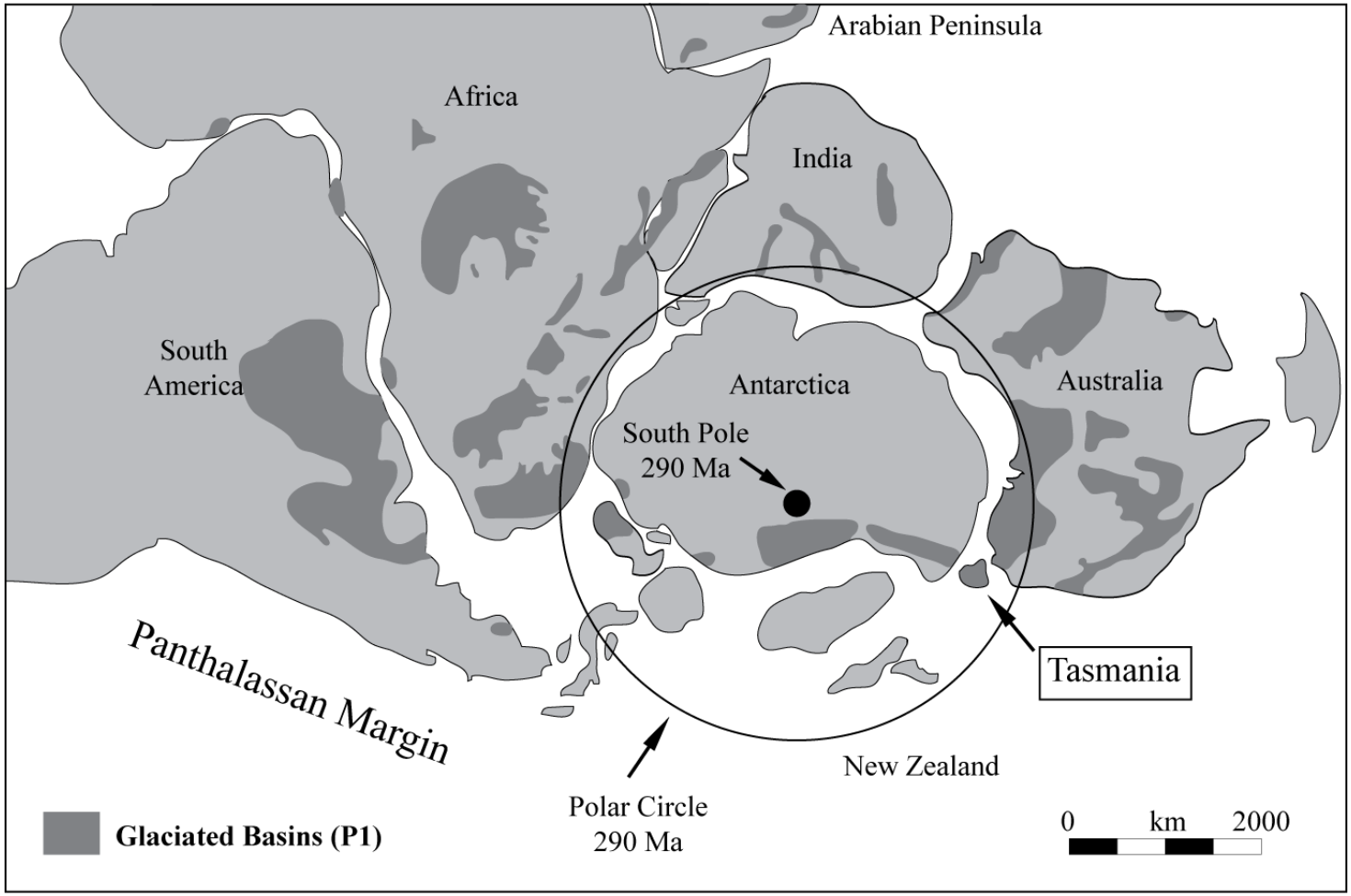

Figure 2.1. Paleogeographic reconstruction of Gondwana at 290Ma highlighting the location of Tasmania within the polar circle. Dark gray polygons represent basins that were glaciated during the Late Paleozoic, P1 glaciation. Modified after Isbell et al. (2003).

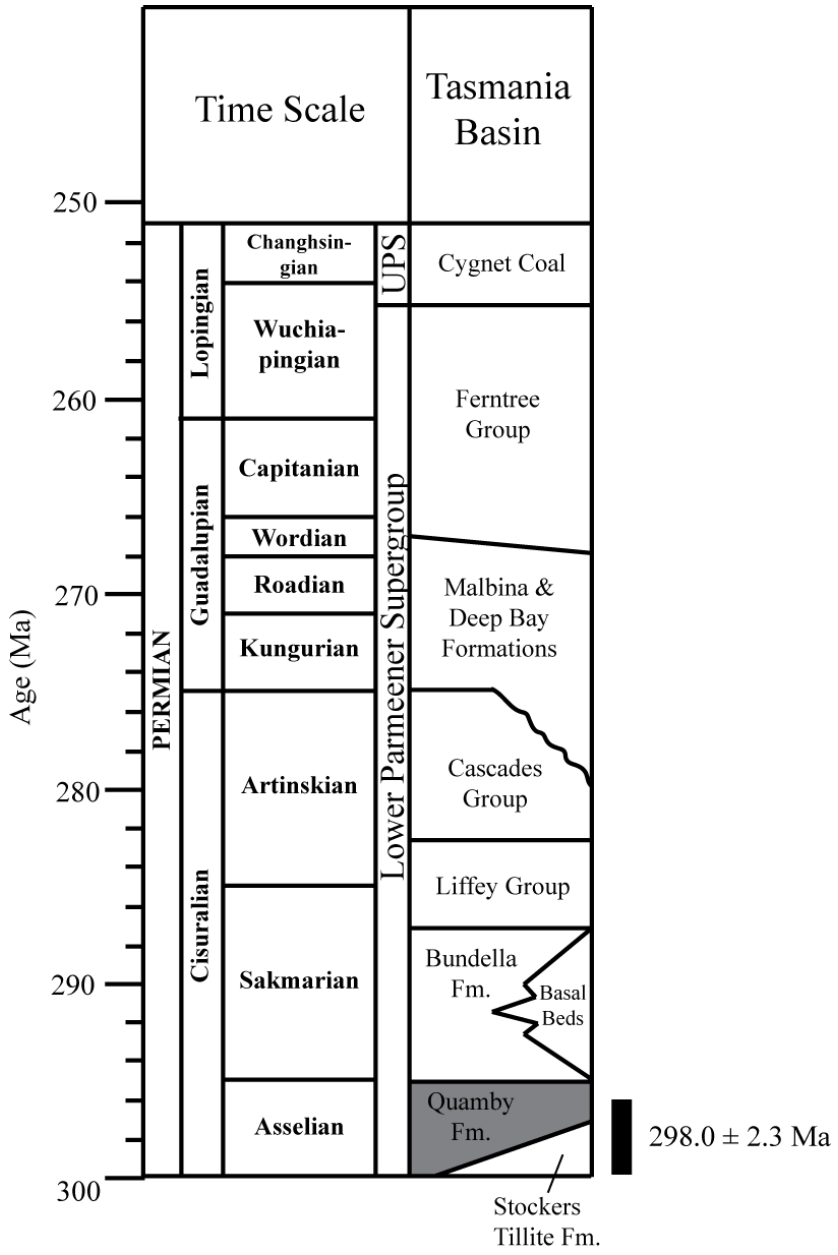

Figure 2.2. Simplified stratigraphic column of the Tasmania Basin during the Permian. UPS = Upper Parmeener Supergroup. Black bar show the Re-Os age for the Tasmanite Oil Shale within the Quamby Mudstone achieved in this study. Modified after Fielding et al. (2010).

The tillite-to-marine-mudstone transition that is observed in Tasmania has been correlated with similar successions in Antarctica, Eastern Australia, and South Africa (Lindsay, 1970; Miller, 1989; Collinson et al., 1994; Isbell et al., 2008; Stollhofen et al., 2000) and is interpreted as the termination of the P1 glaciation episode in the Sakmarian, one of many periodic glacial episodes of the Late Paleozoic Ice Age. This horizon thus provides critical information in providing key correlations between well-known glacigenic successions in Gondwana.

Marine conditions continued into the Late-Sakmarian with gradual filling of the Tasmania Basin through the deposition of the Bundella Formation. The Bundella Formation is a fossiliferous siltstone and sandstone followed by the marginal marine, organic-rich siltstones of the Macrae Mudstone and the non-marine sandstones and carbonaceous siltstones of the Sakmarian-Artinskian Liffey Group. The Liffey Group is interpreted to represent an alluvial plain environment and complete filling of the basin (Banks, 1980; Clarke, 1989; Reid and Burrett, 2004). A marine transgression in the mid-Early Permian brought marine conditions back to the Tasmania Basin with the deposition of marginal marine, then shallow shelf marine fossiliferous siltstones, limestones, and minor sandstones of the Cascades Group (Clarke, 1989). In the Late-Artinskian to Kungurian, the Cascades Group was overstepped by fossiliferous siltstone and sandstone of the Deep Bay and Malbina Formations (Farmer, 1985). By the Late Permian, the deposition of shallow marine to estuarine mudstone and siltstone of the Fern Tree Group resulted in an almost filled Tasmania Basin (Reid and Burrett, 2004). The Late Permian

marks the top of the Lower Parmeener Supergroup, preceding the deposition of the Upper Parmeener Supergroup.

Age control for the tillite-to-marine-mudstone transition at the base of the Quamby is entirely based on biostratigraphic data (Fielding et al., 2010) and primarily on regional zonations of macro-invertebrates of Clarke and Farmer (1976) and micro-flora. These zonations have been correlated in detail to similar successions in eastern Australia and the Australian late Paleozoic palynostratigraphic zonations (Fielding et al., 2010), however, have not been correlated with other portions of Gondwana. A direct, absolute and precise age for this glacigenic-marine transition will provide useful in the test for the episodic glaciation hypothesis to explain the protracted periods of glacial and non-glacial conditions in the Permian phase of the late Paleozoic Ice Age and how they relate to global paleoclimatic changes. In addition, the $(^{187}Os/^{188}Os)_i$ obtained from a Re-Os isochron will provide constraints on the Os isotopic composition of seawater during the earliest Permian and provide another data point toward the construction of a Paleozoic seawater $^{187}Os/^{188}Os$ curve.

2.3. SAMPLING AND ANALYTICAL PROCEDURES

2.3.1. Sampling

Samples used in this study were taken from three research cores (Douglas River, Tunbridge, and Ross B.H. #2) that were drilled in the Tasmania Basin (Figure 2.3). All research cores penetrate the Quamby Mudstone and the entire Tasmanite marker horizon and together represent ~100 km of lateral sampling across Tasmania (Figure 2.3). Six 1-

inch core plugs were taken from the Tasmanite horizon across the three cores. The entire outer surface of the core plugs were sanded with silicon carbide to remove any drill markings and possible metal contamination that could have been obtained during coring, cleaned with ethanol, and left to air dry. Each plug was split into several samples. A 20 g aliquot of each plug, representing a stratigraphic interval of ~2 cm, was then broken into chips and powdered using a mortar and pestle. While the actual amount of powder used for each Re-Os analysis is much less, larger aliquots of powdered sample were used to minimize the effects of Re and Os heterogeneity within a sample (Kendall et al., 2009).

2.3.2. Re-Os Geochemistry

Approximately 0.3 g of powdered sample was weighed and transferred to a thick-walled, internally cleaned, borosilicate glass Carius tube along with a known amount of a mixed ^{185}Re + ^{190}Os spike and 8mL of a chromic acid solution created by dissolving $Cr^{VI}O_3$ powder into 4N H_2SO_4 (0.25g/mL). The CrO_3-H_2SO_4 method was used to preferentially dissolve and oxidize hydrogenous Re and Os which yields more accurate and precise ages (Selby and Creaser, 2003). The Carius tubes were sealed, and sample and spike were digested and equilibrated at 240°C for 48 hours. Digestion dissolves sample powders and oxidizes sample Re and Os to ReO_3^- and OsO_4^- species, respectively. Following digestion the Carius tubes were frozen in a dry ice – ethanol slurry, opened, then thawed, and Os was isolated from the CrO_3-H_2SO_4 solution using $CHCl_3$ solvent extraction at room temperature (Cohen and Waters, 1996), back extracted into 9N HBr and further purified via micro-distillation (Birck et al., 1997). Rhenium was removed from the CrO_3-H_2SO_4 solution by anion column chromatography following reduction of the Cr^{VI} to Cr^{III} using

Milli-Q and bubbling with SO_2 gas. Rhenium was further purified by passing the output of the first column through a second anion column. The isolated Re and Os were then loaded onto ultra-pure (>99.99%) Ni and Pt filaments, respectively, and coated with activator solutions of $Ba(NO_3)_2$ and $Ba(OH)_2$, respectively.

The Re and Os isotopic compositions were determined by isotope-dilution-negative-thermal-ionization mass spectrometry (ID-NTIMS) on a ThermoElectron TRITON TIMS at the University of Houston (Creaser et al., 1991; Volkening et al., 1991). Rhenium was measured as ReO_3 via static Faraday collection and Os as OsO_4 via ion-counting using a secondary electron multiplier in peak-hopping mode. Measured isotopic ratios were spike stripped, corrected for isobaric oxygen interference, instrumental mass fractionation (using $^{185}Re/^{187}Re=0.59738$ and $^{192}Os/^{188}Os=3.08761$), and procedural blank contributions. Uncertainties were obtained through the error propagation of uncertainties in blank abundance and isotopic composition, spike abundance values, mass spectrometry measurements of Re and Os, and the reproducibility of the Re and Os isotopic values of the standard. Average procedural blanks were 19 ± 10 (2σ, n=16) pg for Re and 0.60 ± 1.1 (2σ, n=18) pg for Os with a $^{187}Os/^{188}Os = 0.16 \pm 0.02$ (2σ, n=18).

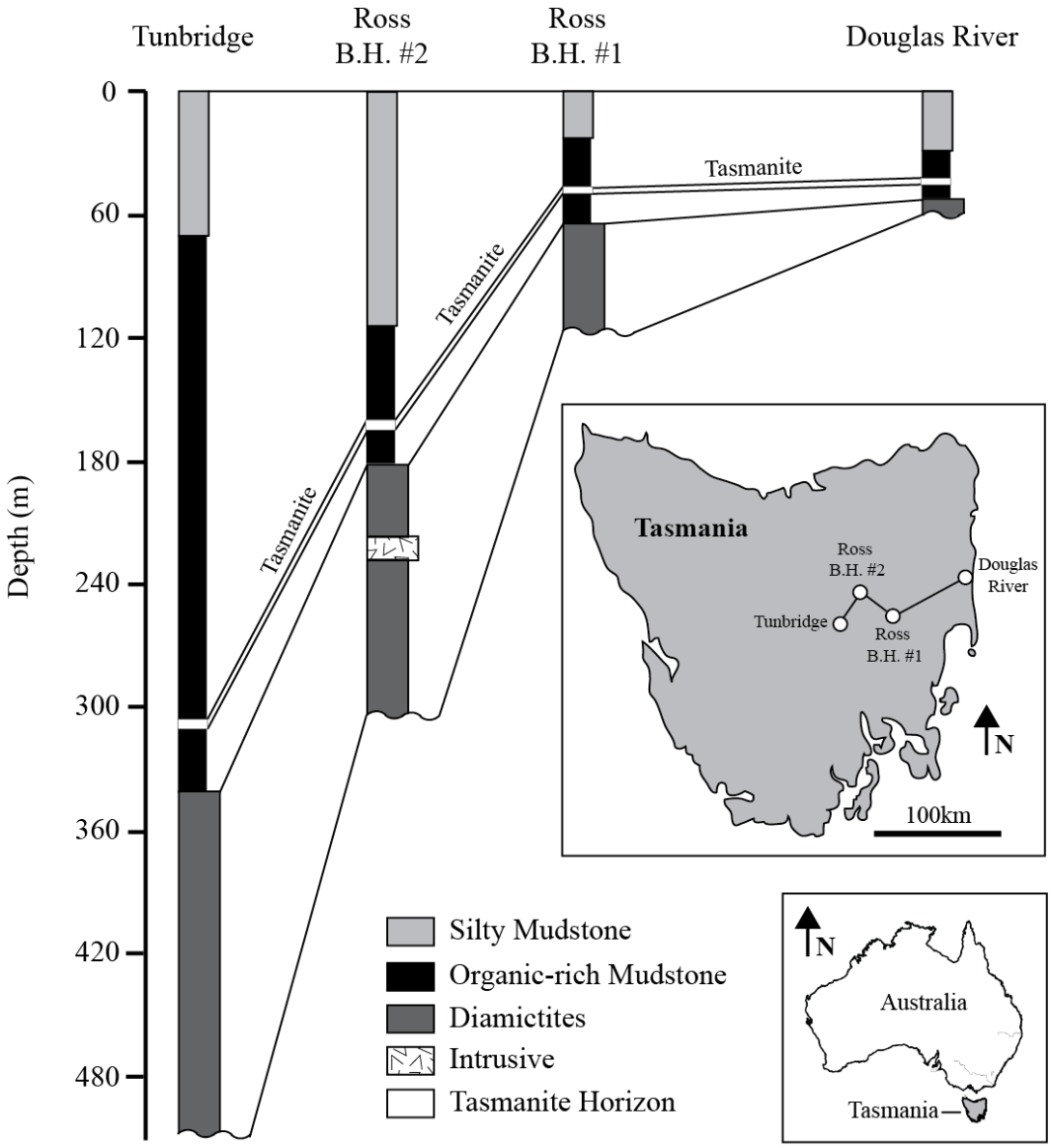

Figure 2.3. Stratigraphic correlation of the Tasmanite Oil Shale within the cores used in this study. Modified after Domack et al. (1993) and Lopez-Gamundi (2010).

Repeat measurements of Re and Os standards were performed throughout the analytical campaign. The Re standard, made from zone-refined Re ribbon, yields an average $^{185}Re/^{187}Re$ ratio of 0.59783 ± 0.00022 (2σ, n=16) for 1.5ng loads using static Faraday collection. The difference between the measured Re standard value and the established standard value of 0.59738 ± 0.0039 (Gramlich et al., 1973) was used to correct the measured $^{185}Re/^{187}Re$ ratios of samples used in this study. The Os standard (University of Maryland, Brandon et al., 1999), yielded a $^{187}Os/^{188}Os$ ratio of 0.11385 ± 0.00026 (2σ, n=18) for 500pg loads using a secondary electron multiplier and is, within uncertainty, identical to that reported by Brandon et al. (1999).

The Re-Os ages and $(^{187}Os/^{188}Os)_i$ are obtained via modified York regression (York, 1969) of the reduced isotopic data and propagated 2σ uncertainties using *Isoplot v. 4.15* (Ludwig, 2008). Errors are calculated using the maximum-likelihood estimation algorithm and are reported as 2σ.

2.4. RESULTS

The Re-Os abundances and isotopic compositions for Tasmanite horizon samples are presented in Table 2.1. All samples are enriched in Re (4-17 ppb) and Os (99-233 ppt) compared to modern-day average continental crust (~1 ppb Re and 30-50 ppt Os; Esser and Turekian, 1993) and have typical abundances of ORM (Ravizza and Turekian, 1989; Cohen et al., 1999; Creaser et al., 2002; Selby and Creaser, 2003; Hannah et al., 2004; Kendall et al., 2004; Finlay et al., 2010; Rooney et al., 2010). The $^{187}Re/^{188}Os$ ratios

range from 236 to 992 and are positively correlated with $^{187}Os/^{188}Os$ ratios of 1.75 to 5.50.

Rhenium and Os abundances and $^{187}Re/^{188}Os$ are lowest in samples from the Ross #1 core (4.0-4.5 ppb, 99-100 ppt, 230-260, respectively). Rhenium abundances and $^{187}Re/^{188}Os$ are highest in the Douglas River samples (11-17 ppb, 753-992), while Os abundances are highest in Tunbridge samples (151-233 ppt).

Linear regression of the Douglas River, Tunbridge, and Ross B.H. #2 provide ages of 293 ± 10 Ma (3.4% age uncertainty, 2σ, n=6, Mean Square Weighted Deviates [MSWD] = 2.1), 298.8 ± 8.3 Ma (2.7% age uncertainty, 2σ, n=4, MSWD = 2.2) and 219 ± 91 Ma (41.5% age uncertainty, 2σ, n=3, MSWD = 0.34), respectively (Figure 2.4). These isochrons yield $(^{187}Os/^{188}Os)_i$ ratios of 0.58 ± 0.04, 0.56 ± 0.12, and 0.91 ± 0.37, respectively. A pooled isochron, using all data yields an age of 298.0 ± 2.3 Ma and an $(^{187}Os/^{188}Os)_i$ of 0.56 ± 0.02 (0.7% age uncertainty, 2σ, n=13, MSWD = 2.1) and represent the best candidate for the age of the Tasmanite oil shale in the Tasmania Basin (Figure 2.4).

Sample	$^{187}Re/^{188}Os$	±	$^{187}Os/^{188}Os$	±	Re (ppb)	±	Os (ppt)	±
Core: Tunbridge								
TB-1	328.99	2.16	2.20	0.01	8.13	0.03	151.29	0.78
TB-2	330.88	2.57	2.21	0.01	8.26	0.04	152.99	0.97
TB-3	281.32	1.53	1.95	0.01	11.01	0.04	233.36	1.00
TB-4	236.95	1.41	1.75	0.01	8.15	0.04	200.77	0.87
Core: Douglas River								
DR-1	753.66	4.29	4.32	0.02	11.84	0.05	117.07	0.68
DR-2	764.74	4.97	4.37	0.03	11.94	0.04	116.93	0.76
DR-3	894.91	3.45	5.05	0.03	15.84	0.06	140.02	0.84
DR-4	992.21	4.57	5.50	0.03	17.35	0.06	143.27	0.90
DR-5	958.30	6.55	5.27	0.05	16.97	0.06	142.53	1.34
DR-6	963.02	4.03	5.37	0.02	15.41	0.06	129.87	0.63
Core: Ross B.H. #2								
BH2-1	260.19	3.72	1.85	0.02	4.50	0.03	102.28	0.82
BH2-2	236.56	3.52	1.76	0.02	4.00	0.03	99.13	0.79
BH2-3	246.28	2.87	1.81	0.01	4.21	0.03	100.46	0.64

Table 1. Rhenium-Os data for the Tasmanite Oil Shale horizon within the Quamby Formation. Uncertainties are reported as 2σ.

2.5. DISCUSSION

2.5.1. Re-Os Geochronology

Linear regressions of samples from individual cores yield Model 1 ages that agree, within uncertainty, with the expected age for the Tasmanite oil shale. The expected age is based on macro-invertebrate and palynostratigraphic zonations in Tasmania which correlate to the GSSP for the base of the Permian across most northern basins of Pangea (Ritter, 1995). U-Pb zircon ages of ash-bearing intervals that straddle the GSSP for the base Permian in the Aidaralash Creek section of the Uralian foredeep provide an absolute age for the base Permian of 298.90 +0.31, -0.15 (2σ) (Ramezani et al., 2007) (Figure 2.2).

As noted earlier, the Douglas River and Tunbridge samples yield Model 1 ages of 293 ± 10 Ma and 298.8 ± 8.3 Ma, respectively (Figure 2.4). The age overlap within their uncertainties for the two isochrons are consistent with minimal to no post-depositional disturbance to the Re-Os system. Ross B.H. #2 Re-Os data provides an age of 219 ± 91 Ma (41.5% age uncertainty, 2σ, n=3, MSWD = 0.34). This is a much higher age uncertainty than Douglas River and Tunbridge samples. Large MSWD values are indicative of large scatter about the isochron. However, the MSWD of less than 1 suggests that the observed scatter is less than that predicted by the analytical uncertainty which is caused by an overestimation of the uncertainties and an underdispersion of the data. The large uncertainty on the age and $(^{187}Os/^{188}Os)_i$ for the Ross B.H. #2 core is a result of the extremely narrow range in both $^{187}Re/^{188}Os$ and $^{187}Os/^{188}Os$ and likely not a result of geologic scatter from post-depositional mobility of Re or Os.

A pooled isochron, using all data yields an age of 298.0 ± 2.3 Ma and an $(^{187}Os/^{188}Os)_i$ of 0.56 ± 0.02 (0.7% age uncertainty, 2σ, n=12, MSWD = 2.1) for the Tasmanite oil shale horizon in the Tasmania Basin. This age correlates the Tasmanite oil shale to the GSSP for the base of the Permian in the Ural Mountains and other globally correlated base Permian maximum flooding surfaces in the midcontinent of the U.S. and Namibia (Ramezani et al., 2007). This age represents the best candidate for the base of the Permian in Gondwana and suggests that it was marked by a global flooding event. This age provides the first absolute age for the correlation of eustatic events between the northern and southern hemispheres during the Permian (Domack et al., in prep.).

2.5.2. Implications of the $(^{187}Os/^{188}Os)_i$ at ~298 Ma

The $(^{187}Os/^{188}Os)_i$ obtained from the isochron regression of 0.56 ± 0.02 for the Tasmanite oil shale horizon is interpreted to represent the $^{187}Os/^{188}Os$ of seawater at the time of deposition (Ravizza and Turekian, 1989; Cohen et al., 1999). As previously described, the $^{187}Os/^{188}Os$ ratio of seawater is derived from a balance of inputs of radiogenic river water during weathering and subsequent continental runoff of upper continental crust ($^{187}Os/^{188}Os = 1.4$) and non-radiogenic inputs from the mantle via seafloor spreading, flood basalt events, hydrothermal alteration of oceanic crust, and from meteorite impacts ($^{187}Os/^{188}Os = 0.13$).

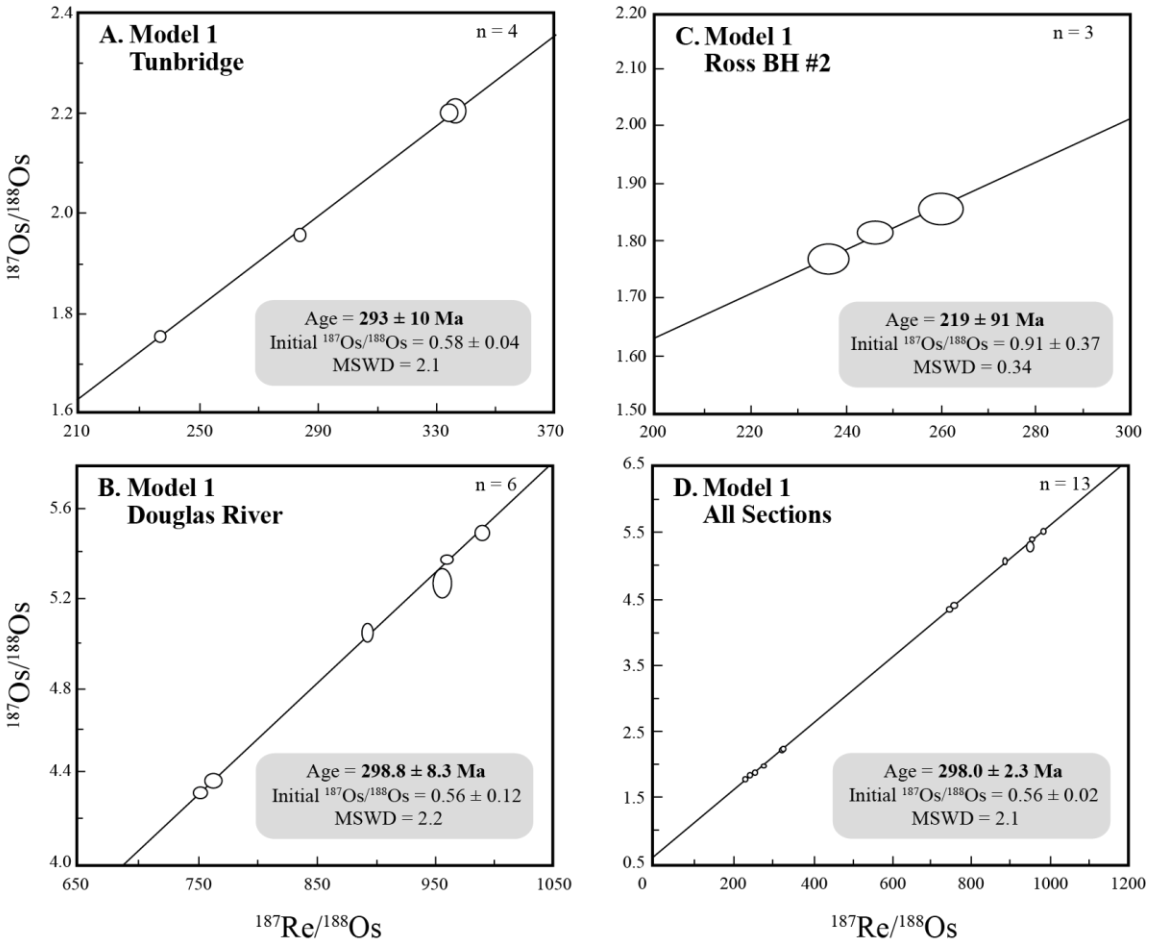

Figure 2.4. Rhenium-Os isochron for the Tasmanite Oil Shale from the Quamby Formation. (A) Samples from Tunbridge core, (B) Sample from Douglas River core, (C) Samples from Ross B.H. #2 core, (D) A pooled isochron using all samples from all cores. Uncertainty is reported as 2σ.

Large temporal shifts in the $^{187}Os/^{188}Os$ of seawater can be detected in the rock record. These shifts can be caused by the relative change in the contribution of the various sources such as during periods of increased seafloor spreading, accelerated crustal weathering during deglaciation, or meteorite impacts. Changes on the order of orbitally forced, glacial-interglacial cycles (~12,000 yrs) can be resolved due to the short residence time of Os in the ocean (Oxburgh, 1998). The isotopic composition of present day seawater (~1.06; Peucker-Ehrenbrink and Ravizza, 2000) suggests a dominance of contribution from radiogenic crustal Os delivered to the oceans via rivers ($^{187}Os/^{188}Os$ = 1.54; Levasseur et al., 1999). The less-radiogenic $^{187}Os/^{188}Os$ for the Tasmanite oil shale of 0.56 ± 0.02 indicates that the Tasmanite Basin received significantly lower relative contributions of crustal Os during the earlier Permian than for the present-day ocean. Similar conditions existed just prior to the Cretaceous-Paleocene boundary and throughout much of the Eocene leading into the Eocene-Oligocene boundary (Pegram et al., 1992; Burton et al., 1999; Turgeon and Creaser, 2008). The less radiogenic nature of seawater at 298 Ma could also be explained by a difference in the composition of exposed crustal material. If a young or mafic crust were exposed to weathering, both of which have unradiogenic Os isotopic signatures, the coeval oceans would reflect this contribution.

Although seawater $^{187}Os/^{188}Os$ at any given time in Earth's history can be known by measuring Os isotopes in marine ORM, constraining the absolute amount of contributions from the various sources is a challenge. This could be manifested geographic and temporal variations in the $^{187}Os/^{188}Os$ of the eroding upper continental crust (e.g.,

weathering of organic-rich mudrocks with $^{187}Os/^{188}Os \leq 13.6$; Peucker-Ehrenbrink and Blum, 1998). The unradiogenic component could be the product of a mixture of contributions from the various unradiogenic sources of Os.

The unradiogenic $(^{187}Os/^{188}Os)_i$ of the Tasmanite oil shale represents the first reported data for the Os isotopic signature of seawater during the earliest Permian.

2.5.3. Osmium Isotopic Evolution of Paleozoic Seawater

The most recent review of the evolution of seawater Os during the Paleozoic reported four data points for the entire Paleozoic, three of which occur at the Devonian-Mississippian boundary (Peucker-Ehrenbrink and Ravizza, 2012). Two of these data points have extremely large uncertainties in the $(^{187}Os/^{188}Os)_i$ (±38 and ±53%) resulting in error bars which span a significant portion of the entire range of possible values for seawater $^{187}Os/^{188}Os$. The few $^{187}Os/^{188}Os$ ratios that are reported for Paleozoic seawater are similar to Cenozoic values (0.42 – 0.75). This may reflect a general secular trend of increasing $^{187}Os/^{188}Os$ values from chondritic values in the Precambrian ($^{187}Os/^{188}Os$ = 0.112; Hannah et al., 2004) toward more continental crustal values during the Paleozoic (Peucker-Ehrenbrink and Ravizza, 2012). This follows the trend of changing values for Precambrian and Early Paleozoic $^{87}Sr/^{86}Sr$ ratios (Halverson et al., 2010).

Previously, constraining secular trends for $^{187}Os/^{188}Os$ during the Paleozoic was limited by the lack of data. This study compiles all previously published $^{187}Os/^{188}Os$ ratios for Paleozoic seawater, including new data presented here and thus provides a five-fold increase in the number of $^{187}Os/^{188}Os$ values for Paleozoic seawater (Figure 2.5).

The $^{87}Sr/^{86}Sr$ ratios of past seawater can be measured through analysis of marine carbonate shells and rocks. Strontium in seawater behaves similarly to Os, in that fluctuation in $^{87}Sr/^{86}Sr$ can be used as a proxy for evaluating relative contributions of radiogenic and unradiogenic Sr to the oceans, but with a much longer residence time as noted above (Cohen et al., 1999; Peucker-Ehrenbrink and Ravizza, 2000). This results in the curve of $^{87}Sr/^{86}Sr$ being smoother than that of $^{187}Os/^{188}Os$ because the temporal resolution of Sr is averaged out over longer time segments than that of Os. The Sr isotopic record of Paleozoic seawater is very well constrained (Figure 2.5).

Because the Sr evolution curve of seawater in the Paleozoic is well constrained, and because Os and Sr behave similarly in the oceans, further discussion will compare the somewhat sparse Os isotopic curve reported here with the established Sr isotopic curve.

Figure 2.5. Temporal $^{187}Os/^{188}Os$ variation of Paleozoic seawater. Large symbols = $^{187}Os/^{188}Os$ achieved through the regression of a Re-Os isochron, Small symbols = $^{187}Os/^{188}Os$ achieved through chemostratigraphic measuremenets. Symbols are as described in the key. Gray bars across the top designate the timing of orogenic or climatic events as discussed in this paper. Caled = Caledonian; A = Decline of Late Paleozoic ice sheets; B = Opening of the Neotethys, C = Cessation of Paleotethys volcanism. Gray line at the bottom = temporal variation of $^{87}Sr/^{86}Sr$ of Paleozoic seawater from Veizer et al. (1999), Sawaki et al. (2008), Sawaki et al. (2010); Korte et al. (2006). MISS. = Mississippian; PENN. = Pennsylvanian. Semi-transparent symbols represent data points that have either too large of uncertainty, or have geologic explanations as to why they shouldn't be included in the secular trend of $^{187}Os/^{188}Os$ (see discussion in text).

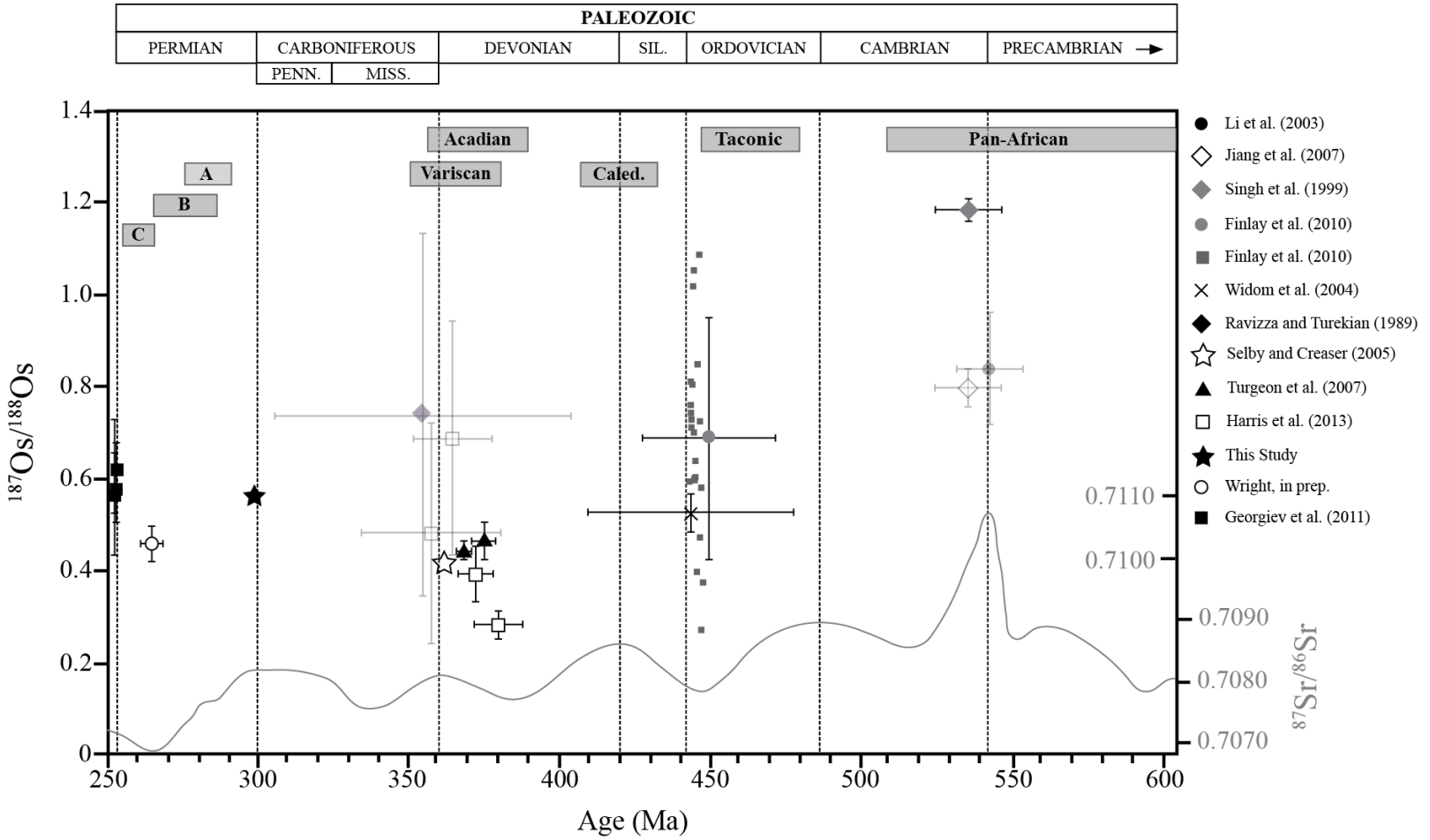
PALEOZOIC
PERMIAN
CARBONIFEROUS
PENN.
MISS.
DEVONIAN
SIL.
ORDOVICIAN
CAMBRIAN
PRECAMBRIAN
Acadian
Variscan
Caled.
Taconic
Pan-African
A
B
C
$^{187}Os/^{188}Os$
Age (Ma)
$^{87}Sr/^{86}Sr$
0.7110
0.7100
0.7090
0.7080
0.7070
Li et al. (2003)
Jiang et al. (2007)
Singh et al. (1999)
Finlay et al. (2010)
Finlay et al. (2010)
Widom et al. (2004)
Ravizza and Turekian (1989)
Selby and Creaser (2005)
Turgeon et al. (2007)
Harris et al. (2013)
This Study
Wright, in prep.
Georgiev et al. (2011)

2.5.3.1. Cambrian

The Os isotopic composition of Cambrian seawater is represented by three data points clustered around 538 ± 14 Ma (Figure 2.5). These show a dichotomy in values. Li et al. (2003) report a $(^{187}Os/^{188}Os)_i$ value of 0.84 ± 0.12 at 542 ± 11 Ma for the marine, Lower Cambrian black rock series of the Hunan-Guizhou provinces in South China. Jiang et al. (2007) report a similar $(^{187}Os/^{188}Os)_i$ value of 0.80 ± 0.04 at 535 ± 11 Ma for marine, Lower Cambrian black shales of the Niutitang Formation, Yangtze Platform in South China, in the Hunan Province, ~550 km away from the area studied by Li et al. (2003). However, lower Cambrian marine, black shales from the Lesser Himalaya have a higher $(^{187}Os/^{188}Os)_i$ value than those obtained from Lower Cambrian black shales of South China (Figure 2.5) (1.181 ± 0.024; Singh et al., 1999).

The Lower Cambrian black shales studied by Li et al. (2003) and Jiang et al. (2007) are part of a regionally distributed polymetallic Ni-Mo-PGE-Au enriched unit. Based on detailed field and laboratory studies, the presence of a middle sulfide bed bounded by chert beds reflects the structure typical of Early quartz stage – middle sulfide stage – and later quartz, carbonate stage, a sequence typical of hydrothermal ore deposits (Li, 1996). This coupled with the enrichment of some platinum group elements (PGE), rare earth elements, trace elements, and noble metals indicate seafloor hydrothermal fluid activities (Li, 1995; Li, 1996; Li, 2000). Previous studies have shown that submarine hydrothermal solutions can depress $^{187}Os/^{188}Os$ values as a result of delivery of hydrothermal, non-radiogenic Os to the oceans likely from venting of hydrothermal fluids that interacted with mafic and ultramafic oceanic lithosphere (Ravizza et al., 1996; Brugmann et al.,

1998; Burton et al., 1999; Peucker-Ehrenbrink and Ravizza, 2000; Sharma et al., 2000; Terakado, 2001; Cave et al., 2003). Snow and Reisberg (1995) estimated that the alteration of ultramafic rocks might provide a flux of Os to seawater that is similar in magnitude to the total riverine Os flux. For example, modern day pyrite ores from the active mound of the TAG hydrothermal field on the Mid-Atlantic Ridge show a progressive increase in $^{187}Os/^{188}Os$ from 0.59 to 1.07 over a 3 m interval (Brugmann et al., 1998). The highest value, observed in the upper part of the interval, most removed from the hydrothermal system is identical to the $^{187}Os/^{188}Os$ value of present day seawater (Brugmann et al., 1998). Rhenium and Os isotopic data from the Miocene Kuroko sulfide ores yield a 18.4 ± 0.6 Ma isochron with an $(^{187}Os/^{188}Os)_i$ value of 0.62 (Terakado, 2001). This value is significantly less than the accepted value for Miocene seawater (0.73; Ravizza, 1993). Cave et al. (2003) reported a systematic increase in $^{187}Os/^{188}Os$ with increasing distance from the Rainbow hydrothermal field in recent sea-floor sediments. The most proximal samples have $^{187}Os/^{188}Os$ ratios of 1.000 to 1.008, lower than present-day seawater values, while the most distant sample, 25 km away from the vent site, has a $^{187}Os/^{188}Os$ ratio of 1.06 which is indistinguishable from modern-day seawater (Cave et al., 2003).

The lack of noticeable polymetallic enrichment typically associated with ORM that are proximal to hydrothermal systems, suggest that the Lower Cambrian black shales from the Lesser Himalaya, India, with $^{187}Os/^{188}Os = 1.181 \pm 0.024$ (Singh et al., 1999) is a better representation of Early Cambrian seawater Os than those from the studies of Jiang et al. (2007) and Li et al. (2003). This is the most radiogenic $^{187}Os/^{188}Os$ value for the

entire Phanerozoic. Assuming the $^{187}Os/^{188}Os$ composition of continental crust exposed in the Early Cambrian is similar to that of the present-day continental crust, a seawater $^{187}Os/^{188}Os$ value of 1.181 is more radiogenic than present-day seawater, suggesting an even higher contribution of radiogenic continental crustal Os likely as a result of weathering, relative to non-radiogenic inputs during the Early Cambrian.

Due to the clustered nature of the Os isotopic record, attempts at identifying temporal trends in the $^{187}Os/^{188}Os$ of seawater during the Cambrian are very limited. There is a ~86 Myr gap between the cluster of Cambrian data points and the $^{187}Os/^{188}Os$ reported for the Late Ordovician (Figure 2.5). However, the Early Cambrian is also characterized by radiogenic $^{87}Sr/^{86}Sr$ values relative to the modern oceanic value of ~0.7090 and supports high continental weathering rates during this time (Veizer et al., 1999).

The Sr record shows an increase, with minor fluctuations, in $^{87}Sr/^{86}Sr$ throughout much of the Precambrian from 0.7052 to 0.7090 in the Late Neoproterozoic (Shields, 1999; Jacobsen and Kaufman, 1999; Melezhik et al., 2001; Shields and Veizer, 2002; Sawaki et al., 2010) (Figure 2.5). At the Precambrian-Cambrian (pC-C) boundary, an abrupt positive Sr isotopic excursion drives the $^{87}Sr/^{86}Sr$ value to 0.7108 followed by an abrupt return to a less radiogenic value of 0.7086 by the Middle Cambrian (Denison et al,. 1998; Sawaki et al., 2008). The $^{87}Sr/^{86}Sr$ value of seawater then rose to a more radiogenic value of 0.7093 by the beginning of the Late Cambrian (Denison et al,. 1998) (Figure 2.5). The $^{87}Sr/^{86}Sr$ value of 0.7108 observed during the Early Cambrian is the highest value of $^{87}Sr/^{86}Sr$ during the entire Phanerozoic. This is consistent with a Phanerozoic maximum in seawater $^{187}Os/^{188}Os$. Following the earliest Late Cambrian peak, seawater $^{87}Sr/^{86}Sr$

values flatten briefly, and then decline slightly to 0.70903 at the Cambrian-Ordovician boundary (Denison et al., 1997).

The long-term increase in seawater $^{87}Sr/^{86}Sr$ throughout the Precambrian is interpreted to record an increase in the flux of radiogenic Sr via riverine input of continental crustal material resulting from high uplift rates and consequent increased denudation rates during the Late Proterozoic-Cambrian Pan-African Orogen (Miller, 1983; Asmerom et al., 1991; Derry et al., 1992; Montanez et al., 1996). Old felsic rocks from Precambrian cratons are an important source of radiogenic Sr ($^{87}Sr/^{86}Sr$ ~0.720) and Os ($^{187}Os/^{188}Os \leq 13.6$) to global seawater (Brass, 1976; Peucker-Ehrinbrink and Blum, 1998). Weathering of these rocks during orogenic events can contribute a large amount of radiogenic Sr and Os to the oceans, thus raising seawater $^{87}Sr/^{86}Sr$ and $^{187}Os/^{188}Os$ values (Burke et al., 1982). The comparable rapid increased in the Cenozoic $^{87}Sr/^{86}Sr$ and $^{187}Os/^{188}Os$ has been explained by rapid exhumation and chemical weathering of Himalayan ^{87}Sr-rich metamorphic and ^{187}Os-rich ORM (Pegram et al., 1992; Richter et al., 1992; Ravizza, 1993; Peucker-Ehrenbrink et al., 1995; Turekian and Pegram, 1997; Pegram and Turekian, 1999; Peucker-Ehrenbrink and Ravizza, 2000).

The large positive $^{87}Sr/^{86}Sr$ excursion at the pC-C boundary was originally explained by a large increase in the amount or radiogenic Sr reaching the oceans during the assembly of Gonwana (Shields, 2007). However, the short duration and magnitude of the excursion requires a reversible change just after the event, inconsistent with the long time-scales of tectonics (Sawaki et al. 2008). Santosh and Omori (2008) proposed that the sudden increase of atmospheric pCO_2, coupled with other environmental changes associated with

the pC-C boundary and the Cambrian explosion, would increase the rate of silicate weathering, and thus provide a much larger amount of radiogenic Sr to the oceans than could be explained by tectonics. Following recovery of pCO_2, weathering slowed causing a decline in the $^{87}Sr/^{86}Sr$ of seawater.

Perhaps the rapid increase and Phanerozoic maximum in $^{87}Sr/^{86}Sr$ during the Early Cambrian may record unroofing and weathering of unstable, ^{87}Sr rich high-grade metamorphic rocks within the Pan-African orogenic zone (Montanez et al., 1996). The overall higher $^{87}Sr/^{86}Sr$ and $^{187}Os/^{188}Os$ observed during the Cambrian may have been accentuated by an overall increase in erosion rates caused by a lack of vegetation on the continents. A reduction in isostatic uplift and chemical weathering during the mature phases of orogenesis may explain the gradual decrease in seawater $^{87}Sr/^{86}Sr$ nearing the end of the Cambrian period (Montanez et al., 1996).

Montanez et al. (1996) observed a high-frequency, sinusoidal overprinting on the Cambrian $^{87}Sr/^{86}Sr$ seawater curve and suggested they may be caused by changes in continental weathering rates governed by sea-level fluctuations of 10^6 yrs. Similar patterns are reported for seawater $^{187}Os/^{188}Os$ during the Ordovician (Finlay et al., 2010) and Pleistocene (Oxburgh, 1998) and are interpreted as the result of sea-level fluctuations during orbitally forced, glacial-interglacial cycles. During sea-level highstands, less continental surface area is exposed, as the edges of previously exposed continents are now submerged (Denison et al., 1997). Therefore, radiogenic pericratonic sediment and strata are not exposed to physical and chemical weathering, thus decreasing the flux of radiogenic continental crust to the oceans via rivers, resulting in a decrease in the

seawater $^{87}Sr/^{86}Sr$ and $^{187}Os/^{188}Os$ ratios. Conversely, during sea-level lowstands, the surface area of the continents increases, exposing fine-grained siliciclastic sediments on the continental shelf. Weathering of these sediments provides an increase in the flux of radiogenic Sr from continental weathering to the oceans, thus resulting in an increase in the $^{87}Sr/^{86}Sr$ and $^{187}Os/^{188}Os$ of coeval seawater.

The Cambrian was a time of continental flooding, following the end of the Precambrian Marinoan glaciation and subsequent sea level rise (Denison et al., 1997). Hallam (1992) interpreted the Late Cambrian highstands to be the greatest of the Phanerozoic. Multiple sea-level events were superimposed on the longer-term rise in sea-level that occurred during the Cambrian (Montanez et al., 1996). Montanez et al. (1996) observed progressively increasing $^{87}Sr/^{86}Sr$ values, which coincided with times of episodically falling sea level, in peritidal carbonates from the Middle to Late Cambrian with the highest $^{87}Sr/^{86}Sr$ correlating with the culmination of falling sea level. The subsequent decrease in the $^{87}Sr/^{86}Sr$ value during the Early Late Cambrian corresponds to a gradual rise in relative sea level recorded by open-marine carbonates (Montanez et al., 1996). Montanez et al. (1996) propose that during greenhouse times, changes in the exposed surface area of continents, governed by sea-level fluctuations, contribute to short-term variations in seawater $^{87}Sr/^{86}Sr$ values. Sea level, however, is not the only control on short-term fluctuations in seawater $^{87}Sr/^{87}Sr$. Denison et al. (1998) suggest climate, and the age and composition of the exposed crystalline rocks also contribute to seawater $^{87}Sr/^{86}Sr$ variations.

Sea-level fluctuations may have had little effect on the long-term variations in seawater $^{87}Sr/^{86}Sr$. This is because the steady increase in sea-level during the Middle to Late Cambrian would theoretically submerge large portions of the continents, therefore reducing the flux of radiogenic Sr to the oceans. Long-term variations in the $^{87}Sr/^{86}Sr$ ratio of seawater appear instead to be controlled by tectonic and climatic events. These can strongly alter the weathering rates of continental material, and/or provide relatively large amounts of unradiogenic Os to the oceans with smaller, high-frequency overprinting due to variations in sea-level.

Although there is limited data to provide a secular trend in the $^{187}Os/^{188}Os$ of Cambrian seawater, the highly radiogenic Early Cambrian value of 1.18 represents a Phanerozoic maximum and is consistent with a maximum in the Phanerozoic $^{87}Sr/^{86}Sr$ value. There is much work to be done on the Os isotopic evolution of Cambrian seawater which will ultimately provide more temporal resolution than the established Sr isotopic curve.

2.5.3.2. Ordovician

The $^{187}Os/^{188}Os$ composition of Ordovician seawater is represented in two ways. These include the $(^{187}Os/^{188}Os)_i$ values obtained from Re-Os isochron regression and a chemostratigraphic study of 8 m of ORM spanning 4.3 Myr across the Ordovician - Silurian boundary in the Linn Branch section, Dob's Linn, Scotland (Figure 2.5) (Finlay et al., 2010). The two $(^{187}Os/^{188}Os)_i$ values determined by isochron regression are indistinguishable within uncertainty. Widom et al. (2004) obtained an $(^{187}Os/^{188}Os)_i$ value of 0.53 ± 0.04 at 443 ± 34 Ma for acetic and hydrochloric acid leachates from marine carbonates from Serpent Mound, Ohio. This age is consistent with the expected age for

these Late Ordovician carbonates based on biostratigraphy (Widom et al., 2004). A second study on marine ORM spanning the Ordovician - Silurian boundary obtained a $(^{187}Os/^{188}Os)_i$ value of 0.69 ± 0.26 at 449 ± 22 Ma (Finlay et al., 2010). The uncertainties of this value overlap that reported by Widom et al. (2004). Finlay et al. (2010) attributes the extremely high uncertainty on both the age and $(^{187}Os/^{188}Os)_i$ value obtained by isochron regression on rapid changes in the Os isotopic composition of Late Ordovician seawater.

Throughout the Katian stage (453 – 445 Ma) of the Late Ordovician, the $^{187}Os/^{188}Os$ value becomes more radiogenic from 0.37 – 1.08 over a 2.25 m interval, representing ~1.2 Myr of time (Finlay et al., 2010). Within this interval, there is an even more abrupt increase from 0.48 to 1.08 over a 40 cm interval, representing ~200 kys. (Finlay et al., 2010). From the peak of $(^{187}Os/^{188}Os)_i$ value of 1.08, values become abruptly less radiogenic and remain stable at ~0.6 until 1.70 m below the Ordovician - Silurian boundary before spiking to a highly radiogenic value of 1.05 over a 19 cm, 100 ky. interval (Finlay et al., 2010). From this point, $^{187}Os/^{188}Os$ values decrease gradually across the Ordovician - Silurian boundary to a value of ~0.6 one meter above the boundary (Finlay et al., 2010).

The $^{87}Sr/^{86}Sr$ ratio of seawater in the Ordovician Period continued the decline that had begun in the Late Cambrian. Several studies reveal decreasing Sr isotope ratios throughout the majority of the Ordovician, from ~0.7090 at the Cambrian-Ordovician boundary to ~0.7078 by the Late Ordovician (Katian: 453 – 445 Ma) (Veizer and Compston, 1974; Burke et al., 1982; Veizer et al., 1986; Denison et al., 1997; Qing et al.,

1998; Gao and Land, 1991; Johnson and Goldstein, 1993; Ebneth et al., 2001; Shields et al., 2003). Seawater $^{87}Sr/^{86}Sr$ decreased gradually from ~0.7090 to ~0.7088 during the Early Ordovician (Qing et al., 1998). A second, larger decrease in the $^{87}Sr/^{86}Sr$ is observed between the Darriwilian (467 – 458 Ma) and Early Caradocian (458 – 448 Ma) from ~0.7088 to ~0.7079 (Gao et al., 1996; Holmden et al., 1996; Qing et al., 1998; Young et al., 2009). This represents the most rapid decrease in seawater $^{87}Sr/^{86}Sr$ of the entire Paleozoic, with a magnitude comparable to the rise in $^{87}Sr/^{86}Sr$ observed in the past ~35 Myr. of the Cenozoic (Young et al., 2009). Finally, the rate of decrease in seawater $^{87}Sr/^{86}Sr$ fell slightly leading into the Katian (453 – 445 Ma) with a period of stasis with an $^{87}Sr/^{86}Sr$ ~0.7078 (Gao et al., 1996; Holmden et al., 1996; Qing et al., 1998; Young et al., 2009) followed by an increase in seawater $^{87}Sr/^{86}Sr$ throughout the Katian (453 – 445 Ma) and Hirnantian (445 – 444 Ma) and continuing into the Silurian (Burke et al., 1982; Shields et al., 2003).

Shields et al. (2003) concluded that the general decreasing trend in seawater $^{87}Sr/^{86}Sr$ during the Ordovician was partly in response to a slowing of tectonic uplift associated with the Pan-African Orogeny. The extent of contractional deformation caused by the Pan-African Orogeny decreased from a maximum during the Late Cambrian to reach an all-time minimum by the mid-Ordovician (Richter et al., 1992). This slowing of uplift would decrease denudation and thus limit the amount of radiogenic Sr that would be contributed to the oceans during that time, resulting in a decrease in the $^{87}Sr/^{86}Sr$ in seawater, consistent with the long term decrease in $^{187}Os/^{188}Os$ discussed previously. Shields et al. (2003) further suggest that such a rapid decrease in the $^{87}Sr/^{86}Sr$ of seawater

likely wasn't solely caused by a gradual decrease in crustal weathering rates. They proposed that an increase in seafloor spreading rates or an increase in the flux of nonradiogenic Sr from weathering of volcanic rocks in island-arc settings associated with the Taconic Orogeny (primary deformation occurred ~458 – 448 Ma) aided in the large decrease in $^{87}Sr/^{87}Sr$ throughout the Ordovician. Initiation of subduction during the Taconic Orogeny correlates with the timing of the large decrease in $^{87}Sr/^{86}Sr$ (Ettensohn, 1990; Finney et al., 1996; Kolata et al., 1996; Wright et al., 2002). Quantitative modeling by Young et al. (2009) conclude that a good fit to the measured Ordovician seawater $^{87}Sr/^{87}Sr$ curve is obtained when a new flux from the weathering of arc basalts (0.7043) is introduced to the system. This flux of unradiogenic Sr represents the weathering of arc basalts of the Taconic arcs, and possibly other regions (Young et al., 2009). In addition, the Middle-Early Late Ordovician was a period of massive island-arc volcanism in Kazakhstan (Nikitin et al., 1990). The increased weatherability of these relatively easily weathered volcanic rocks likely contributed to the increased decline in the $^{87}Sr/^{86}Sr$ of Upper Ordovician seawater (Shields et al., 2003). Such material would have likely resulted in a less radiogenic flux of $^{187}Os/^{188}Os$ as well.

Hence, a combination of factors resulted in the general decreasing trend in the $^{87}Sr/^{86}Sr$ of Ordovician seawater. Overall, it was primarily caused by the slowing of radiogenic flux of Sr to the oceans during slowed uplift and denudation rates during the mature stages of the Pan-African Orogen (Shield et al., 2003). The increased decline in seawater $^{87}Sr/^{86}Sr$ during the Early Late Ordovician was caused by a coupling of (1) an increased flux of unradiogenic Sr to the oceans due to the weathering of island-arc volcanism associated

with the Taconic Orogeny (Young et al., 2009), and (2) a large marine transgression that flooded the edges of continents, ultimately restricting the weatherability of radiogenic continental crustal material (Ross and Ross, 1996; Haq and Schutter, 2008). This large marine transgression in an extended greenhouse interval was likely caused by an increase in sea-floor spreading rates or a general increase in the volume of basalts on the sea-floor, which provides even more unradiogenic Sr to the oceans (Chen, 1990; Denison et al., 1997; Shields et al., 2003; Munnecke et al., 2010). Finally, in the Late Katian (453 – 445 Ma), volcanic outgassing associated with the Taconic Orogeny had ceased while silicate weathering remained high due to the continued weathering of island-arcs, causing pCO_2 to fall and initiated cooling that led into the Hirnantian glacial episode (440 – 444 Ma) (Young et al., 2009). The marked increase in the $^{187}Os/^{188}Os$ ratio throughout the Early Katian (453 – 445 Ma) to a $^{187}Os/^{188}Os$ value of 1.08 also supports increased silicate weathering of radiogenic orogenic material during this time, resulting in atmospheric CO_2 drawdown, global cooling and ultimately the onset of Hirnantian glaciation at the end of the Ordovician (Finlay et al., 2010). Reduced chemical weathering rates and growth of continental ice cover during the Hirnantian glaciation reduced the input of radiogenic Os to the oceans, as supported by a trend to more unradiogenic $^{187}Os/^{188}Os$ values of ~04 – 0.6 following the onset of glaciation (Finlay et al., 2010). As a direct result of the decrease in silicate weathering during the Hirnantian glaciation, atmospheric CO_2 returned to greenhouse levels, causing rapid deglaciation during the Late Hirnantian (Finlay et al., 2010). Following deglaciation, seawater $^{187}Os/^{188}Os$ records a dramatic rise from 0.6 – 1.05 over 100 ky. as a result of the leaching of radiogenic $^{187}Os/^{188}Os$ from

glacial deposits along with increased weathering of now exposed radiogenic $^{187}Os/^{188}Os$ silicates (Finlay et al., 2010).

Work by Finlay et al. (2010) highlights the high temporal variability of the $^{187}Os/^{188}Os$ composition of seawater, controlled by the relatively short residence time of Os in the oceans compared to Sr. The high temporal resolution of Os further highlights the lack of data for Paleozoic seawater Os (Figure 2.5). However, the general trend observed in the $^{187}Os/^{188}Os$ composition of seawater during the Late Ordovician track those of the Sr isotopic composition.

2.5.3.3. *Silurian*

The end of the Ordovician was marked by the Hirnantian glaciation, with two to four principal glacial phases over a brief 4 Myr period (Barnes, 1986; Brenchley et al., 1991, 1994; Qing et al., 1998). The consequent increase in the $^{87}Sr/^{86}Sr$ of seawater during the Silurian from a value of ~0.7078 to ~0.7087 is interpreted by Qing et al. (1998) to represent an increased flux of radiogenic Sr via riverine input during deglaciation following the Hirnantian glaciation. Radiogenic continental weathering products that were generated by the Hirnantian glaciation would have been reworked during the Llandovery transgression following the melting of Hirnantian glaciers (Qing et al., 1998). An additional increase in radiogenic riverine Sr flux could have been caused by mature phases of the Taconic Orogeny that resulted in exhumation and chemical weathering of ^{87}Sr-rich high-grade metamorphic rocks at the eastern margin of Laurentia (Qing et al., 1998). Primary deformation associated with the Taconic Orogeny occurred during the Caradoc (458 – 448 Ma), however, the Sr flux to the oceans may have been delayed until

the Early Silurian because a substantial thickness of marine carbonates needed to be removed from uplifted highlands before exposing Sr-rich basement rocks (Richter et al., 1992). Toward the end of the Silurian, new continental input may have developed due to the Early phases of the Caledonian Orogeny and the initial suturing of Baltica and Laurentia during the closure of the Iapetus Ocean (Dunning et al., 1990; Cawood et al., 1994; Qing et al., 1998).

No Os isotope data exists for tracking the seawater composition during the Silurian. As a prediction, based on the tectonic and climatic events outline above, the $^{187}Os/^{188}Os$ composition of Silurian seawater would increase steadily throughout the Silurian. This would be in response to the relatively stable addition of radiogenic Os to the oceans during deglaciation and denudation of basement rocks exposed during the Taconic Orogeny. High frequency cycles in the $^{187}Os/^{188}Os$ composition of seawater may have developed due to eustatic sea-level changes. Johnson (2010) recorded ten intra-Silurian highstands that ranged in magnitude from several tens of meters to more than 70 m.

2.5.3.4. Devonian

The Devonian Period is the best understood period in the Paleozoic in terms of the $^{187}Os/^{188}Os$ evolution of seawater and is represented by eight data points. In perhaps one of the pioneering studies on Re-Os isotopic in ORM, Ravizza and Turekian (1989) reported an $(^{187}Os/^{188}Os)_i$ of 0.74 ± 0.39 at 354 ± 49 Ma for the Bakken Shale, a Mississippian/Devonian marine black shale using a nickel sulfide fire assay procedure. Since then, chemical and analytical procedures have resulted in a marked decrease in the uncertainty on both Re-Os ages and $(^{187}Os/^{188}Os)_i$ ratios. By accessing only the

hydrogenous component of ORM, Selby and Creaser (2005) achieved an $(^{187}Os/^{188}Os)_i$ ratio of 0.42 ± 0.01 at 361.3 ± 2.4 Ma for the Mississippian/Devonian boundary in the marine Exshaw Formation in Canada.

Turgeon et al. (2007) reported ages for two intervals spanning the Frasnian-Famennian boundary (Late Devonian) in the Hanover Formation, a marine ORM from the Appalachian Basin in western New York, USA. The $(^{187}Os/^{188}Os)_i$ obtained by isochron regression are 0.45 ± 0.02 at 367.7 ± 2.5 Ma and 0.47 ± 0.04 at 374.2 ± 4.0 Ma (Turgeon et al., 2007). These two intervals yield statistically overlapping ages and $(^{187}Os/^{188}Os)_i$ ratios, and are similar to both previous reported values (Ravizza and Turekian, 1989; Selby and Creaser, 2005). The agreement of these data suggests fairly low and constant continental weathering rates across the Frasnian-Famennian boundary (Turgeon et al., 2007).

Harris et al. (2013) reported Re-Os isochrons for four stratigraphic intervals spanning the Frasnian/Famennian and Mississippian/Devonian boundaries of the marine, Upper Devonian Woodford Shale in the Permian Basin, West Texas. The $(^{187}Os/^{188}Os)_i$ obtained by isochron regression are 0.29 ± 0.03 at 379.0 ± 7.1 Ma, 0.40 ± 0.06 at 371.5 ± 5.8 Ma, 0.69 ± 0.25 at 364 ± 13 Ma, and 0.47 ± 0.07 at 357.9 ± 5.3 Ma (Harris et al., 2013). The value for the Frasnian/Famennian boundary reported by Harris et al. (2013) (0.40 ± 0.06) is, within error, identical to the value reported by Turgeon et al. (2007) (0.47 ± 0.04) for the Hanover Formation in New York, USA, suggesting that the Permian Basin was interconnected with other North American basins during the Late Devonian. The similarity between basins and lack of change in $(^{187}Os/^{188}Os)_i$ across the Frasnian-

Famennian boundary also preclude evidence for bolide impact of volcanism as a causal mechanism for the Late Devonian extinction. In addition, the uppermost interval of the Woodford Shale, of Mississippian age, has an $(^{187}Os/^{188}Os)_i$ value of 0.47 ± 0.07 which is very similar to the Devonian-Mississippian boundary interval (0.42 ± 0.01) of the Canadian Exshaw Formation reported by Selby and Creaser et al. (2005) further supporting the interconnectivity of North American basins during the Late Devonian and Early Mississippian.

All $^{187}Os/^{188}Os$ values for Devonian seawater are less radiogenic than present-day seawater. This suggests that the Devonian oceans were receiving a lower contribution of radiogenic continental crustal material than the present-day oceans are receiving. In addition, there is potentially a trend of increasing $^{187}Os/^{188}Os$ throughout the Late Devonian and into the Early Mississippian. However, this should be taken with caution until more accurate Os isotope data is obtained for this time period, as three of the $^{187}Os/^{188}Os$ at the upper end of this potential trend have high $^{187}Os/^{188}Os$ age uncertainties. An increasing trend during this time interval would be consistent with changing $^{87}Sr/^{86}Sr$ for seawater (Figure 2.5).

The $^{87}Sr/^{86}Sr$ of seawater falls through the Early Devonian from a value of 0.70871 at the start of the Devonian to near 0.70782 by the Middle Devonian (Eifelian) (Denison et al., 1997; van Geldern et al., 2006). The $^{87}Sr/^{86}Sr$ curve then remains relatively uniform, with high-order oscillations throughout the Middle Devonian with values between 0.70782 and 0.70784 before rising again starting in the Late Givetian with the rise maintained throughout the Late Devonian to reach a value of 0.70807 at the Devonian/Carboniferous

boundary (Diener et al., 1996; Denison et al., 1997; Veizer et al., 1999; van Geldern et al., 2006).

The final phase of the Caledonian Orogeny occurred in the Early Devonian (McKerrow et al., 2000). The decline in seawater $^{87}Sr/^{86}Sr$ during the Early Devonian correlates well with the end of the orogeny, following a sharp increase during the entire Silurian Period (van Geldern et al., 2006) and can be explained by a decrease in the flux of radiogenic Sr making it to the oceans during decreased denudation following slowed uplift rates associated with the end of the Caledonian Orogeny. A gradual steepening in slope at the Emsian-Eifelian boundary (~393 Ma) is reported by van Geldern et al. (2006) and is explained by an increased mantle strontium flux to the oceans at this time. Increased sea-floor spreading and related hydrothermal activity can be inferred from significant sea-level transgressions in the Late Emsian (408 – 393 Ma) and Early Eifelian (393 – 388 Ma) (Johnson et al., 1985; Johnson and Sandberg, 1988) especially since the Devonian Period is considered an ice-free period with Gondwanan ice-caps reported from only the latest Famennian (Frakes et al., 1992; Streel et al., 2000). The sea-level transgressions would also limit the flux of radiogenic Sr to the oceans by reducing the area of the continent that is exposed to weathering resulting in on overall decrease in the $^{87}Sr/^{86}Sr$ of coeval seawater. The Middle Devonian interval is characterized by a relatively slow, uniform decrease in the $^{87}Sr/^{86}Sr$ of seawater, reflecting an almost equal balance of radiogenic and non-radiogenic Sr (van Geldern et al., 2006). Such a drastic change in the slope must be controlled by a relatively large addition of radiogenic Sr to Middle Devonian seawater. The rise in seawater $^{87}Sr/^{86}Sr$ and $^{187}Os/^{188}Os$ that lasted the duration

of the Late Devonian can be explained by the increase in flux of radiogenic continental crust during uplift associated with the Variscan Orogeny (van Geldern et al., 2006). The collision of Armorica (a piece of rifted Gondwana) with Avalonia occurred in Late Frasnian (383 – 372 Ma) to Famennian (372 – 359 Ma) and led to the formation of the Ellesmerian Fold Belt, the Antler Orogen, part of the Appalachian Orogen and parts of the Hercynian (Variscan) Belt in Europe and north Africa (Pique et al., 1993; Matte, 2001; van Geldern, 2006). In addition, $\delta^{18}O$ isotopic data from van Geldern et al. (2006) indicate higher paleo-temperatures during the Late Devonian, perhaps caused by the continuous northern drift of Gondwana during this time. A warmer climate would have intensified enhanced chemical weathering therefore increasing the flux of radiogenic Sr and Os to the oceans.

2.5.3.5. Carboniferous

The Sr isotopic composition of seawater falls from ~0.70812 in the Early Mississippian to ~0.70755 in the mid-Visean (Kurschner et al., 1993; Denison et al., 1994; Bruckschen et al., 1995). The value then rises to near 0.70812 by the end of the Mississippian and continues to rise to 0.70830 in the mid-Pennsylvanian before declining through the Late Pennsylvanian to a value near 0.70809 at the end of the Carboniferous (Denison et al., 1994) (Figure 2.5).

Superimposed on the Tournaisian to mid-Visean decline in seawater $^{87}Sr/^{86}Sr$ are million year, higher-order oscillations (Bruckschen et al., 1995). Near-field records indicate that glaciation on Gondwana began in the Late Devonian to Early Mississippian (Isbell et al., 2003). Following a brief interval of warmth, glaciers became more widespread

throughout the mid- to Late-Carboniferous and Early Permian as part of the Late Paleozoic Ice Age (Crowley and Baum, 1991; Frakes et al., 1992; Woodard et al., 2013). The observations of alternating glacigenic and post-glacial deposits in South America, Australia, South Africa, and Tasmania document multiple episodes of ice-sheet development on Gondwana during the Carboniferous and Permian, occurring on million-year timescales (Algeo et al., 1991; Isbell et al., 2003; Caputo et al., 2008; Fielding et al., 2008; Stollhofen et al., 2000; Elrick and Scott, 2010; Woodard et al., 2013). Sedimentary cycles that record orbitally-driven climate changes are widely documented throughout Earth's history, recording long-term records of waxing and waning of glaciation on orbital timescales ($10^4 – 10^5$ yrs) (Anderson, 1982; Arthur et al., 1986; Goldhammer, 1987; Olson and Kent, 1999; Gale et al., 2002; Laurin et al., 2005; Culver et al., 2011; Theiling et al., 2012) causing sea-level fluctuations of greater than 50 m (Heckel, 1998; Goldhammer and Elmore, 1984; Soreghan, 1994; Joachimski et al., 2006; Rygel et al., 2008; Elrick et al., 2009). The high-order oscillations in the $^{87}Sr/^{86}Sr$ that are superimposed on the Early Mississippian seawater Sr curve can be explained by variations in the riverine Sr input associated with sea-level rise and fall due to glacial and inter-glacial periods, similar to those observed in the Pleistocene (Clemens et al., 1993). Post-glacial weathering pulses involving the chemical weathering of fined-grained physical weathering product produced by sub-glacial grinding underneath continental glaciers released during glacial melting and retreat would provide an increased in the flux of radiogenic Sr to the oceans (Vance et al., 2009). During period of glaciation, weathering would essentially be shut off resulting in a short-term decrease in the $^{87}Sr/^{86}Sr$ of coeval seawater.

The shift toward more radiogenic $^{87}Sr/^{86}Sr$ values during the Late Mississippian are interpreted as an increased flux of radiogenic Sr due to initiation of the Alleghanian Orogeny and the closure of the Rheic Ocean (Smith and Read, 2000; Saltzman, 2003; Woodard et al., 2013). This potentially resulted in a restructuring of atmospheric and oceanic circulation patterns that caused southern hemisphere ice build-up (Smith and Read, 2000; Saltzman, 2003).

No Os isotope data exists for tracking the seawater composition during the Carboniferous. As a prediction, based on the tectonic and climatic events outline above, the $^{187}Os/^{188}Os$ composition of Carboniferous seawater would parallel that of $^{87}Sr/^{86}Sr$, however, with superimposed, higher-frequency oscillations due to glacial, inter-glacial cycles recognized by Bruckschen et al. (1995).

2.5.3.6. Permian

The unradiogenic $(^{187}Os/^{188}Os)_i$ of 0.56 ± 0.02 at 298.0 ± 2.3 Ma of the Tasmanite oil shale presented in this study represents the first reported data for the Os isotopic composition of seawater during the earliest Permian. Wright et al. (2015) reported an $(^{187}Os/^{188}Os)_i$ ratio of 0.46 ± 0.09 at 264.3 ± 7.5 Ma for Guadalupian marine black shales of the Brushy Canyon Formation in the Delaware Basin, west Texas, USA. This value is slightly less radiogenic than the value reported for the base of the Permian in this study.

The end of the Permian Period is potentially marked by a, slightly resolvable, more radiogenic $^{187}Os/^{188}Os$ value than those for the earlier Permian black shales. However, within the analytical uncertainties, the values are undifferentiable. Rhenium-Os isotopic

data from four marine shale intervals at the Permian-Triassic boundary across two cores from the mid-Norwegian shelf and East Greenland yield ($^{187}Os/^{188}Os)_i$ values of 0.62 ± 0.04 at 252.0 ± 0.9 Ma, 0.57 ± 0.04 at 252.5 ± 1.3 Ma, 0.56 ± 0.12 at 252.2 ± 1.7 Ma, and 0.62 ± 0.11 at 252.1 ± 2.2 Ma (Georgiev et al., 2011).

These unradiogenic $^{187}Os/^{188}Os$ values for the Permian Period indicates a significantly less contribution of radiogenic continental crustal material via riverine input than the present-day ocean.

The Sr isotopic record of seawater records a general decrease in $^{87}Sr/^{86}Sr$ from a radiogenic value of ~0.7080 at the start of the Permian to an unradiogenic value of 0.70685 in the Middle Permian (Capitanian) (Korte et al., 2006). This secular change in the Sr isotopic composition of seawater records the lowest $^{87}Sr/^{86}Sr$ of the entire Phanerozoic, termed the Permian minimum, and suggests a major change in oceanography before the Paleozoic-Mesozoic transition and represents one of the most significant features in the Phanerozoic seawater $^{87}Sr/^{86}Sr$ history (Kani et al., 2008; Kani et al., 2013). The Permian minimum also marks a turnover from a long-term (~280 m.y.) decrease in the seawater $^{87}Sr/^{86}Sr$ starting in the Cambrian to a marked increase going into the Early Mesozoic, suggesting a major global change to the overall Sr-isotope balance in seawater from a mantle flux-dominated to a continental flux-dominated regime (Kani et al., 2008; Kani et al., 2013). Following the Permian minimum, there is a rapid increase, recovering to a $^{87}Sr/^{86}Sr$ value of 0.70715 by the end of the Permian (Korte et al., 2006).

The trend toward unradiogenic Sr throughout the majority of the Permian represents one of the most rapid changes in the Sr isotopic record of the entire Phanerozoic and is explained by a coupling of (1) the waning of glacial ice retreat that covered large parts of the Late Paleozoic Southern Hemisphere continents, and (2) the opening of the Neotethys sea throughout the Cisuralian and into the Guadalupian (Korte et al., 2006). The Gondwanan Permo-Carboniferous glaciation culminated in the Asselian and Early Sakmarian (Frakes et al., 1992) and glacial ice had waned and vanished by the Late Sakmarian (Banks and Clarke, 1987; Dickins and Shah, 1987). The beginning of the Permian is marked by radiogenic $^{87}Sr/^{86}Sr$ and $^{187}Os/^{188}Os$ values, coinciding with a period of deglaciation in the Southern Hemisphere. Deglaciation accelerates continental erosion and thus provides an enhanced riverine flux of radiogenic Sr and Os to the coeval oceans. During the waning stage of deglaciation during the Sakmarian, the rate of continental weathering decreases resulting in a decrease in the flux of radiogenic crustal material to the oceans. This coupled with the enhanced flux of unradiogenic strontium from hydrothermal circulation within the young oceanic crust created during the widespread volcanism associated with the opening of the Neotethys Ocean during the Cisuralian (~299 – 272 Ma) and into the Guadalupian (~272 – 260 Ma) resulted in the steep decrease in the $^{87}Sr/^{86}Sr$ during this time (Korte et al., 2006). There is a significant time gap in the Os isotopic data in the Early to Middle Permian. However, the $^{187}Os/^{188}Os$ values of 0.56 reported here, and 0.52 ± 0.02 from Wright et al. (2015) forms two end-members of a decline in $^{187}Os/^{188}Os$ of Permian seawater, consistent with $^{87}Sr/^{86}Sr$ values. Kani et al. (2013) suggests a simple suppression of the flux of radiogenic Sr to the oceans during decreased continental weathering wouldn't be enough to drive such a drastic

decrease in seawater $^{87}Sr/^{86}Sr$. In addition, due to plate tectonic processes being relatively constant through time, it is difficult to dramatically increase the unradiogenic flux from mid-ocean ridges (Kani et al., 2013). Even in the mid-Cretaceous, where the flux of unradiogenic Sr was significantly accelerated, the seawater $^{87}Sr/^{86}Sr$ was not drastically decreased (Kani et al., 2013). The extraordinarily low $^{87}Sr/^{86}Sr$ observed in the Permian could be enhanced due to an overall decrease of the exposed coast lines due to the assembly of the supercontinent of Pangaea during the Alleghanian Orogeny (Korte et al., 2006) which would limit the availability of radiogenic Sr and Os for weathering. The assembly of Pangaea may have shut down the direct connection of many pre-existing rivers to the Panthalassa Ocean, confining major drainage systems to intra-continental basins (Kani et al., 2008).

Following the cessation of the opening of the Neotethys during the Wordian (~269 – 265 Ma) and the assembly of Pangaea, coeval seawater $^{87}Sr/^{86}Sr$ began a slow trend toward more radiogenic values due to a larger contribution from radiogenic continental material via riverine flux (Korte et al., 2006) likely accelerated by the continental breakup of Gondwana (Kani et al., 2013). Within the few available data for Permian seawater Os, there also appears to be a trend toward more a more radiogenic Os composition between 264.0 Ma and the end of the Permian. Continental breakup initiates with regional uplift of the continental crust followed by rifting under an extensional tectonic regime. Regional uplift provides additional elevation, while normal faulting exposes deeper parts of the continental crust, both of which provide additional radiogenic Sr and Os (Kani et al., 2013).

In addition to these major geologic processes, secondary processes such as climate type (humid vs. arid) may have had an effect on the Sr and Os isotopic record. The Asselian (~299 – 296 Ma) and Early Sakmarian (~296 – 290 Ma) was characterized by a comparatively higher worldwide humidity compared to a more arid climate in the Artinskian-Late Permian interval (~290 – 252 Ma) (Kozur, 1984; Korte et al., 2006). Humid climates are more conducive to chemical weathering of continental materials, and thus provide a larger flux of radiogenic Sr and Os to the oceans compared to arid climate regimes. While the steep slope of the Sr isotopic curve throughout much of the Permian is believed to be the result of decreased continental weathering due to waning of deglaciation, the curve could be affected by decreased weathering under an arid climate regime (Korte et al., 2006). In addition, the slower rate of increase in the $^{87}Sr/^{86}Sr$ following cessation of the opening of the Neotethys could be due to slower weathering rates under an arid climate regime (Korte et al., 2006).

2.5.4. Isotopic curve decoupling

As divalent cations, Sr fractionates readily into major rock-forming minerals in high- and low-temperature environments (Ravizza and Zachos, 1993). However, due to it's highly siderophile and chalcophile nature, Os tends to be associated with trace phases such as sulfides and metal oxides. Because of the difference in geochemical affinity of Sr and Os, the composition of continental crust will reflect that of the rocks of which it is made. The subsequent weathering and transport of dissolved Sr and Os to the oceans would thus provide a spectrum of Sr and Os abundances and isotopic compositions, depending on the lithology that is being eroded. In addition, the association of strontium with carbonates

and osmium with ORM could provide another decoupling mechanism for the marine Sr and Os isotopic records. This difference is magnified as the lower $^{87}Sr/^{86}Sr$ of average riverine flux (0.712) relative to the eroding upper crust (0.716) provides a buffer for seawater $^{87}Sr/^{86}Sr$ (Palmer and Edmond, 1992). In contrast to Sr, the weathering of organic-rich sediments provides large amplitude variations in the seawater $^{187}Os/^{188}Os$ (Ravizza, 1993).

The $^{87}Sr/^{86}Sr$ and $^{187}Os/^{188}Os$ of present-day seawater are representative of the two-component mixing of present-day radiogenic riverine input and hydrothermal or cosmic non-radiogenic inputs (Chesley et al., 2000; Peucker-Ehrenbrink and Jahn, 2001). However, the $^{87}Sr/^{86}Sr$ and $^{187}Os/^{188}Os$ isotopic composition of the Paleogene were significantly different indicating a decoupling of Sr and Os isotopic balances or a substantial shift in the Sr and Os isotopic composition of riverine influx (Chesley et al., 2000; Peucker-Ehrenbrink and Jahn, 2001). Dubin and Peucker-Ehrenbrink (2015) suggest that the increased ubiquity of ORM in the geologic record, coupled with their high weatherability, that their recycling throughout Earth's history exerts a disproportionate driving force of change towards more radiogenic $^{187}Os/^{188}Os$ seawater.

Global variations in crustal composition likely affect the Sr and Os isotopic compositions of seawater on a local, basin scale. However, globally averaged fluxes and isotopic compositions of Sr and Os likely produce homogenous, well-mixed oceans. This is supported by the general coincidence of the trends in $^{187}Os/^{188}Os$ and $^{87}Sr/^{86}Sr$ observed here, and for other portions of Earth's history. In addition, the two end-member controls on seawater $^{187}Os/^{188}Os$ and $^{87}Sr/^{86}Sr$ are from radiogenic upper crustal and non-

radiogenic mantle-derived reservoirs. Thus, changes in the magnitude of these fluxes should result in the same polarity of change in seawater $^{187}Os/^{188}Os$ and $^{87}Sr/^{86}Sr$. Although, a decoupling in the magnitude of increase of these ratios could represent differential weathering. A higher magnitude change in $^{187}Os/^{188}Os$ could represent the weathering of more volume of an Os-rich lithology, such as ORM. This relationship is observed just prior to the Devonian boundary. However, this observation could be affected by the difference in the scales of $^{187}Os/^{188}Os$ and $^{87}Sr/^{86}Sr$ shown on Figure 2.5.

2.6. CONCLUSIONS

Thirty-nine data points spanning the ~290 m.y. time span of the Paleozoic provides the first compilation of Paleozoic seawater $^{187}Os/^{188}Os$ to date. Although the $^{187}Os/^{188}Os$ trend of seawater is largely decoupled from the $^{87}Sr/^{86}Sr$ record, similar trends can be identified, particularly in the interval leading up to the Devonian-Mississippian boundry and during the Permian Period. In addition, the seawater $^{187}Os/^{188}Os$ curve displays a general decreasing trend from a Phanerozoic maximum value of ~1.2 at the Precambrian-Cambrian boundary to ~0.29 within the Middle Devonian. While the Sr curve shows a similar decreasing trend, there are two increase/decrease cycles in $^{87}Sr/^{86}Sr$ values within this interval. The same relationship is observed from the Middle Devonian to the beginning of the Permian. However, the short residence time of Os coupled with the still limited data set for seawater $^{187}Os/^{188}Os$ prevents the construction of a reliable $^{187}Os/^{188}Os$ curve. This is highlighted by work by Finlay et al. (2010) who show a change of 0.60 in the $^{187}Os/^{188}Os$ of seawater over a 40 cm interval representing ~200 kyr (Figure 2.5). With gaps in the $^{187}Os/^{188}Os$ data presented here with magnitude of up to 86 Myr,

small temporal changes, on the order of ten to a hundred thousand years, in the $^{187}Os/^{188}Os$ of seawater will not be recognized with the current data.

A combined isochron, using data from three stratigraphically correlated cores, yields an age of 298.0 ± 2.3 Ma and an $(^{187}Os/^{188}Os)_i$ of 0.56 ± 0.02 (0.7% age uncertainty, 2σ, n=12, MSWD = 2.1) for the Tasmanite oil shale in the Tasmania Basin. This age correlates the Tasmanite oil shale to the GSSP for the base of the Permian in the Ural Mountains in addition to other globally correlated base Permian maximum flooding surfaces in the midcontinent of the U.S. and Namibia. This age therefore represents the best candidate for the base of the Permian in Gondwana and suggests that the base of the Permian was marked by a global flooding event, and provides the first absolute age for the correlation of eustatic events between the northern and southern hemispheres during the Permian.

REFERENCES

Algeo T., Wilson J.L. and Lohmann K.C. (1991) Eustatic and tectonic controls on cyclic sediment accumulation patterns in Lower-Middle Pennsylvanian strata of the Orogrande Basin, New Mexico. *New Mexico Geological Society Guidebook* **42**, 203-212.

Anderson R.Y. (1982) A long geoclimatic record from the Permian. *Journal of Geophysical Research* **87**, 7285-7294.

Arthur M.A., Bottjer D.J., Dean W.E., Fischer A.G., Hattin D.E., Kauffman E.G., Pratt L.M. and Scholle P.A. (1986) Rhythmic bedding in Upper Cretaceous pelagic carbonate sequences: varying sedimentary response to climate forcing. *Geology* **14**, 153-156.

Asmerom Y., Jacobsen S.B., Knoll A.H., Butterfield N.J. and Swett K. (1991) Strontium isotopic variations of Neoproterozoic seawater: Implications for crustal evolution. *Geochimica et Cosmochimica Acta* **55**, 2883-2894.

Banks M.R. (1980) Late Palaeozoic tillites of Tasmania. In: Hambrey M.J. and Harland W.B. (Eds.), Earth's Pre-Pleistocene Glacial Record. *Cambridge University Press, Cambridge*, 495-501.

Banks M.R. and Clarke M.J. (1987) Changes in the geography of the Tasmania Basin in the Late Paleozoic. In: McKenzie G.D. (Ed.), Gondwana Six: Stratigraphy, Sedimentology and Paleontology. *American Geophysical Union* **41**, 1-14.

Barnes C.R. (1986) The faunal extinction event near the Ordovician-Silurian boundary: a climatically induced crisis. In: Walliser O.H. (Ed.), *Global Bio-events: Lecture Notes in Earth Sciences* **8**, 121-126.

Birck J.-L., RoyBarman M. and Capmas F. (1997) Re-Os measurements at the femtomole level in natural samples. *Geostandards Newsletter* **20**, 19-27.

Brakel A.T. and Totterdell J.M. (1993) The Sakmarian-Kungurian of Australia. In: Findlay R.H., Unrug R., Banks M.R. and Veevers J.J. (Eds.), Gondwana Eight: Assembly, Evolution and Dispersal. *Proceedings of the Eighth Gondwana symposium*, 385-396.

Brandon A.D., Norman M.D., Walker R.J. and Morgan J.W. (1999) ^{186}Os-^{187}Os systematics of Hawaiian picrites. *Earth and Planetary Science Letters* **174**, 25-42.

Brass G.W. (1976) The variation of marine $^{87}Sr/^{86}Sr$ ratio during Phanerozoic time: Interpretation using a flux model. *Geochimica et Cosmochimica Acta* **40**, 721-730.

Brenchley P.J., Romano M., Young T.P. and Storch P. (1991) Hirnantian glaciomarine diamictites-Evidence for the spread of glaciation and its effect on Ordovician faunas. In: Barnes C.R. and Williams S.H. (Eds.), *Advances in Ordovician Geology, Geological Survey of Canada* **90-9**, 325-336.

Brenchley P.J., Marshall J.D., Carden G.A.F., Robertson D.B.R., Long D.G.F., Meidla T., Hints L. and Anderson T.F. (1994) Bathymetric and isotopic evidence for short-lived Late Ordovician glaciation in a green-house period. *Geology* **22**, 295-298.

Bruckschen P., Bruhn F., Veizer J. and Buhl D. (1995) $^{87}Sr/^{86}Sr$ isotope evolution of the Lower Carboniferous seawater: Dinantian of western Europe. *Sedimentary Geology* **100**, 63-81.

Brugmann G.W., Birck J.L., Herzig P.M. and Hofmann A.W. (1998) Os isotopic composition and Os and Re distribution in the active mound of the TAG hydrothermal system, Mid-Atlantic Ridge. *Proceedings of the Ocean Drilling Program Scientific Results* **158**, 91-100.

Burke W.H., Denison R.E., Hetherington E.A., Koepnick R.B., Nelson H.F. and Otto, J.B. (1982) Variation of seawater $^{87}Sr/^{86}Sr$ throughout Phanerozoic time. *Geology* **10**, 516-519.

Burton K.W., Bourdon B., Birck J.-L., Allegre C.J. and Hein J.R. (1999) Osmium isotope variations in the oceans recorded by Fe-Mn crusts. *Earth and Planetary Science Letters* **171**, 185-197.

Caputo M.V., Melo J.H.G., Streel M. and Isbell J.L. (2008) Late Devonian and Early Carboniferous glacial records of South America. In: Fielding C.R., Frank T.D. and Isbell J.L. (Eds.), Resolving the Late Paleozoic Ice Age in Time and Space. *Geological Society of America Special Paper* **441**, 161-173.

Cave R.R., Ravizza G.E., German C.R., Thomson J. and Nesbitt R.W. (2003) Deposition of osmium and other platinum-group elements beneath the ultramafic-hosted Rainbow hydrothermal plume. *Earth and Planetary Science Letters* **210**, 65-79.

Cawood P.A., Dunning G.R., Lux D. and van Gool J.A.M. (1994) Timing of peak metamorphism and deformation along the Appalachian margin of Laurentia in Newfoundland: Silurian, not Ordovician. *Geology* **22**, 339-402.

Chen X. (1990) Graptolite depth zonation. *Acta Palaeontologica Sinica* **29**, 507-526.

Chesley J.T., Quade J. and Ruiz J. (2000) The Os and Sr isotopic record of Himalayan paleorivers: Himalayan tectonics and influence on ocean chemistry. *Earth and Planteary Science Letters* **179**, 115-124.

Clarke M.J. and Banks M.R. (1975) The stratigraphy of Lower (Permo-Carboniferous) parts of the Parmeener super-group, Tasmania. In: Campbell K.S.W. (Ed.), Gondwana Geology. *Australian National University Press*, 453-467.

Clarke M.J. and Farmer N. (1976) Biostratigraphic nomenclature for Late Palaeozoic rocks in Tasmania. *Papers and Proceedings of the Royal Society of Tasmania* **110**, 91-109.

Clarke M.J. and Forsyth S.M. (1989) Late Carboniferous-Triassic. In: Burrett C.F. and Marten E.L. (Eds.), Geology and Mineral Resources of Tasmania. *Geological Association of Australia Special Paper* **15**, 209-293.

Clarke M.J. (1989) Lower Parmeener Supergroup. In: Burrett C.F. and Martin E.L. (Eds.) Geology and Mineral Resources of Tasmania. *Geological Society of Australia Special Publication* **15**, 295-309.

Clemens S.C., Farrell J.W. and Gromet L.P. (1993) Synchronous changes in seawater strontium isotope composition and global climate. *Nature* **363**, 607-610.

Cohen A.S. and Waters F.G. (1996) Separation of osmium from geological materials by solvent extraction for analysis by TIMS. *Analytical Chimica Acta* **332**, 269-275.

Cohen A.S., Coe A.L. Bartlett J.M. and Hawksworth C.J. (1999) Precise Re-Os ages of organic-rich mudrocks and the Os isotope composition of Jurassic seawater. *Earth and Planetary Science Letters* **167**, 159-173.

Collinson J.W., Isbell J.L., Elliot D.H., Miller M.F. and Miller J.M.G. (1994) Permian-Triassic Transantarctic Basin. In: Veevers J.J. and Powel .McA. (Eds.), Permian-Triassic Pangean Basins and Foldbelts along the Panthalassan Margin of Gondwanaland. *Geological Society of America Memoir* **184**, 173-222.

Colodner D., Sachs J., Ravizza G., Turekian K.K., Edmond J. and Boyle E. (1993) The geochemical cycles of rhenium: A reconnaissance. *Earth and Planetary Science Letters* **117**, 205-221.

Creaser R.A., Papanastassiou D.A. and Wasserburg G.J. (1991) Negative thermal ion mass spectrometry of osmium, rhenium and iridium. *Geochimica et Cosmochimica Acta* **55**, 397-401.

Creaser R.A., Sannigrahi P., Chacko T. and Selby D. (2002) Further evaluation of the Re-Os geochronometer in organic-rich sedimentary rocks: A test of hydrocarbon maturation effects in the Exshaw Formation, Western Canada Sedimentary Basin. *Geochimica et Cosmochimica Acta* **66**, 3441-3452.

Crowley T.J. and Baum S.K. (1991) Estimating Carboniferous sea-level fluctuations from Gondwana ice extent. *Geology* **19**, 975-977.

Crusius J., Calvert S., Pedersen T. and Sage D. (1996) Rhenium and molybdenum enrichments in sediments as indicator of oxic, suboxic and sulfidic conditions of deposition. *Earth and Planetary Science Letters* **145**, 65-78.

Culver S.J., Farrell K.M., Mallinson D.J., Willard D.A., Horton B.P., Riggs S.R., Theiler E.R., Wehmiller J.F., Parham P., Snyder S.W. and Hillier C. (2011) Micropaleontologic record of Quaternary paleoenvironments in the central Albemarle Embayment, North Carolina, U.S.A. *Palaeogeography, Palaeoclimatology, Palaeoecology* **305**, 227-249.

Cumming V.M., Selby D. and Lillis P.G. (2012) Re-Os geochronology of the lacustrine Green River Formation: Insights into direct depositional dating of lacustrine successions, Re-Os systematics and paleocontinental weathering. *Earth and Planetary Science Letters* **359-360**, 194-205.

Denison R.E., Koepnick R.B., Burke W.H., Hetherington E.A. and Fletcher A. (1994) Construction of the Mississippian, Pennsylvanian and Permian seawater $^{87}Sr/^{s}Sr$ curve. *Chemical Geology* **112**, 145-167.

Denison R.E., Koepnick R.B., Burke W.H., Hetherington E.A. and Fletcher A. (1997) Construction of the Silurian and Devonian seawater $^{87}Sr/^{86}Sr$ curve. *Chemical Geology* **140**, 109-121.

DePaolo D.J. and Ingram B.L. (1985) High-resolution stratigraphy with strontium isotopes. *Science* **227**, 938-841.

Derry L.A., Kaufman A.J. and Jacobsen S.B. (1992) Sedimentary cycling and environmental change in the Late Proterozoic: evidence from stable and radiogenic isotopes. *Geochimica et Cosmochimica Acta* **56**, 1317-1329.

Dickins J.M. and Shah S.C. (1987) The relationship of the Indian and western Australian Permian marine faunas. In: McKenzie G.D. (Ed.), Gondwana Six: Stratigraphy, Sedimentology and Paleontology. *Geophysical Monograms* **41**, 15-21.

Dickins J.M. (1996) Problems of a Paleozoic glaciation in Australia and subsequent climate in the Permian. *Palaeogeography, Palaeoclimatology, Palaeoecology* **125**, 185-197.

Diener A., Ebneth S., Veizer J. and Buhl D. (1996) Strontium isotope stratigraphy of the Middle Devonian: brachiopods and conodonts. *Geochimica et Cosmochimica Acta* **60**, 639-652.

Domack E.W., Burkley L.A., Domack C.R. and Banks M.R. (1993) Facies analysis of glacial marine pebbly mudstones in the Tasmania Basin: Implications for regional paleoclimates during the Paleozoic. In: Findlay R.H., Unrug R., Banks M.R. and Veevers J.J. (Eds.), Gondwana Eight: Assembly, Evolution and Dispersal. *Proceedings of the eighth Gondwana symposium*, 471-484.

Domack E.W., Wright S., Brandon A.D., DeMoor A., Fielding C. and Frank T. (2015) Absolute age for Paleozoic post glacial flooding event in Tasmania and correlation to the Carboniferous-Permian boundary. *Nature Geoscience* **xx**, x-x.

Du Vivier A.D.C., Selby D., Sageman B.B., Jarvis I., Grocke D.R. and Voigt S. (2014) Marine $^{187}Os/^{188}Os$ isotope stratigraphy reveals the interaction of volcanism and ocean circulation during Oceanic Anoxic Event 2. *Earth and Planetary Science Letters* **389**, 23- 33.

Dubin A. and Peucker-Ehrenbrink B. (2015) The importance of organic-rich shles to the geochemical cycles of rhenium and osmium. *Chemical Geology* **403**, 111-120.

Dunning G.R., O'Brien S.J., Colman-Sadd S.P., Blackwood R.F., Dickson W.L., O'Neill P.P. and Krogh T.E. (1990) Silurian orogeny in the Newfoundland Appalachians. *The Journal of Geology* **98**, 895-913.

Ebneth S., Shields G.A., Veizer J., Miller J.F. and Shergold J.H. (2001) High-resolution strontium isotope stratigraphy across the Cambrian-Ordovician transition. *Geochimica et Cosmochimica Acta* **65**, 2273-2292.

Elrick M. and Scott L.A. (2010) Carbon and oxygen isotope evidence for high-frequency (104-105 yr) and My-scale glacioeustasy in Middle Pennsylvanian cyclic carbonates (Gray Mesa Formation), central New Mexico. *Palaeogeography, Palaeoclimatology, Palaeoecology* **285**, 307-320.

Elrick M., Berkyova S., Klapper G., Sharp Z., Joachimski M. and Fryda J. (2009) Stratigraphic and oxygen isotope evidence for My-scale glaciations driving eustasy in the Early-Middle Devonian greenhouse world. *Palaeogeography, Palaeoclimatology, Palaeoecology* **276**, 170-181.

Esser B.K. and Turekian K.K. (1993) The osmium isotopic compositions of the continental crust. *Geochimica et Cosmochimica Acta* **57**, 3093-3104.

Ettensohn F.R. (1990) Flexural interpretation of relationships between Ordovician tectonism and stratigraphic sequences, central and southern Appalachians, USA. In: Barnes C.R. and Williams S.H. (Eds.), *Advances in Ordovician Geology, Geological Survey of Canada* **90-9,** 213-224.

Farmer N. (1985) Geological Atlas 1:50,000 Series, Sheet 88 (8311) Kingborough, Explanatory Report. *Geological Survey of Tasmania*, 1-104.

Fielding C.R., Frank T.D., Birgenheier L.P., Rygel M.C., Jones A.T. and Roberts J. (2008) Stratigraphic imprint of the Late Palaeozoic Ice Age in eastern Australia: A record of alternating glacial and nonglacial climate regime. *Journal of the Geological Society of London* **165**, 129-140.

Fielding C.R., Frank T.D., Isbell J.L. Henry L.C. and Domack E.W. (2010) Stratigraphic signature of the Late Paleozoic Ice Age in the Parmeener Supergroup of Tasmania, SE Australia, and inter-regional comparisons. *Palaeogeography, Palaeoclimatology, Palaeoecology* **298**, 70-90.

Finlay A.J., Selby D. and Grocke D.R. (2010) Tracking the Hirnantian glaciations using Os isotopes. *Earth and Planetary Science Letters* **293**, 339-348.

Finney S.C., Grubb B.J. and Hatcher Jr. R.D. (1996) Graphic correlation of Middle Ordovician graptolite shale, southern Appalachians: An approach for examining the subsidence and migration of a Taconic foreland basin. *Geological Society of America Bulletin* **108**, 355-371.

Frakes L.A., Francis J.E., Syktus J.I. (1992) Climate Modes of the Phanerozoic: The History of the Earth's Climate over the Past 600 Million Years. *Cambridge University Press, Cambridge.*

Gale A.S., Hardenbol J. and Hathaway B. (2002) Global correlation of the Cenomanian (Upper Cretaceous) sequences: evidence for Milankovitch controls on weathering. *Earth and Planetary Science Letters* **30**, 291-294.

Gao G. and Land L.S. (1991) Geochemistry of Cambro-Ordovician Arbuckle limestone, Oklahoma: implications for diagenetic $\delta^{18}O$ alteration and secular $\delta^{13}C$ and $^{87}Sr/^{86}Sr$ variation. *Geochimica et Cosmochimica Acta* **55**, 2911-2920.

Gao G., Dworkin S.I., Land L.S. and Elmore R.D. (1996) Geochemistry of Late Ordovician Viola limestone, Oklahoma: implications for marine carbonate mineralogy and isotopic compositions. *The Journal of Geology* **104**, 359-367.

Georgiev S., Stein H.J., Hannah J.L., Bingen B., Weiss H.M. and Piasecki S. (2011) Hot acidic Late Permian seas stifle life in record time. *Earth and Planetary Science Letters* **310**, 389-400.

Goldhammer R.K. and Elmore R.D. (1984) Paleosols capping regressive carbonate cycles in the Pennsylvanian Black Prince Limestone, Arizona. *Journal of Sedimentary Petrology* **54**, 1124-1137.

Goldhammer R.K. (1987) Platform carbonate cycles, Middle Triassic of northern Italy: the interplay of local tectonics and global eustasy, *Dissertation, Johns Hopkins University, Baltimore,* 548pp.

Gramlich J.W., Murphy T.J., Garner E.L. and Shields W.R. (1973) Absolute isotopic abundance ratio and atomic weight of a reference sample of rhenium. *Journal of Research of the National Bureau of Standards* **77A**, 691-698.

Hallam A. (1992) Phanerozoic sea-level changes. Columbia University Press, New York, 266 pp.

Halverson G.P., Wade B.P., Hurtgen M.T. and Barovich K.M. (2010) Neoproterozoic chemostratigraphy. *Precambrian Research* **182**, 337-350.

Hand S.J. (1993) Paleogeography of Tasmania's Permo-Carboniferous glacigenic sediments. In: Findlay R.H., Unrug R., Banks M.R. and Veevers J.J. (Eds.), Gondwana Eight: Assembly, Evolution and Dispersal. *Proceedings of the eighth Gondwana symposium*, 459-469.

Hannah J.L., Bekker A., Stein H.J., Markey R.J. and Holland H.D. (2004) Primitive Os and 2316 Ma age for marine shale: Implications for Paleoproterozoic glacial events and the rise of atmospheric oxygen. *Earth and Planetary Science Letters* **225**, 43-52.

Haq B.U. and Schutter S.R. (2008) A chronology of Paleozoic sea-level changes. *Science* **322**, 64-68.

Harris N.B., Mnich C.A., Selby D. and Korn D. (2013) Minor and trace element and Re-Os chemistry of the Upper Devonian Woodford Shale, Permian Basin, west Texas: Insights into metal abundance and basin processes. *Chemical Geology* **356**, 76-93.

Heckel P.H., Gibling M.R. and King N.R. (1998) Stratigraphic model for glacial-eustatic Pennsylvanian cyclothems in highstand nearshore detrital regimes. *Journal of Geology* **106**, 373-383.

Hess J., Bender M.L. and Schilling J.-G. (1986) Evolution of the ratio of Strontium-87 to Strontium-86 in seawater from Cretaceous to present. *Science* **231**, 979-984.

Holmden C., Creaser R.A., Muehlenbachs K., Bergstrom S.M. and Leslie S.A. (1996) Isotopic and elemental systematics of Sr and Nd in 454 Ma biogenic apatites: implications for paleoseawater studies. *Earth and Planetary Science Letters* **142**, 425-437.

Isbell J.L., Miller M.L., Wolfe K.L. and Lenaker P.A. (2003) Timing of Late Paleozoic glaciation in Gondwana: Was glaciation responsible for the development of northern hemisphere cyclothems? In: Chan M.A. and Archer A.W. (Eds.), Extreme Depositional Environments: Mega End Members in Geologic Time. *Geological Society of America Special Publication* **370**, 5-24.

Isbell J.L., Koch Z., Szablewski G.M. and Lenaker P.A. (2008) Permian glacigenic deposits in the Transantarctic Mountains, Antarctica. In: Fielding C.R., Frank T.D. and Isbell J.L. (Eds.), Resolving the Late Paleozoic Ice Age in Time and Space. *Geological Society of America Special Paper* **441**, 59-70.

Jacobsen S.B. and Kaufman A.J. (1999) The Sr, C and O isotopic evolution of Neoproterozoic seawater. *Chemical Geology* **161**, 37-57.

Jiang S.-Y., Yang J.-H., Ling H.-F., Chen Y.-Q., Feng H.-Z., Zhao K.-D. and Ni P. (2007) Extreme enrichment of polymetallic Ni-Mo-PGE-Au in lower Cambrian black shales of South China: An Os isotope and PGE geochemical investigation. *Palaeogeography, Palaeoclimatology, Palaeoecology* **254**, 217-228.

Joachimski M.M., von Bitter P.H. and Buggisch W. (2006) Constraints on Pennsylvanian glacioeustatic sea-level changes using oxygen isotopes on conodont apatite. *Geology* **34**, 277-280.

Johnson W.J. and Goldstein R.H. (1993) Cambrian seawater preserved as inclusions in marine low-magnesium calcite cement. *Nature* **22**, 231-234.

Johnson J.G. and Sandberg C.A. (1988) Devonian eustatic events in the Western United States and their biostratigraphic responses. In: McMillan N.J., Embry A.F. and

Glass D.J. (Eds.), Devonian of the world. *Proceedings of the Second International Symposium on the Devonian System* **3**, 171-178.

Johnson J.G., Klapper G. and Sandberg C.A. (1985) Devonian eustatic fluctuations in Euramerica. *Geological Society of America Bulletin* **96**, 567-587.

Kani T., Fukui M., Isozaki Y. and Nohda S. (2008) The Paleozoic minimum of $^{87}Sr/^{86}Sr$ ratio in the Capitanian (Permian) mid-oceanic carbonate: A critical turning point in the Late Paleozoic. *Journal of Asian Earth Science* **32**, 22-33.

Kani T., Hisanabe C. and Isozaki Y. (2013) The Capitanian Permian) minimum of $^{87}Sr/^{86}Sr$ ratio in the mid-Panthalassan paleo-atoll carbonates and its demise by the deglaciation and continental doming. *Gondwana Research* **24**, 212-221.

Kendall B.S., Creaser R.A., Ross G.M. and Selby D. (2004) Constraints on the timing of Marinoan 'Snowball Earth' glaciations by ^{187}Re-^{187}Os dating of a Neoproterozoic post-glacial black shale in Western Canada. *Earth and Planetary Science Letters* **222,** 729-470.

Kendall B.S., Creaser R.A. and Selby D. (2009) ^{187}Re-^{187}Os geochronology of Precambrian organic-rich sedimentary rocks. *Geological Society of London Special Publications* **326**, 85-107.

Koide M., Goldberg E.D., Niemeyer S., Gerlach D., Hodge V., Bertine K.K. and Padova A. (1991) Osmium in marine sediments. *Geochimica et Cosmochimica Acta* **55**, 1641-1648.

Kolata D.R., Huff W.D. and Bergstrom S.M. (1996) Ordovician K-bentonites of eastern North America. *Geological Society of America Special Papers* **313**, 84pp.

Korte C., Jasper T., Kozur H.W. and Veizer J. (2006) $^{87}Sr/^{86}Sr$ record of Permian seawater. *Palaeo* **240**, 89-107.

Kozur H. (1984) Perm. In: Troger K.-A. (Ed.), Abriβ der Historischen Geologie. Akademie-Verlag, Berlin 270-307.

Kurschner W., Becker R.T., Buhl D. and Veizer J. (1993) Strontium isotopes in conodonts: Devonian-Carboniferous transition, the northern Rhenish Slate Mountains, Germany. *Geological Society of Belgium* **115**, 595-622.

Laurin J., Meyers S.R., Sageman B.B. and Waltham D. (2005) Phase-lagged amplitude modulation of hemipelagic cycles: a potential tool for recognition and analysis of sea-level change. *Geology* **33**, 569-572.

Levasseur S., Birck J. and Allegre C.J. (1999) The osmium riverine flux and oceanic mass balance of osmium. *Earth and Planetary Science Letters* **174**, 7-23.

Li Z.X. and Powell C.M. (2001) An outline of the paleogeographic evolution of the Australian regions since the beginning of the Neoproterozoic. *Earth-Science Reviews* **53**, 237-277.

Li S., Xiao Q., Shen J., Sun L., Liu B., Yan B. and Jiang Y. (2003) Rhenium-osmium isotope constraints on the age and source of platinum mineralization in the Lower Cambrian black rock series of Hunan-Guizhou provinces, China. *Science in China* **46**, 919-927.

Li S. and Gao Z. (1995) REE characteristics of black rock series of Niutitang Formation in the Hunan-Guizhou area with discussion on REE model of marine hydrothermal sediments. *Mineralogica Sinica* **5**, 225-229.

Li S. and Gao Z. (2000) Source tracing of noble metal elements in Lower Cambrian black rock series of Guizhou-Hunan provinces, China. *Science in China* **43**, 625-632.

Lindsay J.F. (1970) Depositional environment of Paleozoic glacial rocks in the central Transantarctic Mountains. *Geological Society of America Bulletin* **81**, 1149-1172.

Lopez-Gamundi O.R. (1997) Glacial-postglacial transition in the Late Paleozoic basins of southern South America. In: Martini I.P. (Ed.), Late Glacial and Postglacial Environmental Changes, Quaternary Carboniferous-Permian and Proterozoic. *Oxford, UK, Oxford University Press*, 147-168.

Lopez-Gamundi O.R. (2010) Transgressions related to the demise of the Late Paleozoic Ice Age: Their sequence stratigraphic context. *The Geological Society of America Special Paper* **468**, 1-35.

Ludwig K. (2008) Isoplot, version 4.0: A geochronological toolkit for Microsoft Excel. *Berkeley Geochronology Center Special Publication* **4,** 1-12.

Markey R.J., Stein H.J., Hannah J.L., Zimmerman A., Selby D. and Creaser R.A. (2007) Standardizing Re-Os geochronology: A new molybdenite reference material (Henderson, USA) and the stoichiometry of Os salts. *Chemical Geology* **244**, 74-87.

Matte P. (2001) The Variscan collage and orogeny (480-290 Ma) and the tectonic definition of the Armorica Microplate: a review. *Terra Nova* **13**, 122-128.

McKerrow W.S., Mac Niocaill C., and Dewey J.F. (2000) The Caledonian Orogeny redefined. *Journal of the Geological Society of London* **157**, 1149-1154.

Melezhik V.A., Gorokhov L.M., Kuznetsov A.B. and Fallick A.E. (2001) Chemostratigraphy of Neoproterozoic carbonates: implications for 'blind dating'. *Terra Nova* **13**, 1-11.

Miller R.M. (1983) The Pan-African orogen of Southwest Africa/Namibia. *The Geological Society of South Africa Special Publication* **11**, 431-515.

Miller J.M.G. (1989) Glacial advance and retreat sequences in a Permo-Carboniferous section, central Transantarctic Mountains. *Sedimentology* **36**, 419-430.

Montanez I.P., Banner J.L., Osleger D.A., Borg L.E. and Bosserman P.J. (1996) Integrated strontium isotope variation and sea level history of the Middle to Upper Cambrian platform carbonates: implications for the evolution of Cambrian seawater $^{87}Sr/^{86}Sr$. *Geology* **24**, 917-920.

Morford J.L., Martin W.R., Francois R. and Carney C.M. (2009) A model for uranium, rhenium, and molybdenum diagenesis in marine sediments based on results from coastal locations. *Geochimica et Cosmochimica Acta* **73**, 2938-2960.

Munnecke A., Calner M., Harper D.A.T. and Servais T. (2010) Ordovician and Silurian sea-water chemistry, sea level, and climate: A synopsis. *Palaeogeography, Palaeoclimatology, Palaeoecology* **296**, 389-413.

Nikitin I.F., Frid N.M. and Zvontsov V.S. (1990) Paleogeography and main features of volcanicity in the Ordovician of Kazakhstan and North Tien Shan. In: Barnes C.R. and Williams S.H. (Eds.), *Advances in Ordovician Geology, Geological Survey of Canada* **90-9**, 259-270.

Olson P.E. and Kent D.V. (1999) Long-period Milankovitch cycles from the Late Triassic and Early Jurassic of eastern North America and their implications for the calibration of the Early Mesozoic time-scale and the long-term behavior of planets. *Philosophical Transactions of the Royal Society of London* **357**, 1761-1786.

Oxburgh R. (1998) Variations in the osmium isotope composition of sea water over the past 200,000 years. *Earth and Planetary Science Letters* **159**, 183-191.

Palmer M.R. and Edmond J.M. (1992) Controls over the strontium isotope composition of river water. *Geochimica et Cosmochimica Acta* **56**, 2099-2111.

Paquay F.S., Ravizza G.E., Dalai T.K. and Peucker-Ehrenbrink B. (2008) Determining chondritic impactor size from the marine osmium isotope record. *Science* **320**, 214-218.

Pegram W.J. and Turekian K.K. (1999) The osmium isotopic composition change of Cenozoic sea water as inferred from a deep-sea core corrected for meteoric contributions. *Geochimica et Cosmochimica Acta* **63**, 4053-4058.

Pegram W.J., Krishnaswami S., Ravizza G.E. and Turekian K.K. (1992) The record of sea water $^{187}Os/^{186}Os$ variation through the Cenozoic. *Earth and Planetary Science Letters* **113**, 569-576.

Peucker-Ehrenbrink B. and Blum J.D. (1998) Re-Os isotope systematics and weathering of Precambrian crustal rocks: Implications for the marine osmium isotope record. *Geochimica et Cosmochimica Acta* **62**, 3193-3203.

Peucker-Ehrenbrink B. and Jahn B.-M. (2001) Rhenium-osmium isotope systematics and platinum group element concentrations: Loess and the upper continental crust. *Geochemistry Geophysics Geosystems* **2**, 1-22.

Peucker-Ehrenbrink B. and Ravizza G.E. (2000) The marine osmium isotope record. *Terra Nova* **12**, 205-219.

Peucker-Ehrenbrink B. and Ravizza G.E. (2012) Chapter 8: Osmium Isotope Stratigraphy. In: Gradstein F.M., Ogg J.G., Schmitz M.D., Ogg G.J. (Eds.), *The Geologic Time Scale 2012*, Elsevier, Boston, 145-166.

Peucker-Ehrenbrink B., Ravizza G.E. and Hofmann A.W. (1995) The marine $^{187}Os/^{186}Os$ record of the past 80 million years. *Earth and Planetary Science Letters* **130**, 155-167.

Pique A., Bossiere G., Bouillin J.P., Chalouan A. and Hoepffner C. (1993) Southern margin of the Variscan Belt; the north-western Gondwana mobile zone (eastern Morocco and northern Algeria). *Geologische Rundschau* **82**, 432-439.

Qing H., Barnes C.R., Buhl D. and Veizer J. (1998) The strontium isotopic composition of Ordovician and Silurian brachiopods and conodonts: relationships to geological events and implications for coeval seawater. *Geochimica et Cosmochimica Acta* **62**, 1721-1733.

Ramezani J., Schmitz M.D., Davydov V.I., Bowring S.A., Snyder W.S. and Northrup C.J. (2007) High-precision U-Pb zircon age constraints on the Carboniferous-Permian boundary in the southern Urals Stratotype. *Earth and Planetary Science Letters* **256**, 244-257.

Ravizza G.E. and Peucker-Ehrenbrink B. (2003) The marine $^{187}Os/^{188}Os$ record of the Eocene-Oligocene transition: The interplay of weathering and glaciations. *Earth and Planetary Science Letters* **210**, 151-165.

Ravizza G.E. and Turekian K.K. (1989) Applications of the ^{187}Re-^{187}Os system to black shale geochronometry. *Geochimica et Cosmochimica Acta* **53**, 3257-3262.

Ravizza G.E. and Zachos J.C. (1993) Records of Cenozoic ocean chemistry. In: Holland H.D. and Turekian K.K. (Eds.), *Treatise on Geochemistry*, Elsevier **6**, 551-581.

Ravizza G.E., Martin C.E., German C.R. and Thompson G. (1996) Os isotopes as tracers in seafloor hydrothermal systems; metalliferous deposits from TAG hydrothermal area, 26 degrees N Mid-Atlantic Ridge. *Earth and Planetary Science Letters* **138**, 105-119.

Ravizza G.E., Turekian K.K. and Hay B.J. (2001) The geochemistry of rhenium and osmium in recent sediments from the Black Sea. *Geochimica et Cosmochimica Acta* **55**, 3741-3752.

Ravizza G.E. (1993) Variations of the $^{187}Os/^{186}Os$ ratio of seawater over the past 28 million years as inferred from metalliferous carbonates. *Earth and Planetary Science Letters* **118**, 335-348.

Raymo M.E. and Ruddiman W.F. (1992) Tectonic forcing of Late Cenozoic climate. *Nature* **359**, 117-122.

Reid C.M. and Burrett C.F. (2004) The geology and hydrocarbon potential of the glaciomarine Lower Parmeener Supergroup, Tasmania Basin. *PESA Eastern Australasian Basins Symposium II,* 265-275.

Richter F.M., Rowley D.B. and DePaolo D.J. (1992) Strontium isotope evolution of seawater: the role of tectonics. *Earth and Planetary Science Letters* **109**, 11-23.

Ritter S.M. (1995) Upper Missourian-Lower Wolfcampian (Upper Kasimovian-Lower Asselian) conodont biostratigraphy of the Midcontinent, U.S.A. *Journal of Paleontology* **69**, 1139-1154.

Rooney A.D., Selby D., Houzay J.-P. and Renne P.R. (2010) Re-Os geochronology of a Mesoproterozoic sedimentary succession, Taoudeni Basin, Mauritania: Implications for basin-wide correlations and Re-Os organic-rich sediments systematics. *Earth and Planetary Science Letters* **289**, 486-496.

Rooney A.D., Chew D.M. and Selby D. (2011) Re-Os geochronology of the Neoproterozoic-Cambrian Dalradian Supergroup of Scotland and Ireland: Implications for Neoproterozoic stratigraphy, glaciations and Re-Os systematics. *Precambrian Research* **185**, 202-214.

Rooney A.D., Macdonald F.A., Strauss J.V., Dudas F.O., Hallmann C. and Selby D. (2014) Re-Os geochronology and coupled Os-Sr isotope constraints on the Sturtian snowball Earth. *Proceedings of the National Academy of Sciences* **111**, 51-56.

Ross C.A. and Ross J.R.P. (1996) Silurian sea level fluctuations. In: Witzke B.J., Ludvigson G.A. and Day J. (Eds.), Paleozoic Sequence Stratigraphy: Views from the North American Craton. *Geological Society of America Special Paper* **306**, 187-192.

Rygel M.C., Fielding C.R., Frank T.D. and Birgenheier L.P. (2008) The magnitude of Late Paleozoic glacioeustatic fluctuations: a synthesis. *Journal of Sedimentary Research* **78**, 500-511.

Saltzman M.R. (2003) Late Paleozoic ice age: oceanic gateway or pCO2? *Geology* **31**, 151-154.

Santosh M. and Omori S. (2008) CO_2 flushing: A plate tectonic perspective. *Gondwana Research* **13**, 86-102.

Sawaki Y., Kawai T., Shibuya T., Tahata M., Omori S., Komiya T., Yoshida N., Hirata T., Ohno T., Windley B.F. and Maruyama S. (2010) 87Sr/86Sr chemostratigraphy of Neoproterozoic Dalradian carbonates below the Port Askaig Glaciogenic Formation, Scotland. *Precambrian Research* **179**, 150-164.

Sawaki Y., Ohno T., Fukushi Y., Komiya T., Ishikawa T., Hirata T. and Maruyama S. (2008) Sr isotope excursion across the Precambrian-Cambrian boundary in the Three Gorges area, South China. *Gondwana Research* **14**, 134-147.

Schmitz B., Peucker-Ehrenbrink B., Heilmann-Clausen C., Aberg G., Asaro F. and Lee C.A. (2004) Basaltic explosive volcanism, but no comet impact, at the Paleocene-

Eocene boundary: High-resolution chemical and isotopic records from Egypt, Spain and Denmark. *Earth and Planetary Science Letters* **225**, 1-17.

Selby D. and Creaser R.A. (2005) Direct radiometric dating of the Devonian-Mississippian time-scale boundary using the Re-Os black shale geochronometer. *Geology* **33**, 545-548.

Selby D. and Creaser R.A. (2001) Re-Os geochronology and systematics in molybdenite from the Endako porphyry molybdenum deposit, British Columbia, Canada. *Economic Geology* **96**, 197-204.

Selby D. and Creaser R.A. (2003) Re-Os geochronology of organic rich sediments: An evaluation of organic matter analysis methods. *Chemical Geology* **200**, 225-240.

Selby D., Mutterlose J. and Condon D.J. (2009) U-Pb and Re-Os geochronology of the Aptian/Albian and Cenomanian/Turonian stage boundaries: Implications for timescale calibration, osmium isotope seawater composition and Re-Os isotope systematics in organic-rich sediments. *Chemical Geology* **265**, 394-409.

Sharma M., Wasserburg G.J., Hofmann A.W. and Butterfield D.A. (2000) Osmium isotopes in hydrothermal fluids from Juan de Fuca Ridge. *Earth and Planetary Science Letters* **179**, 139-153.

Shields G.A. and Veizer J. (2002) Precambrian marine carbonate isotope database: Version 1.1. *Geochemistry, Geophysics, Geosystems* **3**, GC000266.

Shields G.A., Carden G.A., Veizer J., Meidla T., Rong J.-Y. And Li R.-Y. (2003) Sr, C, and O isotope geochemistry of Ordovician brachiopods: a major isotopic event around the Middle-Late Ordovician transition. *Geochimica et Cosmochimica Acta* **67**, 2005-2025.

Singh S.K., Trivedi J.R. and Krishnaswami S. (1999) Re-Os isotope systematics in black shales from the Lesser Himalaya: Their chronology and role in the $^{187}Os/^{188}Os$ evolution of seawater. Geochimica *et Cosmochimica Acta* **63**, 2381-2392.

Smith L.B. and Read J.F. (2000) Rapid onset of Late Paleozoic glaciation on Gondwana: evidence from Upper Mississippian strata of the Midcontinent, United States. *Geology* **28**, 279-282.

Smoliar M.I., Walker R.J. and Morgan J.W. (1996) Re-Os isotope constraints on the age of Group IIA, IIIA, IVA, and IVB iron meteorites. *Science* **271**, 1099-1102.

Snow J.E. and Reisberg L. (1995) Os isotopic systematics of the MORB mantle: results from altered abyssal peridotites. *Earth and Planetary Science Letters* **133**, 411-421.

Soreghan G.S. (1994) Stratigraphic responses to geologic processes: Late Pennsylvanian eustasy and tectonics in the Pedrogosa and Orogrande Basins, Ancestral Rocky Mountains. *Geological Society of America Bulletin* **106**, 1195-1211.

Stollhofen H., Stanistreet I.G., Bangert B. and Grill H. (2000) Tuffs, tectonism and glacially related sea-level changes, Carboniferous-Permian, southern Namibia. *Palaeogeography, Palaeoclimatology, Palaeoecology* **161**, 127-150.

Streel M., Caputa M.V., Loboziak S. and Melo J.H.G. (2000). Late Frasnian-Famennian climates based on palynomorph analyses and the question of the Late Devonian glaciations. *Earth Science Reviews* **52**, 121-173.

Terakado Y. (2001) Re-Os dating of the Kuroko ores from the Wanibuchi Mine, Shimane Prefecture, southwestern Japan. *Geochemical Journal* **35**, 169-174.

Theiling B.P., Elrick M. and Asmerom Y. (2012) Increased continental weathering flux during orbital-scale sea-level highstands: Evidence from Nd and O isotope trends in Middle Pennsylvanian cyclic carbonates. *Palaeogeography, Palaeoclimatology, Palaeoecology* **342-343**, 17-26.

Turekian K.K. and Pegram W.J. (1997) Os isotope record in a Cenozoic deep-sea core: its relation to global tectonics and climate. In: Ruddiman W. (Ed.), *Tectonic Uplift and Climate Change*, 384-397.

Turgeon S.C. and Creaser R.A. (2008) Cretaceous oceanic anoxic event 2 triggered by a massive magmatic episode. *Nature Letters* **454**, 323-326.

Turgeon S.C., Creaser R.A. and Algeo T.J. (2007) Re-Os depositional ages and seawater Os estimates for the Frasnian-Famennian boundary: Implications for weathering rates, land plant evolution, and extinction mechanisms. *Earth and Planetary Science Letters* **261**, 649-661.

van Geldern R., Joachimski M.M., Day J., Jansen U., Alvarez F., Yolkin E.A. and Ma X.-P. (2006) Carbon, oxygen and strontium isotope records of Devonian brachiopod shell calcite. *Palaeogeography, Palaeoclimatology, Palaeoecology* **240**, 47-67.

Vance D., Teagle D.A.H. and Foster G.L. (2009) Variable Quaternary chemical weathering fluxes and imbalances in marine geochemical budgets. *Nature* **458**, 493-496.

Veevers J.J. and Powell C.M. (1987) Late Paleozoic glacial episodes in Gondwanaland reflected in transgressive-regressive depositional sequences in Euramerica. *Geological Society of America Bulletin* **98**, 475-487.

Veizer J. and Compston W. (1974) $^{87}Sr/^{86}Sr$ composition of seawater during the Phanerozoic. *Geochimica et Cosmochimica Acta* **38**, 1461-1484.

Veizer J., Fritz P. and Jones B. (1986) Geochemistry of brachiopods: oxygen and carbon isotopic records of Paleozoic oceans. *Geochimica et Cosmochimica Acta* **50**, 1679-1696.

Veizer J., Ala D., Azmy K., Bruckschen P., Buhl D., Bruhn F., Carden G.A.F., Diener A., Ebneth S., Godderis Y., Jasper T., Korte C., Pawellek F., Podlaha O.G. and Strauss H. (1999) $^{87}Sr/^{86}Sr$ and $\delta^{13}C$ and $\delta^{18}O$ evolution of Phanerozoic seawater. *Chemical Geology* **161**, 59-88.

Volkening J., Walczyk T. and Heumann K.G. (1991) Osmium isotope ratio determinations by negative thermal ionization mass spectrometry. *International Journal of Mass Spectrometry and Ion Processes* **105**, 147-159.

Walker R.J., Prichard H.M., Ishiwatari A., Pimentel M. (2002) The osmium isotopic composition of convecting upper mantle deduced from ophiolite chromites. *Geochimica et Cosmochimica Acta* **66**, 329-345.

Widom E., Gaddis S.J. and Wells Jr. N.W. (2004) Re-Os isotope systematics in carbonates from Serpent mound, Ohio: Implications for Re-Os dating of crustal rocks and the osmium isotopic composition of Ordovician seawater. *Geochemistry, Geophysics, Geosystems* **5**, Q03006.

Woodard S.C., Thomas D.J., Grossman E.L., Olszewski T.D., Yancey T.E., Miller B.V. and Raymond A. (2013) Radiogenic isotope composition of Carboniferous seawater from North American epicontinental seas. *Palaeogeography, Palaeoclimatology, Palaeoecology* **370**, 51-63.

Wright S., Brandon A.D. and Casey J.F. (2015) Rhenium-Osmium geochronology and geochemistry of the Permian Brushy Canyon Formation: Insights into the evolution of Permian seawater. *Geochimica et Cosmochimica Acta* **xx,** x-x.

Wright C.A., Barnes C.R. and Jacobsen S.B. (2002) Neodymium isotopic composition of Ordovician conodonts as a seawater proxy: testing paleogeography. *Geochemistry, Geophysics, Geosystems* **3**, GC000195.

York D. (1969) Least-squares fitting of a straight line with correlated errors. *Earth and Planetary Science Letters* **5**, 320-324.

Young S.A., Saltzman M.R., Foland K.A., Linder J.S. and Kump L.R. (2009) A major drop in seawater $^{87}Sr/^{86}Sr$ during the Middle Ordovician (Darriwilian): links to volcanism and climate? *Geology* **37**, 951-954.

CHAPTER 3:

RHENIUM-OSMIUM ISOTOPES AND PLATINUM AND IRIDIUM ABUNDANCES ACROSS THE OCEANIC ANOXIC EVENT 2: SOURCE AND ENRICHMENT MECHANISMS

3.1. INTRODUCTION

The detection of an anomalous enrichment of iridium (Ir) in the globally correlated impact-related ejecta layer marking the Cretaceous-Paleogene (K-Pg) boundary provided the first evidence of a bolide impact as the causal mechanisms for the catastrophic extinction that occurred 65 Ma (Alvarez et al., 1980). Because Ir is highly depleted in the Earth's crust, the Ir enrichment observed at the K-Pg boundary has widely been interpreted to represent the fallout of a large meteorite impact, although some workers have proposed basaltic magmas resulting from mantle melting could also contribute Ir. This discovery triggered an explosion of multidisciplinary research related to the K-Pg boundary, in addition to the identification of other Ir anomalies throughout Earth's history (Playford et al., 1984; Hsu et al., 1985; Gostin et al., 1989; Evans et al., 1993; Sawlowicz, 1993; Evans and Chai, 1997; Lee et al., 2003; Schmitz et al., 2004). Despite over three decades of research, no other robust geochemical relationship between an extraterrestrial impact (and associated Ir anomaly) and a major extinction event has been reported, perhaps because very few terrestrial impacts have preserved ejecta (Grieve, 1991). Weak Ir anomalies at stage boundaries have been reported for the Precambrian-Cambrian (Hsu et al., 1985), Ordovician-Silurian (Wang and Chai, 1989), Devonian-Carboniferous (Chai et al., 1989), Permian-Triassic (Chai et al., 1986; Holser et al., 1991), Triassic-Jurassic (McLaren and Goodfellow, 1990), Late Jurassic-Early Cretaceous (Dypvik et al., 1996), Cenomanian-Turonian (Orth et al., 1988; Orth et al., 1993), Eocene-Oligocene (Alvarez et al., 1982; Glass, 1986), and the Pliocene-Pleistocene (Koeberl, 1993). However, many of these studies report Ir anomalies in mud

rocks at stage boundaries with no clear impact features such as shocked quartz, spherules, or micro-tektites. Making a link between Ir and other PGE anomalies observed in mud rock layers and extraterrestrial impacts prove problematic if the mud rocks do no contain preserved ejecta, as the enrichment mechanisms and geochemical behavior of PGEs in the aquatic environment is likely strongly different than during dispersal during large impacts.

The present understanding of the chemical speciation, distribution pattern and geochemical behavior of the PGEs in aqueous environment is limited, primarily due to the low abundances of these elements in natural rock samples and seawater (Anbar et al., 1996). Rhenium, Os, Ir, Ru, Pt, and Pd are present in present-day sea-water in abundances of 7.5 ppt, 10 ppq, 0.1 ppq, ~1 ppt, 50 ppq, and 60 ppq, respectively, and are among the least-abundant elements in the marine environment (Bekov et al., 1984; Ravizza, 2001).

Sediments rich in organic matter are significant crustal reservoirs of Re and Os with concentrations up to two orders of magnitude higher than average continental crust (Esser and Turekian, 1993; Peucker-Ehrenbrink and Jahn, 2001). Rhenium and Os are redox-sensitive and organophile in nature, and are thought to be sequestered by organisms at, or below the sediment-water interface in both marine and lacustrine basins under suboxic, anoxic or euxinic conditions and are thus hydrogenous in nature and become enriched in marine organic-rich mud rocks (ORM) under these conditions (Koide, 1991; Colodner et al., 1993; Crusius et al., 1996; Morford et al., 2009; Cumming et al., 2012). Because of recent advances in analytical geochemistry, the ^{187}Re-^{187}Os isotopic system ($t_{1/2}$ = 41.6

by; Smoliar et al., 1996) is gaining attention as a useful geochronometer for providing depositional ages for these rocks (Ravizza and Turekian, 1989; Cohen et al., 1999; Creaser et al., 2002; Selby and Creaser, 2003; Hannah et al., 2004; Kendall et al., 2004; Finlay et al., 2010; Rooney et al., 2010), in addition to understanding potentially small chemical changes in the temporal evolution of seawater due to the residence time of ~ 10-50 Kyr (Oxburgh, 1998; Peucker-Ehrenbrink and Ravizza, 2000). The Os isotopic composition of seawater is derived from a balance of two primary inputs: (1) radiogenic Os from river water during weathering and subsequent continental runoff of upper continental crust ($^{187}Os/^{188}Os$ ~1.4 Esser and Turekian, 1993; Peucker-Ehrenbrink and Jahn, 2001), and (2) nonradiogenic Os ($^{187}Os/^{188}Os$: 0.127) from the mantle via seafloor spreading and production of mid-ocean ridge basalts, flood basalt events, hydrothermal alteration of oceanic crust and from meteorite flux (Peucker-Ehrenbrink and Ravizza, 2000; Schmitz et al., 2004). The relative contributions of these sources have varied significantly throughout geologic history leading to significant variations in the $^{187}Os/^{188}Os$ of coeval seawater. The evolution of the Os isotopic composition of seawater over the Earth's history can be reconstructed by measuring the $^{187}Os/^{188}Os$ of ORM throughout the geologic past, which reflects the $^{187}Os/^{188}Os$ composition of seawater at the time their respective sediments were deposited. Inferences can then be made about the degree of continental weathering (Ravizza et al., 2001; Schmitz et al., 2004), seafloor spreading rates, the eruption of flood basalts (Cohen and Coe, 2002; Ravizza and Peucker-Ehrenbrink, 2003; Turgeon and Creaser, 2008) as well as the timing and size of meteorite impacts (Paquay et al., 2008). The variable redox speciations of Re and Os also makes these elements potentially useful in understanding seawater redox conditions in

the geologic past, especially during significant redox changes such as during Oceanic Anoxic Events (OAEs) (Morford and Emerson, 1999; Hannah et al., 2004; Kendall et al., 2009; Jenkyns, 2010).

Oceanic Anoxic Events have widely been accepted as episodes of widespread marine anoxia during which large amounts of organic carbon were buried on the ocean floor under oxygen deficient bottom waters (Schlanger and Jenkyns, 1976; Schlanger et al., 1987). Oceanic Anoxic Event 2 (OAE2) occurred at the Cenomanian-Turonian boundary (93.9 Ma) and is the most widespread and best defined OAE of the mid-Cretaceous (Turgeon and Creaser, 2008; Eldrett et al., 2014; Eldrett et al., 2015b). The OAE2 is generally recognized by a 2 to 4‰ positive excursion in the $\delta^{13}C$ of organic matter interpreted to record extensive periods of enhanced organic carbon burial under global anoxic greenhouse conditions, represented worldwide by sections containing organic-rich marine sedimentary rocks (Jenkyns, 1980; Schlanger et al., 1987;). The OAE2 is globally correlated to the Livello Bonarelli in Italy (Jenkyns, 1985), the Portland #1 core near Pueblo, Colorado (Western Interior Seaway) (Kennedy et al., 2000), the Wunstorf core in Germany (NW European Pelagic shelf) (Voigt et al., 2008), the Vocontian Basin, SE France (Western Tethys) (Grosheny et al., 2006; Jarvis et al., 2011) and DSDP Site 530 (proto-South Atlantic) (Forster et al., 2008). Recently, a diachroneity has emerged between the deposition of organic-rich sediment and the $\delta^{13}C$, with evidence in the Eagle Ford Group, Texas, USA (southern gateway of the Cretaceous Western Interior Seaway) for widespread and persistent oxygenation during OAE2 (Eldrett et al., 2014; Eldrett et al., 2015a).

The actual trigger mechanism, corresponding to the onset of global anoxia and increased carbon sequestration has not been clearly identified. The processes thought to play a role include (1) increased land and sea surface temperatures; (2) an accelerated hydrological cycle, sea level rise and changes in ocean circulation (Erbacher et al., 2001); (3) abrupt episodes of enhanced volcanism and emplacement of large igneous provinces (LIPs) which release large quantities of CO_2 into the atmosphere and hydrothermal iron into the oceans enhancing primary productivity (Orth et al., 1993; Snow et al., 2005; Turgeon and Creaser, 2008; Adams et al., 2010; Du Vivier et al., 2014; Eldrett et al., 2014; Eldrett et al., 2015a); and (4) an extraterrestrial impact (Orth et al., 1988; Orth et al., 1993).

Turgeon and Creaser (2008) reported an abrupt increase in the abundance of Os coupled with a negative $^{187}Os/^{188}Os$ excursion in two sections just prior to the $\delta^{13}C$ defining the onset of OAE2. In Furlo, Italy, Os abundance increases by greater than 10 ppb within 40 cm (Turgeon and Creaser, 2008). Du Vivier et al. (2014) observed the same trend in additional sections containing OAE2, although many were recognized to contain unconformities with uncertain age models. In all sections, the profile shows radiogenic $^{187}Os/^{188}Os$ trends from 0.6 – 1.0 values leading up to OAE2. This is followed by an abrupt unradiogenic $^{187}Os/^{188}Os$ trend to 0.13 to 0.16 at the onset of OAE2. An unradiogenic interval occurs during the first part of OAE2 followed by a return to radiogenic values of 0.4 to 1.1 toward the end of the event, near the Cenomanian-Turonian boundary (Du Vivier et al., 2014). Two-component mixing calculations are consistent with over 97% of the total Os content in seawater at the base of OAE2 being unradiogenic with $^{187}Os/^{188}Os = 0.127$. This is a 30 – 50 fold increase relative to pre-

OAE conditions (Turgeon and Creaser, 2008). These data indicate a relative higher input of unradiogenic Os to contemporaneous seawater. Sources of the unradiogenic Os were likely a result of large scale magmatic activity. Contemporaenous volcanism associated with large igneous provinces, such as the Caribbean Large Igneous Province (CLIP) or High Arctic Large Igneous Province (HALIP) are probably sources (Snow et al., 2005; Tegner et al., 2011). However, an extraterrestrial source of such large quantities of unradiogenic Os cannot be ruled out.

In contrast to Re and Os, few studies have investigated the concentrations of other PGE including Ir, Ru, Pt, and Pd, in marine organic-rich sediments (Orth et al., 1988; Colodner et al., 1992; Ravizza and Pyle, 1997; Ravizza, 1998; Peucker-Ehrenbrink and Hannigan, 2000; Jaffe et al., 2002; Baioumy et al., 2011; Qiu et al., 2015). These studies all document enrichment in Pt and Pd, but not Ir and superchondritic Os/Ir ratios in marine sediments enriched in organic matter. The positive correlation between Pt and Pd abundances and organic carbon content likely indicate that these elements are scavenged from sea-water and are hydrogenous in nature, similar to Re and Os (Baioumy et al., 2011). However, Ir abundances do not significantly differ from continental crust values, indicating that the majority of Ir in marine organic-rich sediments is associated with the inorganic, detrital fractions rather than the organic fraction (Baioumy et al., 2011).

Orth et al. (1988) reported two closely spaced Ir abundance peaks (110 ppt over background of 17 ppt) just below the Cenomanian-Turonian boundary in the upper Cenomanian marine sequence near Pueblo, Colorado and speculated an extraterrestrial source. Iridium abundance peaks at this interval have since been measured in 28 sites

around the world (Orth et al., 1993). In the Cretaceous Western Interior Seaway, the double peak pattern observed in the Pueblo, Colorado section (Orth et al., 1988) is only present south of Colorado, whereas sections to the north only exhibit a single Ir peak (Orth et al., 1993). Orth et al. (1993) suggested the lack of a second peak in the northern sections were the result of the source of Ir being far to the south in northward migrating water masses and the two distinct abundance pulses might not have reached the northern half of the seaway. Elemental abundance patterns within this interval closely resemble those of Mid-Atlantic Ridge basalt or tholeiitic lavas (Orth et al., 1993), and not carbonaceous chondrite. However, linking elemental abundance patterns in water-column-derived sediments to possible sources could prove problematic if the mud rocks do not contain preserved impact ejecta, as the enrichment mechanisms and geochemical behavior of PGEs in the aquatic environment is likely strongly different than from dispersal during large impacts.

In order to better understand the geochemical behavior of the PGEs in the marine environment and to describe the spatial and temporal variability of these enrichments prior to and during OAE2, this study presents high-resolution Re, PGE, and Os isotopic stratigraphy across OAE2 in the Shell Iona-1 core. This core was sampled within a section representing the southern gateway of the Cretaceous Western Interior Seaway near the margin of the Gulf of Mexico. The Iona-1 core was selected as recent work by Eldrett et al. (2014) provides high-resolution chronostratigraphy, $\delta^{13}C$, and trace element geochemical data across a ~60 m interval representing ~3 m.y. of depositional history, spanning the entire OAE2 and the Cenomanian-Turonian boundary. This core provides

the opportunity to measure Re and PGEs in pre-OAE2 anoxic environments as well as OAE2 oxic environments. The results from Eldrett et al. (2014, 2015b) provide a framework for comparing the data presented here.

3.2. GEOLOGIC SETTING

During the Early Mesozoic, extensional rifting and sea-floor spreading associated with the opening of the Gulf of Mexico led to the development of predominant structural and geologic features of south Texas (Pindell et al., 1988; Salvador, 1991; Montgomery et al., 2002). Following rift-related tectonism, regional subsidence caused by cooling of the basement rocks in the Early Cretaceous increased accommodation and promoted carbonate deposition along low-relief coastal areas during cyclic transgressive flooding leading to the development of a shallow-marine carbonate shelf complex (Montgomery et al., 2002; Almon and Cohen, 2008). In response to sea-level transgression and regression, a series of individual carbonate platforms separated by deeper water facies developed during the Cretaceous Period characterized by a series of stacked, prograding carbonate platform-separated by back-stepping, transgressive organic-rich deposits (Scott, 1993; Yurewicz et al., 1993). In the northern Gulf Coast region, these platforms were amalgamated into a single platform called the Comanche Shelf (Montgomery et al., 2002). The Pine Island and Bexar Members of the Pearsall Formation, the Del Rio Formation, and the Eagle Ford Formation each represent periods of primarily organic-rich deposition during marine transgression during the Late Aptian, Cenomanian, and Cenomanian-Turonian, respectively (Scott, 1993; Fritz et al., 2000; Harbor, 2011). The thickest of these transgressive deposits is the Cenomanian-Turonian Eagle Ford Group.

The Eagle Ford Group of south Texas is a mixed siliciclastic and carbonate unconventional resource play deposited in the southern gateway of the Cretaceous Western Interior Seaway near the margin of the Gulf of Mexico and represents one of the largest active unconventional reservoirs in the world (Figure 3.1) (Donovan and Staerker, 2010; Hentz and Ruppel, 2010). It is regionally extensive and extends 640 km from the Rio Grande embayment, near the Texas-Mexico border, to the East Texas Basin (Figure 3.2). Regional well-log correlations indicate that thickness varies from less than 12 m to over 120 m, with thickness and lateral facies distribution of the Eagle Ford Group controlled by pre-existing carbonate platform buildup and structural features such as the San Marcos Arch (an extension of the Llano Uplift), in addition to intra-shelf basins formed during syn-depositional subsidence during tectonic activity associated with the Rio Grande Rift such as the Maverick and East Texas Basins (Figure 3.2) (Rose, 1972; Donovan and Staerker, 2010; McGarity, 2013).

Uplift coupled with eustatic regression produced exposure of the shelf edge and the underlying Buda Limestone throughout much of south Texas creating one of the major unconformities in the Gulf of Mexico Mesozoic record (Galloway, 2008; Denne et al., 2014). This unconformity represents a shift from broad, reef-rimmed carbonate platforms to a ramp profile with alluvial, deltaic, and coastal depositional systems (Galloway, 2008; Phelps et al., 2015). Following this regression, a major eustatic transgression and back-stepping of the Comanche Shelf shifted sedimentation from the shelf margin toward intrashelf depocenters and led to the deposition of the Eagle Ford Group (Galloway, 2008; Phelps et al., 2015). The initial sedimentation of the Cenomanian lower Eagle Ford

are organic-rich marls containing abundant planktonic foraminfera and calcareous nanofossils with rhythmically interbedded limestone and abundant thin bentonites (Denne et al., 2014; Lowery et al., 2014; Corbett et al., 2014; Eldrett et al., 2015a). The upper Eagle Ford is retrogradational in nature and is interpreted as a transgressive unit (Donovan and Staerker, 2010). The Cenomanian-Turonian upper Eagle Ford is characterized by reduced amounts of organic matter and bentonites, and an increase in carbonate content and is interpreted as a regressive member deposited during sea-level highstand (Donovan and Staerker, 2010; Hentz and Ruppel, 2010). In the subsurface, the contact between the lower and upper Eagle Ford is marked by a decrease in gamma-ray values (thorium and uranium) (Donovan and Staerker, 2010). This contact was initially thought to coincide with the Cenomanian-Turonian boundary, however, this boundary has since been placed within the upper Eagle Ford (Eldrett et al., 2014; Eldrett et al., 2015b).

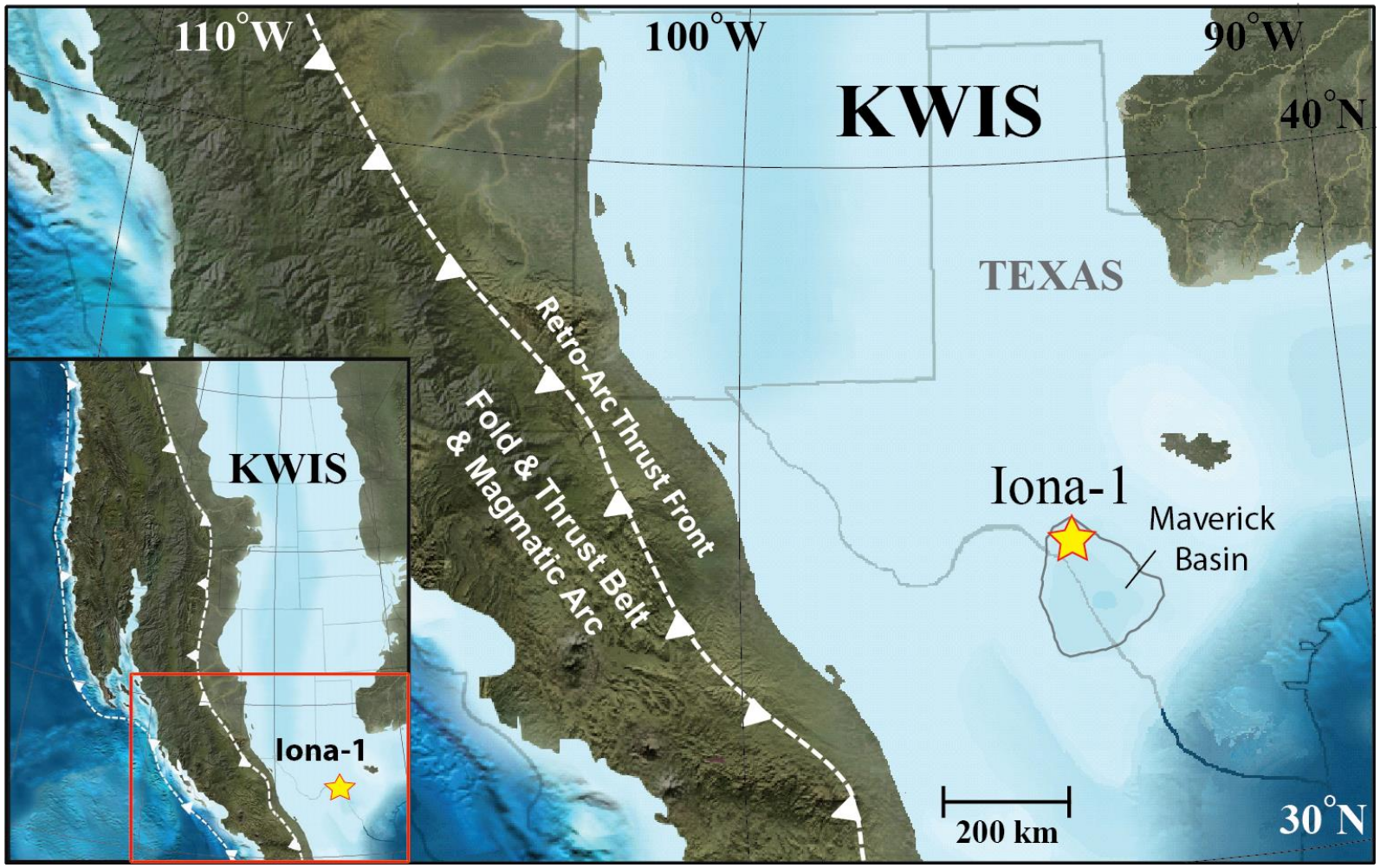

Figure 3.1: Paleogeography of western North America during the Late Cenomanian. Yellow star indicates the location of the Iona-1 core used in this study. KWIS: Cretaceous Western Interior Seaway. Figure modified after Eldrett et al. (2014) after Ron Blakey and Colorado Plateau Geosystems, Inc.

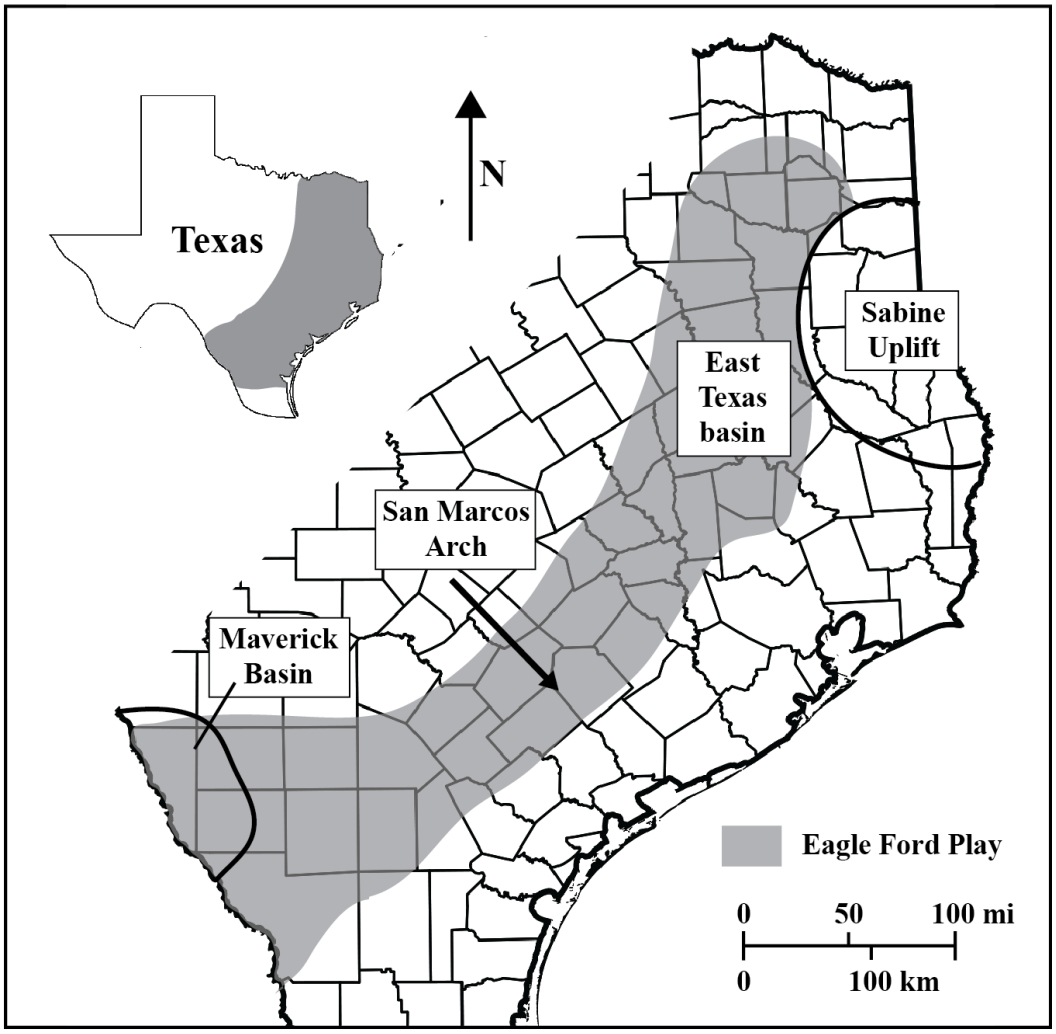

Figure 3.2: Regional extent of the Eagle Ford Group.

The Cretaceous Period Greenhouse was characterized by marine transgressive and regressive cycles of much lower magnitude than the Late Cenozoic Icehouse conditions. The most significant transgressive events occurred during the Albian, Cenomanian-Turonian, and the Early Coniacian-Late Santonian and correspond to global phases of bottom-water anoxia (Phelps et al., 2015). Periods of global bottom-water anoxia are termed oceanic anoxic events (OAEs; Schlanger and Jenkyns, 1976), and are characterized by wide-spread deposition of organic-rich fine-grained sediment and abrupt, globally recognized positive $\delta^{13}C$ excursions (see review in Jenkyns, 2010).

The Cenomanian-Turonian OAE2 in the Eagle Ford Group is characterized by a significant positive $\delta^{13}C$ excurstion of up to 4‰ representing the onset of massive organic carbon burial during a period of dramatic global change that includes widespread global anoxia and the deposition of organic-rich mud rocks (ORM) (Jenkyns, 2010; Eldrett et al., 2014). The OAE2 is globally correlated to the Livello Bonarelli in Italy (Jenkyns, 1985), the Portland #1 core near Pueblo, Colorado (Western Interior Seaway) (Kennedy et al., 2000), the Wunstorf core in Germany (NW European Pelagic shelf) (Voigt et al., 2008), the Vocontian Basin, SE France (Western Tethys) (Grosheny et al., 2006; Jarvis et al., 2011) and DSDP Site 530 (proto-South Atlantic) (Forster et al., 2008). Recently, a diachroneity has emerged between the deposition of organic-rich sediment and the carbon isotope excursion, with evidence in the Eagle Ford for widespread and persistent oxygenation during OAE2, suggesting a much more complex carbon cycle during these globally correlated events (Eldrett et al., 2014).

The diachroneity observed in the Eagle Ford coupled with high-resolution chronostratigraphy by Eldrett et al. (2014, 2015b) makes the Eagle Ford Group a prime target for high-resolution Re and PGE chemostratigraphy in order to better understand the geochemical behavior of the PGEs in the marine environment in addition to attempt to understand the spatial and temporal variability of these enrichments prior to and during OAE2.

3.3. SAMPLING AND ANALYTICAL PROCEDURES

3.3.1. Sampling

Samples used in this study were taken from the Iona-1 research core that was drilled in west Texas by Shell International Exploration and Production in 2011 (Figure 3.2). The Iona-1 core contains a complete record of the Eagle Ford Group Group, spanning the Early Cenomanian to Turonian, and contains organic-rich marls, limestones, and bentonites deposited on the north edge of the Maverick Basin, a distal sediment-starved intrashelf basin, in water depths of ~50 – 200 m (Figures 3.1-3.3) (Eldrett et al., 2014). Core plugs were taken from organic-rich marls of the Cenomanian Lower Eagle

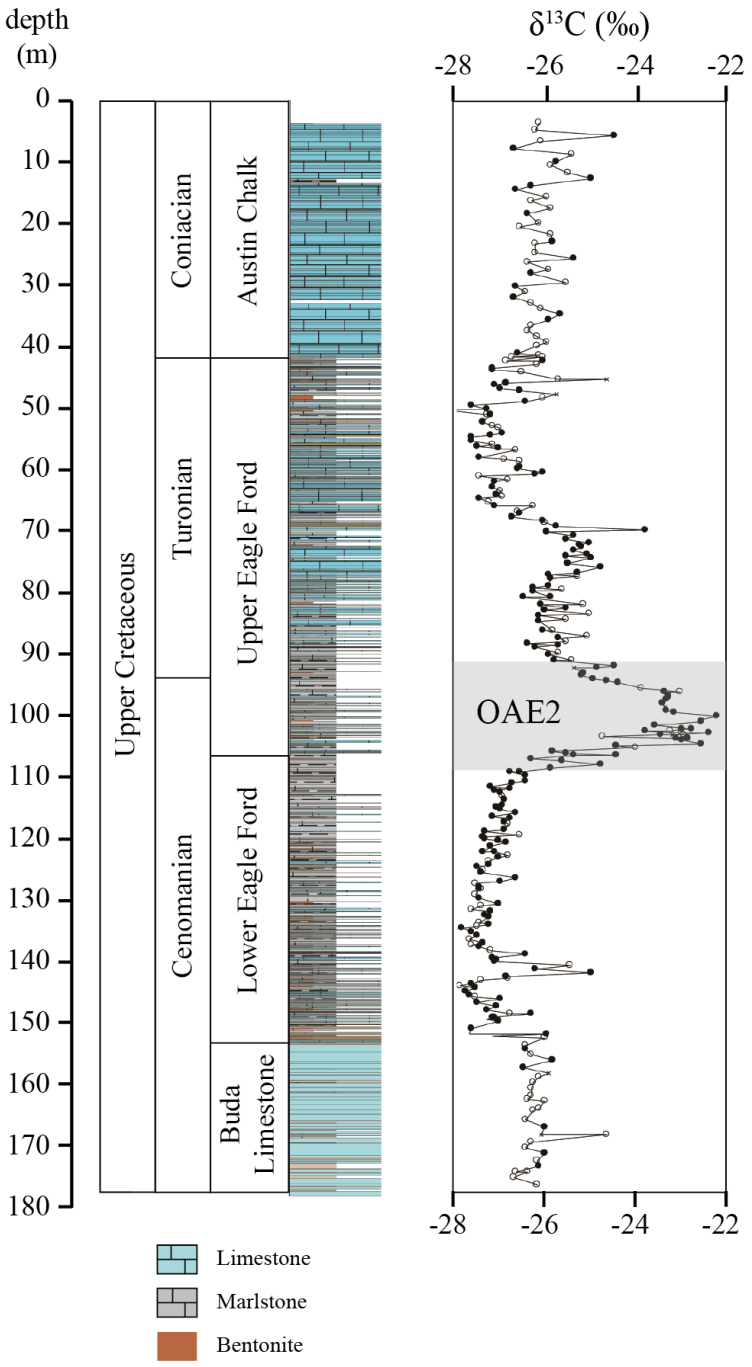

Figure 3.3: A) Lithostratigraphy of the Iona-1 core showing the relative location of the Eagle Ford Gp. and the inter-bedding of limestone and marlstone. B) Organic carbon isotope data ($\delta^{13}C$). OAE2: oceanic anoxic event 2. Figure modified after Eldrett et al. (2014).

Ford at closely spaced intervals (0.65 to 4.48 m) across a ~60 m interval spanning OAE2, representing ~4 Myr of deposition. Work by Eldrett et al. (2015b) provides a robust chronostratigraphic framework thus allowing accurate age determination for each sample (Tables 3.1 & 3.2).

The entire outer surface of the core plugs were sanded with silicon carbide to remove any drill markings and possible metal contamination that could have been obtained during coring, cleaned with ethanol, and left to air dry. A 20 g aliquot of each plug, representing a stratigraphic interval of 1 – 2 cm, was then broken into chips and powdered using a mortar and pestle. Although the actual amount of powder used for each analysis is 0.4 g, the larger aliquots of powdered sample negate the effects of Re and PGE heterogeneity within a sample (Kendall et al., 2009).

3.3.2. Os Analytical Procedures

Approximately 0.4 g of powdered sample was weighed and transferred to a thick-walled, internally cleaned, quartz glass Carius tube along with a known amount of a mixed spike (^{190}Os, ^{191}Ir, ^{194}Pt, and ^{185}Re) and 9 mL of inverse *aqua regia* solution (1:2 12N HCL: 13N HNO_3). The Carius tubes were sealed, and sample and spike were digested at 240°C for 48 hours. Digestion dissolves sample powder and oxidizes sample Os to the OsO_4^- species. Following digestion the Carius tubes were frozen, opened, then thawed, and Os was isolated from the inverse *aqua regia* solution using $CHCl_3$ solvent extraction at room temperature (Cohen and Waters, 1996), back extracted into 9N HBr and further purified via micro-distillation (Birck et al., 1997). The isolated Os was then loaded onto ultra-pure (>99.99%) Pt filaments and coated with a $Ba(OH)_2$ activator solution.

The Os isotopic compositions were determined by isotope-dilution-negative-thermal-ionization mass spectrometry (ID-NTIMS) on a ThermoElectron TRITON Plus thermal-ionization mass spectrometery (TIMS) at the University of Houston (Creaser et al., 1991; Volkening et al., 1991). Osmium was measured as OsO_3^- via ion-counting using a secondary electron multiplier in peak-hopping mode.

Measured isotopic ratios were spike stripped, corrected for isobaric oxygen interference, instrumental mass fractionation ($^{192}Os/^{188}Os$=3.08761), and procedural blank contributions. Uncertainties were obtained through the error propagation of uncertainties in blank abundance and isotopic composition, spike abundance values, mass spectrometry measurements of Os, and the reproducibility of the Os isotopic values of the standard. Average procedural blank was 0.60 ± 0.56 pg/g for Os with a $^{187}Os/^{188}Os$ = 0.16 ± 0.02 (2σ, n=18).

Repeat measurements of an Os standard were performed throughout the four year analytical campaign. The Os standard (University of Maryland, Brandon et al., 1999) yielded a $^{187}Os/^{188}Os$ ratio of 0.11385 ± 0.00026 (2σ, n=18) for 500 pg loads using a secondary electron multiplier and is, within uncertainty, identical to that reported by Brandon et al. (1999).

The $(^{187}Os/^{188}Os)_i$ values used in this study were calculated using the measured Re-Os data, the ^{187}Re decay constant of $\lambda=1.666 \times 10^{-11} a^{-1}$ (Smoliar et al., 1996), and the stratigraphic ages from robust chronostratigraphic framework (Eldrett et al., 2014).

3.3.3. Rhenium and Platinum Group Element Analytical Procedures

Following extraction of Os from the *aqua regia* solutions, the residual solution containing Ir, Pt, and Re, was taken to dryness at ~70°C in internally cleansed Savillex PTFE beakers and brought back up in 3 mL of 12N HCl and taken back to dryness. This procedure was repeated two more times to ensure complete conversion of ions to the chloride species in preparation for cation exchange columns. Bio-rad cation exchange columns were prepared with 1.6 mL of Bio-Rad AG50X-8 100-200 mesh cation resin, then cleaned with successive rinses of 4N HF and 6N HCl and equilibrated with 0.15N HCl. Samples were re-dissolved in 2 mL of 0.15N HCl and passed through the cation columns. The major interfering cations were adsorbed onto the resin while Re and the PGEs passed through the column and were collected in PTFE beakers. Following collection of Re and the PGEs, interfering cations were flushed from the columns using successive rinses of 4N HF and 6N HCl. Cuts containing Re and PGEs were taken to dryness at ~80°C, then brought back up in 0.5 mL 0.15N HCl and passed through a second round of cation exchange columns and taken to dryness once again. The dried Re + PGE cuts were then brought up in 1 mL of 13N HNO_3, taken to dryness, then brought back up in 1 mL of 12N HCl and taken to dryness once more. This is done to dissolve any organic complexes that may be carrying interfering cations. The cation column procedure is then completed once more with the sample loaded onto the column in 0.5 mL 0.15N HCl. Rhenium and PGE were then taken to dryness and brought up in 1 mL of 0.25N HCl for analysis.

Analyses were performed by quadrupole ICP-MS using a Varian 810-MS at the University of Houston. Mass fractionation and instrumental drift were determined by applying sample/standard bracketing with a standard of natural isotopic composition and then applying this correction factor to the individual measurements. Over the course of this analytical campaign, reproducibility on 1 ppb of a mixed PGE standard of natural isotopic composition was better than 2% (2σ) for the isotopic ratios used for isotope dilution calculations ($^{185}Re/^{187}Re$: 0.37%; $^{191}Ir/^{193}Ir$: 1.81%; $^{194}Pt/^{195}Pt$: 0.58%). Signal intensities were corrected for interference from Hg on ^{196}Pt and ^{198}Pt, and Os on ^{187}Re. The intensities of Mo, Rb, Y, Zr, Lu, and Hf were monitored in order to determine possible oxide interferences (LuO: ^{191}Ir; HfO: ^{193}Ir, ^{194}Pt, ^{195}Pt, ^{196}Pt). Procedural blanks were 54 ± 17 pg for Ir, 149 ± 43 pg for Pt, and 2 ± 1 pg for Re (2σ, n=3).

3.4. RESULTS

3.4.1. Rhenium and Osmium Abundances

The Re-Os abundances and isotopic compositions for Eagle Ford samples are presented in Table 3.1. All samples are enriched in Re (5 - 227 ppb) and Os (65 - 6017 ppt) compared to modern-day average continental crust (~1 ppb Re and 30-50 ppt Os; Esser and Turekian, 1993) and have typical Re abundances of ORM (Ravizza and Turekian, 1989; Cohen et al., 1999; Creaser et al., 2002; Selby and Creaser, 2003; Hannah et al., 2004; Kendall et al., 2004; Finlay et al., 2010; Rooney et al., 2010). The $^{187}Re/^{188}Os$ ratios range from 45 to 2937 and are positively correlated with $^{187}Os/^{188}Os$ ratios of 0.24 to 5.52.

Pre-OAE2 values of Re are among the highest (117 – 227 ppb), while Os values are on the lower end of the range reported here (400 – 492 ppt). Across the onset of OAE2 there is an abrupt shift to very high values in the Os concentration. Just prior to OAE2, Os concentrations increase by by a factor of 12 to ~5.4 ppb within ~1.3 m of core (111.36 – 110.01 m) (Figure 3.4). Pre-OAE2 Re abundances decrease leading up to OAE2 from 161 ppb at the base of the section to 65 ppb at the start of OAE2 with the exception of the sample with high Os abundance (227 ppb Re) just prior to OAE2 (Figure 3.4).

Within OAE2, two additional Os peaks are observed. The first occurs at 106.50 m, and the second at 103.54 m and have abundances of 2646 ppt and 1301 ppt, respectively (Figure 3.4). The same trend in Re abundances isn't observed. The measured $^{187}Re/^{188}Os$ ratio shows a decrease from the base of the section (~2742) leading up to OAE2 (~189) and is heavily controlled by the decreasing Re abundance within this interval (Figure 3.4).

Sample	Depth (m)	Age (Ma)[1]	$\frac{^{187}Re}{^{188}Os}$	±	$\frac{^{187}Os}{^{188}Os}$	±	Re (ppb)	±	Os (ppt)	±	$\frac{^{187}Os}{^{188}Os_i}$
Core: Iona-1											
EFC-1	86.65	93.70	512.93	6.67	1.33	0.05	6.03	0.02	65.47	1.23	0.53
EFC-20	90.83	93.94	947.08	12.31	2.13	0.03	53.02	0.20	340.40	2.97	0.65
EFC-21	95.31	94.17	676.82	8.80	1.55	0.02	39.69	0.15	334.98	2.69	0.49
EFC-2	98.08	94.31	630.18	8.19	1.47	0.01	29.09	0.11	261.45	1.55	0.48
EFC-3	100.90	94.45	541.02	7.03	1.14	0.01	28.55	0.11	287.92	1.50	0.29
EFC-23	102.63	94.54	157.76	2.05	0.40	0.00	16.52	0.06	522.44	2.18	0.15
EFC-4	102.95	94.53	116.67	1.52	0.34	0.00	18.98	0.07	805.46	1.93	0.15
EFC-24	103.54	94.54	151.08	1.96	0.37	0.00	39.53	0.15	1301.25	3.08	0.14
EFC-25	104.44	94.58	83.63	1.09	0.28	0.00	20.43	0.08	1201.17	2.60	0.15
EFC-5	104.83	94.62	116.71	1.52	0.38	0.00	17.75	0.07	757.19	1.63	0.20
EFC-26	105.68	94.64	68.38	0.89	0.30	0.00	5.81	0.02	418.41	1.95	0.19
EFC-6	106.45	94.68	109.98	1.43	0.34	0.00	51.87	0.19	2335.22	3.69	0.16
EFC-27	106.50	94.72	74.43	0.97	0.28	0.00	40.07	0.15	2646.16	4.22	0.16
EFC-7	107.17	94.75	45.13	0.59	0.24	0.00	10.50	0.04	1138.41	2.63	0.17
EFC-8	108.77	94.82	216.25	2.81	0.55	0.00	65.48	0.24	1539.17	3.65	0.21
EFC-29	110.01	94.88	189.87	2.47	0.46	0.00	227.28	0.84	6017.55	10.56	0.16
EFC-10	111.36	94.96	1463.74	19.03	2.71	0.02	117.83	0.44	518.64	3.76	0.40
EFC-31	113.42	95.08	2399.23	31.19	4.60	0.16	126.11	0.47	400.91	10.99	0.79
EFC-11	114.50	95.14	2937.31	38.18	5.52	0.06	169.30	0.63	473.26	4.16	0.87
EFC-12	116.79	95.25	2560.57	33.29	4.89	0.07	161.60	0.60	492.87	4.90	0.82

Table 3.1: Rhenium-osmium isotopic data for organic-rich marls from the Eagle Ford Gp.. Uncertainties are reported as 2σ. [1] Age (Ma) provided by detailed chronostratigraphy by Eldrett et al. (2015b).

Sample	Depth (m)	Age (Ma)[1]	Pt (ppb)	±	Ir (ppt)	±
Core: Iona-1						
EFC-1	86.65	93.70	1.46	0.01	12.39	0.22
EFC-20	90.83	93.94	0.81	0.00	7.80	0.14
EFC-21	95.31	94.17	1.03	0.01	7.46	0.14
EFC-2	98.08	94.31	1.64	0.01	16.38	0.30
EFC-3	100.9	94.45	1.20	0.01	8.17	0.15
EFC-23	102.63	94.54	8.76	0.05	94.59	1.71
EFC-4	102.95	94.53	6.26	0.04	83.33	1.51
EFC-24	103.54	94.54	5.90	0.03	179.41	3.25
EFC-25	104.44	94.58	2.94	0.02	90.11	1.63
EFC-5	104.83	94.62	0.64	0.00	12.11	0.22
EFC-26	105.68	94.64	1.47	0.01	11.18	0.20
EFC-6	106.45	94.68	1.38	0.01	18.00	0.33
EFC-27	106.50	94.72	1.23	0.01	20.44	0.37
EFC-7	107.17	94.75	0.85	0.00	12.59	0.23
EFC-8	108.77	94.82	0.91	0.01	9.78	0.18
EFC-29	110.01	94.88	1.48	0.01	25.97	0.47
EFC-10	111.36	94.96	1.20	0.01	21.81	0.39
EFC-31	113.42	95.08	0.99	0.01	12.12	0.22
EFC-11	114.50	95.14	1.24	0.01	44.00	0.80
EFC-12	116.79	95.25	0.99	0.01	21.88	0.40

Table 3.2: Platinum and iridium abundance data for organic-rich marls from the Eagle Ford Gp.. Uncertainties are reported as 2σ. [1] Age (Ma) provided by detailed chronostratigraphy by Eldrett et al. (2015b).

3.4.2. Platinum and Iridium Abundances

Eagle Ford Group samples have Pt and Ir abundances of 0.64 – 8.76 ppb and 12 – 179 ppt, respectively, and are similar to those reported for other marine ORM (Table 3.2) (Orth et al., 1988; Colodner et al., 1992; Ravizza and Pyle, 1997; Baioumy et al., 2011). Both Pt and Ir abundances vary minimally with depth with the exception of a 1.81 m interval within OAE2. Within this interval, Pt and Ir spikes of 8.75 and 179 ppt are observed (Figure 3.4). These spikes represent an increase in Pt and Ir of ~8 ppb (8X) and ~170 ppt (22X) over background, respectively.

3.4.3. $(^{187}Os/^{188}Os)_i$ Stratigraphy

The $(^{187}Os/^{188}Os)_i$ profile for the Eagle Ford Group shows a highly variable trend. Highly radiogenic values occur prior to OAE2, non-radiogenic values during the lower portion of OAE2, then a recovery back to radiogenic values throughout the upper half and following OAE2 (Figure 3.4). Prior to OAE2, $(^{187}Os/^{188}Os)_i$ values of 0.79 – 0.86 are observed for the Iona-1 section. Just prior to and across the onset of OAE2, $(^{187}Os/^{188}Os)_i$ values show an abrupt decrease to 0.15. The $(^{187}Os/^{188}Os)_i$ values are consistently low throughout the lower portion of OAE2, with only minor variation (0.13 – 0.20) over this 7.4 m interval. Starting at 102.63 m, in the upper portion of OAE2, the $(^{187}Os/^{188}Os)_i$ begins to recover, reaching a more radiogenic value of 0.65 at 90.83 m (Figure 3.4). A similar trend is observed in other sections containing OAE2 (Turgeon and Creaser, 2008; Du Vivier et al., 2014), although these sections contain an unconformity at the base of OAE2 and

therefore lack the early part of the $\delta^{13}C$ excursion contained in the Iona-1 section (Eldrett et al., 2015b).

3.5. DISCUSSION

3.5.1. Pre-OAE2 ($^{187}Os/^{188}Os)_i$

The $^{187}Os/^{188}Os$ of seawater at the southern gateway to the KWIS during the short interval (~170 kyr) leading up to OAE2 has a radiogenic composition of 0.79 – 0.86 (Figure 3.4). This is less radiogenic than present day seawater (~1.06; Peucker-Ehrenbrink and Ravizza, 2000) indicating the southern gateway to the WCIS received significantly lower relative contributions of crustal Os from 95.08 to 95.25 Ma than for the present-day ocean. Similar conditions existed throughout the Late Oligocene and much of the Miocene (Peucker-Ehrenbrink and Ravizza, 2012).

Similar $(^{187}Os/^{188}Os)_i$ values are reported for sites within the KWIS, western Tethys and the proto-North Atlantic from the Demerara Rise prior to OAE2 (Figure 3.5) (Turgeon and Creaser, 2008; Du Vivier et al., 2014). All sites show a range of $(^{187}Os/^{188}Os)_i$ values from ~0.5 – 1.0, indicating that seawater was locally heterogeneous during this time. The local heterogeneity was likely controlled by the amount and $^{187}Os/^{188}Os$ composition of the fluxes of Os that was entering the individual basins (Du Vivier et al., 2014). The site reflecting the most radiogenic seawater during this interval is the Portland #1 Core on the western margin of the WCIS with $(^{187}Os/^{188}Os)_i$ values of 0.7 – 1.0 (Du Vivier et al., 2014). Du Vivier et al. (2014) attributed the radiogenic Os isotopic composition to the influence

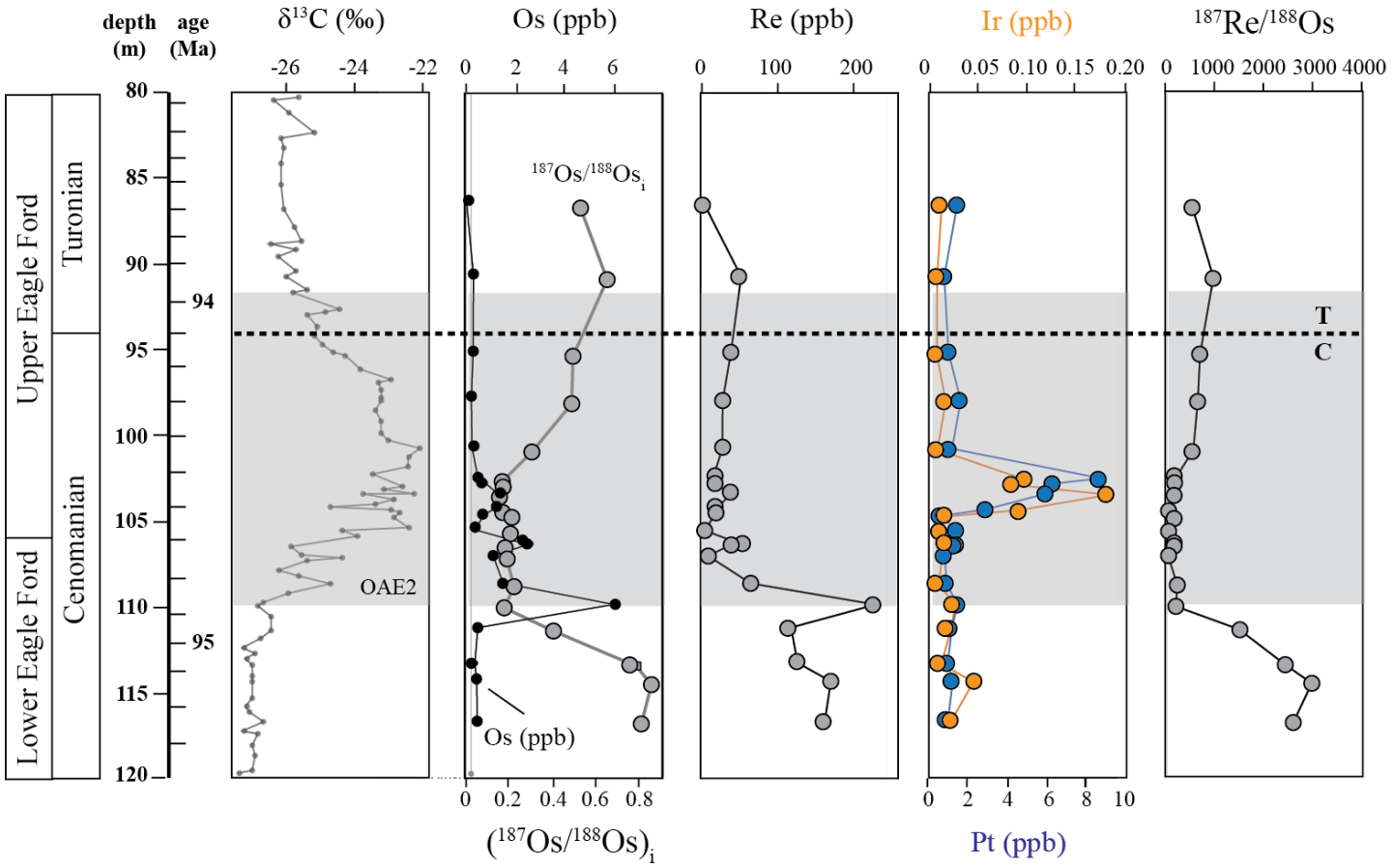

Figure 3.4: Elemental abundances and isotopic ratios with depth for the Iona-1 core. A) Organic carbon isotope data ($\delta^{13}C$) from Eldrett et al (2014). B) Osmium abundance (in parts-per-billion) and the calculated $(^{187}Os/^{188}Os)_i$ ratio. C) Rhenium (in parts-per-billion). D) Iridium (in parts-per-billion) and Platinum (in parts-per-billion). E) Calculated $^{187}Re/^{188}Os$. Gray shaded area represents OAE2. Black dashed line = Cenomanian-Turonian boundary; C = Cenomanian; T = Turonian. Age (Ma) is determined from the detailed chronostratigraphy for the Iona-1 core provided by Eldrett et al. (2015b).

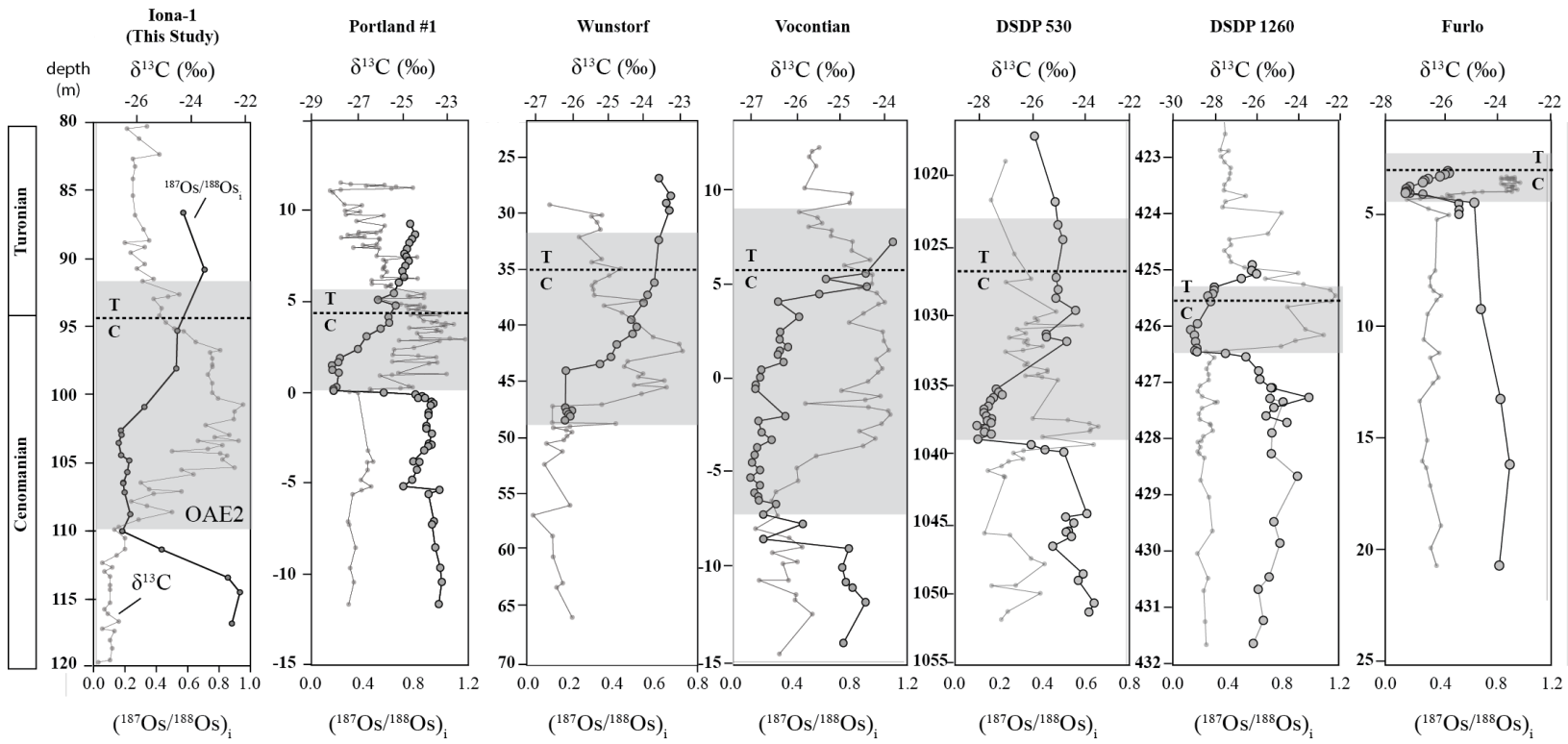

Figure 3.5: Organic carbon isotope data ($\delta^{13}C$) (light gray line) and $(^{187}Os/^{188}Os)_i$ (dark gray line) with depth. The depth scales are not correlated, however, the location of OAE2 (gray shaded area) and Cenomanian-Turonian boundary (black dashed line) as defined by each study are shown for correlation. C: Cenomanian, T: Turonian. $(^{187}Os/^{188}Os)_i$ ratios for the Iona-1 core in this study were calculated from the age of each individual sample. All other $(^{187}Os/^{188}Os)_i$ ratios are calculated using 93.90 Ma by Du Vivier et al., (2014). $\delta^{13}C$ data from: Portland #1 core, Sageman et al. (2006); Site 1260, Forster et al. (2007); Wunstorf, Du Vivier et al. (2014); Vocontian, Jarvis et al. (2011); Furlo, Jenkyns et al. (2007); Site 530, Forster et al. (2008). Osmium data from: Du Vivier et al. (2014) and Turgeon and Creaser (2008).

of a radiogenic crustal component to seawater from the weathering of the Sevier Orogenic Belt and the Canadian Shield.

The $^{187}Os/^{188}Os$ of seawater in the southern gateway to the KWIS, as inferred by the data presented here, is within the range reported by Du Vivier et al. (2014). However, values for the Eagle Ford Group do not reach such radiogenic values as those of the Portland #1 core. Sites that were along the western margin of the WCIS generally contain a large contribution of clastics from erosion of the Sevier highlands (Orth et al., 1993). This is evident by the presence of several well-documented fluvio-deltaic clastic wedges in the KWIS, such as the Cenomanian Dunvegan Formation in Alberta, Canada, and the Turonian Mancos Shale Formation in central Utah (Bhattacharya and MacEachern, 2009). Increased sedimentation along the western margin of the WCIS would provide a more radiogenic, crustal component to seawater than on the eastern or southern margins of the seaway. This would elevate the $^{187}Os/^{188}Os$ of seawater in these regions. In addition, if the shallow epeiric setting in portions of the WCIS became restricted from the global ocean, the radiogenic signal would dominate as the influence of local weathering inputs would be amplified (Du Vivier et al., 2014). In the Portland #1 core, a small depositional hiatus, and bone bed within the uppermost Hartland Shale suggests a minor relative sea-level fall may have occurred within the WCIS just prior to OAE2 (Elder et al., 1994; Gale et al., 2008). Thus the onset of sea-level rise associated with OAE2 may have been preceded by a relative sea-level fall that briefly reduced or inhibited the exchange of water masses within the KWIS. This would explain the variable $^{187}Os/^{188}Os$ of seawater within the KWIS and between other Cenomanian sections discussed here.

3.5.2. Pre-OAE2 Osmium Isotopic Excursion

A negative $^{187}Os/^{188}Os$ excursion occurs just prior to the onset of OAE2 in the Eagle Ford Group. Starting ~95.08 Ma, the $(^{187}Os/^{188}Os)_i$ displays an abrupt shift toward a non-radiogenic value of 0.15. The minimum value of $(^{187}Os/^{188}Os)_i$ at 94.88 Ma is coincident with the start of OAE2 (Figure 3.4). This represent a drastic shift of the Os isotopic composition of seawater over a ~200 kyr interval prior to the onset of OAE2 and reflects a predominance of non-radiogenic Os input to the WCIS at this time. The same trend is observed in the Portland #1 core, from sites in western Tethys and the proto-North Atlantic Ocean (Figure 3.5) (Turgeon and Creaser, 2008; Du Vivier et al., 2014). However, the progressive trend toward non-radiogenic $^{187}Os/^{188}Os$ values in other sections occurred over a ~155 kyr interval. This is likely due to the greater temporal resolution of Os data provided by Du Vivier et al. (2014), rather than an actual condensed time interval. This abrupt shift to non-radiogenic $(^{187}Os/^{188}Os)_i$ values prior to the onset of OAE2 requires a substantial source of non-radiogenic Os to the ocean. Using a simple two-component mixing equation assuming a chondritic $^{187}Os/^{188}Os$ value of 0.127 and an average continental crustal $^{187}Os/^{188}Os$ value of 1.4, ~98% of the total Os content in the Eagle Ford Group at this interval is non-radiogenic in origin. This is similar to a value of 97% reported by Turgeon and Creaser (2008) for pre-OAE2 sites in the Bonarelli section in Furlo, Italy, and ODP Site 1260B in the Demerara Rise. This is in comparison to 43 – 48% of total Os being non-radiogenic prior to the negative isotopic excursion, and ~27% for present-day oceans.

In sites from the WCIS, western Tethys, and the proto-North Atlantic Ocean, Du Vivier et al. (2014) reported a sudden and high increase in Os abundances (up to 10 ppb) coincident with the abrupt decrease in $(^{187}Os/^{188}Os)_i$ prior to OAE2. In the Eagle Ford Group, reported here, there is a decoupling of the negative $(^{187}Os/^{188}Os)_i$ excursion and the increase in Os abundance. The spike in Os abundance occurs ~200 kyr after the trend toward non-radiogenic $(^{187}Os/^{188}Os)_i$ values, and is coincident with the minimum in $(^{187}Os/^{188}Os)_i$ and the onset of OAE2 (Figure 3.4). The delay between the negative isotopic excursion and increased Os abundance could represent the prolonged input of non-radiogenic Os to the oceans, however, more complex mechanisms may be involved and are discussed in more detail below.

3.5.3. Osmium Isotope Systematics During OAE2

The non-radiogenic $^{187}Os/^{188}Os$ values following the negative isotopic excursion prior to the onset of OAE2 persist throughout the lower half of the positive carbon isotopic excursion marking OAE2 (Figure 3.4). Within this 7.4 m section, representing ~360 kyr, there is minimal variation in the $(^{187}Os/^{188}Os)_i$ values (0.13 – 0.20). Starting at ~94.52 Ma, seawater $^{187}Os/^{188}Os$ values returned to more radiogenic values of 0.48 – 0.52 over a 4.6 m interval representing ~210 kyr. Seawater values returned to radiogenic values by ~94.31 Ma and remained radiogenic throughout the remainder of OAE2 (Figure 3.4). This pattern is also observed in the Bonarelli section in Furlo, Italy, and sites within the KWIS, western Tethys and the proto-North Atlantic (Figure 3.5) (Turgeon and Creaser, 2008; Du Vivier et al., 2014). This likely reflects prolonged input of non-radiogenic Os to the oceans before and during the early stages of OAE2. Here, the return of seawater to

radiogenic $^{187}Os/^{188}Os$ values starts at 94.52 Ma, ~360 kyr after the onset of OAE2 (Figure 3.5). Du Vivier et al. (2014) report a return to radiogenic $^{187}Os/^{188}Os$ values to occur ~200 kyr after the onset of OAE2, however, Du Vivier et al. (2014) marks the onset of OAE2 to occur at 94.38 Ma. This study uses a value of 94.85 Ma based on detailed chronostratigraphic work by Eldrett et al. (2015b). When calibrated with the age selected for the onset of OAE2 by Du Vivier et al. (2014), the return to radiogenic $^{187}Os/^{188}Os$ values in this study occurs ~140 kyr after the onset of OAE2, similar to sections discussed by Du Vivier et al. (2014).

Within the interval of low $(^{187}Os/^{188}Os)_i$,Turgeon and Creaser (2008) reported a double spike of Os enrichment in the Bonarelli section and in the Demerara Rise. The similar structure and magnitude of the double spikes at both sites led to the suggestion that these enrichments are primary in nature and record at least two major pulses of non-radiogenic Os to the oceans (Turgeon and Creaser, 2008).

Within the Eagle Ford Group, three distinct peaks in Os abundance are observed (Figure 3.4). These three peaks at 110.01 m (94.88 Ma), 106.50 m (94.72 Ma), and 103.54 m (94.54 Ma) correspond to enrichments in Os abundance of ~6.0 ppb, ~2.6 ppb, and ~1.3 ppb, respectively over background values of <0.01 ppb. Separate peaks in Os abundance were not discussed by Du Vivier et al. (2014). Whereas separate distinct pulses of non-radiogenic contribution to the ocean during this time may provide an explanation for the separate distinct peaks in Os abundance observed here, in the Bonarelli section, and in the Demerara Rise, this study provides a different causal mechanisms.

3.5.4. Sources and Timing of Non-radiogenic Osmium

Possible sources of Os with low $^{187}Os/^{188}Os$ values are (1) an extraterrestrial source, such as a large bolide impact, or (2) mantle-derived Os provided via seafloor hydrothermal processes such as during enhanced spreading rates at mid-ocean ridges or during LIP magmatism. However, any physical signatures of large impacts, such as micro-spherules or shocked quartz have not been reported for OAE2 (Orth et al., 1993; Turgeon and Creaser, 2008). The supposed prolonged input of unradiogenic mantle-derived Os to the oceans is consistent with published data showing an increase in several mafic trace elements at the Bonarelli in Furlo and at site 1260B in the Demerara Rise (Turgeon and Creaser, 2008) and in the WCIS (Orth, 1988; Orth et al., 1993 Snow et al., 2005) and in the Iona-1 core studied here (Eldrett et al., 2014).

Large igneous provinces form by the decompression melting of anomalously hot mantle above mantle plume heads, in a relatively short period of time (<2 – 3 Myr; Coffin and Eldholm, 1994; Torsvik and Burke, 2015). They therefore release mantle-like, non-radiogenic Os to the oceans ($^{187}Os/^{188}Os = 0.13$; Cohen and Coe, 2002). Based on the timing of the $^{187}Os/^{188}Os$ excursion and OAE2, two potential sources of volcanism have been suggested: the Caribbean Large Igneous Province (CLIP) (Orth et al., 1993; Snow et al., 2005; Turgeon and Creaser, 2008; Du Vivier et al., 2014), and the High Arctic Large Igneous Province (HALIP) (Jowitt et al., 2014; Estrada and Henjes-Kunst, 2013). Due to the predominance of published data on the CLIP compared to the HALIP, further discussion will include CLIP magmatism as the source of Os. However, the HALIP has not been excluded as a possible source for these metal enrichments.

The CLIP represents the evidence for one of the largest eruptive event on Earth (Kerr et al., 1997). Portions of the CLIP are preserved mostly as the Caribbean plate and as extensive accreted terranes in Columbia (Kerr et al., 1997). It is generally accepted that the CLIP formed in the eastern Pacific, likely at the Galapagos hot-spot (Duncan and Hargraves, 1984; Kerr et al., 1997; Hoernle et al., 2004). Published $^{40}Ar/^{39}Ar$ ages determined that magmatism occurred from 95 to 69 Ma with the main pulse of flood-basalt magmatism occurring 95 – 83 Ma with a second pulse occurring ~75 Ma (Kerr et al., 1997; Sinton and Duncan, 1997; Hoernle et al., 2002; Hoernle et al., 2004). The volume of lava erupted has been estimated at 4×10^6 km^3 yielding a mean eruption rate of 2 km^3 a^{-1} (Kerr, 1998). The anomalous volcanism related to CLIP eruption is suggested to have been responsible for the environmental disturbances resulting in OAE2 and coincident disruption of the biosphere. This is suggested to have occurred through the emission of large quantities of CO_2 into the atmosphere, leading to global warming. Additionally, the emission of SO_2, H_2S, and CO_2 into the oceans would have acidified sea-water (Kerr, 1998). In addition, nutrient upwelling and increased CO_2 in the atmosphere would have led to increased organic productivity and eventual burial as black shales, creating the positive carbon isotopic excursion which marks OAE2 (Kerr, 1998).

The data presented here indicate that a large flux of non-radiogenic Os reached the southern gateway to the WCIS between 94.94 and 95.06 Ma. This is evident by the abrupt negative $(^{187}Os/^{188}Os)_i$ excursion that occurs starting between 113.42 and 111.36 m in the Eagle Ford Group (Figure 3.4). This trend toward non-radiogenic Os occurs ~240 – 360 kyr prior to the onset of OAE2 as defined by the Global Bounary Stratotype

Section and Point (GSSP). The negative $(^{187}Os/^{188}Os)_i$ excursion for other sites discussed here occurs ~200 kyr prior to OAE2; however unconformities in many of these sections could represent 60 – 100 Kyr of missing section (Figure 3.5) (Du Vivier et al., 2014). The large uncertainty in the timing of initiation of the $(^{187}Os/^{188}Os)_i$ excursion reported in this study is due to sampling resolution. However, the timing agrees with that seen in other sections coincident with OAE2 and with the timing of the main pulse of flood-basalt magmatism of the CLIP (95 – 83 Ma; Hoernle et al., 2004). This provides evidence that supports the influx of non-radiogenic Os observed in the marine record is a direct consequence of volcanism (Ravizza and Peucker-Ehrenbrink, 2003).

Unlike other OAE2 sections, the Eagle Ford Group, as represented by the Iona-1 core, displays a delay of ~200 kyr between the onset of the negative $(^{187}Os/^{188}Os)_i$ excursion and the first peak in Os abundance observed at 110.01 m (94.88 Ma) near the onset of OAE2 (Figure 3.4). The first Os abundance peaks are coincident with the $(^{187}Os/^{188}Os)_i$ excursion in sections from sites within the KWIS, western Tethys and the proto-North Atlantic from the Demerara Rise prior to OAE2 (Turgeon and Creaser, 2008; Du Vivier et al., 2014). This delay in Os enrichment will be discussed in a later section.

Following the decline in $(^{187}Os/^{188}Os)_i$ values prior to OAE2, values remain low from 94.88 Ma to 94.52 Ma (~360 kyr) before returning to more radiogenic values (Figure 3.5). This ~530 kyr period is also observed in other sections discussed here (after timing of OAE2 correction; Turgeon and Creaser, 2008; Du Vivier et al., 2014) and potentially represents the period of volcanism with cessation by 94.52 Ma. Following implied

cessation of volcanism, $^{187}Os/^{188}Os$ values of seawater return to more radiogenic values in all sections.

3.5.5 Platinum-Iridium Anomaly

There is a marked positive anomaly in Pt and Ir within OAE2 in the Eagle Ford Group. This anomaly marks an 8 and 22 fold increase in Pt and Ir of ~8 ppb and ~170 ppt over background, respectively and is decoupled from the large Os abundance peaks (Figure 3.4). This Ir anomaly was first observed by Orth et al. (1988) in the Cenomanian-Turonian boundary interval in marine rocks in the KWIS near Pueblo, Colorado. It was then expanded to 16 other sites within the KWIS and one site in south-central Columbia (Orth et al., 1993). Orth et al. (1993) also reported very weak or complete lack of an Ir peak in sections from England, Poland, Germany, and in the Atlantic and Pacific oceans. The source of the enriched elements was likely located in or near the proto-Caribbean / Gulf of Mexico due to a general decline in the relative intensity of the Ir peak away from this location (Orth et al., 1993). As with the enrichment of Os, the proposed mechanisms for the Ir enrichment are (1) large extraterrestrial impact, (2) increased circulation of deep, metal-rich water associated with the Late Cenomanian-Turonian eustatic sea-level rise, and (3) intense pulses of spreading center or hot-spot activity in the Late Cenomanian, such as eruption of the CLIP (Orth et al., 1993).

The solution chemistry of Pt has been extensively studied (Mountain and Wood, 1988; Kump and Byrne, 1989; Wood, 1990; Wood, 1991; Gammons, 1996; Byrne and Yao, 2000; Cosden et al., 2003). The predominant oxidation states for Pt in seawater are Pt^{II} and Pt^{IV} (Gammons, 1996) forming predominant inorganic forms in seawater of $PtCl_4^{2-}$

and $PtCl_5OH^{2-}$, respectively (Byrne and Yao, 2000). $PtCl_5OH^{2-}$ is more abundant than $PtCl_4^{2-}$ throughout the normal pH range of seawater (Gammons, 1996).

Values of dissolved Pt have been reported for the Pacific (Goldberg et al., 1986), Atlantic (Colodner et al., 1993) and Indian oceans (Jacinto and van den Berg, 1989), with concentrations ranging from 0.2 to 1.6pM. In the Atlantic Ocean, Pt concentrations were invariant with depth (Colodner et al., 1993). However, a scavenged-type profile, with Pt depleted at depth, was observed in the Indian Ocean (Jacinto and van den Berg, 1989).

Platinum is markedly enriched in ferro-manganese nodules over palladium compared to their seawater values (Hodge et al., 1986). The platinum content of marine sediments are strongly governed by the their manganese concentrations (Goldberg et al., 1986). A similar relationship is observed in Co and Ni in marine sediments which are known to be redox-sensitive elements primarily hosted in ferro-manganese minerals (Goldberg, 1962).

Because Pt is enriched in ferro-manganese nodules, and because of the stability of Pt^{IV} in sea-water, it is suggested that Pt is subjected to oxidative removal from sea-water and oxidized during mineral formation from Pt^{II} to Pt^{IV} (Hodge et al., 1985; Hodge et al., 1986; Jacinto and van den Berg, 1989). This mechanism may result in platinum being accumulated in oxic sediments within the marine environment (Hodge et al., 1986).

Further insight into the oxidative behavior of Pt was gained from the analysis of samples taken from various depths from the MANOP site H. in the Guatemala Basin. Site H. is a relatively shallow abyssal area (~3600 m) underlying highly productive surface waters (Kadko and Heath, 1984; Dymond et al., 1984). A high rain rate of organic matter

provides a vigorous benthic macrofaunal community, however, rapid degradation of this organic matter results in the total consumption of oxygen within the upper 4 cm of sediment (Kadko and Heath, 1984). Ferro-manganese minerals from the top of Site H. have typical Pt concentrations of ~157 ppb, whereas the bottom sites have unusually low concentrations of <1 ppb (Goldberg et al.,. 1986). The uptake of Pt in sediment in the bottom of Site H. was limited by the lack of available oxygen (Dymond et al., 1984; Goldberg et al., 1986). The uptake of Co in this same section follows that of Pt, while Ni abundances were the lowest in the sediments from the top of Site H (Goldberg et al., 1986). In addition, there was a lack of correlation between Pt abundance and TOC, further supporting an oxidative uptake of Pt (Goldberg et al., 1986). This is in clear contrast with the reductive enrichment observed by Re and Os and their subsequent enrichment in ORM.

Iridium also shows a marked enrichment in manganese nodules compared to deep-sea sediments (Crocket et al., 1973; Hodge et al., 1986). In seawater, the species of Ir are most likely to be oxy-hydroxy and chloro complex ion forms (Fergusson, 1992). The concentration of Ir in the oceans is fairly uniform, averaging 3.9 $X10^{8}$ atoms kg^{-1} (Anbar et al., 1996). Measured Ir concentrations in anoxic marine waters are four times those in overlying O_2-saturated waters, indicating that Ir is not rapidly removed into sediments under anoxic conditions (Anbar et al., 1996). This is consistent with the lack of enrichment of Ir in anoxic marine sediments (Colodner et al., 1992). In addition, sorption and desorption experiments in bulk coastal sediments when compared to sediments after the removal of sulfides and organic matter showed no difference in the sorption and

desorption distribution coefficients, which indicates that these phases are not significant hosts for Ir (Dai et al., 2000).

These studies show a clear contrast in the enrichment mechanisms between Re-Os and Pt-Ir. Rhenium and Os are redox-sensitive and organophile in nature, and are thought to be sequestered by organisms at, or below the sediment-water interface in both marine and lacustrine basins under suboxic, anoxic or euxinic conditions and are thus hydrogenous in nature and become enriched in marine ORM under these conditions (Koide, 1991; Colodner et al., 1993; Crusius et al., 1996; Morford et al., 2009; Cumming et al., 2012). Platinum and Ir are enriched in oxic sediments during ion exchange reactions and subsequent precipitation from the water column or out of the interstitial waters of sea-floor sediments (Goldberg, 1962; Crocket et al., 1973; Hodge et al., 1986; Goldberg et al.,. 1986; Jacinto and van den Berg, 1989; Fergusson, 1992; Colodner et al., 1992; Anbar et al., 1996). Thus their decoupled enrichment in the strata of the Eagle Ford Group requires variable redox conditions within the water column across OAE2.

3.5.6 Variable Redox across OAE2

The decoupling of the Re-Os and Pt-Ir peaks observed in the Eagle Ford Group before and during OAE2, combined with the previous discussion of the behavior of these elements in the water column, requires changing redox conditions across OAE2. In the interval leading up to OAE2, enrichment in redox-sensitive trace metals (particularly Mo) in addition to the general lack of benthic foraminifera and the occurrence of laminated organic-rich marls indicate anoxic bottom-water conditions at the southern gateway to the KWIS in the Iona-1 core (Figure 3.6) (Eldrett et al., 2014).

Rhenium and Os are both redox-sensitive elements and are concentrated in reducing sediments (Ravizza et al., 1991). Osmium is scavenged from seawater over a wide range of Eh and pH conditions and first enters oxic sediment as Os^{IV}, and is then converted to Os^{III} after further reduction during possible organic complexation (Yamashita et al., 2007). This results in Os being sequestered and/or adsorbed to a variety of phases under a variety of redox conditions. In contrast, high concentrations in recent and ancient reducing sediment and strata coupled with experimental studies show that Re is readily drawn from seawater and fixed in sediment only under reducing conditions (Ravizza et al., 1991; Yamashita et al., 2007; Georgiev et al., 2011). Enrichment of Re over Os therefore requires highly reducing environments. The $^{187}Re/^{188}Os$ ratios for the pre-OAE2 interval, presented here, range from ~1463 to ~2937 (Table 3.1, Figures 3.4 & 3.6). Published $^{187}Re/^{188}Os$ ratios for nearly all shales are less than 2000, with greater than 90% of $^{187}Re/^{188}Os$ values less than 1000 (Georgiev et al., 2011). In exception, Upper Permian black shales from Poland have very high $^{187}Re/^{188}Os$ ratios of up to 5,311 (Pasava et al., 2010). Yang et al. (2004) also reported exceptionally high $^{187}Re/^{188}Os$ ratios of up to 6,114 in Upper Permian Mo-rich black shales of the Laoyaling, Anhui Province, China. The extremely high $^{187}Re/^{188}Os$ ratios presented here support anoxic bottom-water conditions during this pre-OAE2 interval (Figures 3.4 & 3.6).

The decline in $^{187}Re/^{188}Os$ reported here (from 114.50 m to 107.17 m) tracks the fall in redox-sensitive trace metal concentrations observed by Eldrett et al. (2014) (Figure 3.6). The $^{187}Re/^{188}Os$ values reach a minimum of ~45 at 107.17 m, coincident with the minimum in trace metal enrichment (Figure 3.6). The decline in trace metal enrichment

coupled with the coeval sharp increase in bioturbation, the appearance of diverse and abundant benthic foraminifera, and a drop in the TOC of coeval strata indicates a transition to mostly oxic-suboxic bottom-water conditions within a more open oceanographic regime by ~94.75 Ma, coincident with the start of OAE2 (Figure 3.6) (Eldrett et al., 2014).

Between depths of 107.17 and 102.63 m, $^{187}Re/^{188}Os$ values remain low, with only minor variations (Figures 3.4 & 3.6). This likely reflects that oxic-suboxic bottom-water conditions persisted throughout this interval (94.75 – 94.52 Ma). Low abundances of redox-sensitive trace metals within this interval support the persistence of oxic-suboxic bottom-water conditions (Eldrett et al., 2014). Within this oxygenated regime, episodes of intermittent anoxia returned, reflected by periodic trace metal enrichments and a return to organic-rich laminated strata (Eldrett et al., 2014). Starting ~94.52 Ma, a gradual increase in the $^{187}Re/^{188}Os$ ratio indicates slightly less oxic conditions returned (Figure 3.6).

Figure 3.6: Various geochemical data with depth for the Iona-1 core. A) Organic carbon isotope data ($\delta^{13}C$) from Eldrett et al (2014). B) Osmium abundance (in parts-per-billion) (black line) and the calculated ($^{187}Os/^{188}Os)_i$ ratio (gray line). C) Iridium (in parts-per-billion) (orange) and Platinum (in parts-per-billion) (blue). D) Calculated $^{187}Re/^{188}Os$ ratio. E) Trace metal enrichment factor (trace metal abundance normalized to zirconium) of V (black), Mo (blue), and U (green) from Eldrett et al. (2014). F) Mafic trace metal enrichment factor (mafic trace metals normalized to zirconium) of Co (red), Cu (yellow), Sc (blue), and Cr (purple) from Eldrett et al. (2014). Light gray shaded area represents OAE2. BOZ: benthic oxic zone as described by Eldrett et al. (2014). Age (Ma) is determined from the detailed chronostratigraphy for the Iona-1 core provided by Eldrett et al. (2015b).

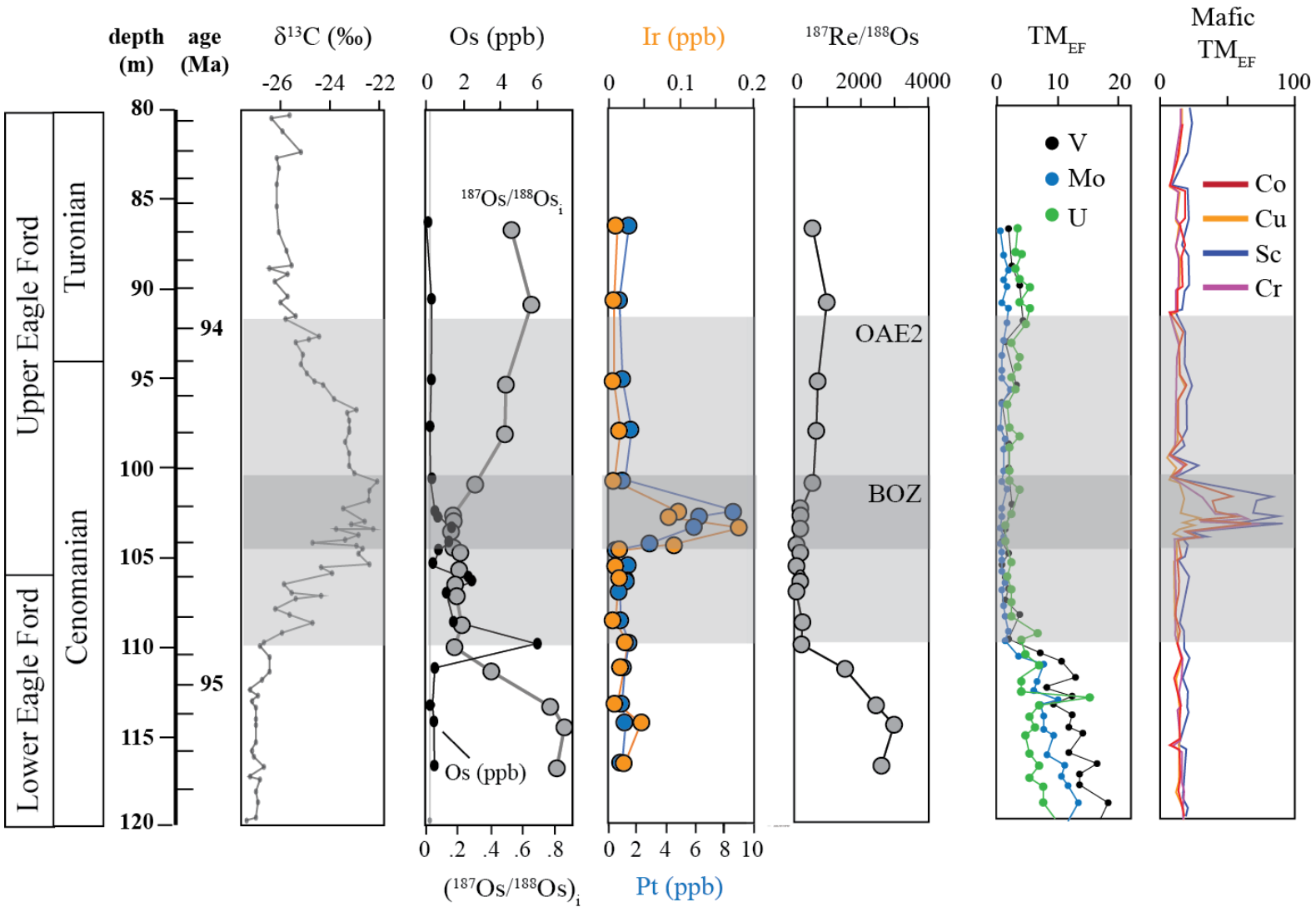
depth (m)
age (Ma)
δ13C (‰)
Os (ppb)
Ir (ppb)
187Re/188Os
TMEF
Mafic TMEF
Upper Eagle Ford
Lower Eagle Ford
Turonian
Cenomanian
OAE2
BOZ
V
Mo
U
Co
Cu
Sc
Cr
187Os/188Os
Os (ppb)
(187Os/188Os)i
Pt (ppb)

The same transition from pre-OAE2 anoxia followed by syn-OAE2 oxic-suboxic bottom-water conditions were observed in the Portland #1 core (Eldrett et al., 2014) and the Manitoba Escarpment (Schroder-Adams et al., 2001) both from the KWIS, and in the southern Tethys (Tsikos et al., 2004; Kolonic et al., 2005; Keller et al., 2009; Trabucho Alexandre et al., 2010; Vahrenkamp, 2013). Anoxia was thus persistent and widespread prior to OAE2, with variable redox conditions prevailing during the "anoxic" event.

3.5.7. Mafic Trace Metal Enrichment

Within the oxic interval of OAE2 in the Eagle Ford Group and the Portland #1 core, Eldrett et al. (2014) reported anomalous enrichment of mafic trace metals, such as scandium, cobalt, chromium, and copper. This enrichment in mafic trace metals is coincident with the enrichment in Pt and Ir reported here (Figure 3.6) and with those reported by Orth et al. (1993). Analysis of elemental abundance ratios within the anomalies closely resemble those of Mid-Atlantic Ridge basalt of Hawaiian tholeiite and not those of chondrite (Orth et al., 1993). The most agreed upon source of these mafic trace metals is via the hydrothermal alteration of basalts that was enhanced during the emplacement of a large igneous province (Orth et al., 1993; Snow et al., 2005; Eldrett et al., 2014).

Eldrett et al. (2014) suggest that due to the coincidence of the mafic trace metal enrichment with the inception of boreal dinocysts in the Eagle Ford Group, the trace metals were likely sourced by the HALIP and transported to the KWIS via the southward flow of boreal waters. In addition, the trace metal anomaly occurs ~70 kyr earlier in the Portland #1 core, suggesting a more northerly source of these metals (Eldrett et al., 2014).

However, Orth et al. (1993) suggest that the source was located in or near the proto-Caribbean / Gulf of Mexico region, due to the distribution and decreased relative magnitude of the anomalies trending away from the proto-Caribbean.

The enrichment in non-radiogenic Os reported here occurs ~340 – 360 kry prior to the enrichment of Pt, Ir, mafic trace metals and the first appearance of boreal dinocysts. This points towards a source other than the HALIP for the enrichment in Re and PGE. Based on the variable behavior of Re-Os and Pt-Ir, the delayed enrichment of Pt and Ir is likely caused by the change of redox regime. Rhenium and Os were enriched in the Eagle Ford sediment during the period with anoxic bottom-water prior to OAE2. Following the onset of OAE2 and a change to oxic-suboxic bottom-waters, Pt and Ir were then sequestered into oxic sediment. The Pt-Ir enrichment and the arrival of the boreal dinocysts into the southern gateway to the KWIS was likely caused by changes in oceanic circulation patterns and subsequent disturbance of the oxycline, perhaps triggered by the eruption of the CLIP.

3.5.8. Milankovitch Cycle Controls on Rhenium and PGE Enrichment

The cyclic inter-bedding of organic-rich marls and limestones observed in the Eagle Ford Group are generally well expressed in the KWIS and have been hypothesized to represents the sedimentological expression of climate cycles (Gilbert, 1895). Proposed causal mechanisms for the deposition of rhythmically inter-bedded strata are climate controlled variations in primary productivity, the input of terrigenous sediments, the intensity of bottom currents, and cycles in benthic oxygenation. Recent work has provided quantitative evidence for astronomic forcing as the primary causal mechanism

in Cenomanian and Turonian sequences within the KWIS (Sageman et al., 1997; Sageman et al., 1998; Meyers et al., 2001; Eldrett et al., 2015a). Based on integrated biostratigraphic, geochemical, petrological, and detailed geochronological data, Eldrett et al. (2015a) demonstrated that lithological variations between marl beds and limestones in the Eagle Ford Group at the southern gateway to the KWIS in the Iona-1 core reflect climatic signatures driving by solar insolation driven by Milankovitch cycles (Figure 3.7).

Eccentricity, obliquity, and precession together make up Milankovitch cycles (Figure 3.8). Eccentricity describes the shape of the Earth's orbit around the sun. The shape of the Earth's orbit constantly fluctuates between a circle and an ellipse (0 – 5% ellipsicity) on the order of ~100,000 year cycles. Variations in eccentricity control the distance the Earths is from the sun, thus changing the amount of the suns radiation that the Earth receives, in addition to effecting seasonal changes in the magnitude of radiation. Obliquity, or axial tilt, is the inclination of the Earth's axis in relation to its solar orbital plane. Oscillations in the angle of the Earth's tilt, from 22.1° to 24.5°, occurs on a periodicity of ~41,000 yrs. With less axial tilt, solar radiation is more evenly distributed between the seasons, however, a greater increase is observed in the radiation received between the equator and Earth's Polar Regions. Precession describes Earth's slow wobble about its spin axis. The precession of Earth is defined by the direction its rotational axis points with variations between pointing at the start Polaris, to pointing at the star Vega. This wobble occurs in 26,000 yr cycles. When the axis is tilted toward Vega the positions of the Northern Hemisphere winter and summer solstices will coincide with the aphelion

and perihelion, respectively. This means that the Northern Hemisphere will experience winter when the Earth is furthest from the Sun and summer when the Earth is closest to the Sun. This coincidence will result in greater seasonal contrasts. Milankovitch cycles thus influence the timing and length of the seasons and the amount of solar radiation received by the Earth. Combined, Milankovitch cycles impact the seasonality and location of solar energy around the Earth, thus impacting seasonal contrasts in total solar insolation.

Figure 3.7: A) Lithostratigraphy of the interval of the Iona-1 core studied here. See legend for lithologic designations. B) Precession (P) (red), Obliquity (O) (green), Short eccentricity (E2) (purple) and Long eccentricity (E) (yellow) obtained for the Eagle Ford Gp. derived from grayscale de-convolution from Eldrett et al. (2015a). Red circles: samples used in this study. 1: sub-maximum solar insolation, discussed in text. 2: minimum solar insolation, discussed in text. Red arrows highlight intervals that are heavily discussed in the text.

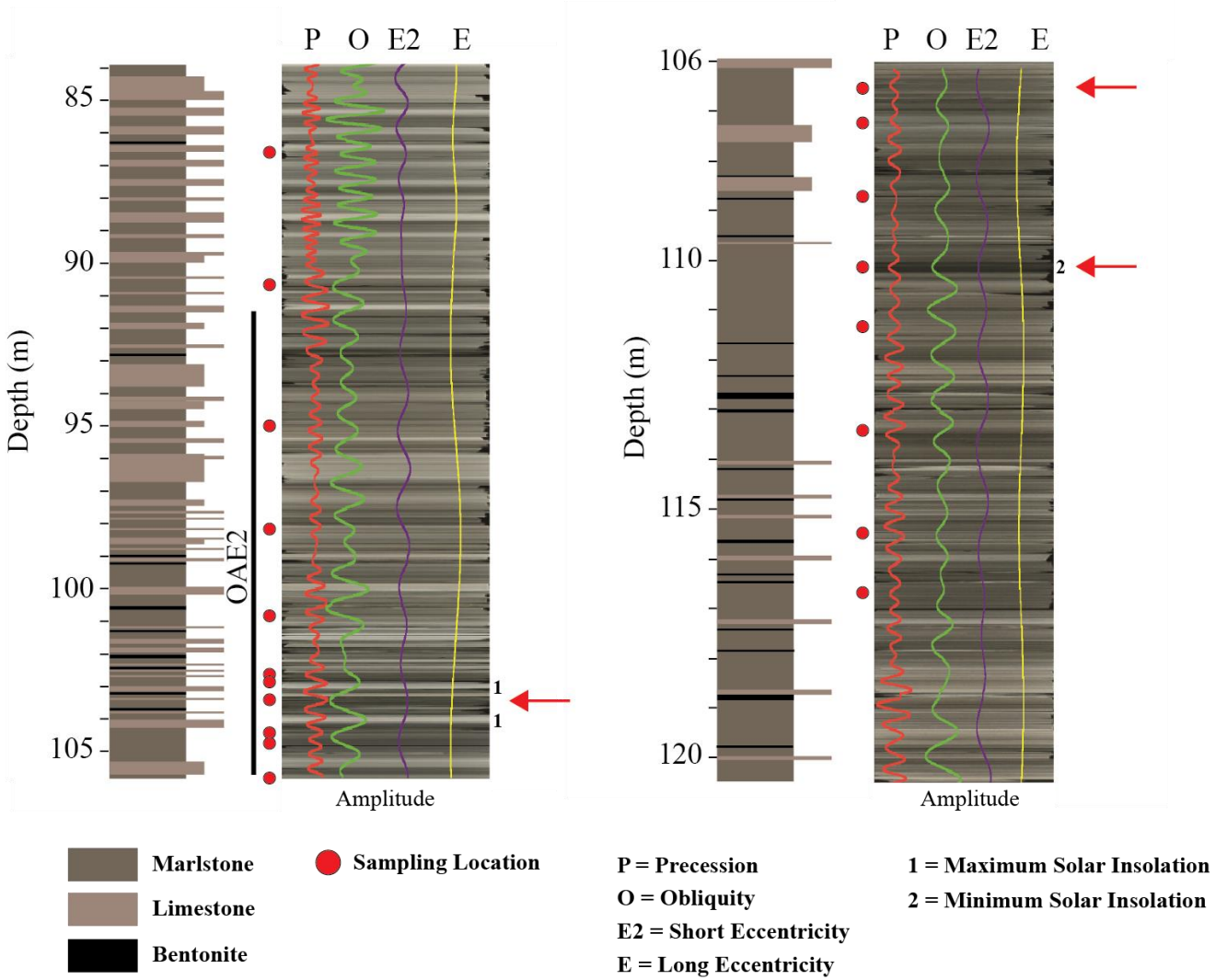
P O E2 E
85
90
95
100
105
Depth (m)
OAE2
1
1
Amplitude
106
110
115
120
2
Marlstone
Limestone
Bentonite
Sampling Location
P = Precession
O = Obliquity
E2 = Short Eccentricity
E = Long Eccentricity
1 = Maximum Solar Insolation
2 = Minimum Solar Insolation

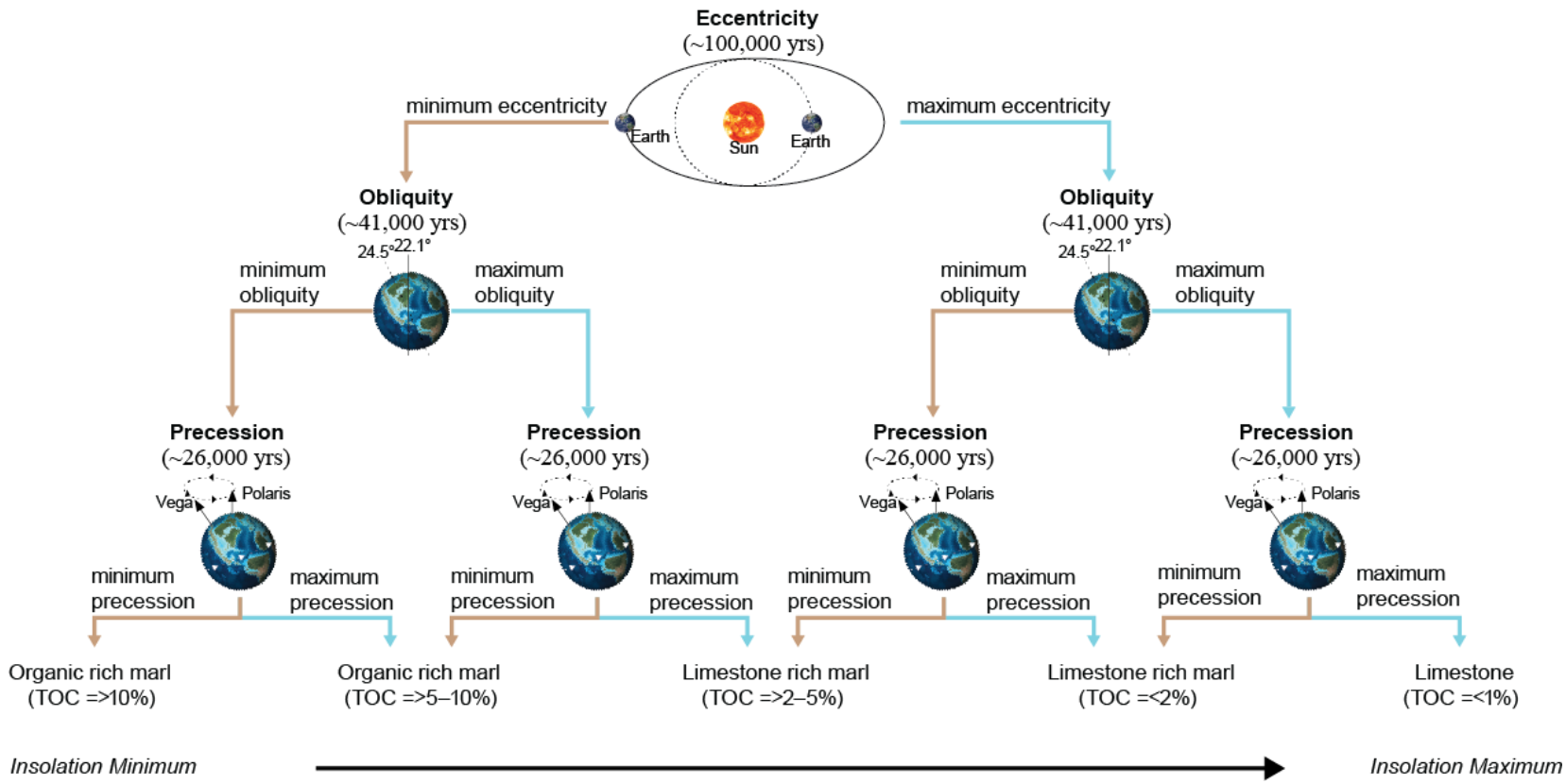

Figure 3.8: A conceptual model for the control of Milankovitch cycles on the lithologies observed in the Iona-1 core. Positive interference in maxima of the three Milankovitch cycles results in maximum insolation. Positive interference in the minima of the cycles results in a minimum in insolation. Modified after Eldrett et al. (2015a). Insolation: the total amount of solar radiation energy received on a given surface area during a given time.

Throughout the Eagle Ford, limestones record improved oxygen conditions in the bottom-waters and/or sediment-water interface as demonstrated by a reduction in redox-sensitive elements, and the abundance of Prasinophyte algae, an algae typically found in more stratified water conditions (Prauss, 2007; Eldrett et al., 2015a). In addition, the limestone beds preserve cross laminations and internal truncations indicative of enhanced current activity (Schieber et al., 2013; Eldrett et al., 2015). Interbedded organic-rich marl beds reflect water column stagnation and stably stratified waters, as evident by enrichments in redox-sensitive trace metals and the preservation of organic matter at the sediment-water interface (Eldrett et al., 2015a).

These observations, in conjunction with their astronomically tuned age model (Eldrett et al. 2015b) for the Iona-1 core led Eldrett et al. (2015a) to conclude that fluctuations in the solar insolation caused by Milankovitch cycles (predominantly obliquity and precession) were responsible for the observed lithological variations. Individual limestone beds correspond to the product of precession and obliquity cycles (Figures 3.7 & 3.8). The amplitude amplification caused by overlapping the maxima of these two Milankovitch cycles caused enhanced latitudinal distribution of solar insolation and consequent increase in the atmospheric-ocean thermal gradients resulting in greater or more frequent storms, stronger bottom-water currents, a de-stratification of the water column, and improved bottom-water oxygenation (Eldrett et al., 2015a). In contrast, the amplitude amplification of minima in precession and obliquity cycles reduced latitudinal energy gradients causing an expansion of the oxygen minimum zone under a more stratified water column, resulting in the deposition of organic-rich marl beds (Figure 3.8) (Eldrett

et al., 2015a). Amplitude interference due to variations in precession, obliquity, and eccentricity produce the variety of lithologies observed in the Eagle Ford Group (Figure 3.8) (Eldrett et al., 2015a).

As discussed, sediments in the pre-OAE2 interval within the southern gateway to the KWIS were dominantly deposited under anoxic bottom-water conditions. However, within this interval, there are intermittent episodes of increased oxygen reflected by periodic trace metal depletions and a decrease in TOC values (Figure 3.6). The three intervals with high Os abundances (110.10, 106.50 and 103.54 m) correlate with intervals with redox-sensitive trace metal enrichment and high TOC values, however, both of these redox-indicators decrease up section, coincident with a decrease in the abundance of Os (Figure 3.6). At a depth of 110.01 m, eccentricity, precession, and obliquity are all at their minima causing minimal solar insolation (Figures 3.7 & 3.8). This results in a more stratified water column and oxygen-deficient bottom waters, reflected by the enrichment in Os and other redox-sensitive trace metals and the deposition of organic-rich marls with >10% TOC. At 106.50 m, eccentricity and precession are at their minima, however the amplitude amplification is muted by a maxima in the obliquity (Figure 3.7 & 3.8). This yields the deposition of a slightly less organic-rich marl with TOC values of 5 – 10, and slightly less enrichment in Os (Figure 3.7 & 3.8). At 103.50 m, eccentricity and precession are at a maxima, however the amplitude amplification is muted by a minima in the obliquity resulting in the deposition of low TOC limestone-rich marls and an even less enrichment in Os (Figures 3.7 & 3.8). At depths of 106.50 and 103.50 m, the degree of bottom-water anoxia decreases, as indicated by the decline in the abundance of Os and

other redox-sensitive trace metals and in the organic-richness of the preserved sediment. This is likely caused by a progressive increase in solar insolation during this interval due to climatic variations controlled by Milankovitch cycles. In contrast, inter-peak intervals, with low abundances of Os redox-sensitive trace metals, represent periods of increased solar insolation and a more well-mixed water column.

In addition, the Pt and Ir enrichments reported here is coincident with the most oxic period within the interval studied. This oxic interval reflects increased solar insolation due to amplitude amplification and modulation of Milankovitch cycles and a consequent increase in the atmospheric-ocean thermal gradients resulting in greater or more frequent storms, stronger bottom-water currents, a de-stratification of the water column, and improved bottom-water oxygenation (Eldrett et al., 2015a). At depths of 102.95 and 104.0 m, within the Pt-Ir enrichment, a maxima in obliquity and precession, and a near maxima in eccentricity results in near maximum solar insolation. The resulting increase in the atmospheric-ocean thermal gradients and a de-stratification of the water column, and improved bottom-water oxygenation is marked by the presence of limestone, a lack of redox-sensitive trace metals, the presents of benthic foraminifera, and an enrichment in oxically enriched trace metals (Pt and Ir). Whereas the Eagle Ford Group studied here only shows one peak in Pt and Ir, Orth et al. (1988) and Orth et al. (1993) show two separate peaks in Pt and Ir. These two peaks likely correlate to these two near-maxima in solar insolation (Figure 3.7). The lack of double peaks observed here is likely due to the general lower sampling resolution in this interval, and further work at higher resolution is required to resolve this difference.

3.6. CONCLUSIONS

A decoupling of Re-Os and Pt-Ir enrichments is observed within the Cenomanian-Turonian Eagle Ford Group from the KWIS prior to and during OAE2. A negative $^{187}Os/^{188}Os$ excursion occurs just prior to the onset of OAE2. Starting ~95.06 Ma, the $(^{187}Os/^{188}Os)_i$ displays an abrupt shift toward a non-radiogenic value of 0.15. The minimum value of $(^{187}Os/^{188}Os)_i$ at 94.88 Ma is coincident with the start of OAE2. This represents a drastic shift of the Os isotopic composition of seawater over a ~240 - 360 kyr interval prior to the onset of OAE2 and reflects a predominance of non-radiogenic Os input to the WCIS at this time. The same abrupt trend to non-radiogenic values is observed the Portland #1 core from the KWIS and from sites in western Tethys and the proto-North Atlantic Ocean and has been explained by a large contribution of mantle-like Os during eruption of the CLIP.

The non-radiogenic trend observed in the Portland #1 core from the KWIS and from sites in western Tethys and the proto-North Atlantic Ocean is coupled with a marked increase in the abundance of Os of up to 10 ppb. However, in the section studied here, the trend toward unradiogenic Os begins ~240 - 360 kyr prior to the marked increase in Os abundance (~6 ppb) and OAE2. This suggests the mechanism responsible for the abrupt increase in non-radiogenic Os provided to the oceans during the pre-OAE2 interval (perhaps the eruption of the CLIP) was likely the triggering mechanism for OAE2.

Following the first enrichment in Os at the start of OAE2, two additional Os enrichments occur with decreasing abundances. These enrichments occur at 94.72 Ma (2650 ppt) and 94.54 Ma (1300 ppt). There is a ~160 - 180 kyr periodicity to these three Os enrichments.

The delayed enrichment of Os and the three Os peaks of decreasing abundance are caused by variations in the redox conditions of the water columns prior to and during OAE2, caused by variations in solar insolation ultimately controlled by Milankovitch cycles. During the pre-OAE2 interval, at the start of the abrupt trend toward non-radiogenic Os values, solar insolation was low resulting in a stratified water-column and sub-oxic to anoxic bottom-waters. At ~94.88 Ma, coincident with the start of OAE2, overlapping minima in eccentricity, obliquity and precession resulted in minimal solar obliquity resulting in anoxic bottom-waters. Rhenium and Os are redox-sensitive elements and thus following their enrichment in seawater during CLIP eruption, they became enriched in organic-rich marls once bottom-water conditions became anoxic. The two younger enrichments in Os of lessening abundances were caused by the variations in redox driven by Milankovitch cycles, specifically, a progressive oxygenation of bottom waters up-section. During inter-peak intervals, marked by low Os abundances, the oceans experienced a more well-mixed water column and oxic bottom-waters.

An abrupt increase in the abundance of Pt and Ir occurs within OAE2, ~340 - 360 kyr after the first Os enrichment. The enrichment of these elements is coincident with the most oxic bottom-waters within the interval studied, following a transition to more oxic conditions during increased solar insolation. Platinum and Ir that were provided to seawater during CLIP eruption remained in solution until oxic bottom-water conditions were achieved. They were then precipitated or sequestered into oxic sediments within this interval.

Previous authors have explained the variable timing and magnitude of the enrichments of Re-Os and Pt-Ir as a factor of distance from the source of these elements. However, this study suggests that it is likely a factor of the oxygen conditions of the bottom-waters in which these sediments are sequestered. Rhenium and Os are sequestered under anoxic bottom-water conditions while Pt and Ir experience uptake during oxic bottom-water conditions. Therefore, the variable enrichments reported for locations around the world are likely due to variations in the redox of the water-column due to variations in basin geometries, water depth, etc. The variability in basin properties ultimately changes how solar insolation caused by Milankovitch cycles affects the water column.

In addition, studies that use PGE abundance ratios as a tool for trace metal source identification should use caution, as the uptake mechanisms for these elements vary. This is especially true if the ratios used include elements that are enriched under different redox conditions (e.g. Pt/Os; Pt: oxically enriched, Os: anoxically enriched). Also, there is likely variable efficiency in the uptake of these elements, even when using an abundance ratio when both elements are similarly behaved. Results achieved through the use of PGE ratios in oceanic sediments are likely of more use in redox studies than in identifying a source for these elements.

REFERENCES

Adams D.D., Hurtgen M.T. and Sageman B.B. (2010) Volcanic triggering of a biogeochemical cascade during Oceanic Anoxic Event 2. *Nature Geoscience* **3**, 201-204.

Almon W.D. and Cohen P.A. (2008) Palaeoecological significance of turritelline gastropod-dominated assemblages from the mid-Cretaceous (Albian-Cenomanian) of Texas and Oklahoma, USA. *Cretaceous Research* **29**, 65-77.

Alvarez L.W., Alvarez W., Asaro F. and Michel H.V. (1980) Extraterrestrial cause for the Cretaceous-Tertiary Extinction. *Science* **208**, 1095-1108.

Alvarez W. Asaro F., Michel H.V. and Alvarez L.W. (1982) Iridium anomaly approximately synchronous with terminal Eocene extinctions. *Science* **216**, 886-888.

Anbar A.D., Wasserburg G.J., Papanastassiou D.A. and Andersson P.S. (1996) Iridium in natural waters. *Science* **273**, 1524-1528.

Baioumy H.M., Eglinton L.B., and Peucker-Ehrenbrink B. (2011) Rhenium-osmium isotope and platinum group element systematics of marine vs. non-marine organic-rich sediments and coals from Egypt. *Chemical Geology* **285**, 70-81.

Bekov G.I., Letokhov V.S., Radaev V.N., Baturin G.N., Egorov A.S., Kursky A.N. and Narseyev V.A. (1984) Ruthenium in the ocean. *Nature* **312**, 748-750.

Bhattacharya J.P. and MacEachern J.A. (2009) Hyperpycnal rivers and prodeltaic shelves in the Cretaceous seaway of North America. *Journal of Sedimentary Research* **79**, 184-209.

Birck J.-L., RoyBarman M. and Capmas F. (1997) Re-Os measurements at the femtomole level in natural samples. *Geostandards Newsletter* **20**, 19-27.

Brandon A.D., Norman M.D., Walker R.J. and Morgan J.W. (1999) ^{186}Os-^{187}Os systematics of Hawaiian picrites. *Earth and Planetary Science Letters* **174**, 25-42.

Byrne R.H. and Yao W. (2000) Formation of palladium(II) hydroxychloride complexes and precipitates in sodium chloride solutions and seawater. *Geochimica et Cosmochimica Acta* **64**, 4153-4153.

Chai C.F., Ma S.L., Mao X.Y., Sun Y.Y., Xu D.Y., Zhang Q.W. and Yang Z.Z. (1986) Geochemical anomaly at the Permian-Triassic boundary Changxin, Zhejiang. *Act Geologica Sinica* **60**, 139-150.

Chai C.F., Mao X.Y., Ma S.L., Bai S.L., Zhou Y.Q., Ma J.G. and Ning Z.S. (1989) Geochemical anomaly at the Devonian-Carboniferous boundary Huangmao, Guangxi, China. *Historical Biology* **2**, 89-100.

Coffin M.F. and Eldholm O. (1994) Large igneous provinces: crustal structure, dimensions, and external consequences. *Reviews of Geophysics* **32**, 1-36.

Cohen A.S. and Coe A.L. (2002) New geochemical evidence for the onset of volcanism in the Central Atlantic magmatic province and environmental change at the Triassic-Jurassic boundary. *Geology* **30**, 267-270.

Cohen A.S. and Waters F.G. (1996) Separation of osmium from geological materials by solvent extraction for analysis by TIMS. *Analytical Chimica Acta* **332**, 269-275.

Cohen A.S., Coe A.L. Bartlett J.M. and Hawksworth C.J. (1999) Precise Re-Os ages of organic-rich mudrocks and the Os isotope composition of Jurassic seawater. *Earth and Planetary Science Letters* **167**, 159-173.

Colodner D.C., Boyle E.A., Edmond J.M. and Thomson J. (1992) Post-depositional mobility of platinum, iridium and rhenium in marine sediments. *Nature* **358**, 402-404.

Colodner D., Sachs J., Ravizza G., Turekian K.K., Edmond J. and Boyle E. (1993) The geochemical cycles of rhenium: A reconnaissance. *Earth and Planetary Science Letters* **117**, 205-221.

Corbett M.J, Watkins D.K. and Pospichal J.J. (2014) A quantitative analysis of calcareous nannofossil bioevents of the Late Cretaceous (Late Cenomanian-

Coniacian) Western Interior Seaway and their reliability in established zonation schemes. *Marine Micropaleontology* **109**, 30-45.

Cosden J.M., Schijf J. and Byrne R.H. (2003) Fractionation of platinum group elements in aqueous systems: comparative kinetics of palladium and platinum removal from seawater by Ulva lactuca L. *Environmental Science and Technology* **37**, 555-560.

Creaser R.A., Papanastassiou D.A. and Wasserburg G.J. (1991) Negative thermal ion mass spectrometry of osmium, rhenium and iridium. *Geochimica et Cosmochimica Acta* **55**, 397-401.

Creaser R.A., Sannigrahi P., Chacko T. and Selby D. (2002) Further evaluation of the Re-Os geochronometer in organic-rich sedimentary rocks: A test of hydrocarbon maturation effects in the Exshaw Formation, Western Canada Sedimentary Basin. *Geochimica et Cosmochimica Acta* **66**, 3441-3452.

Crocket J.H., MacDougall J.D. and Harriss R.C. (1973) Palladium and iridium in marine sediments. *Geochimica et Cosmochimica Acta* **37**, 2547-2556.

Crusius J., Calvert S., Pedersen T. and Sage D. (1996) Rhenium and molybdenum enrichments in sediments as indicator of oxic, suboxic and sulfidic conditions of deposition. *Earth and Planetary Science Letters* **145**, 65-78.

Cumming V.M., Selby D. and Lillis P.G. (2012) Re-Os geochronology of the lacustrine Green River Formation: Insights into direct depositional dating of lacustrine successions, Re-Os systematics and paleocontinental weathering. *Earth and Planetary Science Letters* **359-360**, 194-205.

Dai X., Chai Z., Mao X. and Ouyang H. (2000) Sorption and desorption of iridium by coastal sediment: effects of iridium speciation and sediment components. *Chemical Geology* **166**, 15-22.

Dawson W.C. (2000) Shale microfacies: Eagle Ford Group (Cenomanian-Turonian), north-central Texas outcrops and subsurface equivalents. *Gulf Coast Association of Geological Societies Transactions* **50**, 607-621.

Denne R.A., Hinote R.E., Breyer J.A., Kosanke T.H., Lees J.A., Engelhardt-Moore N., Spaw J.M. and Tur N. (2014) The Cenomanian-Turonian Eagle Ford Group of south Texas: insights on timing and paleoceanographic conditions from geochemistry and micropaleontologic analyses. *Palaeogeography, Palaeoclimatology, Palaeoecology* **413**, 2-28.

Donovan A.D. and Staerker T.S. (2010) Sequence stratigraphy of the Eagle Ford (Boquillas) Formation in the subsurface of South Texas and outcrops of west Texas. *Gulf Coast Association of Geological Societies Transactions* **60**, 861-899.

Du Vivier A.D.C., Selby D., Sageman B.B., Jarvis I., Grocke D.R. and Voigt S. (2014) Marine $^{187}Os/^{188}Os$ isotope stratigraphy reveals the interaction of volcanism and ocean circulation during Oceanic Anoxic Event 2. *Earth and Planetary Science Letters* **389**, 23-33.

Duncan R.A. and Hargraves R.B. (1984) Plate tectonic evolution of the Caribbean region in the mantle reference frame. In: Bonini W., Hargraves R.B. and Shagam R. (Eds.), *The Caribbean-South American plate boundary and regional tectonics*. Boulder, Geological Society of America, GSA Memoir **162**, 81-93.

Dymond J., Lyle M., Finney B., Piper D.Z., Murphy K., Conrad R. and Pisias N.L. (1984) Ferromanganese nodules from MANOP Sites H, S, and R – control of mineralogical and chemical compositions by multiple accretionary processes. *Geochimica et Cosmochimica Acta* **48**, 931-949.

Dypvik H., Gudlaugsson S.T., Tsikalas F., Attrep M., Ferrell R.E., Krinsley D.H., Mork A., Faleide J.I and Nagy J. (1996) Mjolnir structure: an impact crater in the Barents Sea. *Geology* **24**, 779-782.

Elder W.P., Gustason E.R. and Sageman B.B. (1994) Correlation of basinal carbonate cycles to nearshore parasequences in the Late Cretaceous Greenhorn Seaway, Western Interior, U.S. *Geological Society of America Bulletin* **106**, 892–902.

Eldrett J.S., Ma C., Bergman S.C., Ozkan A., Minisini D., Lutz B., Jackett S.-J., Macaulay C. and Kelly A.E. (2015a) Origin of limestone-marlstone cycles: Astronomic forcing of organic-rich sedimentary rocks from the Cenomanian to Early Coniacian of the Cretaceous Western Interior Seaway, USA. *Earth and Planetary Science Letters* **423**, 98-113.

Eldrett J.S., Ma C., Bergman S.C., Lutz B., Gregory J.F., Dodsworth P., Phipps M., Hardas P., Minisini D., Ozkan A., Ramezani J., Bowring S.A., Kamo S.L., Ferguson K., Macaulay C. and Kelly A.E. (2015b) An astronomically calibrated stratigraphy of the Cenomanian, Turonian and earliest Coniacian from the Cretaceous Western Interior Seaway, USA: Implications for global chronostratigraphy. *Cretaceous Research* (in press.).

Eldrett J.S., Minisini D. and Bergman S.C. (2014) Decoupling of the carbon cycle during Oceanic Anoxic Event 2. *Geology* **42**, 567-570.

Esser B.K. and Turekian K.K. (1993) The osmium isotopic compositions of the continental crust. *Geochimica et Cosmochimica Acta* **57**, 3093-3104.

Estrada S. and Henjes-Kunst F. (2013) 40Ar-39Ar and U-Pb dating of Cretaceous continental rift-related magmatism on the northeast Canadian Arctic margin. *Zeitschrift der Deutschen Gesellschaft fur Geowissenschaften* **164**, 107-130.

Evans N.J. and Chai C.F. (1997) The distribution and geochemistry of platinum-group elements as event markers in the Phanerozoic. *Palaeogeography, Palaeoclimatology, Palaeoecology* **132**, 373-390.

Evans N.J., Gregoire D.C., Grieve R.A.F., Goodfellow W.D. and Veizer J. (1993) Use of platinum-group elements for impactor identification: Terrestrial impact craters and Cretaceous-Tertiary boundary. *Geochimica et Cosmochimica Acta* **57**, 3737-3748.

Fergusson J.E. (1992) Noble metals in the environment: In: Brooks R.R. (Ed.), *Noble Metals and Biological Systems*. CRC Press, FL, USA. 246-247.

Finlay A.J., Selby D. and Grocke D.R. (2010) Tracking the Hirnantian glaciations using Os isotopes. *Earth and Planetary Science Letters* **293**, 339-348.

Forster A., Schouten S., Moriya K., Wilson P.A. and Sinninghe Damste J.S. (2007) Tropical warming and intermittent cooling during the Cenomanian/Turonian oceanic anoxic event 2: Sea surface temperature records from the equatorial Atlantic. *Paleoceanography* **22**, PA1219.

Forster A., Kuypers M.M.M., Turgeon S.C., Brumsack H.-J., Petrizzo M.R. and Sinninghe Damste J.S. (2008) The Cenomanian/Turonian oceanic anoxic event in the South Atlantic: New insights from a geochemical study of DSDP 530A. *Palaeogeography, Palaeoclimatology, Palaeoecology* **267**, 256-283.

Fritz D.A., Belsher T.W., Medlin J.M., Stubbs J.L., Wright, R.P. and Harris P.M. (2000) New exploration concepts for the Edwards and Sligo margins, Cretaceous of onshore Texas. *AAPG Bulletin* **84**, 905-922.

Gale A.S., Voigt S., Sageman B.B. and Kennedy W.J. (2008) Eustatic sea-level record for the Cenomanian (Late Cretaceous) – Extension to the Western Interior Basin, USA. *Geology* **36**, 859-862.

Galloway W.E. (2008) Depositional evolution of the Gulf of Mexico sedimentary basin. In: Miall A.D. (Ed.), *The sedimentary basins of the United States and Canada*, New York, Elsevier, 610 p.

Gammons C.H. (1996) Experimental investigations of the hydrothermal geochemistry of platinum and palladium: V. Equilibria between platinum metals, Pt(II), and Pt(IV) chloride complexes at 25 to 300^{o}C. *Geochimica et Cosmochimica Acta* **60**, 1683-1694.

Georgiev S., Stein H.J., Hannah J.L., Bingen B., Weiss H.M. and Piasecki S. (2011) Hot acidic Late Permian seas stifle life in record time. *Earth and Planetary Science Letters* **310**, 389-400.

Gilbert G.K. (1895) Sedimentary measurement of geologic time. *Journal of Geology* **3**, 121-127.

Glass B.P. (1986) Late Eocene microtektites and clinopyroxene-bearing spherules. In: Pomerol C. and Premoli-Silva I. (Eds.), Terminal Eocene Events. Elsevier, Amsterdam, pp. 395-401.

Goldberg E.D., Hodge V., Kay P., Stallard M. and Koide M. (1986) Some comparative marine chemistries of platinum and iridium. *Applied Geochemistry* **1**, 227-232.

Goldberg E.D. (1962) Marine geochemistry I: Chemical scavengers of the sea. *Journal of Geology* **62**, 249-265.

Gostin V.A., Keays R.R. and Wallace M.W. (1989) Iridium anomaly form the Acraman ejecta horizon: impacts can produce sedimentary iridium peaks. *Nature* **340**, 542-544.

Grieve R.A.F. (1991) Terrestrial impact: The record in the rocks. *Meteoritics* **26**, 175-194.

Grosheny D., Beaudoin B., Morel L. and Desmares D. (2006) High-resolution biostratigraphy and chemostratigraphy of the Cenomanian/Turonian boundary event in the Vocontian Basin, southeast France. *Cretaceous Research* **27**, 629-640.

Hannah J.L., Bekker A., Stein H.J., Markey R.J. and Holland H.D. (2004) Primitive Os and 2316 Ma age for marine shale: Implications for Paleoproterozoic glacial events and the rise of atmospheric oxygen. *Earth and Planetary Science Letters* **225**, 43-52.

Harbor R. (2011) Facies characterization and stratigraphic architecture of organic-rich mudrocks, Upper Cretaceous Eagle Ford Formation, south Texas. Master's Thesis, University of Texas at Austin, 195 p.

Hentz T.F. and Ruppel S.C. (2010) Regional lithostratigraphy of the Eagle Ford shale: Maverick Basin to East Texas Basin. *Gulf Coast Association of Geological Societies Transactions* **60**, 325-337.

Hodge V.F., Stallard M., Koide M. and Goldberg E.D. (1985) Platinum and the platinum anomaly in the marine environment. *Earth and Planetary Science Letters* **72**, 158-162.

Hodge V.F., Stallard M., Koide M. and Goldberg E.D. (1986) Determination of platinum and iridium in marine waters, sediments, and organism. *Analytical Chemistry* **58**, 616-620.

Hoernle K., van den Bogaard P., Werner R., Lissina B., Hauff F., Alvarado G. and Garbe-Schonberg D. (2002) Missing history (16-71 Ma) of the Galapagos hotspot: Implications for the tectonic and biological evolution of the Americas. *Geology* **30**, 795-798.

Hoernle K., Hauff F. and van den Bogaard P. (2004) 70 m.y. history (139-69 Ma) for the Caribbean large igneous province. *Geology* **32**, 697-700.

Holser W.T., Schonlaub H.P., Boeckelmann K. and Magaritz M. (1991) The Permian-Triassic of the Gartnerkofel-1 core (Carnic Alps, Austria): synthesis and conclusions. *Abh. Geol. Bundesanst.* ***45****, 213-232.*

Hsu K.J., Oberhansli H., Gao J.Y., Shu S., Haihong C. and Krahenbuhl V. (1985) "Strangelove ocean" before the Cambrian explosion. *Nature* **316**, 809-811.

Jacinto G.S. and van den Berg C.M.G. (1989) Different behavior of platinum in the Indian and Pacific Oceans. *Letters to Nature* **338**, 332-334.

Jaffe L.A., Peucker-Ehrenbrink B. and Petsch S.T. (2002) Mobility of rhenium, platinum group elements and organic carbon during black shale weathering. *Earth and Planetary Science Letters* **198**, 339-353.

Jarvis I., Lignum J.S., Grocke D.R., Jenkyns H.C. and Pearce M.A. (2011) Black shale deposition, atmospheric CO2 drawdown, and cooling during the Cenomanian-Turonian Oceanic Anoxic Event. *Paleoceanography* **26**, PA3201.

Jenkyns H.C. (1980) Cretaceous anoxic events: from continents to oceans. *Memoirs of the Geological Society of London* **137**, 171-188.

Jenkyns H.C. (1985) The Early Toarcian and Cenomanian-Turonian anoxic events in Europe: comparisons and contrasts. *Geologische Rundschau* **74**, 505-508.

Jenkyns H.C., Matthews A., Tsikos H. and Erel Y. (2007) Nitrate reduction, sulfate reduction, and sedimentary iron isotope evolution during the Cenomanian-Turonian oceanic anoxic event. *Paleoceanography* **22**, PA3208.

Jenkyns H.C. (2010) Geochemistry of oceanic anoxic events. *Geochemistry, Geophysics, Geosystems* **60**, Q03004.

Jowitt S., Williamson M.-C. And Ernst R.E. (2014) Geochemistry of the 130-80 Ma Canadian High Arctic LIP (HALIP) event and implications for Ni-Cu-PGE prospectivity. *Economic Geology and the Bulletin of the Society of Economic Geologists* **109**, 281-307.

Kadko D. and Heath G.R. (1984) Models of depth dependent bioturbation at MANOP site H in the Eastern Equatorial Pacific. *Journal of Geophysical Research* **89**, 6567-6570.

Keller G., Adatte T., Berner Z., Chellai E.H. and Steuben D. (2009) Oceanic events and biotic effects of the Cenomanian-Turonian anoxic event, Tarfaya Basin, Morocco. *Cretaceous Research* **29**, 976-994

Kendall B.S., Creaser R.A., Ross G.M. and Selby D. (2004) Constraints on the timing of Marinoan 'Snowball Earth' glaciations by ^{187}Re-^{187}Os dating of a Neoproterozoic post-glacial black shale in Western Canada. *Earth and Planetary Science Letters* **222,** 729-470.

Kendall B.S., Creaser R.A. and Selby D. (2009) ^{187}Re-^{187}Os geochronology of Precambrian organic-rich sedimentary rocks. *Geological Society of London Special Publications* **326**, 85-107.

Kennedy W.J., Walaszezyk I. And Cobban W.A. (2000) Pueblo, Colorado, USA, candidate Global Boundary Stratotype Section and Point for the base of the Turonian Stage of the Cretaceous and for the base of the Middle Turonian Substage, with a revision of the Inoceramidae (Bivalvia). *Acta Geologica Polonica* **50**, 295-334.

Kerr A.C., Tarney J., Marriner G.F., Nivia A. and Saunders A.D. (1997) The Caribbean-Columbian Cretaceous igneous province: the internal anatomy of an oceanic plateau. In: Mahoney J.J. and Coffins M. (Eds.) *Large Igneous Provinces.* American Geophysical Union Monographs **100**, 123-144.

Kerr A.C. (1998) Oceanic plateau formation: a cause of mass extinction and black shale deposition around the Cenomanian-Turonian boundary? *Journal of the Geological Society of London* **155**, 619-626.

Koeberl C. (1993) Extraterrestrial component associated with Australasian microtektites in a core from ODP site 758b. *Earth and Planetary Science Letters* **119**, 453-458.

Koide M., Goldberg E.D., Niemeyer S., Gerlach D., Hodge V., Bertine K.K. and Padova A. (1991) Osmium in marine sediments. *Geochimica et Cosmochimica Acta* **55**, 1641-1648.

Kolonic S., Wagner T., Forster A., Sinninghe Damsté J.S., Walsworth-Bell B., Erba E., Turgeon S., Brumsack H-J., Chellai E. H., Tsikos H., Kuhnt W. and Kuypers, M.M.M. (2005) Black shale deposition on the northwest African Shelf during the Cenomanian//Turonian oceanic anoxic event: Climate coupling and global organic carbon burial. *Paleoceanography* **20**, PA1006.

Kump L.R. and Byrne R.H. (1989) Palladium chemistry in seawater. *Environmental Science and Technology* **23**, 663-662.

Lee C.-T., Wasserburg G.J. and Kyte F.T. (2003) Platinum-group elements (PGE) and rhenium in marine sediments across the Cretaceous-Tertiary boundary: Constraints on Re-PGE transport in the marine environment. *Geochimica et Cosmochimica Acta* **67**, 655-670.

Lowery C.M., Corbett M.J., Leckie R.M., Watkins D., Romero A. and Pramudito A. (2014) Foraminiferal and nannofossil paleoecology and paleoceanography of the Cenomanian-Turonian Eagle Ford shale of southern Texas. *Palaeoceanography, Palaeoclimatology, Palaeoecology* **413**, 49-65.

Markey R.J., Stein H.J., Hannah J.L., Zimmerman A., Selby D. and Creaser R.A. (2007) Standardizing Re-Os geochronology: A new molybdenite reference material (Henderson, USA) and the stoichiometry of Os salts. *Chemical Geology* **244**, 74-87.

McGarity H.A. (2013) Facies and stratigraphic framework of the Eagle Ford shale in south Texas. Masters Thesis, University of Houston, 105 p.

McLaren D.J. and Goodfellow W.D. (1990) Geological and biological consequences of giant impacts. *Annual Review of Earth and Planetary Science* **18**, 123-171.

Meyers S.R., Sageman B.B. and Hinnov L. (2001) Integrated quantitative stratigraphy of the Cenomanian-Turonian Bridge Creek Limestone member using Evolutive Harmonic Analysis and stratigraphic modeling. *Journal of Sedimentary Research* **71**, 627-643.

Montgomery S.W., Petty A.J. and Post P.J. (2002) James Limestone, northeastern Gulf of Mexico: Refound opportunity in a Lower Cretaceous trend. *AAPG Bulletin* **86**, 381-397.

Morford J.L. and Emerson S. (1999) The geochemistry of redox sensitive trace metals in sediments. *Geochimica et Cosmochimica Acta* **63**, 1735-1750.

Morford J.L., Martin W.R., Francois R. and Carney C.M. (2009) A model for uranium, rhenium, and molybdenum diagenesis in marine sediments based on results from coastal locations. *Geochimica et Cosmochimica Acta* **73**, 2938-2960.

Mountain B. and Wood S.A. (1988) Chemical controls on the solubility, transport, and deposition of platinum and palladium in hydrothermal solutions: a thermodynamic approach. *Economic Geology* **83**, 492-510.

Orth C.J., Attrep M., Mao X.Y., Kauffman E.G., Diner R. and Elder W.P. (1988) Iridium abundance maxima in the Upper Cenomanian extinction interval. *Geophysical Research Letters* **15**, 346-349.

Orth C.J., Attrep M., Quintana L.R., Elder W.P., Kauffman E.G., Diner R. and Villamil T. (1993) Elemental abundance anomalies in the Late Cenomanian extinction interval: A search for the source(s). *Earth and Planetary science Letters* **117**, 189-204.

Oxburgh R. (1998) Variations in the osmium isotope composition of sea water over the past 200,000 years. *Earth and Planetary Science Letters* **159**, 183-191.

Paquay F.S., Ravizza G.E., Dalai T.K. and Peucker-Ehrenbrink B. (2008) Determining chondritic impactor size from the marine osmium isotope record. *Science* **320**, 214-218.

Pasava J., Oszczepalski S. and Du A.S. (2010) Re-Os age of non-mineralized black shales from the Kupferschiefer, Poland, and implications for metal enrichments. *Miner. Deposita* **45**, 189-199.

Peucker-Ehrenbrink B. and Hannigan R.E. (2000) Effects of black shale weathering on the mobility of rhenium and platinum group elements. *Geology* **28**, 475-478.

Peucker-Ehrenbrink B. and Jahn B.-M. (2001) Rhenium-osmium isotope systematics and platinum group element concentrations: Loess and the upper continental crust. *Geochemistry Geophysics Geosystems* **2**, 1-22.

Peucker-Ehrenbrink B. and Ravizza G. (2000) The marine osmium isotope record. *Terra Nova* **12**, 205-219.

Peucker-Ehrenbrink B. and Ravizza G.E. (2012) Chapter 8: Osmium Isotope Stratigraphy. In: Gradstein F.M., Ogg J.G., Schmitz M.D., Ogg G.J. (Eds.), *The Geologic Time Scale 2012*, Elsevier, Boston, 145-166.

Phelps R.M., Kerans C., Da-Gama R.O.B.P., Jeremiah J., Hull D. and Loucks R.G. (2015) Response and recovery of the Comanche carbonate platform surrounding multiple Cretaceous oceanic anoxic events, northern Gulf of Mexico. *Cretaceous Research* **54**, 117-144.

Pindell J.L., Cande S.C., Pitman W.C., Rowley D.B., Dewey J.F., LaBreeque J. and Haxby W. (1988) A plate-kinematic framework for models of Caribbean evolution. *Tectonophysics* **155**, 121-139.

Playford P.E., McLaren D.J., Orth C.J., Gilmore J.S. and Goodfellow W.D. (1984) Iridium anomaly in the Upper Devonian of the Canning Basin, Western Australia. *Science* **226**, 437-439.

Qiu X., Liu C., Mao G., Deng Y., Wang F. and Wang J. (2015) Major, trace and platinum-group element geochemistry of the Upper Triassic nonmarine hot shales in the Ordos Basin, Central China. *Applied Geochemistry* **53**, 42-52.

Ravizza G.E. and Peucker-Ehrenbrink B. (2003) The marine $^{187}Os/^{188}Os$ record of the Eocene-Oligocene transition: The interplay of weathering and glaciations. *Earth and Planetary Science Letters* **210**, 151-165.

Ravizza G. and Pyle D. (1997) PGE and Os isotopic analysis of single sample aliquots with NiS fire assay preconcentrations. *Chemical Geology* **141**, 251-268.

Ravizza G. and Turekian K.K. (1989) Applications of the ^{187}Re-^{187}Os system to black shale geochronometry. *Geochimica et Cosmochimica Acta* **53**, 3257-3262.

Ravizza G., Turekian K.K. and Hay B.J. (2001) The geochemistry of rhenium and osmium in recent sediments from the Black Sea. *Geochimica et Cosmochimica Acta* **55**, 3741-3752.

Ravizza G. (1998) Osmium-Isotope geochemistry of site 959: Implications for Re-Os sedimentary geochronology and reconstruction of past variations in the Os-isotopic composition of seawater. *Proceedings of the Ocean Drilling Program, Scientific Results* **159**, 181-186.

Ravizza G., Turekian K.K. and Hay B.J. (1991) The geochemistry of rhenium and osmium in recent sediments from the Black Sea. Geochimica *et Cosmochimica Acta* **55**, 3741-3752.

Rooney A.D., Selby D., Houzay J.-P. and Renne P.R. (2010) Re-Os geochronology of a Mesoproterozoic sedimentary succession, Taoudeni Basin, Mauritania: Implications for basin-wide correlations and Re-Os organic-rich sediments systematics. *Earth and Planetary Science Letters* **289**, 486-496.

Rose P.R. (1972) Edwards Group, surface and subsurface, central Texas. *University of Texas at Austin Bureau of Economic Geology Report of Investigations* **74**, 198 p.

Sageman B.B., Rich J., Arthur M.A., Birchfield G.E. and Dean W.E. (1997) Evidence for Milankovitch periodicities in Cenomanian-Turonian lithologic and geochemical cycles, Western interior U.S. *Journal of Sedimentary Research* **67**, 285-301.

Sageman B.B., Rich J., Savrda C.E., Bralower T., Arthur M.A. and Dean W.E. (1998) Multiple Milankovitch cycles in the Bridge Creek Limestone (Cenomanian-Turonian), Western interior basin. In: Arthur M.A. and Dean W.E. (Eds.), *Stratigraphy and paleoenvironments of the Cretaceous Western Interior seaway, USA.* Society of Sedimentary Geology, Concepts in Sedimentology and Paleontology **6**, 153-171.

Sageman B.B., Meyers S.R. and Arthur S.R. (2006) Orbital time scale and new C-isotope record for Cenomanian-Turonian boundary stratotype. *Geology* **34**, 125-128.

Salvador A. (1991) Origin and development of the Gulf of Mexico Basin. In: Salvador A. (Ed.), *The Gulf of Mexico Basin: Boulder, Colorado*, Geological Society of America, The Geology of North America **J**, 389-444.;

Sawlowicz Z. (1993) Iridium and other platinum-group elements as geochemical marks in sedimentary environments. *Palaeogeography, Palaeoclimatology, Palaeoecology* **104**, 253-270.

Schieber J., Southard J.B., Kissling P., Rossman B. and Ginsburg R. (2013) Experimental deposition of carbonate mud from moving suspension: importance of flocculation and implications for modern and ancient carbonate mud deposition. *Journal of Sedimentary Research* **83**, 1025-1031.

Schlanger S.O. and Jenkyns H.C. (1976) Cretaceous anoxic events: causes and consequences. *Geologie en Mijnbouw* **55**, 179-184.

Schlanger S.O., Arthur M.A., Jenkyns H.C. and Scholle P.A. (1987) The Cenomanian-Turonian Oceanic Anoxic Event, I. Stratigraphy and distribution of organic carbon-rich beds and the marine $\delta^{13}C$ excursion. *Special Publications of the Geological Society of London* **26**, 371-399.

Schmitz B., Peucker-Ehrenbrink B., Heilmann-Clausen C., Aberg G., Asaro F. and Lee C.A. (2004) Basaltic explosive volcanism, but no comet impact, at the Paleocene-Eocene boundary: High-resolution chemical and isotopic records from Egypt, Spain and Denmark. *Earth and Planetary Science Letters* **225**, 1-17.

Schroder-Adams C.J., Cumbaa S.L., Bloch J., Leckie D.A., Craig J., Seif El-Dein S.A.,Simons D-J.H.A.E. and Kenig F. (2001) Late Cretaceous (Cenomanian to Campanian) paleoenvironmental history of the Eastern Canadian margin of the Western Interior Seaway: bonebeds and anoxic events. *Palaeogeography, Palaeoclimatology, Palaeoecology* **170**, 261-289.

Scott R.W. (1993) Cretaceous carbonate platform, U.S. Gulf coast. In: Simo J.A., Scott R.W. and Masse J.P. (Eds.), *Cretaceous Carbonate Platforms,* AAPG Memoir **56**, 97-109.

Selby D. and Creaser R.A. (2001) Re-Os geochronology and systematics in molybdenite from the Endako porphyry molybdenum deposit, British Columbia, Canada. *Economic Geology* **96**, 197-204.

Selby D. and Creaser R.A. (2003) Re-Os geochronology of organic rich sediments: An evaluation of organic matter analysis methods. *Chemical Geology* **200**, 225-240.

Sinton C.W. and Duncan R.A. (1997) Potential links between ocean plateau volcanism and global ocean anoxia at the Cenomanian-Turonian boundary. *Economic Geology* **92**, 836-842.

Smoliar M.I., Walker R.J. and Morgan J.W. (1996) Re-Os isotope constraints on the age of Group IIA, IIIA, IVA, and IVB iron meteorites. *Science* **271**, 1099-1102.

Snow L.J., Duncan R.A. and Bralower T.J. (2005) Trace element abundances in the Rock Canyon Anticline, Pueblo, Colorado, marine sedimentary section and their relationship to the Caribbean plateau construction and oxygen anoxic event 2. *Paleoceanography* **20**, PA3005.

Tegner C., Storey M., Holm P.M., Thorarinsson S.B., Zhao X., Lo C.-H. And Knudsen M.F. (2011) Magmatism and Eurekan deformation in the High Arctic Large Igneous Province: ^{40}Ar-^{39}Ar age of Kap Washington Group volcanics, North Greenland. *Earth and Planetary Science Letters* **303**, 203-214.

Torsvik T.H. and Burke K. (2015) Large igneous province locations and their connections with the core-mantl boundary. In: Schmidt A., Fristad K.E. and Elkins-Tanton L.T. (Eds.), *Volcanism and Global Environmental Change,* Cambridge University Press, Cambridge University Press, 30-46.

Trabucho Alexandre J., Tuenter E., Henstra G.A., van der Zwan K.J., van de Wal R.W.W., Dijkstra H.A. and de Boer P.L. (2010). The mid-Cretaceous North Atlantic nutrient trap: Black shales and OAEs. *Paleoceanography* **25**, PA4201.

Turgeon S.C. and Creaser R.A. (2008) Cretaceous oceanic anoxic event 2 triggered by a massive magmatic episode. *Nature Letters* **454**, 323-326.

Tsikos H., Jenkyns H.C., Walsworth-Bell B., Petrizzo M.R., Forster A., Kolonic S., Erba E., Premoli Silva I., Baas M., Wagner T. and Sinninghe Damste H.S. (2004) Carbon-isotope stratigraphy recorded by the Cenomanian-Turonian Oceanic Anoxic Event: Correlation and implications based on three key localities. *Journal of the Geological Society of America* **161**, 711-719.

Vahrenkamp C.C. (2013) Carbon-isotope signatures of Albian to Cenomanian (Cretaceous) shelf carbonates of the Natih Formation, Sultanate of Oman. *GeoArabia* **18**, 65-82.

Voigt S., Erbacher J., Mutterlose J., Weiss W., Westerhold T., Wiese F., Wilmsen M. and Wonik T. (2008) The Cenomanian-Turonian of the Wunstorf section (North Germany): Global stratigraphic reference section and new orbital time scale for Oceanic Anoxic Event 2. *Newsletters on Stratigraphy* **43**, 65-89.

Volkening J., Walczyk T. and Heumann K.G. (1991) Osmium isotope ratio determinations by negative thermal ionization mass spectrometry. *International Journal of Mass Spectrometry and Ion Processes* **105**, 147-159.

Wang X. and Chai Z. (1989) Terminal Ordovician mass extinction and discovery of iridium anomaly – An example from the Ordovician-Silurian boundary section, eastern Yangtze Gorges area, China. *Progress of Geosciences of China 1985-1988, Vol. III*, Geological Publishing House, 11-16.

Wood S.A. (1990) The interaction of dissolved platinum with fulvic acid and simple organic acid analogues in aqueous solutions. *Canadian Mineralogy* **28**, 665-673.

Wood S.A. (1991) Experimental determination of the hydrolysis constants of Pt^{2+} and Pd^{2+} at 25^{o}C from the solubility of Pt and Pd in aqueous hydroxide solutions. *Geochimica et Cosmochimica Acta* **55**, 1759-1767.

Yamashita Y., Takahashi Y., Haba H., Enomoto S. and Shimizu H. (2007) Comparison of reductive accumulation of Re and Os in seawater-sediment systems. *Geochimica et Cosmochimica Acta* **71**, 3458-3475.

Yang W., Muzzullo S.J. and Teal C.S. (2004) Sediments, facies tracts, and variations in sedimentation rates of Holocene platform carbonate sediments and associated deposits, Northern Belize-Implications for "representative" sedimentation rates. *Journal of Sedimentary Research* **74**, 498-512.

Yurewicz D.A., Marler T.B., Meyerholtz K.A. and Siroky F.X. (1993) Early Cretaceous carbonate platform, north rim of the Gulf of Mexico, Mississippi and Louisiana. In: Simo A., Scott R.W. and Masse J.P. (Eds.), *Cretaceous Carbonate Platforms*, AAPG Memoir **56**, 81-96.

CHAPTER 4:

RHENIUM AND OSMIUM ISOTOPES IN ORGANIC CONSTITUENTS, PYRITE, AND BULK-ROCKS FROM THE EAGLE FORD SHALE: CONSTRUCTING AN INTERNAL ISOCHRON

4.1. INTRODUCTION

Temporal changes in local and global sea-water geochemistry have been preserved in the rock record and are traditionally recovered using predominantly O, C, and Sr isotopes. Because of recent advances in analytical geochemistry, the ^{187}Re-^{187}Os isotopic system ($t_{1/2}$ = 41.6 by; Smoliar et al., 1996) has also become a useful geochronometer and isotopic tracer that has begun to be applied to understanding the evolution of sea-water during different time intervals. The Os isotopic composition of organic-rich mud rocks (ORM) reflects the $^{187}Os/^{188}Os$ composition of sea-water at the time their respective sediments were deposited. Rhenium and Os are redox-sensitive and organophilic in nature, and are suggested to be sequestered by organisms at, or below the sediment-water interface in marine and lacustrine basins under suboxic, anoxic or euxinic conditions and are thus hydrogenous in nature (Koide, 1991; Colodner et al., 1993; Crusius et al., 1996; Morford et al., 2009; Cumming et al., 2012). Studies of sea-water evolution using $^{87}Sr/^{86}Sr$ ratios have described Sr isotope variation throughout the Phanerozoic (Veizer and Compston, 1974; Burke et al., 1982; Denison et al., 1994; Denison et al., 1997; Veizer et al., 1999; Ebneth et al., 2001). However, the long residence time of Sr of 1-4 Myr means that Sr isotopes are averaged out, or muted and on these timescale. Hence Sr isotopes potentially miss influences on sea-water chemistry on shorter timescales. The residence time of Os in sea-water is a ~10,000 – 50,000 yrs. (Peucker-Ehrenbrink and Ravizza, 2000). Because of this, high frequency, Os isotopic changes on the order of tens to hundreds of thousands of years in sea-water chemistry (such as orbitally forced, glacial-interglacial cycles) are potentially resolvable with Os isotopes. The $^{187}Os/^{188}Os$

ratio of sea-water is derived from a balance of two primary inputs: (1) Radiogenic Os from river water during weathering and subsequent continental runoff of upper continental crust (Esser and Turekian, 1993; Peucker-Ehrenbrink and Jahn, 2001), and (2) non-radiogenic Os from the mantle via seafloor spreading and production of mid-ocean ridge basalts, flood basalt events, hydrothermal alteration of oceanic crust, or from meteorite influx (Peucker-Ehrenbrink and Ravizza, 2000; Schmitz et al., 2004). The relative contributions of these sources have varied significantly throughout geologic history leading to significant variations in the $^{187}Os/^{188}Os$ of coeval sea-water. From the $(^{187}Os/^{188}Os)_i$ of ORM at any given time of formation, a mass balance calculation can be used to determine the relative contribution of radiogenic and non-radiogenic Os to sea-water. Inferences can then be made about the degree of continental weathering (Ravizza et al., 2001; Schmitz et al., 2004), seafloor spreading rates, the eruption of flood basalts (Cohen et al., 1999; Ravizza and Peucker-Ehrenbrink, 2003; Turgeon and Creaser, 2008) as well as the timing and size of meteorite impacts (Paquay et al., 2008).

Hydrogenous ^{187}Re that is sequestered from sea-water decays to ^{187}Os with a half-life of 41.6 Ga making the Re-Os system a novel geochronometer for ORMs. The application of the Re-Os geochronometer to marine petroleum systems has allowed for the precise (<0.5% 2σ) and accurate determination of source rock depositional ages (Ravizza and Turekian, 1989; Cohen et al., 1999; Creaser et al., 2002; Hannah et al., 2004; Selby et al., 2005; Kendall et al., 2009; Finlay et al., 2010; Rooney et al., 2010). This has been especially useful for timescale calibration of sedimentary horizons that lack more established chronostratigraphic markers (Rooney et al., 2012). In addition, many basins

with active petroleum systems lack bentonites that are typically used for zircon ages to create basin models in order to recreate the depositional histories and constrain timing of petroleum generation.

Recently, the use of the Re-Os isotopic system has been expanded to other portions of the petroleum system including the timing of petroleum generation (Selby et al., 2005; Selby and Creaser, 2005; Finlay et al., 2011). These studies yielded ages that are in agreement with basin models for the timing of hydrocarbon generation and are suggested to constrain petroleum-generation events. Furthermore, Os isotopes have been successfully used in the fingerprinting of oils for source rock identification (Finlay et al., 2012).

Despite the promising success of the Re-Os isotopic system, the present understanding of the behavior or Re and Os in the water column and their complexation with various organic and inorganic phases is incomplete. Rhenium and Os are redox-sensitive and organophile and are suggested to be sequestered by organism at, or below the sediment-water interface under reducing conditions (Koide, 1991; Colodner et al., 1993; Crusius et al., 1996; Morford et al., 2009; Cumming et al., 2012). It has been proposed that Re and Os are bound within heteroatomic ligands and other metallo-organic complexes, similar to other trace metals in ORMs, although, a naturally occurring organic complex containing Re or Os has not been identified (Selby et al., 2007). The main assumptions associated with the use of the Re-Os isotopic system in the marine environment is that both Re and Os are hydrogenous in origin and are rapidly immobilized following deposition, thus determined Re-Os dates via bulk-rock isochrons reflect the age of sediment deposition. However, a thorough understanding of the partitioning systematics

of Re and Os between the water column and host phases within ORMs doesn't exist. In addition, the transfer behavior of Re and Os between the domiant ORM phases such as kerogen, bitumen, pyrite, and oil, during burial and hydrocarbon generation is limited.

To improve our understanding of the host phases of Re and Os in addition to the transfer behavior of these elements between the phases of ORMs, this study examines the Re and Os abundances and Os isotopic composition in bulk-rock, kerogen (insoluble organic matter), bitumen (soluble organic matter), and pyrite, from a natural petroleum system source rock, the Cenomanian-Turonian Eagle Ford shale. In addition a generated crude oil from the Eagle Ford is measured for its Re-Os systematics. The abundances and isotopic compositions of the various fractions, all isolated from the same bulk-rock sample will enhance our understanding of the residence of Re and Os within ORMs and provide clues toward the transfer behavior of these elements during sediment burial and hydrocarbon generation.

4.2. GEOLOGIC SETTING

During the Early Mesozoic, extensional rifting and sea-floor spreading associated with the opening of the Gulf of Mexico led to the development of predominant structural and geologic features of south Texas (Pindell et al., 1988; Salvador, 1991; Montgomery et al., 2002). Following rift-related tectonism, regional subsidence caused by cooling of the basement rocks in the Early Cretaceous increased accommodation and promoted carbonate deposition along low-relief coastal areas during cyclic transgressive flooding leading to the development of a shallow-marine carbonate shelf complex (Montgomery et al., 2002; Almon and Cohen, 2008). In response to sea-level transgression and regression,

a series of individual carbonate platforms separated by deeper water facies developed during the Cretaceous Period characterized by a series of stacked, prograding carbonate platform separated by back-stepping, transgressive organic-rich facies (Scott, 1993; Yurewicz et al., 1993). In the northern Gulf Coast region, these platforms were amalgamated into a single platform called the Comanche Shelf (Montgomery et al., 2002). The Pine Island and Bexar Members of the Pearsall Formation, the Del Rio Formation, and the Eagle Ford Formation each represent periods of organic-rich deposition during marine transgression during the Late Aptian, Cenomanian, and Cenomanian-Turonian, respectively (Scott, 1993; Fritz et al., 2000; Harbor, 2011). The thickest of these transgressive deposits is the Cenomanian-Turonian Eagle Ford shale.

The Eagle Ford shale of south Texas is a mixed siliciclastic and carbonate unconventional resource play deposited in the southern gateway of the Cretaceous Western Interior Seaway near the margin of the Gulf of Mexico and represents one of the largest active unconventional reservoirs in the world (Donovan and Staerker, 2010; Hentz and Ruppel, 2010) (Figure 4.1). It is regionally extensive and extends 640 km from the Rio Grande embayment, near the Texas-Mexico border, to the East Texas Basin (Figure 4.2). Regional well-log correlations indicate that thickness varies from less than 12 m to over 120 m, with thickness and lateral facies distribution of the Eagle Ford Shale controlled by pre-existing carbonate platform buildup and structural features such as the San Marcos Arch (an extension of the Llano Uplift), in addition to intra-shelf basins which formed during syn-depositional subsidence during tectonic activity associated with the Rio Grande Rift (Rose, 1972; Donovan and Staerker, 2010; McGarity, 2013).

Uplift coupled with eustatic regression produced exposure of the shelf edge and the underlying Buda Limestone throughout much of south Texas creating one of the major unconformities in the Gulf of Mexico Mesozoic record (Galloway, 2008; Denne et al., 2014). This unconformity represents a shift from broad, reef-rimmed carbonate platforms to a ramp profile with alluvial, deltaic, and coastal depositional systems (Galloway, 2008; Phelps et al., 2015).

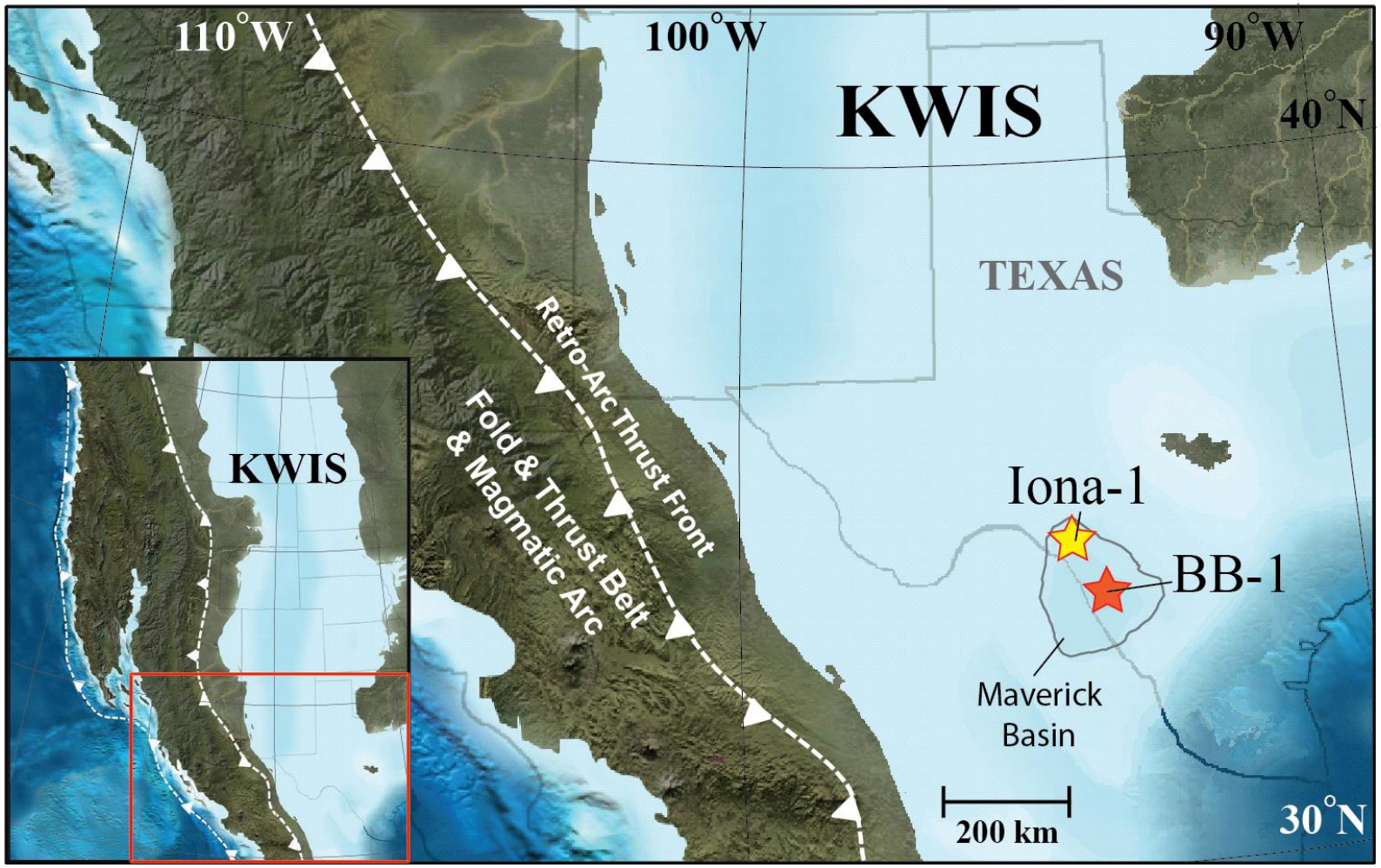

Figure 4.1: Paleogeography of western North America during the Late Cenomanian. Yellow and orange stars indicate the location of the cores used in this study. KWIS: Cretaceous Western Interior Seaway. Figure modified after Eldrett et al. (2014) after Ron Blakey and Colorado Plateau Geosystems, Inc.

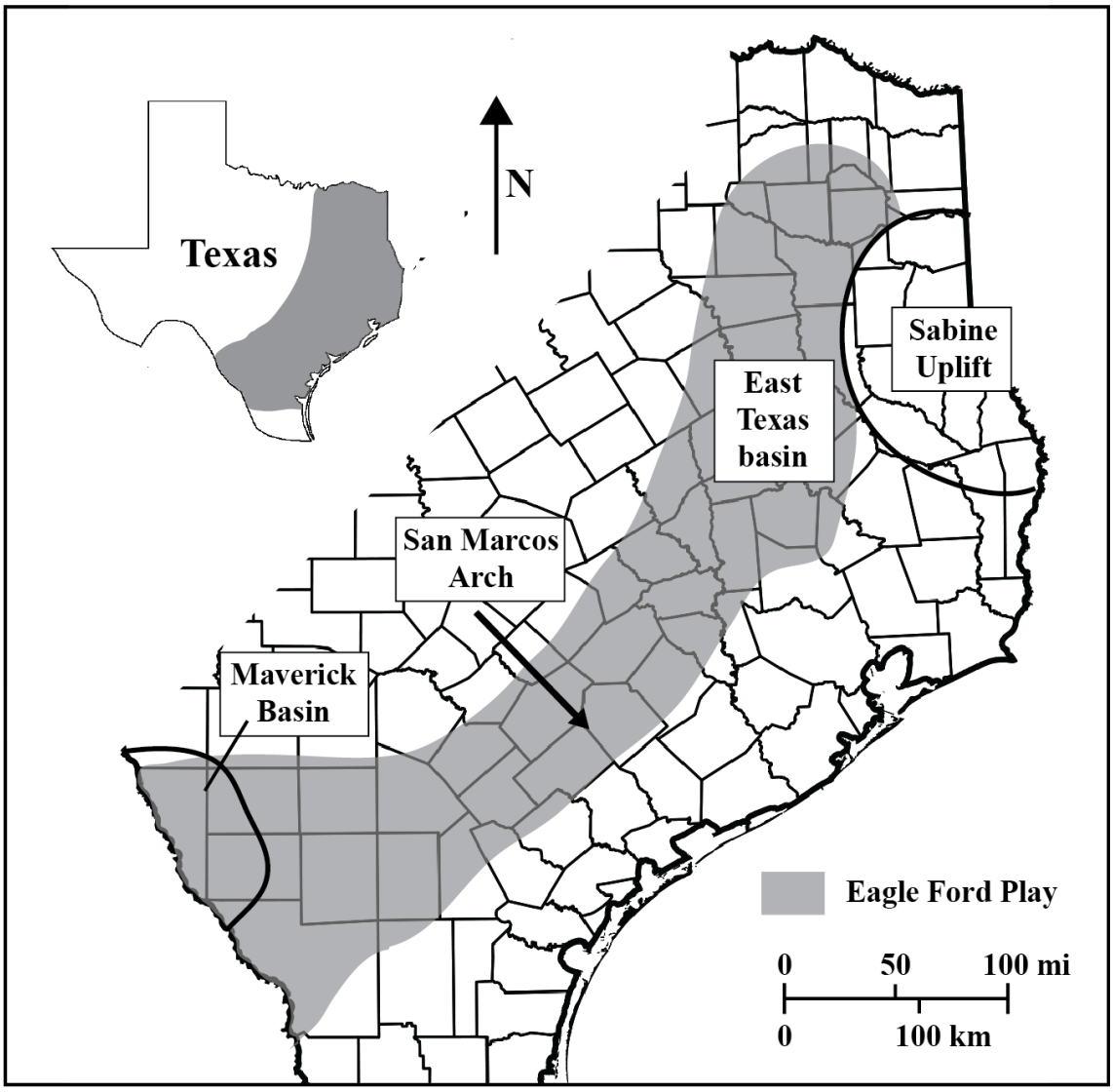

Figure 4.2: Regional extent of the Eagle Ford Group.

Following this regression, a major eustatic transgression and back-stepping of the Comanche Shelf shifted sedimentation from the shelf margin toward intrashelf depocenters and led to the deposition of the Eagle Ford shale (Galloway, 2008; Phelps et al., 2015). The initial sedimentation of the Cenomanian lower Eagle Ford are organic-rich marls containing abundant planktonic foraminfera and calcareous nanofossils with interbedded limestone and abundant thin bentonites (Denne et al., 2014; Lowery et al., 2014; Corbett et al., 2014; Eldrett et al., 2015a). The upper Eagle Ford is retrogradational in nature and is interpreted as a transgressive unit (Donovan and Staerker, 2010). The Cenomanian-Turonian upper Eagle Ford is characterized by reduced amounts of organic matter and bentonites, and an increase in carbonate content and is interpreted as a regressive member deposited during sea-level highstand (Donovan and Staerker, 2010; Hentz and Ruppel, 2010).

The Eagle Ford is thickest in the Maverick Basin and thins toward the San Marcos Arch (Donovan and Staerker, 2010; Hentz and Ruppel, 2010). The Maverick Basin is an intrashelf depocenter that developed on the southeast flank of the Comanche Shelf. It originated from underlying basement structures and half-grabens that developed during the failed Rio Grande rift (Rose, 1972; Donovan and Staerker, 2010). Thermal subsidence led to prolonged development of accommodation and therefore increased sedimentation within the Maverick Basin (Harbor, 2011). Accommodation was further influenced by the development of regional and local fault zones which affected patterns of sedimentation. Samples used in this study are taken from two cores from the Maverick Basin, one proximal and one distal.

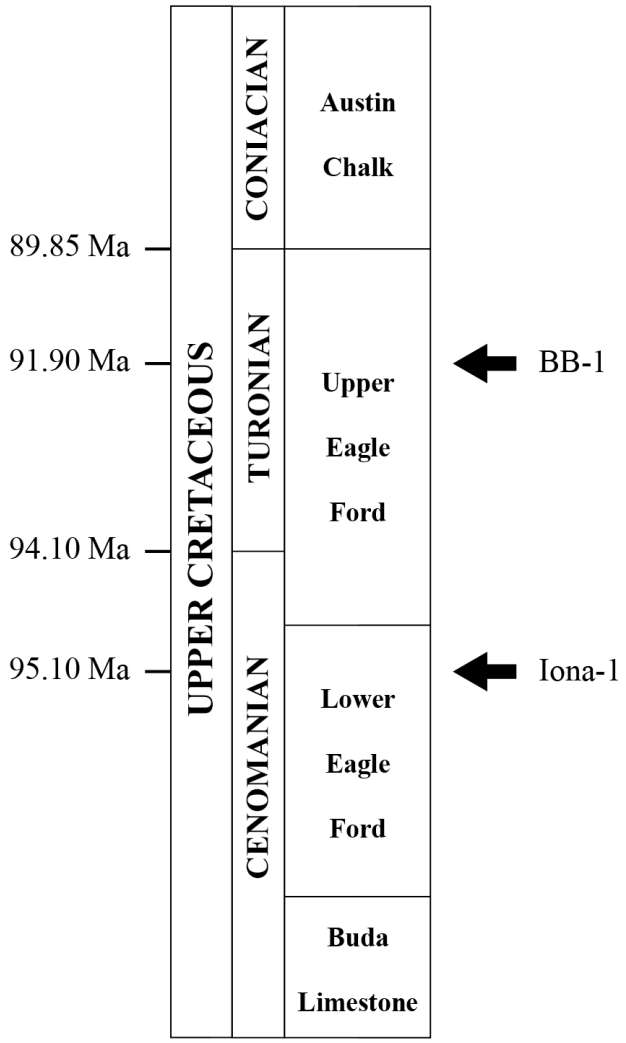

Figure 4.3. Simplified stratigraphic column of the Eagle Ford Group showing the relative location and ages for samples used in this study. Reference ages are from Eldrett et al. (2015b).

4.3. SAMPLING AND ANALYTICAL PROCEDURES

4.3.1. Sampling

Samples used in this study were taken from two research cores, Iona-1 and BB-1, drilled in the Maverick Basin, west Texas, by Shell International Exploration and Production (Figures 4.1 & 4.2). The Iona-1 core contains a complete record of the Eagle Ford Formation, spanning the Early Cenomanian to Turonian, and contains organic-rich marls, limestones, and bentonites deposited on the north edge of the Maverick Basin, a distal sediment-starved intrashelf basin, in water depths of ~50 – 200 m (Eldrett et al., 2014). Samples were taken from organic-rich marls of the Cenomanian lower Eagle Ford at 25 cm intervals across a 1 m section of core 2 m below the upper Eagle Ford / lower Eagle Ford contact (Figure 4.3). Work by Eldrett et al. (2015a) provides a robust chronostratigraphic framework for this core allowing accurate age comparison. Ages for each sample are shown in Table 4.1. The BB-1 core was drilled SE of the Iona-1 well in a more distal setting within the Maverick Basin (Figures 4.1 & 4.2) and contains portions of the Turonian upper Eagle Ford shale. Samples were taken from organic-rich marls of the Turonian upper Eagle Ford shale at 10 cm intervals across a 1 m section of core (Figure 4.3). Lateral correlation between the two cores has not been performed, therefore exact timing of deposition is unclear. The entire outer surface of the core plugs were sanded with silicon carbide to remove any drill markings and possible metal contamination that could have been obtained during coring, cleaned with ethanol, and left to air dry. ~5 – 50 g aliquots of each plug were taken for bulk-rock analysis and organic fraction isolation, broken into chips and powdered using a mortar and pestle. While the

actual amount of powder used for each analysis is much less, larger aliquots of powdered sample negate the effects of Re and Os heterogeneity within a sample (Kendall et al., 2009).

4.3.2. Organic Characterization (TOC and Pyrolysis)

Total organic carbon (TOC) content was determined by the dry combustion of an aliquot of the powdered sample using a Leco CS244 carbon analyzer at the Center for Petroleum Geochemistry at the University of Houston using methods pioneered by Jarvie (1991). In brief, samples were pretreated with 2% HCl acid in order to remove any carbonate associated carbon, then dried in an oven at 60°C. The demineralized sample was then placed in a crucible and heated to 1,350°C in an oxygen atmosphere. Carbon is oxidized to form CO_2 which is then carried by the gaseous oxygen flow through scrubbers in order to remove chlorine gas and any residual moisture. The CO_2 is then measured by an infrared detector and corrected to weight percent carbon (TOC %).

Organic matter type and maturity was determined via Rock-Eval pyrolysis at the Center for Petroleum Geochemistry at the University of Houston. The Rock-Eval pyrolysis method involves step-heating of a sample in an inert atmosphere (Peters, 1986; Hunt, 1996). Samples are heated to 300°C for 3 minutes in order to volatilize free hydrocarbons (bitumen) within the sample. Free hydrocarbons are hydrocarbons that have already, naturally, been generated in the sample and are reported in mg of hydrocarbons per gram of rock (mg/g) and are termed S_1. The temperature is then increased slowly from 300°C to 550°C in order to artificially thermally crack and volatilize the heavy carbon compounds (kerogen) and are termed S_2. The temperature of maximum hydrocarbon

formation after free hydrocarbons are removed is termed T_{max} and is dependent upon the thermal maturity and organic matter type present in the sample. CO_2 that is created during the thermal cracking of the heavy carbon compounds is measured and reported as S_3 and is an indication of the amount of oxygen in the kerogen which is also dependent upon organic matter type.

Sample	Depth (m)	Age (Ma)[1]	TOC %	S1	S2	S3	T_{max}	HI	OI
Core: Iona-1									
EF-100a	114.25	95.06	4.08	0.99	24.14	0.74	423	592	18
EF-100b	114.25	95.06	4.16	1.03	25.58	0.98	420	615	24
EF-100c	114.25	95.06	4.21	0.82	23.98	1.37	425	570	33
EF-100d	114.25	95.06	3.94	0.76	23.24	0.99	421	590	25
EF-101a	114.50	95.08	4.21	0.65	22.09	0.38	415	525	9
EF-101b	114.50	95.08	4.16	0.50	17.21	0.48	419	414	12
EF-101c	114.50	95.08	4.24	0.54	22.06	0.49	414	520	12
EF-101d	114.50	95.08	4.07	0.50	20.05	0.55	417	493	14
EF-103a	115.00	95.10	3.11	0.89	17.98	1.24	421	578	40
EF-108a	115.00	95.10	2.64	0.46	13.30	0.62	418	504	23
EF-108b	114.75	95.09	3.06	0.45	16.51	1.07	423	540	35
Core: BB-1									
EF-104a	9801.35	91.90	2.79	1.49	0.92	0.53	481	33	19
EF-104c	9801.35	91.90	2.77	1.47	0.76	0.44	479	27	16
EF-104d	9801.35	91.90	2.76	1.52	0.74	0.48	481	27	17
EF-105d	9801.45	91.90	2.75	1.53	0.91	0.47	483	33	17
EF-106d	9801.55	91.90	2.69	1.32	0.79	0.41	480	29	15
EF-106c	9801.55	91.90	2.80	1.48	1.02	0.44	477	36	16
EF-107a	9801.55	91.90	2.84	1.56	1.01	0.40	482	36	14
EF-107c	9801.55	91.90	2.73	1.54	0.85	0.47	482	31	17

Table 4.1. TOC and Rock-Eval data for Eagle Ford samples. TOC = Total organic carbon and is given in weight percent. S1, S2 are in mg of hydrocarbons per gram of TOC (mgHC/gTOC), S3 is in mg CO_2 per gram of TOC ($mgCO_2$/gTOC), T_{max} is in °C, Oxygen Index (OI) = S3/TOC, Hydrogen Index (HI) = S2/TOC.

4.3.3. Bitumen Extraction

Bitumen, the organic solvent soluble organic matter, was extracted from Eagle Ford samples using a soxhlet extractor. A ~ 20 – 40 g aliquot of bulk-rock powder was loaded into a cellulose extraction thimble and placed into the Soxhlet apparatus. A rounded flask, half filled with dichloromethane (CH_2Cl_2, DCM) was placed beneath the sample and heated to reflux. The solvent vapor travels up a distillation arm and above the sample into a reflux condenser. The solvent vapors then cool, condense, and drip back down into the chamber housing the sample in the cellulose thimble. The bitumen dissolves in the solvent and empties through a siphon back into the rounded flask containing the DCM beneath. This process is repeated until the solvent that empties through the siphon is clear (~2 days) indicating complete extraction of the bitumen. The refluxed solvent containing the bitumen was filtered through a 0.45μm polytetrafluroethylene (PTFE) filter and subsequently dried down by rotary vacuum evaporation at 34^{o}C at 55rpm. The insoluble residue following bitumen extraction is termed the extracted rock and contains insoluble organic (kerogen) and inorganic mineral matter. Bitumen extraction was performed at Weatherford Laboratories in Houston, Texas.

4.3.4. Kerogen Isolation

Kerogen, the organic solvent insoluble organic matter, was isolated from Eagle Ford samples through a demineralization procedure using non-oxidizing acids which dissolve the rock matrix without modifying the chemical properties of the kerogen. The method involves progressive soaks of the extracted rock (bulk-rock – bitumen) in HCl to dissolve carbonates, sulfates, oxides, hydroxides and some sulfides, and HF for the dissolution of

silicates (Dancy and Giedroys, 1950; Forsman and Hunt, 1958; Smith, 1961; Durand and Nicaise, 1980; Ibrahimov and Bissada, 2010). Between reactions, the acids are decanted and the samples are rinsed with ultra-pure water. After demineralization, the kerogen is rinsed to neutrality and dried at 100^{o}C. Once dry, the kerogen concentrate is homogenized. The residue of HCl – HF acidiziation consists of a relatively pure kerogen concentrate. Kerogen isolation was performed at Weatherford Laboratories in Houston, Texas.

4.3.5. Pyrite Isolation from Kerogen

While the open beaker demineralization procedure for kerogen isolation produces a relatively pure kerogen isolate, pyrite, some heavy mineral oxides such a rutile and anatase, silicates such as zircon, and Ca and Mg neofluorides such as ralstonite are commonly present (Robinson, 1969; Hitchon et al., 1976; Durand and Nicaise, 1980; Ibrahimov and Bissada, 2010). For the purpose of this study, it was necessary to further refine the kerogen isolate through heavy liquid separation for the isolation of undissolved pyrite, as pyrite commonly contains abundant Re and Os. Heavy liquid separation was performed on isolated kerogen using $ZnBr_2$ (density: 4.20 g/cc) at National Petrographic in Houston, Texas. During heavy liquid separation, those minerals with densities higher than 4.20 g/cc (pyrite: 5.01 g/cc; pyrrhotite: 4.61 g/cc; rutile: 4.23 g/cc; zircon: 4.6 g/cc) will sink, while those with densities less than 4.20 g/cc will remain in the float (anatase: 3.79 – 3.97 g/cc; ralstonite: 2.55 g/cc; and likely other neofluorides). Pyrite was then manually picked from the kerogen sink using a binocular microscope, thoroughly washed, and dried at 60^{o}C.

4.3.6. Asphaltene Isolation from Oil

The heavy fraction of crude oil (asphaltenes) contains large molecular compounds that are insoluble in n-heptane (Speight, 1998). Trace element abundances in oil, particularly Ni, V, and Mo are often present in ppm levels (Curiale, 1987; Manning and Gize, 1993). The asphaltene component of oil is the major host for these metals (Manning and Gize, 1993; Selby et al., 2007). For asphaltene separation, ~2 g of oil was accurately weighed into a 120 mL glass vial along with ~80 mL of n-heptane (1:40 ratio) and sealed with PTFE lined cap. The contents were agitated for 10 mins to thoroughly mix the oil and n-heptane. The oil and n-heptane were left to react for 24 hours with agitation occurring every 30 – 60 mins for 5 mins. Following the 24 hour period, the contents of the glass vial were transferred to a centrifuge tube and centrifuged at 3000 rpm for 30 mins in order to separate the n-heptane insoluble fraction (asphlatene) and soluble fractions (maltene). The maltene fraction was then transferred to a separate glass vial while the asphaltene fraction was brought up in ~1 mL of n-heptane and transferred to an accurately weighed PTFE coated watch glass. The watch glass was placed on a hot-plate at 50°C in order to evaporate the n-heptane. The watch glass was then re-weighed and the abundance of the asphaltene fraction was calculated. The ~2 g aliquot of oil contained 18.3 mg (0.9%) of asphaltenes.

4.3.7. Re-Os Geochemistry

For bulk-rock and extracted rocks, approximately 0.3g of powdered sample was accurately weighed and transferred to a thick-walled, internally cleaned, borosilicate glass Carius tube along with a known amount of a mixed ^{185}Re + ^{190}Os spike and 8mL of

a chromic acid solution created by dissolving $Cr^{VI}O_3$ powder into 4N H_2SO_4 (0.25g/mL). The CrO_3-H_2SO_4 method was used to preferentially dissolve and oxidize hydrogenous Re and Os which yields more accurate and precise ages (Selby and Creaser, 2003). The Carius tubes were sealed, and sample and spike were digested and equilibrated at 240°C for 48 hours. Digestion dissolves sample powders and oxidizes sample Re and Os to ReO_3^- and OsO_4^- species, respectively. Following digestion the Carius tubes were frozen in a dry ice – ethanol slurry, opened, then thawed, and Os was isolated from the CrO_3-H_2SO_4 solution using $CHCl_3$ solvent extraction at room temperature (Cohen and Waters, 1996), back extracted into 9N HBr and further purified via micro-distillation (Birck et al., 1997). Rhenium was removed from the CrO_3-H_2SO_4 solution by anion column chromatography following reduction of the Cr^{VI} to Cr^{III} using Milli-Q and bubbling with SO_2 gas. Rhenium was further purified by passing the output of the first column through a second anion column. The isolated Re and Os were then loaded onto ultra-pure (>99.99%) Ni and Pt filaments, respectively and coated with activator solutions of $Ba(NO_3)_2$ and $Ba(OH)_2$, respectively.

The procedure for the pyrite and organic fractions was similar, however, sample were dissolved in inverse *aqua regia* (1:3 12N HCL: 13N HNO_3) instead of CrO3-H_2SO_4 as these are pure fractions with no need for selective dissolution provided by the chromic acid solution. Sample weights were: ~0.1 g of kerogen, 0.2 – 0.5g of pyrite, 0.01 - 0.1 g of bitumen. Following Os solvent extraction from the *aqua regia* solution, the residue containing Re was taken to dryness at 70°C and brought back up in 3 mL 0.2N HNO3 for the anion exchange column procedure described above.

The Re and Os isotopic compositions were determined by isotope-dilution-negative-thermal-ionization mass spectrometry (ID-NTIMS) on a ThermoElectron TRITON Plus TIMS at the University of Houston (Creaser et al., 1991; Volkening et al., 1991). Re was measured as ReO_4^- via static Faraday collection and Os as OsO_3^- via ion-counting using a secondary electron multiplier in peak-hopping mode.

Measured isotopic ratios were spike stripped, corrected for isobaric oxygen interference, instrumental mass fractionation (using $^{185}Re/^{187}Re=0.59738$ and $^{192}Os/^{188}Os=3.08761$), and procedural blank contributions. Uncertainties were obtained through the error propagation of uncertainties in blank abundance and isotopic composition, spike abundance values, mass spectrometry measurements of Re and Os, and the reproducibility of the Re and Os isotopic values of the standard. Average procedural blanks were 19 ± 10 (2σ, n=16) pg for Re and 0.60 ± 1.1 (2σ, n=18) pg for Os with a $^{187}Os/^{188}Os = 0.16 \pm 0.02$ (2σ, n=18).

Repeat measurements of Re and Os standards were performed throughout the four year analytical campaign. The Re standard, made form zone-refined Re ribbon, yields an average $^{185}Re/^{187}Re$ ratio of 0.59783 ± 0.00022 (2σ, n=16) for 1.5 ng loads using static Faraday collection. The difference between the measured Re standard value and the established standard value of 0.59738 ± 0.0039 (Gramlich et al., 1973) was used to correct the measured $^{185}Re/^{187}Re$ ratios of samples used in this study. The University of Maryland Os standard (Brandon et al., 1999) (Selby and Creaser, 2001; Markey et al., 2007) yields a $^{187}Os/^{188}Os$ ratio of 0.11385 ± 0.00023 (2σ, n=18) for 500 pg loads using a

secondary electron multiplier and is, within uncertainty, identical to that reported by Brandon et al. (1999).

Re-Os ages and $(^{187}Os/^{188}Os)_i$ are obtained via modified York regression (York, 1969) of the reduced isotopic data and propagated 2σ uncertainties using *Isoplot v. 4.15* (Ludwig, 2008). Errors are calculated using the maximum-likelihood estimation algorithm and are reported as 2σ.

4.4. RESULTS

4.4.1. Organic Characterization (TOC and Pyrolysis)

Total organic carbon values, a measure of the organic richness of ORMs, for Eagle Ford samples range from 2.64 to 4.24% with Iona-1 sample possessing higher TOC values (2.64% - 4.24%; 3.81% average) than samples from the BB-1 core (2.69 – 2.84%; 2.77% average) (Table 4.2). All samples have TOC values > 2% making them good source rocks, with respect to organic richness.

Rock-Eval pyrolysis yielded T_{max} values (a measure of thermal maturity using the temperature of maximum generation of hydrocarbons during pyrolysis) of 414 – 425°C for Iona-1 samples indicating these samples are thermally immature and have not been buried to significant depths to generate hydrocarbons (Table 4.2). Samples from BB-1 have T_{max} values of 477 – 493°C indicating thermal over-maturity and significant burial in order to generate hydrocarbons (Table 4.2).

Sample	Depth (m)	Age (Ma)[1]	$\frac{^{187}Re}{^{188}Os}$	±	$\frac{^{187}Os}{^{188}Os}$	±	Re (ppb)	±	Os (ppt)	±
Core: Iona-1										
EF-100a	114.25	95.06	2751.51	13.77	5.26	0.03	150.49	0.52	440.05	2.74
EF-100b	114.25	95.06	2771.33	12.47	5.23	0.02	165.80	0.57	480.05	2.53
EF-100c	114.25	95.06	2780.88	12.90	5.25	0.02	159.42	0.55	460.97	2.50
EF-100d	114.25	95.06	2526.22	16.61	4.81	0.05	155.32	0.54	477.06	4.28
EF-101a	114.50	95.08	2328.75	11.51	4.38	0.02	150.90	0.61	485.52	2.52
EF-101b	114.50	95.08	2835.23	17.67	5.30	0.02	150.98	0.78	429.74	2.56
EF-101c	114.50	95.08	2517.71	13.27	4.73	0.02	151.60	0.66	464.50	2.51
EF-101d	114.50	95.08	2869.84	15.72	5.38	0.03	149.53	0.61	423.19	2.61
EF-103a	115.00	95.10	2429.78	12.38	4.70	0.02	115.34	0.40	365.19	2.08
EF-108a	115.00	95.10	2841.78	17.54	5.27	0.03	97.44	0.35	276.13	1.85
EF-108b	114.75	95.09	2682.81	14.53	5.09	0.02	113.83	0.40	336.90	2.03
Core: BB-1										
EF-104a	9801.35	91.90	579.50	2.31	1.62	0.01	30.25	0.11	300.56	1.02
EF-104c	9801.35	91.90	609.61	4.65	1.68	0.01	30.65	0.11	291.35	1.63
EF-104d	9801.35	91.90	610.31	4.66	1.68	0.01	30.39	0.11	288.57	1.62
EF-105d	9801.45	91.90	614.83	4.51	1.68	0.01	30.99	0.11	292.12	1.60
EF-106d	9801.55	91.90	670.88	2.93	1.77	0.01	35.73	0.13	311.64	1.31
EF-106c	9801.55	91.90	685.88	4.83	1.78	0.01	38.30	0.14	326.91	1.75
EF-107a	9801.55	91.90	613.36	4.54	1.68	0.01	32.82	0.12	309.93	1.71
EF-107c	9801.55	91.90	612.95	4.81	1.68	0.01	30.54	0.11	288.63	1.67

Table 4.2. Re-Os isotopic data for Eagle Ford samples. Uncertainties for Re-Os isotopic data are 2σ.

The type of organic matter that make up the samples is determined through the co-variance of ratios (hydrogen index and oxygen index) that are proxies for the amount of H, C, and O in the kerogen, traditionally represented on the classic van Krevelen atomic H/C versus O/C diagram (Espitalie et al., 1977; Peters, 1986) (Figure 4.4). Hydrogen Index (HI) ([100*S_2]/TOC), a proxy for atomic H/C, is a measure of the amount of hydrogen in the kerogen. Marine organisms and algae are generally composed of lipid- and protein-rich organic matter, which has a higher proportion of hydrogen than the carbohydrate-rich land plant constituents. Oxygen Index (OI) ([100*S_3]/TOC), a proxy for atomic O/C, is a measure of the amount of oxygen in the kerogen. Polysaccharide-rich remains of land plants and inert organic matter are generally much higher in OI than marine sediments. Therefore a thermally immature Type II, marine kerogen will have a higher HI and lower OI than a thermally immature kerogen created from the remains of terrestrial organic matter (Type III). The co-variation of HI and OI is also useful in the estimation of thermal maturity, as samples follow paths on a modified van Krevelen diagram during burial and thermal maturity due to a loss of H and O relative to C during hydrocarbon generation (Figure 4.4). The HI (414 - 615 mgHC/gTOC) and OI (9 - 40 mgCO_2/gTOC) data for Rock-Eval data for the Iona-1 core illustrates that the samples are comprised of Type II kerogen, consistent with previous studies of the Eagle Ford Formation (Hays and Tieh, 1992; Sageman et al., 1998) (Figure 4.4). Eagle Ford samples from BB-1 core possess HI and OI values of 27 – 36 and 14 – 19, respectively and are consistent with a Type II nature of the Iona-1 core (Figure 4.4).

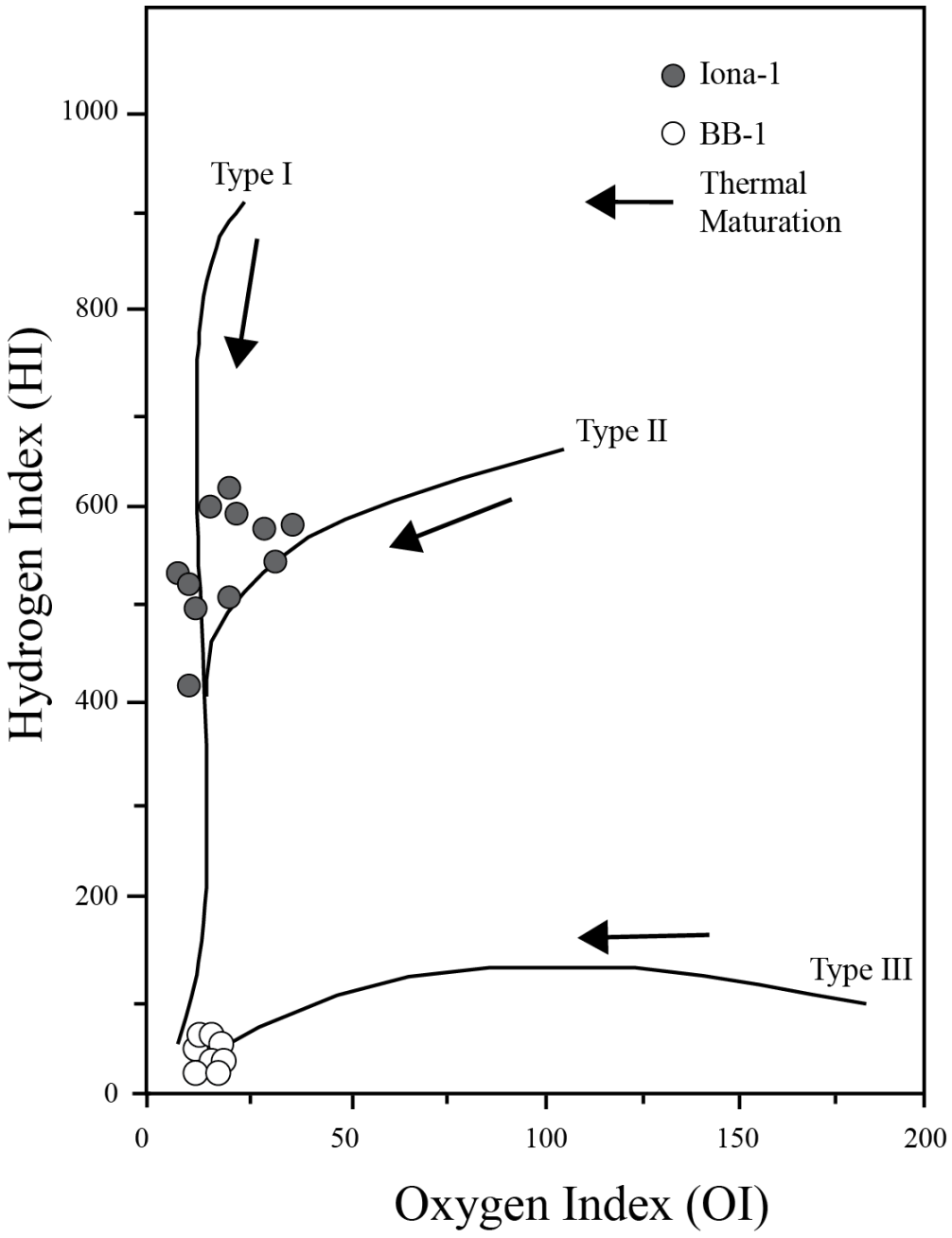

Figure 4.4. Modified Van Krevelen diagram showing the co-variation of Hydrogen Index (S2/TOC) and Oxygen Index (S3/TOC), both indicators of organic matter type. Black arrow indicates increasing thermal maturity for each organic matter type.

The TOC and Rock-Eval data indicates both cores contain Type II organic matter and represent two end-members of thermal maturity. Samples from Iona-1 are thermally immature while samples from BB-1 are thermally over-mature.

4.4.2. Bulk-rock Rhenium and Osmium

Rhenium and Os abundances and isotopic compositions for Eagle Ford samples are presented in Table 4.1. All Iona-1 samples are enriched in Re (97 - 165 ppb) and Os (276 - 485 ppt) compared to modern-day average continental crust (~1ppb Re and 30-50ppt Os; Esser and Turekian, 1993) and have abundances typical of ORMs (Ravizza and Turekian, 1989; Cohen et al., 1999; Creaser et al., 2002; Selby and Creaser, 2003; Hannah et al., 2004; Kendall et al., 2004; Finlay et al., 2010; Rooney et al., 2010). The $^{187}Re/^{188}Os$ ratios range from 2328 to 2869, are markedly higher than most published marine ORMs, and are positively correlated with $^{187}Os/^{188}Os$ ratios of 4.38 to 5.38. Linear regression of all data points from Iona-1 provides an isochron with a Model 3 age of 105 ± 12 Ma (11.4% age uncertainty, 2σ, n=11, mean square of weighted deviates [MSWD] = 9.9). The isochron yields an $(^{187}Os/^{188}Os)_i = 0.37 \pm 0.54$ (Figure 4.5a).

Samples from the BB-1 core are also enriched in Re (30 – 38 ppb) and Os (288 – 326 ppt). The $^{187}Re/^{188}Os$ have a limited range from 579 to 685, and are positively correlated with $^{187}Os/^{188}Os$ ratios of 1.62 to 1.78. Linear regression of all data points from BB-1 provides an isochron with a Model 1 age of 93.6 ± 6.0 Ma (6.4% age uncertainty, 2σ, n=8, MSWD = 1.5). The isochron yields an $(^{187}Os/^{188}Os)_i = 0.71 \pm 0.06$ (Figure 4.5c).

4.4.3. Rhenium and Osmium in Organic and Inorganic Phases

4.4.3.1. Kerogen

Kerogen isolated from a sample from the Iona-1 core (EF-101.2) has abundances of Re and Os of ~1184 ppb and ~4710 ppt, respectively, and is heavily enriched relative to the bulk-rock samples (Table 4.3). The $^{187}Re/^{188}Os$ ratio of 1958 ± 121 is significantly less than its host bulk-rock (~2300 – 2800), even at the upper limit of uncertainty. The measured $^{187}Os/^{188}Os$ of kerogen is 4.85 ± 0.46 is. Within uncertainty, this $^{187}Os/^{188}Os$ is identical to this ratio for the bulk-rock sample (~4.38 – 5.38). A replicate analysis of this kerogen (EF-101.2[2]) yields identical results, within analytical uncertainty.

A second kerogen isolated from the Iona-1 core (EF-108.2), taken from a sample with large amounts of pyrite, is less enriched in Re and Os (~197 ppb and ~904 ppt, respectively) than kerogen from EF-101 (Table 4.3). The Re and Os abundances of this kerogen isolate are also elevated relative to the bulk-rock samples which range from ~97 - 113 ppb and ~276 - 336 ppt, respectively. The $^{187}Re/^{188}Os$ and $^{188}Os/^{188}Os$ ratios from this second kerogen are 1606 ± 108 and 4.19 ± 0.43, respectively. These are significantly smaller than the $^{187}Re/^{188}Os$ and $^{187}Os/^{188}Os$ ratios for the host bulk-rocks of ~2600 - 2800 and ~5.09 – 5.27, respectively. A replicate analysis of this kerogen (EF-108.2[2]) yielded identical results, within analytical uncertainty. Following the heavy liquid removal of inorganic minerals (predominantly pyrite, with some rutile and zircon), the "pyrite-free" kerogen (EF-108.2.1) became even more enriched, with Re and Os abundances of ~1200

Figure 4.5: Bulk-rock isochrons for Eagle Ford samples. (A) All Iona-1 samples, (B) All Iona-1 samples with a forced $(^{187}Os/^{188}Os)_i$ of 0.7, (C) All BB-1 samples. Uncertainty is reported as 2σ.

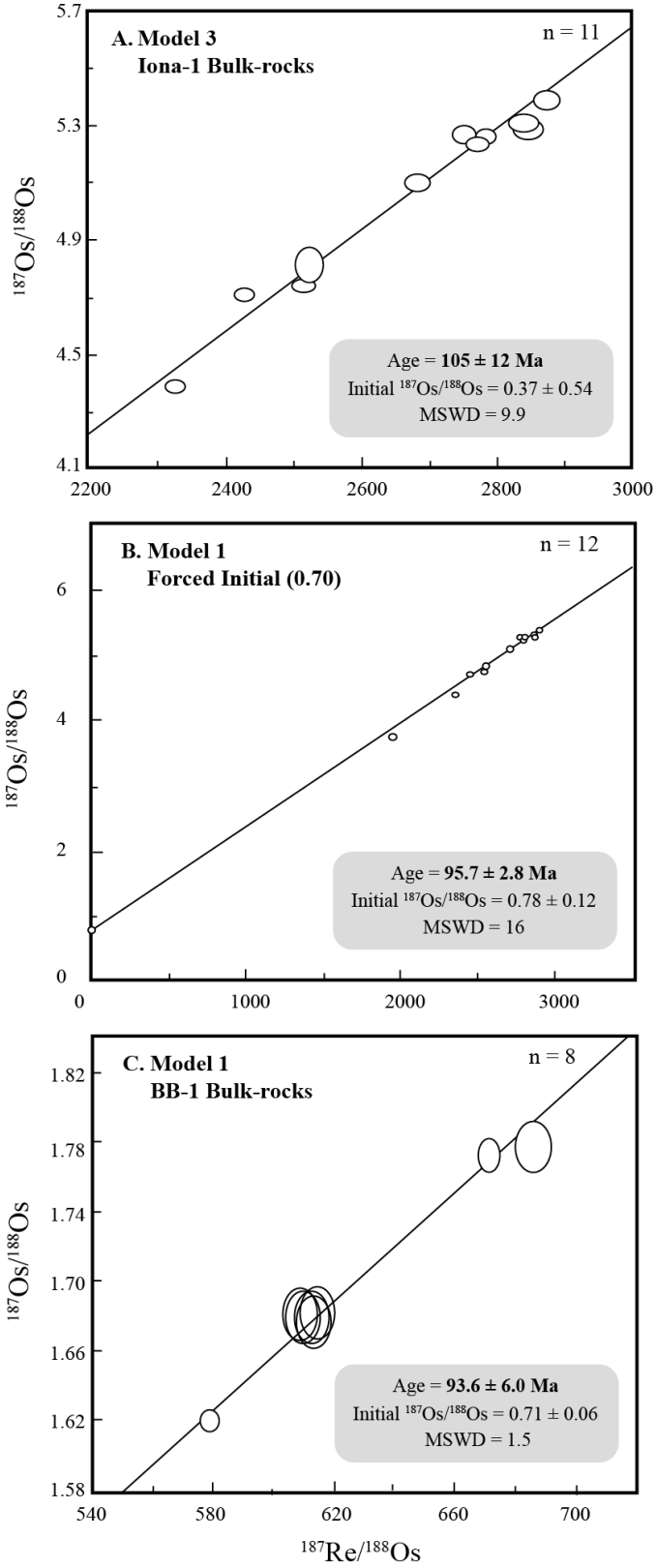
A. Model 3
Iona-1 Bulk-rocks
n = 11
Age = 105 ± 12 Ma
Initial 187Os/188Os = 0.37 ± 0.54
MSWD = 9.9
187Os/188Os
B. Model 1
Forced Initial (0.70)
n = 12
Age = 95.7 ± 2.8 Ma
Initial 187Os/188Os = 0.78 ± 0.12
MSWD = 16
C. Model 1
BB-1 Bulk-rocks
n = 8
Age = 93.6 ± 6.0 Ma
Initial 187Os/188Os = 0.71 ± 0.06
MSWD = 1.5
187Re/188Os

Sample	Description	$\frac{^{187}Re}{^{188}Os}$	±	$\frac{^{187}Os}{^{188}Os}$	±	Re (ppb)	±	Os (ppt)	±
Core: Iona-1									
EF-101.3	Extracted Rock	2635.14	9.79	5.61	0.02	153.35	0.54	481.16	2.23
EF-101.2	Kerogen	1958.97	121.85	4.85	0.46	1184.18	4.13	4710.78	197.49
EF-101.2[2]	Kerogen	2026.67	106.83	4.87	0.41	1141.23	4.53	4394.35	169.55
EF-101.1	Bitumen	5989.48	667.54	5.91	0.66	91.58	0.32	129.31	5.23
EF-108.3	Extracted Rock	2650.62	23.97	5.05	0.04	56.95	0.21	169.98	1.40
EF-108.3[2]	-	2679.28	38.37	5.10	0.07	56.94	0.21	168.85	1.81
EF-108.2	Kerogen	1606.71	108.33	4.19	0.43	197.04	1.29	904.51	39.05
EF-108.2[2]	-	1623.73	82.92	4.24	0.33	209.94	0.77	957.33	33.21
EF-108.2.1	Pyrite-Free Kerogen	2450.14	163.79	4.60	0.45	1200.23	4.15	3738.69	159.28
EF-108.4	Pyrite	691.47	44.84	1.27	0.08	5.03	0.05	40.30	1.13
EF-108.1	Bitumen	2184.25	766.47	3.99	1.40	28.51	0.37	94.63	10.74
Core: BB-1									
EF-107.3	Extracted Rock	662.06	3.02	1.75	0.01	33.80	0.15	298.08	1.04
EF-107.3[2]	-	665.15	5.10	1.77	0.01	33.76	0.12	296.85	1.70
EF-107.2	Kerogen	795.82	26.18	1.78	0.09	340.76	1.37	2508.79	49.83
EF-107.1	Bitumen	406.41	126.75	0.53	0.18	8.57	0.51	106.93	14.01

Table 4.3. Re-Os isotopic data for organic and inorganic fractions from Eagle Ford samples. [2] = Replicate analysis. Uncertainties for Re-Os isotopic data are 2σ.

ppb and ~3738 ppt, respectively, and the $^{187}Re/^{188}Os$ and $^{187}Os/^{188}Os$ ratios increased to 2450 and 4.60, respectively. These are, within uncertainty, similar to those of the host bulk-rocks. Due to a small number of samples, a replicate analysis could not be performed.

Kerogen isolated from one sample of the BB-1 core (EF-107.2) has Re and Os abundances of ~340 ppb and 2508 ppt, respectively. These values are also enriched relative to its host bulk-rock with Re of ~30 – 32 ppb and Os of ~288 – 309 ppt (Table 4.3). In contrast to samples from Iona-1, the $^{187}Re/^{188}Os$ and $^{188}Os/^{188}Os$ ratios of 795 ± 26 and 1.78 ± 0.09 for kerogen isolated from samples of BB-1 are higher than in the host bulk-rock which have $^{187}Re/^{188}Os$ ratios of ~612 and $^{187}Os/^{188}Os$ ratios of of 1.68. A replicate analysis of this kerogen (EF-107.2[2]) yields identical results, within analytical uncertainty.

4.4.3.2. Pyrite

Pyrite removed from bulk kerogen from Iona-1 by heavy liquid separation (EF-108.4) has Re and Os abundances of ~5 ppb and ~40 ppt, respectively, which are markedly lower than those for the bulk kerogen or the bulk-rocks (Table 4.3). The $^{187}Re/^{188}Os$ and $^{187}Os/^{188}Os$ ratios of 694 ± 44 and 1.26 ± 0.08, respectively, are significantly less than in the bulk-rock or any other fractions reported here.

In addition to the pyrite separate, Re and Os isotopes were measured in a ~1 cm thick sulfide layer within the same depth interval as all other samples from the Iona-1 core (EF-108.4). This pyrite layer has Re and Os abundances of ~9 ppb and ~32 ppb

respectively, similar to those of the pyrite isolated from the kerogen (Table 4.3). However, the $^{187}Re/^{188}Os$ and $^{187}Os/^{188}Os$ ratios of this pyrite layer of 2186 ± 21 and 4.19 ± 0.04, respectively. These are much higher than those of the pyrite separate, and more similar to those of the other fractions.

4.4.3.3. Extracted Rock

The extracted rock, which is the insoluble residue after bitumen extraction, contains insoluble organic matter (kerogen) and inorganic minerals. The extracted rock from a thermally immature sample from the Iona-1 core (EF-101.3) has Re and Os abundances of ~153 ppb and ~481 ppt, respectively. These are similar to the bulk-rock with Re and Os abundances of ~149 - 151 ppb and ~423 - 485 ppt, respectively (Table 4.3). The $^{187}Re/^{188}Os$ ratio of 2635 ± 9 is indistinguishable from the $^{187}Re/^{188}Os$ of the bulk-rocks with values of 2328 – 2869. However, the measured $^{187}Os/^{188}Os$ ratio of 5.61 ± 0.02 of the extracted rock is slightly higher than those of the bulk-rocks with values of 4.38 – 5.38.

Extracted rock from the pyrite-rich sample from Iona-1 (EF-108.3) contains Re and Os abundances of ~56 ppb and ~169 ppt, respectively. These are significantly lower than the bulk-rock samples with Re and Os abudnacnes of ~97 – 113 ppb and 276 – 336 ppt, respectively (Table 4.3). The $^{187}Re/^{188}Os$ and $^{187}Os/^{188}Os$ ratios of the extracted rock are 2650 ± 23 and 5.05 ± 0.04, respectively. These are indistinguishable from the bulk-rocks with $^{187}Re/^{188}Os$ and $^{187}Os/^{188}Os$ ratios of ~2682 – 2841 and 5.09 – 5.27, respectively. A

replicate analysis of this extracted rock (EF-108.3[2]) yields identical results, within analytical uncertainty.

Extracted rock from the thermally mature sample from the BB-1 core (EF-107.3) has Re and Os abundances of ~33 ppb and ~298 ppt, respectively, and are indistinguishable from the abundances in the bulk-rock (~30 – 33 ppb and 288 – 309 ppt Os) (Table 4.3). The $^{187}Re/^{188}Os$ and $^{187}Os/^{188}Os$ ratios of the extracted rock of 662 ± 3 and 1.75 ± 0.01, respectively, are higher than these ratios in the bulk-rock samples (612 – 613 and 1.68, respectively). A replicate analysis of this extracted rock (EF-107.3[2]) yields identical results, within analytical uncertainty.

4.4.3.4. Bitumen

Bitumen extracted from a sample from the Iona-1 core (EF-101.1) has Re and Os abundances of ~91 ppb and 129 ppt, respectively, which are moderately lower than in the bulk-rock samples (Table 4.3). The $^{187}Re/^{188}Os$ ratio of 5989 ± 667 is considerably higher than in the bulk-rock samples which have values of 2328 – 2869. However, the $^{187}Os/^{188}Os$ of 5.91 ± 0.6 is, within uncertainty, similar to that of the bulk-rocks that have values of 4.38 – 5.38. Similar abundances were reported for bitumen extracts from the Staffin Formation, Scotland (Rooney et al., 2012) and from lacustrine source rocks of the Green River Formation (Cumming, 2013).

Bitumen extracted from the pyrited sample from Iona-1 (EF-108.1) has Re and Os abundances of 28 ppb and 94 ppt respectively, and are similar to those of the other Iona-1

sample (Table 4.3). The $^{187}Re/^{188}Os$ and $^{187}Os/^{188}Os$ ratios of 2184 ± 766 and 3.99 ± 1.40 are indistinguishable from the bulk-rock values, within uncertainty.

The bitumen extracted from the thermally mature BB-1 core sample has Re and Os abundances of 8 ppb and 106 ppt, respectively, much lower than the bulk-rocks (30 – 32 ppb and 288 – 309 ppt, respectively) (Table 4.3). The $^{187}Re/^{188}Os$ and $^{187}Os/^{188}Os$ ratios of 406 ± 126 and 0.53 ± 0.18 are much less than these ratios in the bulk-rock (~612 and 1.68, respectively).

All bitumen data reported here have large uncertainties. Due to the requirement of using a small sample size in order to prevent failure of glass Carius tubes, a procedural blank correction of 19.27 pg for Re and 0.60 pg for Os introduced the large uncertainties. In addition, bitumen typically makes up ~10% of the organic matter in these Eagle Ford samples. With TOC values of ~2 – 4%, the sample size of ~60 g often didn't yield enough bitumen in order to provide precise analyses. Typical bitumen yields range from 6 – 83 mg. Other studies perform bitumen analysis on ~0.1 g aliquots of bitumen extracted from source rocks with a much higher proportion of bitumen than the ~10% reported here, which resulted in more precise data (Rooney et al., 2012; Cumming, 2013).

4.4.3.5. Oil and Asphaltenes

Light crude oil produced from the Eagle Ford shale has Re and Os abundances of -60 ± -53 ppt and 7 ± 2 ppt, respectively (Table 4.3). For Re-Os analysis, ~0.1 g of oil was loaded into the Carius tube. With such low abundances of Re and Os, these values are less than the procedural blank values of 19.27 pg for Re and 0.60 pg for Os, leading to a

large blank correction. The $^{187}Re/^{188}Os$ and $^{187}Os/^{188}Os$ are -40 ± -41 and 0.19 ± 0.15, respectively, with the large uncertainty caused by the large blank correction. Similar low abundances were reported by Selby et al. (2007) for light oils with asphaltene content of <1% from the Pembina Field, Alberta, Canada.

The Eagle Ford oil sample used in this study has an asphlatene content of ~0.4%. Rhenium and Os abundances in the asphaltene fraction are -467 ± -410 ppt and 49 ± 12 ppt, respectively. The $^{187}Re/^{188}Os$ and $^{187}Os/^{188}Os$ ratios are -45 ± -47 and 0.21 ± 0.16, respectively and, within uncertainty are identical to these ratios in the bulk oil. As with the bulk oil sample, the low abundances coupled with small sample size caused a large blank correction causing negative abundances and large analytical uncertainties, similar to those reported for other oils with low asphaltene content (Selby et al., 2007).

4.5. DISCUSSION

4.5.1. Re-Os Systematics in Bulk-rocks

Bulk-rock samples from the Iona-1 core have Re and Os abundances of 97-165 ppb and 276-485 ppt, respectively. These values are typical for ORM (Ravizza and Turekian, 1989; Cohen et al., 1999; Creaser et al., 2002; Selby and Creaser, 2003; Hannah et al., 2004; Kendall et al., 2004; Finlay et al., 2010; Rooney et al., 2010). To test lateral variability in Re and Os, at least on the scale of a core plug, a slice of the plug was taken in order to bracket ~1 cm of stratigraphy. This core slice was then divided into separate samples and processed independently. For example, sample EF-100 from the Iona-1 core was divided into three samples (EF-100a-c; Table 4.2), each from the ~1 cm same

stratigraphic interval. The $^{187}Re/^{188}Os$ and $^{187}Os/^{188}Os$ values for these separate aliquots are identical, within uncertainty. Rhenium and Os abundances of ~150 – 165 ppb and 440 – 480 ppt, respectively, are minimally variable. These abundances show no directional trends across the core (Table 4.2). Different aliquots sampled from EF-101 in the same manner have the same relationship indicating minimal variability in the submarine conditions on this scale.

Bulk-rock samples from Iona-1 that contains abundant pyrite (EF-108) have Re and Os abundances of 97 – 113 ppb and 276 – 336 ppt, respectively. These abundances are less enriched than those from the Iona-1 samples with significantly less pyrite. The $^{187}Re/^{188}Os$ and $^{187}Os/^{188}Os$ ratios of the pyrited samples range from 2682 – 2841 and 5.09 – 5.27, respectively. These values are similar to those of the bulk-rocks, however, with much more internal variability. This variability is likely due to the nugget effect, where each sample has varying amounts of pyrite which could strongly change the abundances of Re and Os in the bulk-rocks.

Bulk-rock samples from BB-1 have a much tighter range in Re and Os abundances of 30 – 38 ppb and 288 – 326 ppt, respectively. These samples also have much smaller internal variability between multiple aliquots of the same stratigraphic interval (e.g., EF-107a,c; EF-104a,c, etc.) which supports the lack of variability in submarine condition on this scale.

4.5.2. Re-Os Geochronology of Bulk-rocks

Detailed chronostratigraphic work conducted by Eldrett et al. (2015) provides an astronomically tuned age model for the Iona-1 core. Integrated age models anchored by biostratigraphy and U/Pb ages of zircons within interbedded bentonites provide high resolution geochronology for this section. Based on this model, the Iona-1 samples used in this study were deposited 95.06 – 95.14 Ma (Table 4.1) (Eldrett et al., 2015b).

Regression of all data points from the Cenomanian Lower Eagle Ford shale from the Iona-1 core yields a Model 3 age of 105 ± 12 Ma (11.4% age uncertainty, 2σ, n=11, mean square of weighted deviates [MSWD]=9.9) and an $(^{187}Os/^{188}Os)_i = 0.37 \pm 0.54$ (Figure 4.5a). Within uncertainty, this age agrees with the expected age for this formation, but with large uncertainties on both the age and $(^{187}Os/^{188}Os)_i$.

In order to obtain precise and accurate isochron ages, three conditions must be met: (1) The initial sea-water conditions $(^{187}Os/^{188}Os)_i$ for all samples must have been the same, (2) There must be no post-depositional mobilization of Re or Os, and (3) There must be a significant spread in measured $^{187}Re/^{187}Os$, which leads to a significant spread in measured $^{187}Os/^{188}Os$. Calculated $(^{187}Os/^{188}Os)_i$ at 95.1 Ma (using $\lambda=1.666 \times 10^{-11}a^{-1}$; Smoliar et al., 1996) for all samples range from 0.68 to 0.89 with no clear correlation with stratigraphic level. This is consistent with either a rapidly changing $^{187}Os/^{188}Os$ of sea-water around ~95 Ma, or some degree of post-depositional mobility of Re or Os. A range in $^{187}Re/^{188}Os$ from 2328 to 2869 and the measured $^{187}Os/^{188}Os$ from 4.38 - 5.38 provides a limited range in both ratios. Precise Re-Os geochronology requires samples

with similar ($^{187}Os/^{188}Os)_i$, with a spread in $^{187}Re/^{188}Os$ ratios of at least a few hundred units (Cohen et al., 1999; Selby and Creaser, 2005; Kendall et al., 2009).

Eagle Ford samples from Iona-1 have significant spread in the $^{187}Re/^{188}Os$ ratio with a range of 541 units. However, because the samplea re relatively young, they have a very limited spread in the $^{187}Os/^{188}Os$ ratio of ~1 unit. This limited spread results in the data points being tightly clustered which produces a large uncertainty in the regression of the isochron. In addition, data points that cluster far from the y-intercept magnifies the uncertainty of the extrapolation of the isochron to the y-intercept, providing additional uncertainty in the age and $(^{187}Os/^{188}Os)_i$ (Figure 4.5a).

One of the assumptions of using the Re-Os system in the marine environment is that, due to the short residence time of Os in the oceans, the world's oceans are well mixed and thus homogeneous with respect to Os. An added advantage of examining the Eagle Ford shale is its coincidence with the Cenomanian-Turonian boundary and the oceanic anoxic event 2 (OAE2). This interval has been globally correlated to the Livello Bonarelli in Italy, the Portland #1 core near Pueblo, Colorado, the Wunstorf core in Germany, the Vocontian Basin, SE France and DSDP Site 530 in the proto-South Atlantic using Os isotopes (Du Vivier et al., 2014). The $(^{187}Os/^{188}Os)_i$ curve of all of these sections are similar, with $^{187}Os/^{188}Os$ values in the interval studied here of ~0.7 (Du Vivier et al., 2014). This suggests homogeneity of the oceans with respect to Os during this portion of the Cenomanian.

In an attempt to constrain an accurate and precise age for this portion of the Eagle Ford shale, an isochron was regressed forcing the $(^{187}Os/^{188}Os)_i$ to 0.7 (Figure 4.5b). This

forced isochron yielded an age of 95.7 ± 2.8 Ma (2.9% age uncertainty, 2σ, n=11, MSWD=16). This is within uncertainty is identical to the expected age for this formation, however, with much more precision than the previously discussed isochron. This indicates that the primary control on the original Iona-1 uncertainty is the distance between the data cluster and the y-intercept, and not post depositional mobility or rapidly changing $(^{187}Os/^{188}Os)_i$. This gap is visually highlighted on Figure 4.5b.

Regression of all data points from the Turonian Upper Eagle Ford shale from the BB-2 core yields a Model 1 age of 93.6 ± 6.0 Ma (6.4% age uncertainty, 2σ, n=8, MSWD=1.5) with a $(^{187}Os/^{188}Os)_i$ of 0.71 ± 0.06 (Figure 4.5c). Within uncertainty, this age agrees with the expected age for this formation (~91.9 Ma; Shell E-mail), which is more precise than the original Re-Os isochron from the Iona-1 core. Age verification for this core is from an independent U/Pb age of zircons of ~91.9 Ma from an interval 6 inches below the interval studied here (Amy Kelly, personal communication). Calculated initials at 93.6 Ma form a very tight range from 0.71 to 0.73 indicating minimal change in sea-water $^{187}Os/^{188}Os$ during deposition of this section of the Eagle Ford. These calculated $^{187}Os/^{188}Os$ initials agree with other sections of Turonian strata (Du Vivier et al., 2014).

Although the uncertainty in the BB-1 isochron is significantly better than for the Iona-1 isochron, an uncertainty of ±6.4% (2σ) is still higher than can be explained by analytical error alone. Calculated $(^{187}Os/^{188}Os)_i$ ratios indicated limited variation in the $^{187}Os/^{188}Os$ of coeval sea-water, however, there is an extremely limited range in both the measured $^{187}Re/^{188}Os$ of ~106 units and $^{187}Os/^{188}Os$ of ~0.15 units, producing a data cluster which introduces significant uncertainty in the regression computation. Also, the data cluster for

BB-1 samples lies significantly away from the y-intercept, magnifying that uncertainty as discussed above for the Iona core data (Figure 4.5c).

4.5.3. Relationship between Re-Os and Organic Matter

The uptake of Re and Os in the water column occurs under suboxic to anoxic conditions with complexation likely occurring through a combination of reductive capture (Colodner et al., 1993; Yamashita et al., 2007) and adsorption onto organic complexes (Koide, 1991; Crusius et al., 1996; Levasseur et al., 1998; Oxburgh, 1998; Cohen et al., 1999; Morford and Emerson, 1999). Several experimental studies have demonstrated that the uptake mechanism varies for each element with soluble Re ($Re^{VII}O_4^-$) being removed from sea-water by reductive capture during diffusion into anoxic pore waters and converted to the insoluble Re^{IV} under low oxidation potential (Eh) conditions (Colodner et al., 1993). Removal of Os from sea-water (as soluble Os^{IV}) is suggested to be directly associated with the presence of organic matter. Over a wide range of Eh and pH conditions, Os enters oxic sediment, first as Os^{IV}, and is then converted to Os^{III} after further reduction during organic complexation (Yamashita et al., 2007). Osmium removal from sea-water is fast compared to Re removal and is complexed into ferro-manganese oxides as well as organic-rich sediments, while Re is only removed to sediment under highly reducing conditions. This leads to high $^{187}Re/^{188}Os$ ratios in organic-rich sediments (Yamashita et al., 2007; Poirier et al., 2011).

Although the removal of Re and Os from sea-water has been directly linked to the presence of organic matter, through positive correlations of both elements with TOC, the rate of removal is therefore controlled not only by the type and abundance of organic

matter, but also the redox conditions and sediment accumulation rates. The rate of removal of Re from sea-water, however, is controlled by precipitation kinetics and has been demonstrated to be unaffected by changes in sediment accumulation rate and sulfide abundance (Crusius and Thompson, 2000; Sundby et al., 2004). Rooney et al. (2010) suggests that the enrichment of Re and Os in ORM may be related to local factors such as the duration that the pore-water sediment interface is open, and changes in the oxic-anoxic boundary of the water column, both of which can be related to sediment accumulation rate. Further, the behavior of other redox-sensitive elements such as Ni and Mo who's dominant enrichment factor is sediment accumulation rate, are very similar to that of Re and Os, indicates a common dominant enrichment factor (Lewan and Maynard, 1982; Kendall et al., 2009; Rooney et al., 2010).

Recent studies have shown that Re and Os abundances do not always correlate with TOC values. However, these studies either used inverse *aqua-regia* instead of CrO_3-H_2SO_4 for sample digestion (Cohen et al., 1999), or were performed on organic-rock mud rocks from restricted basins (McArthur et al., 2008; Baioumy et al., 2011; Cumming et al., 2012). Sample digestion using inverse *aqua-regia* alleviates and oxidizes Re and Os from both hydrogenous and detrital, non-hydrogenous sources. Since non-hydrogenous sources aren't related to sea-water and therefore unrelated to organic matter, if the detrital component is large, then a strong correlation between Re and Os abundances and TOC isn't expected. In fact, there is a weak correlation between Re and Os abundance and TOC for the Jurassic ORM reported by Cohen et al. (1999) and perhaps a stronger correlation would result from analysis using the CrO_3-H_2SO_4 method.

Baioumy et al. (2011) reported Re-Os data for laterally correlated marine and non-marine shales and coals from Egypt and showed a strong positive correlation between TOC and both Re and Os abundances for the marine shales (R^2=0.87 and 0.89, respectively), and a lack of correlation in the laterally correlated non-marine gray shales and coals (R^2=0.19 and 0.37, respectively). Cumming et al. (2012) also reported a lack of correlation between TOC and Os in both distal and proximal (R^2= 0.56 and 0.41, respectively) lacustrine deposits from the Green River Basin. There was also a lack of correlation between TOC and Re in the proximal, lake margin Douglas Creek Member (R^2=0.17). However, the Mahogany Zone, which represents distal lake center deposits showed a moderate positive correlation between TOC and Re (R^2 = 0.73) (Cumming et al., 2012). The Mahogany Zone was deposited in the lake center when lake levels were at their maximum and sedimentation rates were slow and steady under a stratified water column (Bradley, 1931; Boyer, 1982; Tuttle and Goldhaber, 1993; Cumming et al., 2012). In contrast, the Douglas Creek Member was deposited on the lake margin during fluctuating lake-levels and a variation in sedimentation rate, possibly allowing much higher variation in the Re-Os uptake and fractionation compared to the more stable lake center where association of Re and Os with organic matter would have been greater (Cumming et al., 2012). It has been suggested that in restricted basins, organic matter sedimentation draws down dissolved Re and Os from the water column resulting in a shortening of the residence time, subsequently causing rapid variations in the availability of those elements in the water column (McArthur et al., 2008). This results in rapid variations in the $(^{187}Os/^{188}Os)_i$ of the sediments. However, the proximal lacustrine zones discussed in

Cumming et al. (2012) that had the weakest correlation between TOC and both Re and Os, provided a more precise isochron than the distal shales from the lake center.

If there is a relationship between TOC, sedimentation rate, and the abundances of Re and Os, it can be expected that the slope of a line correlating points from various ORM on a TOC versus Re (or Os) plot would be related to the sediment accumulation rate (Figure 4.6). Because TOC decreases during decreased sedimentation rates due to scavenging of organic matter by benthic organisms, while Os (or Re) abundances would increase due to a longer duration of interaction between pore-waters and the sediment interface, this correlation would be negative, with larger slopes (higher Re/TOC or Os/TOC) representing slower accumulation rates. There is a rough correlation between the slope of correlation lines and the R^2 values for most marine and non-marine shales, with slopes of Re/TOC and Os/TOC of up to 18.7 and 350.7, respectively and R^2 values of 0.97 for both (Figure 4.6). This indicates that the slower accumulation rates in less restricted, marine conditions, provides adequate time for the complexation of Re and Os with organic

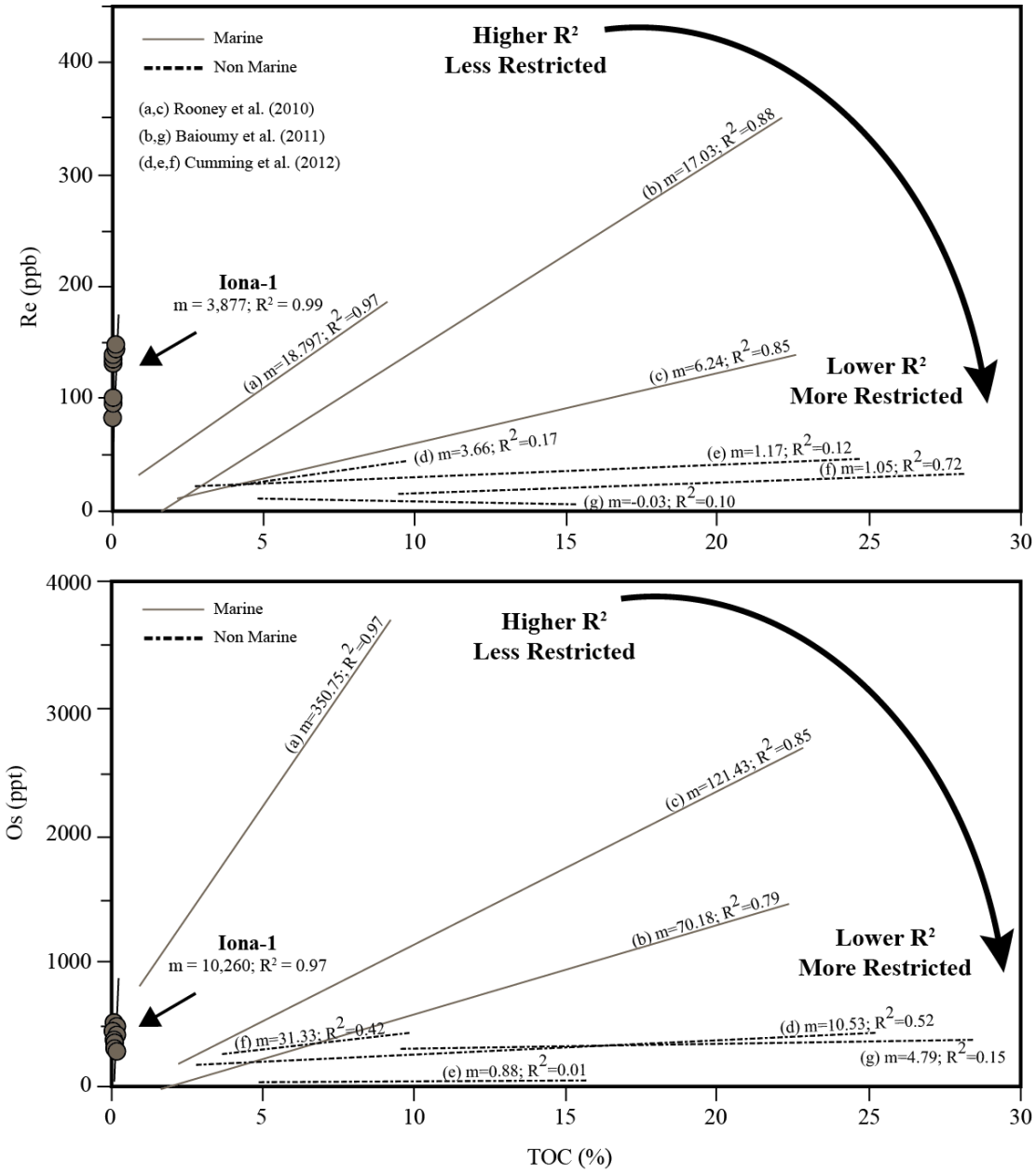

Figure 4.6. (A) Re abundance (in ppb) vs. Total organic carbon (in weight percent), (B) Os abundance (in ppt) vs. Total organic carbon (in weight percent). Solid gray lines represent marine shales from: (a, c) Rooney et al. (2010) and (b) Baioumy et al. (2011). Dashed black lines represent non-marine shales from: (g) Baioumy et al. (2011), (d, e) proximal lacustrine shale from Cumming et al. (2012) and (f) distal lacustrine shales from Cumming et al. (2012).

matter. However, the implication of this correlation may not be straightforward. In addition to sedimentation rate, the amount of preserved organic matter in sediment can be related to water depth, redox conditions, and diagenesis following deposition and burial, as well as degree of restriction of the basin. Molybdenum concentration in organic-rich sediments is a particularly useful indicator of paleoredox state because the uptake of Mo from sea-water requires low O_2 to anoxic waters with H_2S present in the sediment pore fluid (Zheng et al., 2000). Georgiev et al. (2011) reported a positive relationship between TOC and molybdenum abundance for Upper Permian shales from Greenland and the mid-Norwegian shelf. They also attributed the correlation to the degree of basin restriction. In stagnant, restricted basins with limited deep water renewal, Mo drawdown into basin floor sediments progressively depletes the dissolved Mo of sea-water. This drawdown results in shales that are deposited in this setting to have lower Mo/TOC than shales deposited in less restricted basins with continued Mo renewal (Georgiev et al., 2011). Therefore, ORM with low Mo/TOC are likely to have been deposited in more restricted basin settings than those with high Mo/TOC (Tribovillard et al., 2006). Non-marine shales discussed here all plot with low Re/TOC and Os/TOC, in a distinct field, separate from the marine shales with high Re/TOC and Os/TOC (Figure 4.6). If the only factor controlling the slopes of the correlation lines in this diagram is sediment accumulation rates, it would be expected that this would not be the case, as sediment accumulation rates are similar for some lacustrine and marine settings. The covariation of Re and Os with TOC likely has implications for Re and Os renewal which is controlled by the degree of basin restrictivity, similar to that of Mo. However, the degree of basin restrictivity does have some control on the rate of sediment accumulation as well.

The TOC values for Eagle Ford samples from Iona-1 range from 2.64 to 4.24% and are positively correlated with both Re and Os abundances (Figure 4.6). The slope of Re/TOC and Os/TOC for Iona-1 samples is 3,877 and 10,260, respectively, with R^2 values of 0.99 and 0.97, respectively. These samples have the highest slope of Re/TOC and Os/TOC of all plotted samples. Based on the discussion above, samples from Iona-1 were deposited in an open, unrestricted marine setting possibly under very slow sediment accumulation. To further support this conclusion are the high Re/Os ratios reported here for Iona-1 samples of 2328 – 2869. To date, the published $^{187}Re/^{188}Os$ ratios for nearly all shales is less than 2000, with greater than 99% of $^{187}Re/^{188}Os$ values less than 2300 (Georgiev et al., 2011). In exception, Upper Permian black shales from Poland have very high $^{187}Re/^{188}Os$ ratios of up to 5,311 (Pasava et al., 2010). Yang et al. (2004) also reported exceptionally high $^{187}Re/^{188}Os$ ratios of up to 6,114 in Upper Permian Mo-rich black shales of the Laoyaling, Anhui Province, China. Georgiev et al. (2011) also reported high $^{187}Re/^{188}Os$ ratios of 3,138-6,028 for Upper Permian black shales from the mid-Norwegian shelf and East Greenland sections.

As noted above, Re and Os are redox-sensitive elements and are concentrated in reducing sediments (Ravizza et al., 1991). Osmium is scavenged from sea-water over a wide range of Eh and pH conditions and first enters oxic sediment as Os^{IV}, and is then converted to Os^{III} after further reduction during organic complexation (Yamashita et al., 2007). This results in Os being sequestered and/or adsorbed to a variety of phases under a variety of conditions. In contrast, high concentrations in recent and ancient reducing sediments coupled with experimental studies show that Re is readily drawn from sea-water and

fixed in sediment only under reducing conditions (Ravizza et al., 1991; Yamashita et al., 2007; Georgiev et al., 2011). Enrichment of Re over Os therefore requires highly reducing environments. The extraordinarily high $^{187}Re/^{188}Os$ ratios reported here for the Eagle Ford, in addition to those from the Upper Permian are likely caused by extreme deep-water anoxia. This is supported by redox-sensitive trace element enrichment and lack of benthic bioturbation reported in this section of the Eagle Ford shale indicating anoxic conditions in the Maverick Basin during the Upper Cenomanian (Eldrett et al., 2014).

The TOC values for Turonian samples from BB-1 range from 2.69 to 2.84%. A correlation between Re-Os and TOC cannot be made for the BB-1 samples due to a tight clustering of these data points. However, $^{187}Re/^{188}Os$ ratios for BB-1 samples are 597 – 685 and fall within the typical range for ORM (Georgiev et al., 2011) indicating less extreme anoxia in this portion of the Maverick Basin during the Turonian.

In summary, our present understanding of the uptake and fractionation behavior of Re and Os in the water column requires further examination. It is however, likely an intricate balance of degree of anoxia, depositional rates, organic matter type, water depth, salinity, pH, and temperature that controls the kinetics of Re and Os removal from sea-water. A better understanding of the types of inorganic and organic molecules that are involved in Re and Os sequestration is clearly necessary to understand their behavior in the water column.

4.5.4. Re-Os Systematics in Organic and Inorganic Phases

Within an ORM, organic-matter typically comprises only a small mass of the rock. Eagle Ford samples contain 2 – 4 wt% total organic carbon. This means that a 100 g bulk-rock sample with these TOC values contains 2 – 4 g of organic carbon. The rest is made up of various inorganic phases. The 2 – 4 g of organic carbon is further subdivided into kerogen, which is the organic-solvent insoluble organic matter, and bitumen, which is the organic-solvent soluble organic matter, or extractable organic matter.

Kerogen comprises the majority of the organic-matter in an ORM. During the break-down process of organic matter during diagenesis, biopolymers from proteins and carbohydrates dismantle either partially or completely (Tucker, 1988). These dismantled components can then polycondense to form new polymers, or kerogen. Kerogen is the complex organic matter that generates petroleum and natural gas (Tissot and Welte, 1984; Vandenbroucke and Largeau, 2007).

The remainder of organic-matter, the extractable organic matter, is comprised of carbon contained in the oil and gas already formed during burial and catagenesis but not yet expelled from the rock (Jarvie, 1991).

For this study, three samples were selected for separation and analysis of Re and Os in the different organic and inorganic fractions. From Iona-1, EF-101 and EF-108 were used. EF-100 represents a thermally immature, Type II source rock. EF-108 is also a thermally immature, Type II source rock, however, it contains an appreciable amount of pyrite. From BB-1, EF-107 was selected. EF-107 represents a thermally mature, Type II

source rock. These samples allow for the determination of Re and Os isotopes and abundances in two thermal end-member, Type II marine source rocks. In addition, EF-108 provides a means for understanding the effect sulfides have on the Re-Os systematics within ORM. The percent, by weight of bitumen in EF-101, EF-108 and EF-107 is 0.38, 0.08, and 0.11, respectively. The remainder of the organic-matter is kerogen (3.81, 2.72, 2.68 wt%, respectively).

The distribution of Re and Os in different fractions within ORM have been relatively well studied. In addition, Re-Os systematics in crude oil and heavy oil (bitumen) have been studied in natural systems (Selby et al., 2005; Selby and Creaser, 2005; Finlay et al., 2011) as well as laboratory based experiments using hydrous pyrolysis for the artificial thermal maturation of marine and lacustrine source rocks (Rooney et al., 2012; Cumming, 2013).

In this study, the Re-Os abundances and isotopic compositions are determined in organic and inorganic phases within an ORM in order to determine the Re-Os systematics within the petroleum system source rock and produced hydrocarbons. In order to minimize confusion, a systematic approach in the following discussion has been used. The Re-Os systematics in the bulk-rocks were discussed above. From here, the discussion will involve sequential removal of phase(s) from the bulk-rock; bitumen, kerogen, then pyrite. The extraction of the soluble organic matter (bitumen) through Soxhlet extraction produces a bitumen-free residue, this is termed the extracted rock. The extracted rock is then subjected to kerogen isolation through the previously described demineralization

procedure. Finally, pyrite (and other heavy minerals) is removed from the kerogen though heavy-liquid separation.

4.5.4.1. Extracted Rock

Extracted rock from Iona-1 has Re and Os abundances indistinguishable from the bulk-rock (Tables 4.1 & 4.3). The same relationship is observed in extracted rock from BB-1. A first order interpretation is that the extracted bitumen has very little Re and Os, as the abundances in the bulk-rock and in the residue are identical. The Eagle Ford samples from the Iona-1 and BB-1 cores contain very little bitumen (0.38 and 0.11 wt%, respectively). In order for bitumen to have an effect on the bulk-rock budget by only 1 ppb, it would have to contain ~260 ppb Re for bitumen from the Iona-1 core sample and ~900 ppb Re for bitumen from the BB-1 core. Therefore, a lack of change in Re and Os abundances between bulk and extracted rocks doesn't imply low abundances of these elements in the bitumen, rather just a low proportion of bitumen in the bulk-rock budget.

Extracted rock from the thermally immature Iona-1 sample has a $^{187}Re/^{188}Os$ ratio, within uncertainty, identical to that of the bulk-rock but has a slightly higher $^{187}Os/^{188}Os$. The extracted rock from the thermally mature BB-1 also has a $^{187}Os/^{188}Os$ ratio slightly higher than its host bulk-rock, however, with a $^{187}Re/^{188}Os$ ratio significantly larger than the bulk-rock. Rooney et al. (2012) reported similar results from experiments of artificial thermal maturation of samples from the Jurassic Staffin Formation, Scotland, using hydrous pyrolysis. Thermally immature bulk-rock and extracted rock had similar Re and Os abundances (13.4 vs. 14.0 and 199.1 vs. 200.6, respectively) with very similar $^{187}Re/^{188}Os$ and $^{187}Os/^{188}Os$ ratios (355 vs. 353 and 1.47 vs. 1.47, respectively) (Rooney

et al., 2012). Following hydrous pyrolysis at 350 ^{o}C for 72 h, Re and Os abundances of the bulk-rock and extracted rock varied minimally while a difference of ~10% was introduced in the $^{187}Re/^{188}Os$ ratio between the thermally mature bulk and extracted rocks (333 vs. 369, respectively), suggesting a selective transfer of Os over Re to generated bitumen (Rooney et al., 2012). While it is difficult to compare the thermally immature Iona-1 samples to the thermally mature BB-1 samples due to varying age and associated lack of lateral correlation of these samples, it is possible to compare relationships between the bulk and extracted rocks of each core independently.

In both the Iona-1 and BB-1 samples, the $^{187}Os/^{188}Os$ ratios are slightly higher in the extracted rock than in the bulk-rock, indicating bitumen has a less radiogenic $^{187}Os/^{188}Os$ than the bulk-rock. The thermally mature BB-1 sample shows a marked increase in the $^{187}Re/^{188}Os$ ratios between bulk and extracted rocks indicating removal of a phase with lower $^{187}Re/^{188}Os$ than the bulk-rock. This selective transfer of Os over Re into bitumen during burial and thermal maturation would cause the bitumen to have less ^{187}Re available for decay to ^{187}Os while increasing the $^{187}Re/^{188}Os$ of the kerogen. This is supported by the implied less radiogenic nature of bitumen in both the immature and mature samples.

Rhenium and Os abundances in the extracted rock from the heavily pyrited sample (EF-108) from Iona-1 are significantly less than for the host bulk-rock (~56 vs. ~100 ppb and ~169 vs. ~300 ppt, respectively) (Tables 4.1 & 4.3) indicating that the removal of bitumen removed a phase enriched in Re and Os. EF-108 contains 0.11wt% bitumen. A simple mass balance calculation yields theoretical Re and Os abundances of ~100,000

ppb and ~181,000 ppt, respectively, in the extracted bitumen in order to see such differences in the abundances of Re and Os between the bulk and extracted rocks. These values are significantly higher than any previously reported bitumen abundances (Selby et al., 2005; Rooney et al., 2011; Cumming, 2013) or for ORM (Ravizza and Turekian, 1989; Cohen et al., 1999; Creaser et al., 2002; Selby and Creaser, 2003; Hannah et al., 2004; Kendall et al., 2004; Finlay et al., 2010; Rooney et al., 2010). These abundances are unrealistic, as even if the bulk-rock were comprised of 100% bitumen, Re and Os abundances in the bulk-rock are only 100 ppb and 300 ppt, respectively. Two mechanisms that could explain this imbalance are (1) An error in the calculation of the relative abundance of bitumen in the bulk-rock, or (2) Loss of Os during solvent extraction. The $^{187}Re/^{188}Os$ and $^{187}Os/^{188}Os$ ratios of the extracted rock are, within uncertainty, identical to those of the bulk-rock. Therefore a loss of Os must be coupled with an equal loss of Re for these two phases to have similar $^{187}Re/^{188}Os$ ratios. Although, small differences in the $^{187}Re/^{188}Os$ ratios of the two fractions could be present, but are masked by the slightly higher uncertainty in the $^{187}Re/^{188}Os$ ratio of extracted rock (Table 4.3).

4.5.4.2. Bitumen

Diagenesis of kerogen gives way to catagenesis which is the thermally involved transformation of kerogen. Long chain hydrocarbons that make up kerogen are broken down into simpler molecules. This thermal decomposition of kerogen results in the generation of bitumen and minor amounts of expelled oil (Lewan et al., 1985). During

increased burial, kerogen decomposition slows, while the decomposition of bitumen results in the primary generation of expelled oil (Lewan et al., 1985).

It should be noted that data for bitumen in this study are reported with large uncertainty (11 – 35%, 2σ) due to the small sample size coupled with the low amount of bitumen within the Eagle Ford samples used. The discussion of the data in this section should be taken lightly.

Bitumen extracted from the thermally immature Iona-1 sample (EF-101.1) has Re and Os abundances of 91 ppb and 129 ppt, respectively. Extracted rock data from Iona-1 predicted that extracted bitumen would have $^{187}Re/^{188}Os$ ratios similar to the bulk-rock, but with less radiogenic $^{187}Os/^{188}Os$. The $^{187}Os/^{188}Os$ of 5.91 ± 0.66 is, within uncertainty, similar to that of the bulk and extracted rocks. However, the $^{187}Re/^{188}Os$ ratio of 5989 ± 667 is markedly higher than the bulk-rock, even at the lower limits of the uncertainty. As previously mentioned, changes in the Re and Os abundances between bulk-rock and extracted rock would be undetectable with such low abundances of Re and Os in bitumen coupled with the low amount of bitumen in these Eagle Ford samples. The higher than predicted $^{187}Re/^{188}Os$ ratio in the extracted bitumen indicates loss of Os during the chemical extraction procedure, perhaps due to volatility. This would raise the $^{187}Re/^{188}Os$ ratio without affecting the $^{187}Os/^{188}Os$ ratio.

Bitumen extracted from BB-1 (EF-107.1) has Re and Os abundances of ~8 ppb and ~106 ppt, respectively. The $^{187}Re/^{188}Os$ and $^{187}Os/^{188}Os$ ratios of 406 ± 126 and 0.53 ± 0.18, respectively, are both smaller than in the respective bulk-rock, as predicted by the extracted rock data. These results reflect the selective transfer of Os over Re to bitumen

during source rock burial and bitumen generation as discussed by Rooney et al. (2012). In contrast to Iona-1 extracted rock, there doesn't appear to be loss of Os during the bitumen extraction process for this sample.

Bitumen from the pyrited samples from Iona-1 (EF-108.1) has Re and Os abundances of ~28 ppb and ~95 ppt, respectively. These are much lower than predicted by the extracted rock data (Tables 4.1 & 4.3). The $^{187}Re/^{188}Os$ and $^{187}Os/^{188}Os$ ratios of 2184 ± 766 and 3.99 ± 1.40 are, within uncertainty, identical to those of the bulk and extracted rocks. However, such large uncertaintainties in these values (35%, 2σ) should warrant caution in using this data for any meaningful interpretation or application.

There are large discrepancies between the reported and predicted (from bulk and extracted rock data) abundances and isotopic ratios in the Iona-1 samples discussed here. This discrepancy is partially explained by such large analytical uncertainties, however, there also seems to be a loss of Os and/or Re either during the chemical extraction of bitumen from the bulk-rock (perhaps during the boiling of the dichloromethane), or during the loading of bitumen into the Carius tubes, as there is a heating step involved.

The large discrepancy in the abundances of Re and Os predicted from the bulk-rock and extracted rock data compared to that of the measured bitumen for the pyrited Iona-1 sample indicates missing Re and Os. As the products of the bitumen extraction make up the whole of the rock, the only explanation for missing Re and Os is their volatility during the procedure. Osmium is known to be volatile and in the VII oxidation state, as OsO_4, sublimes at room temperature (Butler and Harrod, 1989). OsO_4 is formed when Os powder reacts with O_2 at ambient temperatures (Housecroft and Sharpe, 2004). In the

bitumen extraction procedure, bitumen in solution (DCM) is heated to boiling and thus could provide a means of volatilizing Os. The most common oxide of Re is the volatile Re_2O_7 (Greenwood and Earnshaw, 1997).

In addition, the large abundance discrepancy isn't observed in the non-pyrited sample from Iona-1, therefore, the variation in behavior of Re and Os either within the natural system or during the chemical extraction of bitumen seems to be controlled by the presence of sulfides.

Within a kerogen its carbon-sulfur bonds may cleave more readily to generate more liquid hydrocarbons that its carbon-carbon bonds. Therefore, the greater the amount of organic sulfide incorporation into the matrix of a Type II kerogens, the lower the thermal stress necessary for their generation of oil (Lewan, 1985). This hypothesis may hold true for the extraction of Re and Os from the organic molecules of the kerogen during bitumen extraction.

4.5.4.3. Kerogen

Kerogen, defined as the insoluble macromolecular organic matter dispersed in sedimentary rocks, is by far the most abundant form of organic matter on Earth with abundances on the order of 10^{16} tons in the global carbon cycle (Durand, 1980; Vandenbroucke and Largeau, 2007). This is compared to ~10^{12} tons in living biomass (Durand, 1980). Accordingly, it has much importance in disciplines other than petroleum research, such as biogeochemistry and oceanography. Kerogen is of prime importance in

petroleum systems, as it is the sedimentary organic matter which generates petroleum and natural gas (Vandenbroucke and Largeau, 2007).

Kerogen dominantly represents the residues from two photoautotrophic primary producers: algae and terrestrial higher plants, and various heterotrophic organisms that escaped mineralization during the C cycle (Vandenbroucke and Largeau, 2007). The photoautotrophic primary producers transform atmosphere CO_2 or inorganic C dissolved in the water column into their own metabolites using solar energy for photosynthesis (Vandenbroucke and Largeau, 2007). Life for these organisms is thus restricted to the land surface and the upper hundred meters of the water column, where sun light is available. On land, higher plants make up the majority of primary producers. In lakes and oceans, phytoplankton is the major contributor. Following death of the primary producers, they are mineralized through the food chain by a consortium of heterotrophic organism that use energy provided by oxidation reactions to synthesize their own metabolites (Vandenbroucke and Largeau, 2007). The organic debris settling at the sediment-water interface in lakes or in the ocean is the sum of all residues escaping the biological process including primary producers and heterotrophic organisms that were involved in organic matter mineralization (Froelich et al., 1979; Deming and Baross, 1993).

During the break-down process of the primary producers large biopolymers from proteins and carbohydrates dismantle either partially or completely (Tucker, 1988). These dismantled components can then polycondense to form new polymers. The formation of

polymers in this way accounts for the large molecular weight and diverse chemical compositions of kerogen (Tucker, 1988).

Kerogen isolated from the thermally immature Iona-1 sample (EF-101.2) is 8 to 10 times enriched in Re and Os compared to the extracted rock (Tables 4.1 & 4.3). A first-order observation, is that the removal of the inorganic matter during demineralization removed phases with comparatively lower abundances of Re and Os. The $^{187}Re/^{188}Os$ and $^{187}Os/^{188}Os$ ratios of isolated kerogen are also lower than these ratios in the extracted rock, indicating the removal of phases(s) with more radiogenic $^{187}Os/^{188}Os$ and higher $^{187}Re/^{188}Os$ ratios than the kerogen. The inorganic material removed during demineralization is predominantly detrital minerals representative of the upper continental crust. The $^{187}Os/^{188}Os$ of ORM, as derived from the $^{187}Os/^{188}Os$ composition of sea-water, is controlled by the two dominant inputs of Os: radiogenic continental crust with a high $^{187}Os/^{188}Os$ and non-radiogenic mantled-derived Os with a low $^{187}Os/^{188}Os$. Therefore, the removal of detrital, inorganic material during demineralization removes a component with a high $^{187}Os/^{188}Os$, leaving the residue with a lower $^{187}Os/^{188}Os$.

Kerogen isolated from the thermally mature BB-1 sample (EF-107.2) is also 8 to 10 times enriched in Re and Os compared to its extracted rock (Tables 4.1 & 4.3). The $^{187}Os/^{188}Os$ of isolated kerogen is, within uncertainty, identical to that of the extracted rock. However, the $^{187}Re/^{188}Os$ of kerogen is markedly higher than the extracted rock. In contrast to EF-101.2, the removal of the inorganics from EF-107 indicates a removal of a phase with a $^{187}Re/^{188}Os$ lower than the extracted rock, but with a $^{187}Os/^{188}Os$ similar to the extracted rock. While it's tempting to explain this contrast by a process related to

thermal maturity, this isn't possible as these two samples represent different basin settings and are of vastly different age. In addition, the demineralization procedure that isolates the kerogen only removes inorganic phases that are independent of thermal maturity. Therefore, the differences observed in the $^{187}Os/^{188}Os$ composition of the demineralized phases are related to the composition of the inorganic material within the sample (quartz, clays, pyrite, etc.). In addition, sedimentation rate could control the amount of inorganics present which would ultimately affect the differences in abundances and isotopic ratios observed.

Kerogen isolated from the pyrited Iona-1 sample (EF-108.2) is also enriched in Re and Os, however, not as much as the previously discussed kerogens. The $^{187}Re/^{188}Os$ ratio of 1606 ± 108 is lower than that of the extracted rock (~2600) indicating that the removal of the inorganics during demineralization removed phases with higher $^{187}Re/^{188}Os$ ratios than the extracted rock. Measured $^{187}Os/^{188}Os$ of the kerogen (4.19 ± 0.43) is lower than that of the extracted rock (5.61 ± 0.02) suggesting the removal of a more radiogenic phase. This is consistent with the removal of radiogenic crustal material during demineralization and kerogen isolation.

There is again a discrepancy between the extracted rock-kerogen couples from Iona-1 and BB-1. Iona-1 samples (both 'pyrite-free' and pyrited) demonstrate a decrease in the $^{187}Re/^{188}Os$ ratio in the kerogen following demineralization. Whereas, following demineralization, kerogen from BB-1 shows an increase in this ratio. As discussed above, Os is scavenged from sea-water over a wide range of Eh and pH conditions and first enters oxic sediment Os^{IV}, and is then converted to Os^{III} after further reduction during

organic complexation (Yamashita et al., 2007). This results in Os being sequestered and/or adsorbed to a variety of phases under a variety of conditions. In contrast, high concentrations in recent and ancient reducing sediments coupled with experimental studies show that Re is readily drawn from sea-water and fixed in sediment only under reducing conditions (Ravizza et al., 1991; Yamashita et al., 2007; Georgiev et al., 2011). The significantly higher $^{187}Re/^{188}Os$ ratios of Iona-1 samples (~2300 - ~2800) compared to those of BB-1 samples (~579 – 685) indicate a decrease in the oxygenation of the bottom-waters preserved in the samples from Iona-1. In this context, phases that are present in samples deposited under highly anoxic bottom-waters of the Iona-1 core will have a higher abundance of Re than sample deposited under more oxic conditions, such as in BB-1. In contrast, host phases of Re and Os in the BB-1 core will have higher abundance of Os, as Os is sequestered under more oxic conditions than Re. This is observed here, as inorganic phases removed during demineralization of Iona-1 samples removes much more Re than it does Os. This results in a drastically reduced $^{187}Re/^{188}Os$ for the isolated kerogen. This is contrast to BB-1 samples that show an increase in the $^{187}Re/^{188}Os$ of kerogen following demineralization indicating a removal of phases enriched in Os.

Following the heavy liquid removal of pyrite (and other heavy minerals), the Re and Os abundances of "pyrite-free" kerogen (EF-108.2.1) increased to ~1200 ppb and ~3738 ppt, respectively. These abundances represent 10 to 12 times enrichment over the bulk-rock and are consistent with the results reported for the two previously discussed samples. This marked increase in the abundances of Re and Os following heavy liquid removal of

pyrite (and other heavy minerals) indicates that these heavy minerals have low abundances. These low abundance, high mass phases are diluting the pyrited-kerogen, causing the bulk pyrited-kerogen abundances to be suppressed when compared to the "pyrite-free" kerogen. The $^{187}Re/^{188}Os$ increased to 2450 ± 163 in the pyrite-free kerogen while the $^{187}Os/^{188}Os$ remained the same (4.60 ± 0.45), within uncertainty, following pyrite removal. These data suggest the removal of heavy minerals removed a phases or phases with $^{187}Os/^{188}Os$ similar to bulk kerogen, but with much lower $^{187}Re/^{188}Os$.

4.5.4.4. Pyrite

Pyrite in sediments forms under anoxic bottom-water conditions via the reaction of detrital iron minerals with dissolved H_2S (Berner, 1985). The H_2S is produced by the reduction of interstitial dissolved sulfate by bacteria during their anaerobic respiration and consequent reduction of sedimentary organic matter (Berner, 1985). This reaction does not directly precipitate pyrite, however, a series of reactions starting with metastable iron monosulfides occurs, which, under most conditions, ends with the transformation to pyrite (Berner, 1984).

In this study, Re and Os isotopes were measured in two different pyrite morphologies (1) disseminated pyrite framboids that were separated from kerogen via heavy liquid separation and (2) a discrete pyrite layer.

Ubiquitous in modern sediments, pyrite framboids are small, near-spherically shaped aggregates of pyrite, ranging in diameter from about 1um to tens of um's, composed of tiny, discrete, and equigranular pyrite crystals (Love, 1967). In order for pyrite framboids

to form, iron must migrate to the site of framboid formation. For this to happen, pore waters must be non-sulfidic (Berner, 1981). In addition, for the dissolution of iron oxyhydroxides to occur (for the release of labile iron), pore waters must contain some amount of free oxygen, as iron is only insoluble in oxic waters (Brett and Allison, 1998; Curtis et al., 2000). This occurs during the migration of the redox interface changing a sub-oxic zone (iron enrichment) to an anoxic zone (iron sulfide precipitation) (Brett and Allison, 1998; Curtis et al., 2000).

Iron sulfide concretions and pyritic layers in sediments vary in size from a few millimeters to tens of centimeters. Although pyrite is usually considered the primary sulfide mineral within concretions or layers, other sulfides such as marcasite are typically present (Schieber, 2002). The features of pyrite layers attest to growth prior to substantial compaction and growth within stratiform, anoxic bottom-waters (Berner, 1981). Horizons with abundant iron sulfide concretions or abundant pore filling iron sulfide may imply very slow sedimentation rates at the time of pyrite formation (Schieber and Riciputi, 2005). Another proposed mechanism for the formation of pyrite layers within sediments is to cover iron-oxide rich layers with an organic-rich anoxic sediment drape, followed by migration of sulfide-rich reduction front into the iron bearing layer effectively converting the iron oxide to pyrite (Ingri and Ponter, 1986).

Regardless of morphology, pyrite is hydrogenous in nature and forms during the very Early stages of diagenesis. Pyrite therefore contains valuable information regarding the chemical composition of sea-water, specifically the Os isotopic composition. In addition, several studies have demonstrated the utility of the Re-Os isotopic system in obtaining

depositional ages for organic-rich mud rocks using early diagenetic pyrite (e.g., Hannah et al., 2004).

Rhenium and Os abundances in the disseminated pyrite are ~10 ppb and ~32 ppb, respectively (Table 4.3). These values are significantly less than those in the bulk-rock and in the kerogen, as predicted by the difference in abundances of bulk and "pyrite-free" kerogen discussed above. The measured $^{187}Re/^{188}Os$ and $^{187}Os/^{188}Os$ of pyrite are 691 ± 45 and 1.27 ± 0.08, respectively, and are much lower than these ratios in the bulk kerogen and the bulk-rock. The kerogen data predicted that the $^{187}Re/^{188}Os$ of the heavy-liquid phase was much lower than bulk-rock values. This is also observed in the measured pyrite. However, the $^{187}Os/^{188}Os$ was predicted to be similar to that of the bulk-kerogen. However, the $^{187}Os/^{188}Os$ of disseminated pyrite is significantly less than that of the bulk-kerogen. The heavy mineral fraction obtained through heavy liquid separation contains a variety of heavy minerals, not just pyrite. While only pyrite was picked and analyzed, it is evident that the heavy mineral fraction contains additional fractions enriched in Re and Os. Some of these phases are required to have $^{187}Os/^{188}Os$ ratios higher than bulk kerogen in order to mass balance the $^{187}Os/^{188}Os$ ratios observed in the kerogen and "pyrite-free" kerogen.

It can be expected that since pyrite is formed under anoxic bottom-water conditions via the reaction of detrital iron minerals with dissolved H_2S, that it should present a high $^{187}Re/^{188}Os$ ratios, similar to anoxic sediment. However, the $^{187}Re/^{188}Os$ ratio for disseminated pyrite observed here is the lowest of any phase measured. In addition, it is among the least enriched phases with respect to Re and Os. These data indicate that Re

and Os were likely already removed from the water column prior to pyrite formation. This suggests that Re and Os are rapidly sequestered into organic matter or into a phase that is precipitated very Early in the anaerobic process.

Pyrite from the discrete pyrite layer has Re and Os abundances of ~9 ppb and 32 ppb, respectively, similar to those observed in the disseminated pyrite. The $^{187}Re/^{188}Os$ and $^{187}Os/^{188}Os$ ratios of ~2125 ± 49 and 4.04 ± 0.09, respectively, are much higher than those observed in the disseminated pyrite. The features of pyrite layers attest to growth prior to substantial compaction and growth within stratiform, anoxic bottom-waters (Berner, 1981), possibly under very slow sedimentation rates (Schieber and Riciputi, 2005). The markedly higher $^{187}Re/^{188}Os$ observed in the pyrite layer compared to the disseminated pyrite may reflect the non-competition for Re and Os in the water-column. A high $^{187}Re/^{188}Os$ at the time of deposition would result in a higher $^{187}Os/^{188}Os$. This is consistent with the higher $^{187}Os/^{188}Os$ observed in the pyrite layer compared to this ratio in the disseminated pyrite.

4.5.4.5. Oil

Crude oil includes a wide assortment of material consisting of mixtures of hydrocarbons and other organic compounds containing varying amounts of nitrogen, sulfur, oxygen and trace metals (Selby et a., 2007). Trace element abundances in oil, particularly Ni, V, and Mo are present on the order of ppm levels (Curiale, 1987; Manning and Gize, 1993). These elements are known to exist as part of a porphyrin structure, as a tetrapyrrole complex (Manning and Gize, 1993). In addition to these trace metals, Re and Os have been reported to occur in oil, with abundances in the ppb and ppt range, respectively, and

are thought to be transferred from the source rocks during oil generation (Poplavko et al., 1975; Barre et al., 1995; Selby and Creaser, 2005; Selby et al., 2005). Oil from deposits of the Alberta Oil Sands, Canada, contain Re (2 – 50 ppb) and Os (34 – 288 ppt) abundances similar to those observed in ORM (Selby and Creaser, 2005). Analysis of 12 worldwide oil samples by Selby et al. (2007) show that Re and Os abundances of 0.003 – 50 ppb and 0.01 – 285 ppt, respectively, positively correlate with the asphaltene content of oil, with light oils (<1% asphaltene content) having no measurable Re or Os. Selby et al. (2007) determined that Re and Os are present dominantly in the asphaltene fraction (>83%) of oil, with abundances of Re and Os up to 264 ppb and 1443 ppt, respectively. This relationship is observed in other trace metals such as V and Mo (Manning and Gize, 1993).

The abundances of Re in the bulk oil and asphaltene fraction of Eagle Ford oil are less than that of the procedural blank (9.27 ± 5.05 pg) resulting in negative abundances and large analytical uncertainty (Table 4.3). Osmium abundance, while still low in the bulk oil, is measurable at 7 ± 2 ppt (Table 4.3). This is similar to Os abundances reported by Selby et al. (2007) for oil with low amounts of asphaltenes. Eagle Ford oil contains ~0.4% asphaltenes. The asphaltene fraction has considerably more Os than the bulk oil (~50 ppt vs. ~7 ppt), even considering the high analytical uncertainties of each. The $^{187}Re/^{188}Os$ and $^{188}Os/^{188}Os$ ratios of bulk oil and the asphaltene fraction are identical, within uncertainty (Table 4.3). Relative to whole oil, only ~1 – 5 % of the Os is present in the asphaltene fraction. This is drastically different than the >83% reported by Selby et

al. (2007), however, the results reported in this study should be used with caution due to their high analytical uncertainty.

A couple of recent studies have demonstrated the utility of the Re-Os isotopic system in dating the timing of hydrocarbon generation (Selby and Creaser, 2005; Selby et al., 2005; Finlay et al., 2010; Finlay et al., 2011). The conclusions of these studies were that during hydrocarbon generation, Re and Os are transferred to crude oil from the source rock, effectively resetting the Re-Os isochron. Therefore, Re-Os isochrons obtained from a suite of generated oils represents the time of hydrocarbon generation. However, oil generated during hydrous pyrolysis experiments contain extremely low abundances of Re and Os in contrast to those reported for natural oils (Rooney et al., 2012; Cumming, 2013). Rooney et al. (2012) suggested the experimental conditions used in the hydrous pyrolysis experiments, most notably the duration of the experiments (72 hours), didn't mimics those of a natural petroleum system, and thus the abundances of Re and Os that is observed in oils in natural systems wasn't observed in the experiments.

Questions have been raised concerning the mechanism for isotopic homogenization of oil on a basin scale (Mahdaoui et al. 2015). In order for a Re-Os isochron of generated oils to have any temporal significance, all oil samples that make up the isochron must have had the same $(^{187}Os/^{188}Os)_i$. Hydrocarbon generation is a process that commonly occurs over millions year time-scales. Therefore, some secondary process must be present if entire reservoirs of oil are to be isotopically homogenized. In addition, several studies have demonstrated that petroleum fluid and mantle-derived hydrothermal fluid interaction may modify the Re-Os contents of petroleum and potentially reset the geochronometer (Finlay

et al., 2010; Lillis and Selby, 2013). In an experiment where oil samples of varying compositions were left in contact with artificially enriched Re and Os solutions, up to 97% of Re and Os that were initially present in the aqueous solutions was captured by the oil within just a few days, and occurs over temperatures between 45^{o}C and 150^{o}C (Mahdaoui et al., 2015). A similar relationship is seen for uranium in natural crude oils (Landais, 1993). Extensive transfer of Re and Os at the oil-water interface is thus a geologically instantaneous process that can operate at temperatures typical of petroleum systems (Mahdaoui et al., 2015). In a natural petroleum system, following generation and expulsion, oil comes in contact with formation fluids within water saturated permeable reservoir rocks. In addition, during secondary migration, oil migrates into the trap by displacing the water within the rock porosity, thus allowing further contact with formation fluids (Mahdaoui et al., 2015). Assuming Re and Os abundances of formation fluids mimic those of groundwater (4 ppt for Re and 70 ppq for Os; Colodner et al., 1993; Paul et al., 2010), a water/oil ratio of 250:1 is required to create the abundances of Re and Os observed in experimentally contaminated oils (Mahdaoui et al., 2015). Mahdaoui et al. (2015) also demonstrated there is no different in the uptake of Re and Os between oils of varying sulfur concentrations, however, oil that contained more asphaltenes sequestered more Re and Os than those oils with lower asphaltene content, a relationship also observed in natural systems.

These results reflect the complicated nature of the petroleum system, and our current lack of understanding of the transfer (or lack of) of Re and Os between source rock and crude

oil. These together highlight that caution should be used for Re-Os studies of generated bitumen and crude oils.

4.5.5. Internal Isochron

One of the disadvantages of using the Re-Os isotopic system for the dating of organic-rich mud rocks is the necessity to have multiple time-equivalent samples. Although the identification of such samples is relatively simple (e.g., maximum flooding surfaces), obtaining these samples is often difficult and requires the drilling of multiple boreholes that intersect the interval that is to be dated. In other applications of isotopic dating, internal isochrons are constructed from the isotopic analysis of individual mineral grains that make up a rock sample. This eliminates the need for multiple samples. Here, an attempt has been made at constructing an internal isochron for organic-rich mud rocks using time-equivalent fractions of the rock: kerogen, bulk-rock, extracted rock, and in the case of EF-108, pyrite (Figure 4.7).

The internal isochron for EF-101 includes data points from 4 bulk-rock aliquots, kerogen, and extracted rock (Figure 4.7a). This internal isochron yields an age of 57 ± 94 Ma (165%, 2σ, MSWD = 342), and within uncertainty, agrees with the accepted age for this formation (95.1 Ma; Eldrett et al., 2015b). These results should be taken extremely lightly due to the excessively large uncertainty on this age. Within this isochron, the bulk-rocks form a trend of 109.9 ± 4.3 Ma, which is older than the expected age for this formation. As discussed earlier, this is due to the narrow range of $^{187}Os/^{188}Os$ and the distance this data plots from the $(^{187}Os/^{188}Os)_i$ on the diagram. The two outliers (kerogen and extracted rock) lie significantly off of this trend. In this study, kerogen was digested

using inverse *aqua-regia*. Therefore, any trace phases that were not effectively removed during kerogen isolation would be dissolved. As previously mentioned, these phases have no time-significance, and therefore would drive the kerogen off of the isochron. The internal isochron shows the kerogen plotting in a trend away from the bulk with lower $^{187}Re/^{188}Os$ and similar $^{187}Os/^{188}Os$ to bulk rock. However, this observation could be hampered by the large uncertainty on the kerogen data. The extracted rock also plots significantly off of the isochron and can only be explained by the loss of Re and/or Os during bitumen extraction, as this aliquot is dissolved in Jones Reagent and thus should only access the hydrogenous component. It is therefore expected to lie on the isochron. A precise internal isochron was not achieved with the EF-101 samples.

The internal isochron for thermally mature BB-1 samples (EF-107) includes data points for 2 bulk-rock aliquots, 2 extracted rock aliquots, and kerogen. The regression of these points yields an age of 43 ± 60 Ma (139%, 2σ, MSWD = 4.5), and once again agrees with the expected age for this formation (Figure 4.7b) (~91.9; Shell E-mail). However, once again, the uncertainty on the age (~140%, 2σ), caused by the extreme outlier (kerogen) invalidates any realistic geologic applications. The bulk-rocks and extracted rocks form a much steeper trend, with kerogen lying significantly to the right. As with EF-101, the location of the kerogen significantly away from the trend provided by the time-significant phases indicates incomplete kerogen isolation. From the direction that kerogen falls away from the trend, the incompletely removed phases have $^{187}Re/^{188}Os$ higher than bulk-rock values, and $^{187}Os/^{188}Os$ greater to or equal than bulk-rock values.

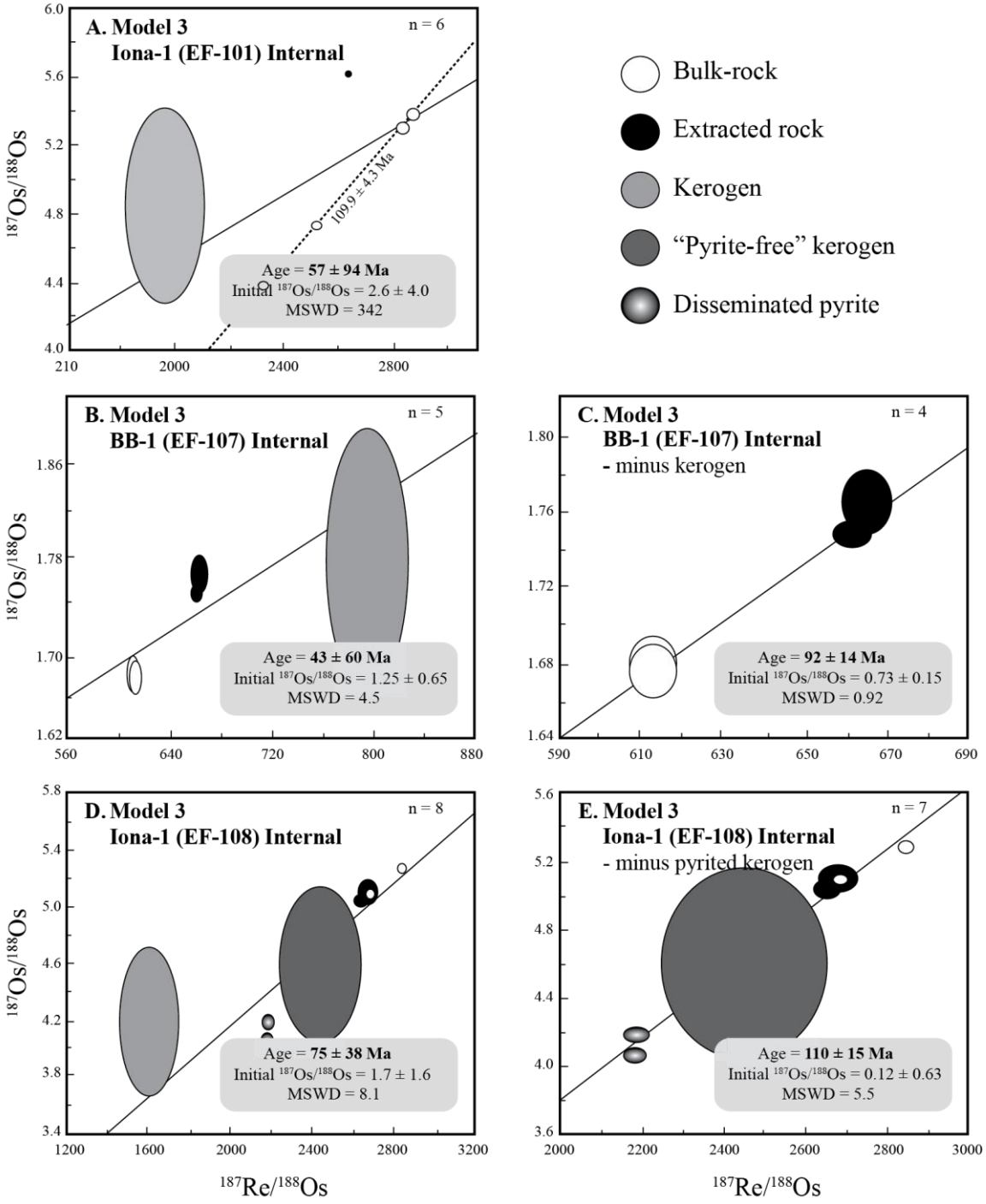

Figure 4.7: Internal isochrons for Eagle Ford samples. Uncertainty is reported as 2σ.

By removing the kerogen data point and regressing the bulk-rocks and extracted rocks data, an age of 92 ± 14 Ma (15%, 2σ, MSWD = 0.92) is achieved, and is within agreement with the expected age for this formation (Figure 4.7c). A ($^{187}Os/^{188}Os)_i$ of 0.73 ± 0.15 provided by the isochron is also in agreement with other marine Turonian strata (Du Vivier et al., 2014). An accurate and somewhat precise internal isochron was achieved for BB-1 samples.

Finally, the internal isochron for the pyrited Iona-1 sample (EF-108) includes data points for 2 bulk-rock aliquots, 2 extracted rock aliquots, 2 disseminated pyrite aliquots, bulk-kerogen, and "pyrite-free" kerogen. The regression of these points yields an age of 75 ± 38 Ma (51%, 2σ, MSWD = 8.1) and again, agrees with the expected age for this interval of the Iona-1 core (Figure 4.7d) (~95.1 Ma; Eldrett et al., 2015b). This data is presented with extremely large uncertainty stemming from large uncertainty surrounding the kerogen data and the outlying nature of the bulk-kerogen. Bulk-kerogen plots with lower $^{187}Re/^{188}Os$ and $^{187}Os/^{188}Os$ ratios than the trend defined by the remaining data points. This likely reflects the composition of incompletely removed, time-insignificant phases, as discussed for the other samples. However, following heavy liquid removal of these phases, "pyrite-free" kerogen plots on the trend defined by the other phases. Regression of the remaining phases yields an age of 110 ± 15 Ma (14%, 2σ, MSWD = 5.5) and agrees with the expected age for this interval of the Iona-1 core, with more accuracy and precision (Figure 4.7e). These results indicate that heavy liquid separation of heavy minerals removes the majority of time-insignificant phases; however, this conclusion may be hampered by the large uncertainty associated with the kerogen data.

4.6. CONCLUSIONS

Rhenium and Os abundances in the insoluble residue following bitumen extraction (extracted rock) are very similar to those of the bulk-rocks indicating that bitumen is not a significant host of Re and Os in ORM. The $^{187}Re/^{188}Os$ ratio of extracted rock from the thermally mature sample is higher than this ratio in the thermally immature sample. This indicates a selective transfer of Os (over Re) to bitumen and crude oil during thermal maturation. This selective transfer of Os results in a bitumen with a much less radiogenic $^{187}Os/^{188}Os$, as there is little ^{187}Re available in the bitumen for decay to ^{187}Os. In addition, the difference in Re and Os abundances between the bulk and extracted rocks for a heavily pyrited sample are much greater than in those samples with significantly less pyrite. This indicates that sulfides play a role in hosting Re and Os, and/or in the transfer of Re and Os during thermal maturation. Both forms of pyrite contain low abundances of Re and Os indicating that they are also not a substantial host for these elements within ORM.

A markedly lower $^{187}Re/^{188}Os$ ratio for disseminated pyrite compared to this ratio in a discrete pyrite layer indicates differences in the availability of Re and Os in the water column or sediment pore fluids. Rhenium and Os are likely rapidly sequestered from the water column by organic matter or other redox-sensitive phases prior to the formation of pyrite. This competition for Re and Os isn't present during bottom-water conditions that are conducive to the formation of the pyrite layer.

Kerogens are markedly enriched in Re and Os (~8 – 10X) compared to bulk rocks indicating that kerogen is a dominant host phase for these elements. However, a heavily

pyrited kerogen has significantly less Re and Os than those kerogens with less pyrite. This is consistent with the low abundance of Re and Os in pyrite, as the presence of pyrite dilutes the bulk-rock Re and Os budget. Following the heavy-liquid removal of heavy minerals from the pyrited kerogen, Re and Os abundances increased significantly suggesting the removal of a phase or phases with low abundance of Re and Os.

These data indicate that the dominant host phase for Re and Os is kerogen. However, incomplete removal of microscopic phases (such as oxides, or platinum-group metals) from kerogen during heavy liquid separation could be causing high abundances in the kerogen. However, heavy liquid separation likely removes a significant volume of these phases and due to the increase in Re and Os abundances following heavy liquid separation, they heavy minerals are likely not significant hosts of Re and Os. Minerals of lower density will, however, remain in the kerogen during heavy liquid separation and could be hosts for Re and Os.

Internal isochrons using time-significant, hydrogenous phases were achieved for two sections of the Eagle Ford shale. Isochron regression from phases from the Eagle Ford shale provide internal isochron ages of 110 ± 15 Ma (14%, 2σ, MSWD = 5.5) for the Cenomanian Lower Eagle Ford shale, and 92 ± 14 Ma (15%, 2σ, MSWD = 0.92) for the Turonian Upper Eagle Ford shale, both of which agree with the expected age for these intervals of the Eagle Ford shale.

REFERENCES

Almon W.D. and Cohen P.A. (2008) Palaeoecological significance of turritelline gastropod-dominated assemblages from the mid-Cretaceous (Albian-Cenomanian) of Texas and Oklahoma, USA. *Cretaceous Research* **29**, 65-77.

Baioumy H.M., Eglinton L.B., and Peucker-Ehrenbrink B. (2011) Rhenium-osmium isotope and platinum group element systematics of marine vs. non-marine organic-rich sediments and coals from Egypt. *Chemical Geology* **285**, 70-81.

Barre A.B., Prinzhofer A., and Allegre C.J. (1995) Osmium isotopes in the orgnic matter of crude oil and asphaltenes. *Terra Abstracts* **7**, 199.

Berner R.A. (1985) Sulfate reduction, organic matter decomposition, and pyrite formation. *Transactions of the Royal Society of London* **48**, 25-38.

Birck J.-L., RoyBarman M. and Capmas F. (1997) Re-Os measurements at the femtomole level in natural samples. *Geostandards Newsletter* **20**, 19-27.

Boyer B.W. (1982) Green River laminites: Does the playa-lake model really invalidate the stratified-lake model? *Geology* **10**, 321-324.

Bradley W.H. (1931) Origin and microfossils of the oil shale of the Green River Formation of Colorado and Utah. *U.S. Geological Survey, Professional Paper* **168.**

Brandon A.D., Norman M.D., Walker R.J. and Morgan J.W. (1999) ^{186}Os-^{187}Os systematics of Hawaiian picrites. *Earth and Planetary Science Letters* **174**, 25-42.

Brett C.E. and Allison P.A. (1998) Paleontological approaches to the environmental interpretation of mudrocks. In: Schieber J., Zimmerle W. and Sethi P. (Eds.), *Mudstones and Shales 1: Basin Studies, Sedimentology, and Paleontology*, Stuttgart, Schweizerbartsche Verlagsbuchhandlung, 301-349.

Burke W.H., Denison R.E., Hetherington E.A., Koepnick R.B., Nelson H.F. and Otto, J.B. (1982) Variation of seawater $^{87}Sr/^{86}Sr$ throughout Phanerozoic time. *Geology* **10**, 516-519.

Butler I.S. and Harrod J.F. (1989) *Inorganic Chemistry: Principles and Applications*, Benjamin-Cummings Publishing Co., 799 pp.

Cohen A.S. and Waters F.G. (1996) Separation of osmium from geological materials by solvent extraction for analysis by TIMS. *Analytical Chimica Acta* **332**, 269-275.

Cohen A.S., Coe A.L. Bartlett J.M. and Hawksworth C.J. (1999) Precise Re-Os ages of organic-rich mudrocks and the Os isotope composition of Jurassic seawater. *Earth and Planetary Science Letters* **167**, 159-173.

Colodner D., Sachs J., Ravizza G., Turekian K.K., Edmond J. and Boyle E. (1993) The geochemical cycles of rhenium: A reconnaissance. *Earth and Planetary Science Letters* **117**, 205-221.

Creaser R.A., Papanastassiou D.A. and Wasserburg G.J. (1991) Negative thermal ion mass spectrometry of osmium, rhenium and iridium. *Geochimica et Cosmochimica Acta* **55**, 397-401.

Creaser R.A., Sannigrahi P., Chacko T. and Selby D. (2002) Further evaluation of the Re-Os geochronometer in organic-rich sedimentary rocks: A test of hydrocarbon maturation effects in the Exshaw Formation, Western Canada Sedimentary Basin. *Geochimica et Cosmochimica Acta* **66**, 3441-3452.

Crusius J. and Thompson J. (2000) Comparative behavior of authigenic Re, U, and Mo during reoxidation and subsequent long-term burial in marine sediments. *Geochimica et Cosmochimica Acta* **64**, 2233-2242.

Crusius J., Calvert S., Pedersen T. and Sage D. (1996) Rhenium and molybdenum enrichments in sediments as indicator of oxic, suboxic and sulfidic conditions of deposition. *Earth and Planetary Science Letters* **145**, 65-78.

Cumming V.M., Selby D. and Lillis P.G. (2012) Re-Os geochronology of the lacustrine Green River Formation: Insights into direct depositional dating of lacustrine successions, Re-Os systematics and paleocontinental weathering. *Earth and Planetary Science Letters* **359-360**, 194-205.

Cumming V.M. (2013) Rhenium-osmium geochronology and geochemistry of ancient lacustrine sedimentary and petroleum systems, Durham theses, Durham University. Available at Durham E-Thesis Oline: http://ethesis.dur.ac.uk/6945

Curiale J.A. (1987) Steroidal hydrocarbons of the Kishenehn Formation, northwest Montana. *Organic Geochemistry* **11**, 233-244.

Curtis C.D., Cope J.C.W., Plant D. and Macquaker J.H.S. (2000) "Instantaneous" sedimentation, Early microbial sediment strengthening and a lengthy record of chemical diagenesis preserved in Lower Jurassic ammonitiferous concretions from Dorset. *Journal of the Geological Society of London* **157**, 165-172.

Dancy T.E. and Giedroys V. (1950) Further research on the determination of the chemical composition of oil shales. *Journal of the Institute of Petroleum* **36**, 593-603.

Deming J.W. and Baross J.A. (1993) The Early diagenesis of organic matter: bacterial activity. In: Engel M.H. and Macko S.A. (Eds.) *Organic Geochemistry*, Plenum Press, New York, 119-144.

Denison R.E., Koepnick R.B., Burke W.H., Hetherington E.A. and Fletcher A. (1994) Construction of the Mississippian, Pennsylvanian and Permian seawater $^{87}Sr/^{s}Sr$ curve. *Chemical Geology* **112**, 145-167.

Denison R.E., Koepnick R.B., Burke W.H., Hetherington E.A. and Fletcher A. (1997) Construction of the Silurian and Devonian seawater $^{87}Sr/^{86}Sr$ curve. *Chemical Geology* **140**, 109-121.

Denne R.A., Hinote R.E., Breyer J.A., Kosanke T.H., Lees J.A., Engelhardt-Moore N., Spaw J.M. and Tur N. (2014) The Cenomanian-Turonian Eagle Ford Group of south Texas: insights on timing and paleoceanographic conditions from geochemistry and micropaleontologic analyses. *Palaeogeography, Palaeoclimatology, Palaeoecology* **413**, 2-28.

Donovan A.D. and Staerker T.S. (2010) Sequence stratigraphy of the Eagle Ford (Boquillas) Formation in the subsurface of South Texas and outcrops of west Texas. *Gulf Coast Association of Geological Societies Transactions* **60**, 861-899.

Du Vivier A.D.C., Selby D., Sageman B.B., Jarvis I., Grocke D.R. and Voigt S. (2014) Marine $^{187}Os/^{188}Os$ isotope stratigraphy reveals the interaction of volcanism and ocean circulation during Oceanic Anoxic Event 2. *Earth and Planetary Science Letters* **389**, 23- 33.

Durand B. and Nicaise G. (1980) Procedures of kerogen isolation. In: Durand B. (Ed.), *Kerogen, Insoluble Organic Matter from Sedimentary Rocks,* Editions Technip Paris, 35-53.

Durand B. (1980) Sedimentary organic matter and kerogen. Definition and quantitative importance of kerogen. In: Durand B. (Ed.), *Kerogen,* Editions Technip, Paris.

Ebneth S., Shields G.A., Veizer J., Miller J.F. and Shergold J.H. (2001) High-resolution strontium isotope stratigraphy across the Cambrian-Ordovician transition. *Geochimica et Cosmochimica Acta* **65**, 2273-2292.

Eldrett J.S., Ma C., Bergman S.C., Ozkan A., Minisini D., Lutz B., Jackett S.-J., Macaulay C. and Kelly A.E. (2015a) Origin of limestone-marlstone cycles: Astronomic forcing of organic-rich sedimentary rocks from the Cenomanian to Early Coniacian of the Cretaceous Western Interior Seaway, USA. *Earth and Planetary Science Letters* **423**, 98-113.

Eldrett J.S., Ma C., Bergman S.C., Lutz B., Gregory J.F., Dodsworth P., Phipps M., Hardas P., Minisini D., Ozkan A., Ramezani J., Bowring S.A., Kamo S.L., Ferguson K., Macaulay C. and Kelly A.E. (2015b) An astronomically calibrated stratigraphy of the Cenomanian, Turonian and earliest Coniacian from the Cretaceous Western Interior Seaway, USA: Implications for global chronostratigraphy. *Cretaceous Research* **(in press.).**

Eldrett J.S., Minisini D. and Bergman S.C. (2014) Decoupling of the carbon cycle during Oceanic Anoxic Event 2. *Geology* **42**, 567-570.

Espitalie J., Laporte J.L., Madec M., Marquis F., Leplat P., Paulet J. and Boutefeu A. (1977) Rapid method for source rock characterization, and for determination of their petroleum potential and degree of evolution. *Revue de l'Institut Francais du Petrole Annales des Combustibles Liquides* **32/1**, 23-42

Esser B.K. and Turekian K.K. (1993) The osmium isotopic compositions of the continental crust. *Geochimica et Cosmochimica Acta* **57**, 3093-3104.

Finlay A.J., Selby D. and Grocke D.R. (2010) Tracking the Hirnantian glaciations using Os isotopes. *Earth and Planetary Science Letters* **293**, 339-348.

Finlay A.J., Selby D. and Osborne M.J. (2011) Re-Os geochronology and fingerprinting of United Kingdom Atlantic margin oil: Temporal implications for regional petroleum systems. *Geology* **39**, 475-478.

Finlay A.J., Selby D. and Osborne M.J. (2012) Petroleum source rock identification of United Kingdom Atlantic Margin oil fields and the Western Canadian Oil Sands using platinum, palladium, osmium and rhenium: Implications for global petroleum systems. *Earth and Planetary Science Letters* **313-314**, 95-104.

Forsman J.P and Hunt J.M. (1958) Insoluble organic matter (kerogen) in sedimentary rocks. *Geochimica et Cosmochimica Acta* **15**, 170-182.

Fritz D.A., Belsher T.W., Medlin J.M., Stubbs J.L., Wright, R.P. and Harris P.M. (2000) New exploration concepts for the Edwards and Sligo margins, Cretaceous of onshore Texas. *AAPG Bulletin* **84**, 905-922.

Froelich P.N., Klinkhammer G.P., Bender M.L., Luedtke N.A., Heath G.R., Cullen D., Dauphin P. and Maynard V. (1979) Early oxidation of organic matter in pelagic sediments of the eastern equatorial Atlantic: Suboxic diagenesis. *Geochimica et Cosmochimica Acta* **43**, 1075-1090.

Galloway W.E. (2008) Depositional evolution of the Gulf of Mexico sedimentary basin. In: Miall A.D. (Ed.), *The sedimentary basins of the United States and Canada*, New York, Elsevier, 610 p.

Georgiev S., Stein H.J., Hannah J.L., Bingen B., Weiss H.M. and Piasecki S. (2011) Hot acidic Late Permian seas stifle life in record time. *Earth and Planetary Science Letters* **310**, 389-400.

Gramlich J.W., Murphy T.J., Garner E.L. and Shields W.R. (1973) Absolute isotopic abundance ratio and atomic weight of a reference sample of rhenium. *Journal of Research of the National Bureau of Standards* **77A**, 691-698.

Greenwood N.N. and Earnshaw A. (1997) *Chemistry of the Elements*, 2nd Edition, Butterworth-Heinemann, 1600 pp.

Hannah J.L., Bekker A., Stein H.J., Markey R.J. and Holland H.D. (2004) Primitive Os and 2316 Ma age for marine shale: Implications for Paleoproterozoic glacial events and the rise of atmospheric oxygen. *Earth and Planetary Science Letters* **225**, 43-52.

Harbor R. (2011) Facies characterization and stratigraphic architecture of organic-rich mudrocks, Upper Cretaceous Eagle Ford Formation, south Texas. Master's Thesis, University of Texas at Austin, 195 p.

Hays P.D. and Tieh T.T. (1992) Organic geochemistry and diagenesis of the Delaware Mountain Group, west Texas and southeast New Mexico. *Transactions of the American Association of Petroleum Geologists* **92-90**, 155-175.

Hentz T.F. and Ruppel S.C. (2010) Regional lithostratigraphy of the Eagle Ford shale: Maverick Basin to East Texas Basin. *Gulf Coast Association of Geological Societies Transactions* **60**, 325-337.

Hitchon B., Holloway L.R. and Bayliss P. (1976) Formation of ralstonite during low-temperature acid digestion of shales. *The Canadian Mineralogist* **14**, 391-392

Housecroft C. and Sharpe A.G. (2004) *Inorganic Chemistry*, 2nd Edition, Prentice Hall, 992 pp.

Hunt J.M. (1996) *Petroleum Geochemistrty and Geology*, 2nd Edition, W.H. Freeman and Co., San Francisco, 707 pp.

Ibrahimov R.A. and Bissada K.K. (2010) Comparative analysis and geologic significant of kerogen isolated using open-system (palynological) versus chemically and volumetrically conservative closed-system methods. *Organic Geochemistry* **41**, 800-811.

Ingri J. and Ponter C. (1986) Iron and manganese layering in recent sediments of the Gulf of Bothnia. *Chemical Geology* **56**, 105-116.

Jarvie D.M. (1991) Total Organic Carbon (TOC) Analysis. In: Merrill R.K. (Ed.), *Treatise of petroleum geology: Handbook of petroleum geology, source and migration processes and evaluation techniques*. American Association of Petroleum Geologists, 113-118.

Kendall B.S., Creaser R.A., Ross G.M. and Selby D. (2004) Constraints on the timing of Marinoan 'Snowball Earth' glaciations by ^{187}Re-^{187}Os dating of a Neoproterozoic post-glacial black shale in Western Canada. *Earth and Planetary Science Letters* **222,** 729-470.

Kendall B.S., Creaser R.A. and Selby D. (2009) ^{187}Re-^{187}Os geochronology of Precambrian organic-rich sedimentary rocks. *Geological Society of London Special Publications* **326**, 85-107.

Koide M., Goldberg E.D., Niemeyer S., Gerlach D., Hodge V., Bertine K.K. and Padova A. (1991) Osmium in marine sediments. *Geochimica et Cosmochimica Acta* **55**, 1641-1648.

Landais P. (1993) Bitumen in ore deposits. In: Parnell J., Kucha H. and Landais P. (Eds.), *Bitumen in Ore Deposits*, Special Publicatation of the Society for Geology Applied to Mineral Deposits **9**, 213-239.

Levasseur S., Birck J. and Allegre C.J. (1999) The osmium riverine flux and oceanic mass balance of osmium. *Earth and Planetary Science Letters* **174**, 7-23.

Lewan M.D. and Maynard J.B. (1982) Factors controlling enrichment of vanadium and nickel in the bitumen and organic sedimentary rocks. *Geochimica et Cosmochimica Acta* **46**, 2547-2560.

Lewan M.D., Spiro B., Illich H., Raiswell R., Mackenzie A.S., Durand B., Manning D.A.C., Comet P.A., Berner R.A. and De Leeuw J.W. (1985) Evaluation of petroleum generation by hydrous pyrolysis experimentation [and discussion]. *Philosophical Transactions of the Royal Society of London* **315**, 123-134.

Lillis P.G. and Selby D. (2011) Evaluation of the rhenium-osmium geochronometer in the Phosphoria petroleum system, Bighorn Basin of Wyoming and Montana, USA. *Geochimica et Cosmochimica Acta* **118**, 312-330.

Love L.G. (1967) Early diagenetic iron sulphide in recent sediments of the Wash (England). *Sedimentology* **9**, 327-352.

Ludwig K. (2008) Isoplot, version 4.0: A geochronological toolkit for Microsoft Excel. *Berkeley Geochronology Center Special Publication* **4,** 1-12.

Mahdaoui F., Michels R., Reisberg L., Pujol M. and Poirier Y. (2015) Behavior of Re and Os during contact between an aqueous solution and oil: Consequences for the application of the Re-Os geochronometer to petroleum. *Geochimica et Cosmochimica Acta* **158**, 1-21.

Manning D.A.C. and Gize A.P. (1993) The role of organic matter in ore transport processes. In: Engels M.H. and Macko S.A. (Eds.), *Organic Geochemistry, Principles and Applications,* Plenum Press. New York, 547-563.

Markey R.J., Stein H.J., Hannah J.L., Zimmerman A., Selby D. and Creaser R.A. (2007) Standardizing Re-Os geochronology: A new molybdenite reference material (Henderson, USA) and the stoichiometry of Os salts. *Chemical Geology* **244**, 74-87.

McArthur J.M., Algeo T.J., van de Schootbrugge B., Li Q. and Howarth R.J. (2008) Basinal restriction, black shales, Re-Os dating, and the Early Toarcian (Jurassic) oceanic anoxic event. *Paleoceanography* **23**, PA4217.

McGarity H.A. (2013) Facies and stratigraphic framework of the Eagle Ford shale in south Texas. Masters Thesis, University of Houston, 105 p.

Montgomery S.W., Petty A.J. and Post P.J. (2002) James Limestone, northeastern Gulf of Mexico: Refound opportunity in a Lower Cretaceous trend. *AAPG Bulletin* **86**, 381-397.

Morford J.L. and Emerson S. (1999) The geochemistry of redox sensitive trace metals in sediments. *Geochimica et Cosmochimica Acta* **63**, 1735-1750.

Morford J.L., Martin W.R., Francois R. and Carney C.M. (2009) A model for uranium, rhenium, and molybdenum diagenesis in marine sediments based on results from coastal locations. *Geochimica et Cosmochimica Acta* **73**, 2938-2960.

Oxburgh R. (1998) Variations in the osmium isotope composition of sea water over the past 200,000 years. *Earth and Planetary Science Letters* **159**, 183-191.

Paquay F.S., Ravizza G.E., Dalai T.K. and Peucker-Ehrenbrink B. (2008) Determining chondritic impactor size from the marine osmium isotope record. *Science* **320**, 214-218.

Pasava J., Oszczepalski S. and Du A.S. (2010) Re-Os age of non-mineralized black shales from the Kupferschiefer, Poland, and implications for metal enrichments. *Miner. Deposita* **45**, 189-199.

Paul M., Reisberg L., Vigier N., Zheng Y., Matin Ahmed K., Charlet L. and Hug M.R. (2010) Dissolved osmium in Bengal plain groundwater: implications for the marine Os budget. *Geochimica et Cosmochimica Acta* **74**, 3432-3448.

Peters K.E. (1986) Guidelines for evaluation petroleum source rocks using programmed pyrolysis. *American Association of Petroleum Geologists Bulletin* **70**, 318-329.

Peucker-Ehrenbrink B. and Jahn B.-M. (2001) Rhenium-osmium isotope systematics and platinum group element concentrations: Loess and the upper continental crust. *Geochemistry Geophysics Geosystems* **2**, 1-22.

Peucker-Ehrenbrink B. and Ravizza G. (2000) The marine osmium isotope record. *Terra Nova* **12**, 205-219.

Phelps R.M., Kerans C., Da-Gama R.O.B.P., Jeremiah J., Hull D. and Loucks R.G. (2015) Response and recovery of the Comanche carbonate platform surrounding multiple Cretaceous oceanic anoxic events, northern Gulf of Mexico. *Cretaceous Research* **54**, 117-144.

Pindell J.L., Cande S.C., Pitman W.C., Rowley D.B., Dewey J.F., LaBreeque J. and Haxby W. (1988) A plate-kinematic framework for models of Caribbean evolution. *Tectonophysics* **155**, 121-139.

Poirier A., Hillaire-Marcel, C. (2011) Improved Os-isotopic stratigraphy of the Arctic Ocean. *Ocean. Geophys. Res. Lett.* **38**, L14607.

Poplavko Y.M, Ivanov V.V., Karasik T.G., Miller A.D., Fadeyeva V.A., Orekohov V.S., Taliyev S.D. and Tarkhov Y.A. (1975) On the concentration of rhenium and petroleum, petroleum bitumens and oil shales. *Geochemistry International* **11**, 969-972.

Ravizza G.E. and Peucker-Ehrenbrink B. (2003) The marine $^{187}Os/^{188}Os$ record of the Eocene-Oligocene transition: The interplay of weathering and glaciations. *Earth and Planetary Science Letters* **210**, 151-165.

Ravizza G. and Turekian K.K. (1989) Applications of the ^{187}Re-^{187}Os system to black shale geochronometry. *Geochimica et Cosmochimica Acta* **53**, 3257-3262.

Ravizza G., Turekian K.K. and Hay B.J. (1991) The geochemistry of rhenium and osmium in recent sediments from the Black Sea. Geochimica *et Cosmochimica Acta* **55**, 3741-3752.

Ravizza G., Turekian K.K. and Hay B.J. (2001) The geochemistry of rhenium and osmium in recent sediments from the Black Sea. *Geochimica et Cosmochimica Acta* **55**, 3741-3752.

Robinson W.E. (1969) Isolation procedures for kerogens and associated soluble organic materials. In: Eglinton G. and Murphy M.T.J. (Eds.), *Organic Geochemistry – Methods and Results*, Springer-Verlg, Berlin, Heidelberg, New York, 181-195.

Rooney A.D., Selby D., Houzay J.-P. and Renne P.R. (2010) Re-Os geochronology of a Mesoproterozoic sedimentary succession, Taoudeni Basin, Mauritania: Implications for basin-wide correlations and Re-Os organic-rich sediments systematics. *Earth and Planetary Science Letters* **289**, 486-496.

Rooney A.D., Chew D.M. & Selby D. (2011) Re-Os geochronology of the Neoproterozoic-Cambrian Dalradian Supergroup of Scotland and Ireland: Implications for Neoproterozoic stratigraphy, glaciations and Re-Os systematics. *Precambrian Research* **185**, 202-214.

Rooney A.D., Selby D., Lewan M.D., Lillis P.G. and Houzay J.-P. (2012) Evaluating Re-Os systematics in organic-rich sedimentary rocks in response to petroleum generation using hydrous pyrolysis experiments. *Geochimica et Cosmochimica Acta* **77**, 275-291.

Rose P.R. (1972) Edwards Group, surface and subsurface, central Texas. *University of Texas at Austin Bureau of Economic Geology Report of Investigations* **74**, 198 p.

Sageman B.B., Rich J., Savrda C.E., Bralower T., Arthur M.A. and Dean W.E. (1998) Multiple Milankovitch cycles in the Bridge Creek Limestone (Cenomanian-Turonian), Western interior basin. In: Arthur M.A. and Dean W.E. (Eds.), *Stratigraphy and paleoenvironments of the Cretaceous Western Interior seaway, USA.* Society of Sedimentary Geology, Concepts in Sedimentology and Paleontology **6**, 153-171.

Salvador A. (1991) Origin and development of the Gulf of Mexico Basin. In: Salvador A. (Ed.), *The Gulf of Mexico Basin: Boulder, Colorado*, Geological Society of America, The Geology of North America **J**, 389-444.;

Schieber J. and Riciputi L. (2005) Pyrite-marcasite coated grains in the Ordovician Winnipeg Formation, Canada: An intertwined record of surface conditions, stratigraphic condensation, geochemical "reworking" and microbial activity. *Journal of Sedimentary Research* **75**, 905-918.

Schieber J. (2002) Sedimentary pyrite: A window into the microbial past. *Geology* **30**, 531-534.

Schmitz B., Peucker-Ehrenbrink B., Heilmann-Clausen C., Aberg G., Asaro F. and Lee C.A. (2004) Basaltic explosive volcanism, but no comet impact, at the Paleocene-Eocene boundary: High-resolution chemical and isotopic records from Egypt, Spain and Denmark. *Earth and Planetary Science Letters* **225**, 1-17.

Scott R.W. (1993) Cretaceous carbonate platform, U.S. Gulf coast. In: Simo J.A., Scott R.W. and Masse J.P. (Eds.), *Cretaceous Carbonate Platforms,* AAPG Memoir **56**, 97-109.

Selby D. and Creaser R.A. (2001) Re-Os geochronology and systematics in molybdenite from the Endako porphyry molybdenum deposit, British Columbia, Canada. *Economic Geology* **96**, 197-204.

Selby D. and Creaser R.A. (2003) Re-Os geochronology of organic rich sediments: An evaluation of organic matter analysis methods. *Chemical Geology* **200**, 225-240.

Selby D. and Creaser R.A. (2005) Direct radiometric dating of hydrocarbon deposits using rhenium-osmium isotopes. *Science* **308**, 1293-1295.

Selby D., Creaser R.A., Dewing K. and Fowler M. (2005) Evaluation of bitumen as a ^{187}Re-^{187}Os geochronometer for hydrocarbon maturation and migration: A test case from the Polaris MVT deposits, Canada. *Earth and Planetary Science Letters* **235**, 1-15.

Selby D., Creaser R.A. and Fowler M.G. (2007) Re-Os elemental and isotope systematics in crude oils. *Geochimica et Cosmochimica Acta* **71**, 378-386.

Smith J.W. (1961) Ultimate composition of organic material in green river oil shale. *United States Bureau of Mines Report,* **5725.**

Smoliar M.I., Walker R.J. and Morgan J.W. (1996) Re-Os isotope constraints on the age of Group IIA, IIIA, IVA, and IVB iron meteorites. *Science* **271**, 1099-1102.

Speight J.G. (1988) Evidence for types of polynuclear aromatic systems in nonvolatile fractions of petroleum. In: Ebert L.B. (Ed.), *Polynuclear Aromatic Compounds,* ACS Advances in Chemistry Series **217**, 201-255.

Sundby B., Martinez P. and Gobeil C. (2004) Comparative geochemistry of cadmium, rhenium, uranium, and molybdenum in continental margin sediments. *Geochimica et Cosmochimica Acta* **68**, 2485-2493.

Tissot R.P. and Welte D.H. (1984) *Petroleum Formation and Occurrence,* 2nd Edition, Springer Berlin Heidelberg New York, 699 pp.

Tribovillard N., Algeo T., Lyons T.W. and Riboulleau A. (2006) Trace metals as paleoredox and paleoproductivity proxies: An update. *Chemical Geology* **232**, 12-32.

Tucker M.E. (1998) *Sedimentary Petrology, an Introduction*, Blackwell London, 197 pp.

Turgeon S.C. and Creaser R.A. (2008) Cretaceous oceanic anoxic event 2 triggered by a massive magmatic episode. *Nature Letters* **454**, 323-326.

Tuttle M.L. and Goldhaber M.B. (1993) Sedimentary sulfur geochemistry of the Paleogene Green River Formation, western USA: Implications and geochemical approach, Devonian Appalachian Basin. *Paleogeography, Paleoclimatology, Paleoecology* **304**, 54-73.

Vandenbroucke M. and Largeau C. (2007) Kerogen origin, evolution and structure. *Organic Geochemistry* **28**, 719-833.

Veizer J. and Compston W. (1974) $^{87}Sr/^{86}Sr$ composition of seawater during the Phanerozoic. *Geochimica et Cosmochimica Acta* **38**, 1461-1484.

Veizer J., Ala D., Azmy K., Bruckschen P., Buhl D., Bruhn F., Carden G.A.F., Diener A., Ebneth S., Godderis Y., Jasper T., Korte C., Pawellek F., Podlaha O.G. and Strauss H. (1999) $^{87}Sr/^{86}Sr$ and $\delta^{13}C$ and $\delta^{18}O$ evolution of Phanerozoic seawater. *Chemical Geology* **161**, 59-88.

Volkening J., Walczyk T. and Heumann K.G. (1991) Osmium isotope ratio determinations by negative thermal ionization mass spectrometry. *International Journal of Mass Spectrometry and Ion Processes* **105**, 147-159.

Yamashita Y., Takahashi Y., Haba H., Enomoto S. and Shimizu H. (2007) Comparison of reductive accumulation of Re and Os in seawater-sediment systems. *Geochimica et Cosmochimica Acta* **71**, 3458-3475.

York D. (1969) Least-squares fitting of a straight line with correlated errors. *Earth and Planetary Science Letters* **5**, 320-324.

Yurewicz D.A., Marler T.B., Meyerholtz K.A. and Siroky F.X. (1993) Early Cretaceous carbonate platform, north rim of the Gulf of Mexico, Mississippi and Louisiana. In: Simo A., Scott R.W. and Masse J.P. (Eds.), *Cretaceous Carbonate Platforms*, AAPG Memoir **56**, 81-96.

Zheng Y., Anderson R.F. van Geen A. and Kuwabara J.S. (2000) Authigenic molybdenum formation in marine sediments: a link to pore water sulfide in the Santa Barbara Basin. *Geochimica et Cosmochimica Acta* **64**, 4165-4178.